DESIGN AND SYNTHESIS OF BLOCK COPOLYMERS THAT SELF ASSEMBLE INTO MICELLES WITH CONTROLLED ACID AND LIPASE CATALYZED DEGRADATION

A Dissertation
Submitted to
the Temple University Graduate Board

---

in Partial Fulfillment
of the Requirements for the Degree
DOCTOR OF PHILOSOPHY

---

by
Xiaobo Zhu
January, 2014

Examining Committee Members:

Bradford B. Wayland, Ph. D., Dissertation Supervisor, Chemistry
Stephanie L. Wunder, Ph. D., Advisory Chair, Chemistry
Ann M. Valentine, Ph. D., Chemistry
Michael Fryd, Ph. D., External Member, University of Pennsylvania

ABSTRACT

DESIGN AND SYNTHESIS OF BLOCK COPOLYMERS THAT SELF ASSEMBLE INTO MICELLES WITH CONTROLLED ACID AND LIPASE CATALYZED DEGRADATION

Xiaobo Zhu

Professor Bradford B. Wayland

Poly (ε-caprolactone) block poly (ethylene glycol) (PCL-*b*-PEG) is typical amphiphilic block copolymer that self assembles into micelles in water where the hydrolytically stable hydrophilic PEG segment forms the exterior corona and the core contains the hydrophobic degradable PCL block. Micelles from PCL-*b*-PEG block copolymers are among the top candidates for application as transport and delivery systems. The efficiency for micellar transported therapeutics to reach the desired site is currently limited by processes that prematurely degrade the micelle and this issue is stimulating increased effort in evaluating how micelles respond to the conditions encountered in the digestive and circulatory systems. Drug loaded micelles introduced into the blood and digestive systems encounter a wide range of conditions, enzymes and other substances that can promote micelle precipitation, degradation and premature release of therapeutics. Furthermore, PEG-*b*-PCL diblock copolymer micelle stability in aqueous suspension, low drug loading content and burst drug releasing are also the critical issues in drug delivery system.

One central objective for this research is to identify and utilize polymer structural features that influence the hydrolytic stability of micelles toward acid, base and enzyme catalyzed hydrolysis of the polyester cores. The strategy of by preparing a set of triblock copolymers (PEG-*b*-PBO-*b*-PCL) formed by inserting a short hydrophobic non-

hydrolyzable PBO segment between the PEG and PCL blocks as an approach to increase the barrier for water to reach the sensitive interface ester at the surface of the PCL core and thus increase the micelle stability at acidic aqueous medium. However, the triblock micelle doesn't significantly reduce the rate of lipase enzyme catalyzed degradation of micelle from PCL-*b*-PEG-OMe.

Another objective for this research is to prepare PCL-*b*-PEG diblock copolymer micelles that have high stability in aqueous suspensions, high drug loading content and selective reactions with lipase enzymes. The working hypothesis is that the micelles with charged groups at the terminus of PEG corona will increase the micelle dispersion stability and stabilize micelles with much larger hydrophobic cores through intermicelle electrostatic repulsions. When the micelle corona and lipase enzyme have the same charge there will be an increased barrier to reaction. The comparison of micelle dispersion stabilities micelles from HO-PCL-*b*-PEG-$CH_2CH{=}CH$, $[\text{PCL-}b\text{-PEG-RCO}_2]^-Na^+$ and $[\text{PCL-}b\text{-PEG-RSO}_3]^-Na^+$ demonstrates that the micelles with ionic coronas have significantly higher suspension stability. Kinetic of lipase catalyzed degradation of micelles with corona charges shows that lipases selective reaction with corona charged micelles which could be used as design feature to selectivity for therapeutic transport and release.

Modification hydrophilic-hydrophobic interface and corona charges of PCL-*b*-PEG diblock copolymer micelle are successful chemical strategies to increase micelle stability and control acid and lipase enzymes catalytic degradation.

ACKNOWLEDGEMENTS

I would like to express my deepest appreciation to Professor Bradford B. Wayland, my advisor. He has generously provided his invaluable insights, inspiring ideas, precious time, constant guidance, and warm encouragement. Also, his kind advice for my career and life are highly appreciated.

I would like to give my great thanks to Professor Michael Fryd. He is always available when I need help on my research. Many great ideas were generated during the weekly discussion with him. I also express my appreciation to him for his help on my career.

I would like to acknowledge my committee members: Professor Stephanie L. Wunder and Professor Ann M. Valentine for their priceless time, comments and guidance on my research. I really appreciate their recommendation for my outstanding research award and dissertation completion fellowship.

I want to thank Professor Ann M. Valentine's help on my lipase separation experiments, Dr. DeBrosse for his help on my solvent suppressed ^{1}H NMR experiments, Dr. Zhou for his help on my TEM experiments, Dr. Ilies for his help on DLS.

Thanks also goes to my colleagues and close friends: Salome, Sounak, Jerry, Behzad, Greg, Yingjian, QQ, Peng, Senzhi, Chongsong, Bolei and many others. They have contributed their suggestions and experience to my research. They also make my journey here full of joys and fun.

Special thanks to my wife, Xiaolei Zhang, for her love, support, and sacrifice on family reunion. She brings me a joyful life with happiness and love.

Finally, but the most important part, I want to show my deepest thanks to my parents for their guidance, encouragement and forever love and support.

TABLE OF CONTENTS

LIST OF FIGURES

LIST OF TABLES

LIST OF SCHEMES

CHAPTER 1:

INTRODUCTION: BLOCK COPOLYMER MICELLES IN DRUG DELIVERY SYSTEM

1.1 Amphiphilic block copolymer for drug delivery

Amphiphilic block copolymers self assemble into micelles with hydrophilic corona (shell) and hydrophobic cores[1-10] provide a broad platform for development of drug and gene delivery vehicles[11-18] that function through their capability for loading, transport and release of lipophilic substances incorporated in the hydrophobic core. The block copolymer micelles with size range from 10-200 nm are considered as one of the most promising platforms for targeted and controlled drug and gene delivery since the fact that they increase the solubility of poorly water soluble hydrophobic drugs, prolong the drug circulation time and avoid excretion through the kidney[12, 19-20]. In addition, polymer micelles have received great interest due to their versatile structures that can be easily modified according to the specific aim of drug loading and delivery system.

A variety of hydrophilic polymers such as poly(ethylene glycol) (PEG) or poly(vinyl pyrrolidone) (PVP)[21] with a flexible nature can be selected as shell-forming segments. Among them, poly (ethylene glycol) (PEG) that has a repeat unit of -CH_2CH_2O- is the most commonly used as a hydrophilic segment due to PEG has unique properties such as: i) high solubility in water and many organic solvents, ii) biocompatible and non-toxicity; iii) absence of antigenicity and immunogenicity[22-26]. Besides, the PEG corona on the polymer micelles can inhibit hydrophobic interactions between the inner cores of different micelles thus inhibiting intermicelle aggregation. The selection of hydrophobic polymers for the micelle core determine the properties of polymeric micelles, such as micelle stability, drug loading capacity and drug release profile. Biodegradable polyesters such as poly(lactic acid) (PLA)[27-28], poly (glycolic acid)(PGA)[29] and poly(ε-caprolactone) (PCL)[30-31] have been widely studied for drug delivery materials.

In spite of such advantages of using amphiphilic diblock copolymer micelles as a hydrophobic drugs carriers, there are still several barriers such as micelle stability in vivo or vitro and drug loading efficiency are waiting to be overcome in the area of micellar drug delivery.

1.2 PEG-*b*-PCL diblock copolymer micelles

Block copolymers from Poly (ethylene glycol) and poly (ε-caprolactone) (PEG-*b*-PCL) are prototypical amphiphilic block copolymers that form micelles in water where the hydrolytically stable hydrophilic segment (PEG) forms the exterior corona and the core contains the hydrolytically degradable hydrophobic block (PCL) (Figure 1.1).

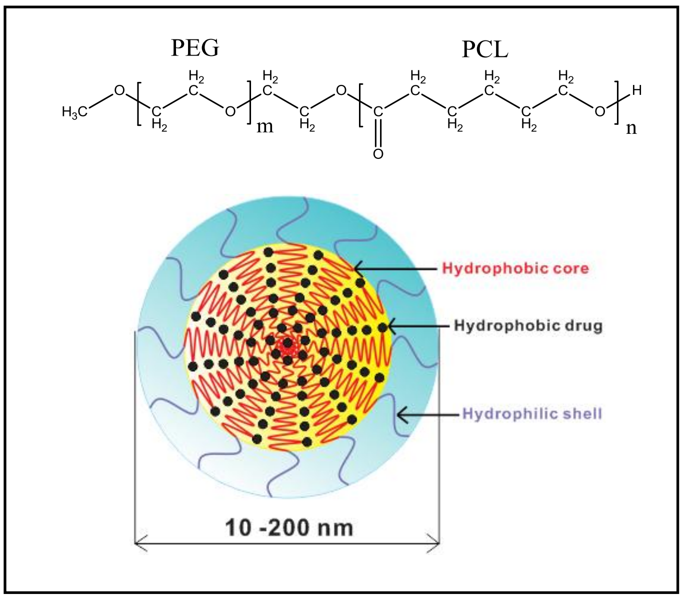

Figure 1.1: Structure of MeO-PEG-*b*-PCL diblock copolymer and drug loaded micelle.

The most common method to synthesize PEG-*b*-PCL diblock copolymers was the ring opening polymerization of caprolactone (CL) using methoxy-PEG (MeO- PEG) as a macroinitiator and stannous octoate as a catalyst[32-33] at T= 110-120 ^{o}C. One of the widely used methods to form PEG-*b*-PCL diblock copolymer micelle is nano-precipitation method[21, 34-36]. Stock solution of the block copolymer and hydrophobic drugs in organic solvent was added into water where polymers self assemble into micelles and drugs go into the core of the micelles (Figure 1.2).

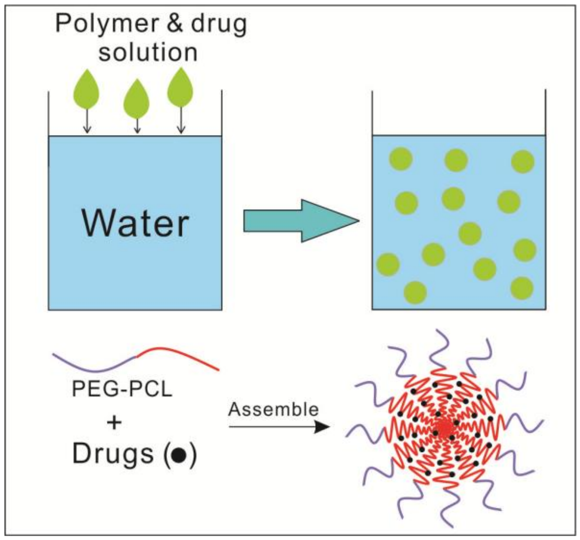

Figure 1.2: Schematic demonstration of self assembly of PEG-*b*-PCL diblock copolymer in water.

Amphiphilic block copolymers containing PEG and PCL segments have been utilized effectively in the preparation of structurally modified polymers designed to improve micelle stability and efficiency of targeted therapeutic delivery. Studies of cell specific drug delivery from polymer micelles that have appended functionalities such as proteins[37], antibodies[38] and sugars[39] have reported remarkable successes, but the fraction of drug that reaches the target site is small even when the target selectivity is high because of in vivo micelle instability[40]. The efficiency for micellar transported therapeutics to reach the desired site is currently limited by processes that prematurely degrade the micelle. Drug loaded micelles introduced into the blood and digestive systems encounter a wide range of conditions, enzymes and other substances that can promote micelle precipitation, degradation and premature release of therapeutics. Furthermore, PEG-*b*-PCL diblock copolymer micelle stability in aqueous suspension, low drug loading content and burst drug releasing are also the critical issues in drug delivery system.

1.3 Stability issue of PEG-*b*-PCL diblock copolymer micelles

1.3.1 Micelle stability in aqueous solutions

Polymer micelles must remain intact to prevent the cargoes release before reaching the target sites. One of the barriers on the development of effective micelle drug carriers is the poor stability of micelles in an aqueous environment. The polymer micelle is a physically assembled structure. In aqueous medium, the stability of polymer micelle is determined by many factors, such as polymer concentration, ratio of hydrophilic and hydrophobic segments, solution ion concentration and temperature etc. It is well known that the micelle stability depends on the polymer concentration. A polymer micelle has a critical micelle concentration (CMC) that is the minimum concentration of polymer required for micelle formation[41-42]. At low polymer concentrations, there are not enough numbers of chains to self-assemble and instead the chains are found distributed throughout the solution.

The stability of PEG-*b*-PCL micelles is highly dependent on the PEG corona. It is the PEG coronas that inhibit hydrophobic interactions between the inner cores from different micelles thus inhibiting intermicelle aggregation. The PEG chains interact with the water by hydrogen bonding forcing the PEG into a rigid and extended configuration[43-44], which protects the hydrophobic PCL core from exposure to the aqueous solution and stabilizes the micelle (Figure 1.3A). In contrast, when the solubility in solution decreases at conditions such as high temperature or high ionic strength, the PEG chains become coiled and soft (less stretched), leading to aqueous exposure to the hydrophobic core and micelle destabilization[44](Figure 1.3B).

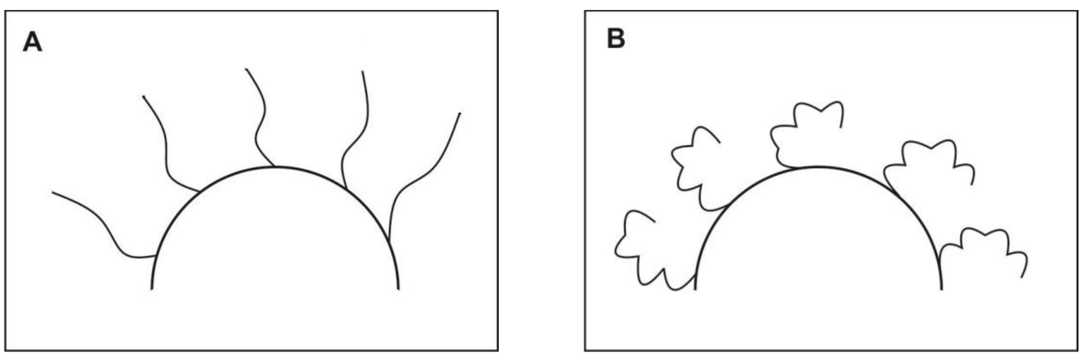

Figure 1.3: Schematic diagrams of PEG configurations on the micelle: stable micelles with PEG corona in a rigid and extended configuration (A); instable micelles with PEG corona in coiled and soft configuration (B).

Drug loaded PEG-*b*-PCL diblock copolymer micelles introduced into the digestive and circulatory systems[45-52] encounter a wide range of conditions that can promote micelle precipitation and destabilization. Strategies need to be developed to increase the solubility of PEG at various conditions.

1.3.2 Micelle stability in biological environments

After drug loaded micelles are injected into the blood systems, polymer micelles become much diluted by blood[53]. If the polymer concentration is lower than the CMC after the blood dilution, then the micelles disassociates to early release the drug. Furthermore, after the injection, the polymer micelles are confronted with numerous blood components, such as proteins and cells. PEG interacts with biomolecules, especially proteins via the attractive forces (hydrogen bonding, electrostatic, and van der Waals interactions)[54]. PEG has been reported to have direct interaction with proteins including lysozyme[55], serum albumin[56], pepsin[57], and α-chymotrypsin[58]. Maysinger et al. reported that PEG-b-PCL diblock copolymer micelle is unstable in serum-containing culture media with or without cells, but stable in phosphate-buffered saline[59]. The formation of complex between PEG and proteins possibly induces micelle aggregation which may significantly affect the micelle stability in vivo.

1.3.3 Micelle stability in acidic and basic aqueous medium

The PEG-*b*-PCL block copolymers that were designed for drug delivery have a hydrolytically sensitive ester[21, 60-62] link between the hydrophilic and hydrophobic segments. This ester group is normally located at the aqueous/hydrophobic interface in core-shell micelles and thus is readily accessed for reactions with the aqueous medium. Hydrolysis of the interface ester leads to shedding of the PEG block and destabilization of the micelle[47, 63-65]. At acidic and basic aqueous medium[46-48, 64-65], the acid and base catalyzed degradation of this unique interface ester group is much faster compared to this ester hydrolysis happens at neutral medium (pH=7). The rate limiting step in the acid catalyzed degradation of micelles from PEG-*b*-PCL diblock copolymer micelles was identified as the initial PCL hydrolysis event which occurs at the PCL ester group that is bonded to the PEG. The shedding of PEG coronas to certain degree and when the remaining PEG couldn't stabilize the PCL cores, the micelles will aggregate and precipitate out. The fast hydrolysis of the ester groups at the hydrophilic-hydrophobic interface results in the micelle precipitation is the key issue for these micelles used as drug carriers for oral drug delivery since the pH in the digestive system such as stomach can drop to the range from 1.0-2.0.

1.3.4 Micelle stability in enzymatic aqueous medium

Block copolymers containing PEG and PCL segments have been utilized effectively in the preparation of structurally modified polymers designed to improve micelle stability and efficiency of targeted therapeutic delivery. Studies of cell specific drug delivery from polymer micelles that have appended functionalities such as proteins[37], antibodies[38] and sugars[39] have reported remarkable successes, but the fraction of drug that reaches the target site is small even when the target selectivity is high because of in vivo micelle instability[40]. The efficiency for micellar transported therapeutics to reach the desired site is currently limited by processes that prematurely degrade the micelle. Drug loaded micelles introduced into the blood encounter a wide range of conditions, enzymes and other substances that can promote micelle degradation and premature release of therapeutics. Several lipase enzymes have been observed to catalyze polyester hydrolysis and degradation of micelles derived from water insoluble PEG-*b*-PCL block copolymers[31, 46, 64, 66]. Kinetics of micelle degradation obtained by light scattering[31, 46, 48,

[66] were interpreted as indicating that the micelle particles reacted away in a "one by one" sequential manner first proposed by Wu[31, 66]. A rate law for the lipase catalyzed micelle degradation that is zero order in the micelle concentration and first order in the enzyme concentration was reported by Jiang[46]. The kinetic studies of lipase enzymes catalyzed degradation of PEG-*b*-PCL block copolymers micelles demonstrated that all the micelles were reacted away within hours after lipase enzymes were added into the solutions[31, 46, 64, 66]. One major issue is to identify and exploit polymer structural features that can be used to influence the hydrolytic stability of polymers in micelles toward extremely enzyme catalyzed hydrolysis of the polyester cores that trigger micelle degradation and drug release.

1.4 Drug loading capacity issue of PEG-*b*-PCL diblock copolymer micelles

Block copolymer micelles have a variety of biomedical applications[11-12, 19], and are particularly prominent as drug and gene delivery vehicles[13-14, 67] that function through their capability for loading, transport and release of lipophilic substances incorporated in the hydrophobic core. One of the biggest issues for using the PEG-*b*-PCL diblock copolymer micelles to loading the deliver hydrophobic therapeutics is the low drug loading efficiency in the core. Most of the prior reported PEG-*b*-PCL diblock copolymer micelles drug loading content (DL% = weight of drug in the micelles/total weight of the drug loaded micelles $\times$100%) is less than 10%[7, 68-70]. For a specific polymer micelle drug delivery system, a higher drug loading content permits the administration of an equivalent dose of the actual drug with a smaller amount of polymer, which is necessary to minimize unwanted side effects from the polymer after the drug has been delivered to its target[1]. Previous studies reported that the capacity of a micelle to store and transport a hydrophobic substance is proportional to the size of the core[68, 70-71] which in block copolymer micelles is related to the length of the hydrophobic polymer segment. The general approach to increase the loading capacity for a micelle carrier is simply to increase the volume of the hydrophobic core which is limited by the capability of the hydrophilic corona to maintain a stable aqueous dispersion of the insoluble hydrophobic core.

1.5 Drug burst releasing issue of PEG-*b*-PCL diblock copolymer micelles

Amphiphilic diblock copolymer micelles loaded with the hydrophobic anticancer drug are supposed to deliver the drugs to the targeted tumor cells, diseased blood vessel, etc and then controlled release all the drugs (Figure 1.4). However, a major problem encountered for most diblock micellar carriers is the undesirable burst release of drugs after the micelles are injected into the blood. Burst release leads to the large initial drug release that limits clinical successes of block copolymer micelles for targeted delivery of lipophilic anticancer drugs. Two major causes of the micelle drug burst releasing have been reported during the prior studies. First of all, the burst drug release in blood circulation is mainly due to blood dilution and subsequent micelle disassembly[72-73] which is highly related to the micelle stability issue. Another cause of the drug burst release results from the drug loading process. When PEG-*b*-PCL diblock copolymers self-assemble into micelles, some of the hydrophobic drugs go into the PCL cores and a large portion of the drugs stays at the surface of the PCL cores[74-75]. Those drugs adsorb on the PCL surface prematurely release into the blood system after the micelle dilution. The way to avoid the fast release of these drugs loaded at the surface of the PCL core is to do the dialysis of the drug encapsulated micelles to remove these drugs. Meanwhile, this also reduces the drug loading content of the micelles which is also a top issue.

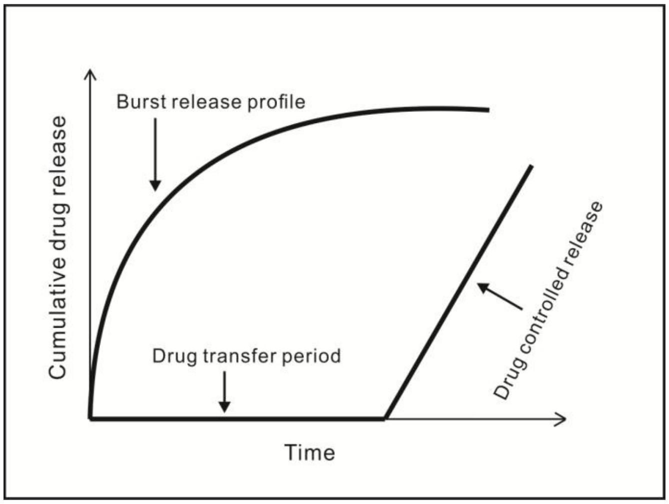

Figure 1.4: Schematic demonstration of drug burst release and controlled release.

1.6 Scope and Dissertation Objectives

Design of PEG-*b*-PCL block copolymer micelles that manifest enhanced efficiency of drug delivery could benefit substantially from having a kinetic-mechanistic understanding for the array of potential reactions that can contribute to the degradation of the transport micelles. One major goal for this research is to identify and exploit polymer structural features that can be used to influence the hydrolytic stability of polymers in micelles toward acid, base and enzyme catalyzed hydrolysis of the polyester cores that trigger micelle degradation and drug release. At the same time, other critical issues such as micelle stability in aqueous solution, low drug loading content and burst drug releasing will be evaluated though chemical modification of PEG-*b*-PCL diblock copolymer structures.

Chapter 2 studies the destabilization issue of MeO-PEG-*b*-PCL diblock copolymer micelle after the junction ester group at the hydrophilic PEG and hydrophobic PCL interface is hydrolyzed. In acidic and basic medium, the rate of hydrolysis of this unique ester is significantly increased. Our working hypothesis is that by preparing a set of triblock copolymers (MeO-PEG-*b*-PBO-*b*-PCL) formed by inserting a short hydrophobic non-hydrolyzable poly (1,2-butylene oxide) (PBO) segment between the PEG and PCL blocks as an approach to increase the barrier for water to reach the interface ester at the surface of the PCL core. The acid catalyzed hydrolysis of the interface ester groups should occur substantially slower in the triblock copolymer micelles when compared to micelles of the parent diblock copolymer and thus the micelle stability for MeO-PEG-*b*-PCL diblock copolymer is increased at the acidic medium by such hydrophilic-hydrophobic interface modification strategy. Mechanistic features of acid catalyzed degradation of MeO-PEG-*b*-PCL diblock copolymer micelle over a long period of reaction time is also studied in Chapter 2 to understand the whole process of the micelle degradation.

Chapter 3 mainly focuses on the issue of fast instability of diblock copolymer micelle at the enzymatic medium. The lipase enzymes catalyzed degradation of MeO-PEG-*b*-PCL diblock copolymer micelle was prior reported to be very fast. The efficiency observed for micelle deliver therapeutics to the targeted sites is currently limited by processes that prematurely degrade the micelle and early release of the drugs. Lipase enzymes from *P. cepacia*, *C. rugosa* and *P. fluorescens* are utilized to test if the inserted PBO segment between the PEG and PCL blocks could retard the lipase to catalyze the degradation of the PCL cores. ^{1}H NMR, GPC and DLS studies are used to evaluate the micelle and solution compositions, determine the kinetics of diblock and triblock copolymer micelle degradation and advance the mechanistic understanding for lipase catalyzed processes.

Chapter 4 reports the detailed kinetic and mechanistic studies of lipase-polymer micelle binding and catalytic degradation. The lipase catalyzed degradation of MeO-PEG-*b*-PCL micelles at different micelle and lipase concentrations demonstrates that the degradation is zero order in micelle concentration ([M]) and first order in the initial enzyme concentration ($[E_0]$) which is equivalent to first order in the enzyme-micelle complex [EM] when the micelle concentration is excess. Analysis and computer simulation of kinetics for *P. cepacia* lipase catalyzed MeO-PEG-*b*-PCL micelle degradation show that the process conforms to a ($E + M \rightleftharpoons EM \rightarrow P + E$) with enzyme-micelle complex product inhibition ($EM + P \rightleftharpoons EMP$). Formation and tight binding of the lipase enzyme-micelle complex, activation of lipase catalysis and sequential micelle degradation are characteristics of MeO-PEG-*b*-PCL micelle degradation which parallel features of enzyme interfacial activation associated with lipase catalyzed hydrolysis of lipids in membranes.

Chapter 5 discusses the strategy of preparation of PCL-*b*-PEG diblock copolymer micelles that have high stability in aqueous suspensions, high drug loading content and selective reactions with lipase enzymes. This chapter reports on initial test on the comparison of micelle dispersion stabilities from HO-PCL-*b*-PEG-$CH_2CH{=}CH$, [PCL-*b*-PEG-$RCO_2]^-$ Na^+ and [PCL-*b*-PEG-$RSO_3]^-Na^+$ (R=-$O(CH_2)_3S(CH_2)_2$-). Thiol-ene click chemistry of an allyl terminated block copolymer (HO-PCL_n-*b*-PEG_{32}-$CH_2CH{=}CH_2$) is used to place -CO_2Na and -SO_3Na end groups on the PEG segment and generate micelles that have negatively charged groups at the terminus of the corona. The general approach to increase the loading capacity for a micelle carrier is simply to increase the volume of the hydrophobic core which is limited by the capability of the hydrophilic corona to maintain a stable aqueous dispersion of the insoluble hydrophobic core. The working hypothesis is that micelles with ionic corona will increase the micelle dispersion stability through intermicelle electrostatic repulsions and will stabilize micelles with much larger hydrophobic cores.

Chapter 6 explores the lipase enzymes catalyzed degradation of the corona charged micelles from HO-PCL-*b*-PEG-RX (R= $-O(CH_2)_3S(CH_2)_2-$, X= $-CO_2^-$,$-RSO_3^-$,$-NH_3^+$). All the kinetic and mechanistic studies in Chapter 6 are based upon the lipase-micelle interfacial activation model proposed in Chapter 4. The original motivation for placing charged groups on the corona of is that when the micelle corona and lipase enzyme have the same charge there will be an increased barrier to reaction which could be used as a design feature to obtain selectivity for therapeutic transport and release. This chapter discusses on the influence that the electronic charge on the micelle corona has on lipase enzyme catalyzed hydrolytic degradation of micelles. Kinetic studies of *P. cepacia* lipase catalyze detected the presence of two *P. cepacia* lipase isoforms that have opposite corona charge selectivity for catalyzing the degradation of micelles with positively and negatively charged corona. One lipase selectively reacts with the micelles with a negative corona and the other lipase only reacts with the micelles with a positive corona. Both lipases catalyze degradation of micelles with a neutral corona. An initial effort to separate the two lipase isoforms with molecular weight of about 33 kD in the commercial sample by trituration and hydrophobic interaction chromatography supports the presence of two lipases, but only partial separation is observed.

Chapter 7 provides some suggestions for future works on this research project. Chapters 2-6 mainly focus on the kinetic and mechanistic studies acid and lipase catalyzed degradation of PCL-*b*-PEG block copolymer micelles with modified hydrophilic-hydrophobic interface and corona charge. The drug loading experiments for all the prepared micelles used in the studies of this dissertation are missing. In this Chapter, the drug loading and in vitro drug releasing using current polymer micelles are suggested for future works. Besides, core cross linkable PCL-*b*-PMCL-*b*-PEG micelles are recommended to be synthesized for inhibiting the fast lipase catalyzed degradation of PCL core. Most importantly, one interfacially cross linked [PCL-*b*-PMCL-*b*-PBO-*b*-PEG-$RSO_3]^-Na^+$ micelle with negatively charged corona has been predicted as an ideal candidate for the drug delivery application.

1.7 References

(1) Tyrrell, Z. L.; Shen, Y.; Radosz, M. *Prog. Polym. Sci.* 2010, 35, 1128-1143.

(2) Zhang, Q.; Remsen, E. E.; Wooley, K. L. *J. Am. Chem. Soc.* 2000, 122, 3642-3651.

(3) Hickey, R. J.; Haynes, A. S.; Kikkawa, J. M.; Park, S.-J. *J. Am. Chem. Soc.* 2011, 133, 1517-1525.

(4) Zhu, W.; Nese, A.; Matyjaszewski, K. *J. Polym. Sci., Part A: Polym. Chem.* 2011, 49, 1942-1952.

(5) Lee, H.-i.; Wu, W.; Oh, J. K.; Mueller, L.; Sherwood, G.; Peteanu, L.; Kowalewski, T.; Matyjaszewski, K. *Angew. Chem. Int. Ed.* 2007, 46, 2453-2457.

(6) Discher, B. M.; Won, Y.-Y.; Ege, D. S.; Lee, J. C.-M.; Bates, F. S.; Discher, D. E.; Hammer, D. A. *Science* 1999, 284, 1143-1146.

(7) Zhang, X.; Cheng, J.; Wang, Q.; Zhong, Z.; Zhuo, R. *Macromolecules* 2010, 43, 6671-6677.

(8) Geng, Y.; Discher, D. E. *J. Am. Chem. Soc.* 2005, 127, 12780-12781.

(9) Mai, Y.; Eisenberg, A. *Chem. Soc. Rev.* 2012, 41, 5969-5985.

(10) Rajagopal, K.; Mahmud, A.; Christian, D. A.; Pajerowski, J. D.; Brown, A. E. X.; Loverde, S. M.; Discher, D. E. *Macromolecules* 2010, 43, 9736-9746.

(11) Langer, R.; Tirrell, D. A. *Nature* 2004, 428, 487-492.

(12) Elsabahy, M.; Wooley, K. L. *Chem. Soc. Rev.* 2012, 41, 2545-2561.

(13) Endres, T. K.; Beck-Broichsitter, M.; Samsonova, O.; Renette, T.; Kissel, T. H. *Biomaterials* 2011, 32, 7721-7731.

(14) Zhu, Z.; Li, Y.; Li, X.; Li, R.; Jia, Z.; Liu, B.; Guo, W.; Wu, W.; Jiang, X. *J. Controlled Release* 2010, 142, 438-446.

(15) Aliabadi, H. M.; Mahmud, A.; Sharifabadi, A. D.; Lavasanifar, A. *J. Controlled Release* 2005, 104, 301-311.

(16) Kataoka, K.; Harada, A.; Nagasaki, Y. *Adv. Drug Deliv. Rev.* 2001, 47, 113-131.

(17) Ensign, L. M.; Schneider, C.; Suk, J. S.; Cone, R.; Hanes, J. *Adv. Mater.* 2012, 24, 3887-3894.

(18) Shuvaev, V. V.; Ilies, M. A.; Simone, E.; Zaitsev, S.; Kim, Y.; Cai, S.; Mahmud, A.; Dziubla, T.; Muro, S.; Discher, D. E.; Muzykantov, V. R. *ACS Nano* 2011, 5, 6991-6999.

(19) Deng, C.; Jiang, Y.; Cheng, R.; Meng, F.; Zhong, Z. *Nano Today* 2012, 7, 467-480.

(20) Kim, S.; Shi, Y.; Kim, J. Y.; Park, K.; Cheng, J.-X. *Expert Opinion on Drug Delivery* 2010, 7, 49-62.

(21) Chung, T. W.; Cho, K. Y.; Lee, H.-C.; Nah, J. W.; Yeo, J. H.; Akaike, T.; Cho, C. S. *Polymer* 2004, 45, 1591-1597.

(22) Metters, A. T.; Anseth, K. S.; Bowman, C. N. *Polymer* 2000, 41, 3993-4004.

(23) Greenwald, R. B.; Choe, Y. H.; McGuire, J.; Conover, C. D. *Adv. Drug Delivery Rev.* 2003, 55, 217-250.

(24) Allmeroth, M.; Moderegger, D.; Gündel, D.; Buchholz, H.-G.; Mohr, N.; Koynov, K.; Rösch, F.; Thews, O.; Zentel, R. *J. Controlled Release* 2013, 172, 77-85.

(25) Lai, T.; Bae, Y.; Yoshida, T.; Kataoka, K.; Kwon, G. *Pharm. Res.* 2010, 27, 2260-2273.

(26) Zhang, Y.; Yin, Q.; Lu, H.; Xia, H.; Lin, Y.; Cheng, J. *ACS Macro Lett.* 2013, 2, 809-813.

(27) Hagan, S. A.; Coombes, A. G. A.; Garnett, M. C.; Dunn, S. E.; Davies, M. C.; Illum, L.; Davis, S. S.; Harding, S. E.; Purkiss, S.; Gellert, P. R. *Langmuir* 1996, 12, 2153-2161.

(28) Lee, J.; Cho, E. C.; Cho, K. *J. Controlled Release* 2004, 94, 323-335.

(29) Singh, V.; Tiwari, M. *Int. J. Polymer. Sci.* 2010, 2010.

(30) Allen, C.; Han, J.; Yu, Y.; Maysinger, D.; Eisenberg, A. *J. Controlled Release* 2000, 63, 275-286.

(31) Gan, Z.; Jim, T. F.; Li, M.; Yuer, Z.; Wang, S.; Wu, C. *Macromolecules* 1999, 32, 590-594.

(32) Storey, R. F.; Sherman, J. W. *Macromolecules* 2002, 35, 1504-1512.

(33) Meier, M. A. R.; Aerts, S. N. H.; Staal, B. B. P.; Rasa, M.; Schubert, U. S. *Macromol. Rapid Commun.* 2005, 26, 1918-1924.

(34) Schubert, S.; Delaney, J. J. T.; Schubert, U. S. *Soft Matter* 2011, 7, 1581-1588.

(35) Giacomelli, C.; Borsali, R. *Macromol. Symp.* 2006, 245-246, 147-153.

(36) Lassalle, V.; Ferreira, M. L. *Macromol. Biosci.* 2007, 7, 767-783.

(37) Giacomelli, F. C.; Stepanek, P.; Schmidt, V.; Jager, E.; Jager, A.; Giacomelli, C. *Nanoscale* 2012, 4, 4504-4514.

(38) Noh, T.; Kook, Y. H.; Park, C.; Youn, H.; Kim, H.; Oh, E. T.; Choi, E. K.; Park, H. J.; Kim, C. *J. Polym. Sci., Part A: Polym. Chem.* 2008, 46, 7321-7331.

(39) Nagasaki, Y.; Yasugi, K.; Yamamoto, Y.; Harada, A.; Kataoka, K. *Biomacromolecules* 2001, 2, 1067-1070.

(40) Dobrovolskaia, M. A.; McNeil, S. E. *Nat. Nanotechnol.* 2007, 2, 469-478.

(41) Richter, A.; Olbrich, C.; Krause, M.; Hoffmann, J.; Kissel, T. *Eur. J. Pharm. Biopharm.* 2010, 75, 80-89.

(42) Oerlemans, C.; Bult, W.; Bos, M.; Storm, G.; Nijsen, J. F.; Hennink, W. *Pharm. Res.* 2010, 27, 2569-2589.

(43) Owen, S. C.; Chan, D. P. Y.; Shoichet, M. S. *Nano Today* 2012, 7, 53-65.

(44) Owens Iii, D. E.; Peppas, N. A. *Int. J. Pharm.* 2006, 307, 93-102.

(45) Hu, Y.; Zhang, L.; Cao, Y.; Ge, H.; Jiang, X.; Yang, C. *Biomacromolecules* 2004, 5, 1756-1762.

(46) Jiang, Z.; Zhu, Z.; Liu, C.; Hu, Y.; Wu, W.; Jiang, X. *Polymer* 2008, 49, 5513-5519.

(47) Shen, C.; Guo, S.; Lu, C. *Polym. Adv. Technol.* 2008, 19, 66-72.

(48) Hu, Y.; Jiang, Z.; Chen, R.; Wu, W.; Jiang, X. *Biomacromolecules* 2010, 11, 481-488.

(49) Nie, T.; Zhao, Y.; Xie, Z.; Wu, C. *Macromolecules* 2003, 36, 8825-8829.

(50) Li, S.; Garreau, H.; Pauvert, B.; McGrath, J.; Toniolo, A.; Vert, M. *Biomacromolecules* 2002, 3, 525-530.

(51) Samarajeewa, S.; Shrestha, R.; Li, Y.; Wooley, K. L. *J. Am. Chem. Soc.* 2011, 134, 1235-1242.

(52) D'Addio, S. M.; Saad, W.; Ansell, S. M.; Squiers, J. J.; Adamson, D. H.; Herrera-Alonso, M.; Wohl, A. R.; Hoye, T. R.; Macosko, C. W.; Mayer, L. D.; Vauthier, C.; Prud'homme, R. K. *J. Controlled Release* 2012, 162, 208-217.

(53) Mu, L.; Elbayoumi, T. A.; Torchilin, V. P. *Int. J. Pharm.* 2005, 306, 142-149.

(54) Rixman, M. A.; Dean, D.; Ortiz, C. *Langmuir* 2003, 19, 9357-9372.

(55) Priya, M. H.; Pratt, L. R.; Paulaitis, M. E. *Langmuir* 2011, 27, 13713-13718.

(56) Asadi, A.; Saboury, A. A.; Moosavi-Movahedi, A. A.; Divsalar, A.; Sarbolouki, M. N. *Int. J. Biol. Macromol.* 2008, 43, 262-270.

(57) Xia, J.; Dubin, P. L.; Kokufuta, E. *Macromolecules* 1993, 26, 6688-6690.

(58) Topchieva, I. N.; Sorokina, E. M.; Efremova, N. V.; Ksenofontov, A. L.; Kurganov, B. I. *Bioconjugate Chem.* 1999, 11, 22-29.

(59) Savić, R.; Azzam, T.; Eisenberg, A.; Maysinger, D. *Langmuir* 2006, 22, 3570-3578.

(60) Cuong, N.-V.; Jiang, J.-L.; Li, Y.-L.; Chen, J.-R.; Jwo, S.-C.; Hsieh, M.-F. *Cancers* 2010, 3, 61-78.

(61) Ge, H.; Hu, Y.; Jiang, X.; Cheng, D.; Yuan, Y.; Bi, H.; Yang, C. *J. Pharm. Sci.* 2002, 91, 1463-1473.

(62) Cuong, N.-V.; Hsieh, M.-F.; Chen, Y.-T.; Liau, I. *J. Appl. Polym. Sci.* 2010, 117, 3694-3703.

(63) Ahmed, F.; Discher, D. E. *J. Controlled Release* 2004, 96, 37-53.

(64) Carstens, M. G.; van Nostrum, C. F.; Verrijk, R.; de Leede, L. G. J.; Crommelin, D. J. A.; Hennink, W. E. *J. Pharm. Sci.* 2008, 97, 506-518.

(65) Shen, C.; Guo, S.; Lu, C. *Polym. Degrad. Stab.* 2007, 92, 1891-1898.

(66) Lam, H.; Gong, X.; Wu, C. *J. Phys. Chem. B* 2007, 111, 1531-1535.

(67) Yang, R.; Meng, F.; Ma, S.; Huang, F.; Liu, H.; Zhong, Z. *Biomacromolecules* 2011, 12, 3047-3055.

(68) Elhasi, S.; Astaneh, R.; Lavasanifar, A. *Eur. J. Pharm. Biopharm.* 2007, 65, 406-413.

(69) Shi, B.; Fang, C.; You, M.; Zhang, Y.; Fu, S.; Pei, Y. *Colloid. Polym. Sci.* 2005, 283, 954-967.

(70) Shuai, X.; Ai, H.; Nasongkla, N.; Kim, S.; Gao, J. *J. Controlled Release* 2004, 98, 415-426.

(71) Letchford, K.; Liggins, R.; Burt, H. *J. Pharm. Sci.* 2008, 97, 1179-1190.

(72) Bae, Y. H.; Yin, H. *J. Controlled Release* 2008, 131, 2-4.

(73) Moghimi, S. M.; Hunter, A. C.; Murray, J. C. *Pharmacol. Rev.* 2001, 53, 283-318.

(74) Shen, Y.; Zhan, Y.; Tang, J.; Xu, P.; Johnson, P. A.; Radosz, M.; Van Kirk, E. A.; Murdoch, W. J. *AlChE J.* 2008, 54, 2979-2989.

(75) Tyrrell, Z. L.; Shen, Y.; Radosz, M. *Macromolecules* 2012, 45, 4809-4817.

CHAPTER 2:

ACID CATALYZED DEGRADATION OF MeO-PEG_{45}-*b*-$PBO_{0,6,9}$-*b*-PCL_{60} MICELLES: INCREASE HYDROLYTIC STABILITY BY ENGINEERING THE HYDROPHILIC-HYDROPHOBIC INTERFACE

2.1 Introduction

Amphiphilic diblock copolymers self-assemble into a variety of supramolecular aggregate structures including core-shell micelles[1-5], filomicelles[6-8] and polymersomes[9-11] that are finding applications as drug and gene delivery systems[12-16]. In particular, micelles formed from block copolymers that contain poly (ethylene glycol) (PEG) and poly (ε-caprolactone) (PCL) segments are widely applied in the design of drug delivery systems because the hydrophilic PEG block is biocompatible and the hydrophobic PCL block is biodegradable[17-21]. The PEG-*b*-PCL block copolymers that were designed for drug delivery have a hydrolytically sensitive ester[22-25] link between the hydrophilic and hydrophobic segments. This ester group is normally located at the aqueous/hydrophobic interface in core-shell micelles and thus is readily accessed for reactions with the aqueous medium. Hydrolysis of the interface ester leads to shedding of the PEG block and destabilization of the micelle[26-29]. When applying PEG-*b*-PCL block copolymer as an oral drug carrier, the acid medium in the stomach catalyzes the hydrolysis of the interface ester and accelerates the shedding of PEG corona to precipitates the micelles. This chapter reports on an initial effort to tune the stability of micelles by moving the hydrolytically accessible ester linkage away from the core-shell interface. This is achieved by inserting a short non-biodegradable hydrophobic segment of poly (1,2-butylene oxide) (PBO) between the PCL core and PEG corona. Our working hypothesis is that the rate of PEG shedding can be retarded by separating the interface between the biodegradable PCL and non-degradable PEG blocks from the hydrophilic-hydrophobic interface and thus extends micelle stability without affecting the self-assembly process (Scheme 2.1).

This chapter reports on the preparation of low polydispersity PEG-*b*-PCL diblock and PEG-*b*-PBO-*b*-PCL triblock polymers that self-assemble into spherical micelles. Kinetics of acid catalyzed hydrolysis of the interface ester groups are shown to occur substantially slower in the triblock copolymer micelles when compared to micelles of the parent diblock copolymer.

Scheme 2.1: Modifying the hydrophilic-hydrophobic interface of PEG-*b*-PCL micelle.

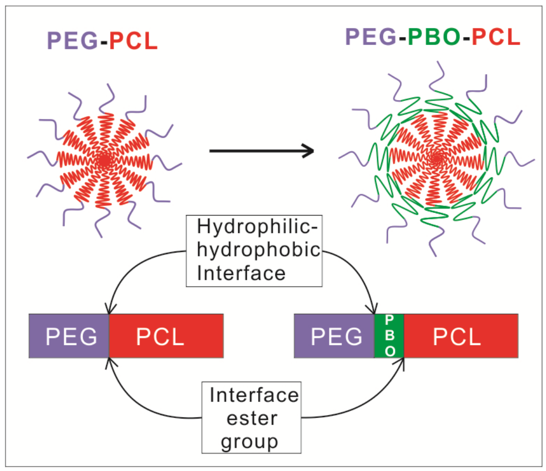

2.2 Results and Discussion

2.2.1 Polymerization kinetic of caprolactone (CL)

A series of parallel caprolactone (CL) polymerization experiments were carried to study the kinetic of CL polymerization. The methoxy terminated poly (ethylene glycol) (MeO-PEG$_{45}$-OH) was used as the macroinitiator for the ring-opening polymerization (ROP) of ε-caprolactone (CL) in the presence of stannous octoate ($Sn(Oct)_2$) as a catalyst[14, 21]. The initial feeding ratio ([CL]:[PEG]=160) and all the other reaction conditions were set constant, but the reaction were terminated at different reaction time. The increase of number average molecular weight (M_n) of PCL and the conversion of CL toward the reaction time are plotted in Figure 2.1. The kinetic result shows that the M_n of PCL is almost linear increasing within the first 10 hours of reaction and ~70% of CL was polymerized at t = 10 h. GPC traces of MeO-PEG$_{45}$-*b*-PCL diblock copolymers obtained from different polymerization time in Figure 2.2 illustrates that early termination of the reaction is able to prepare low polydispersity (PDI) polymers. When the conversion of CL gets high (t = 20 h), the GPC trace for the MeO-PEG$_{45}$-*b*-PCL diblock copolymer becomes broad and not unimodal anymore. It is very possible that side reactions such as chain transfer and polymer chains coupling are dominant when the polymerization reaches to the end. Based up on the CL polymerization kinetic and GPC results, the strategy of making low PDI PEG-*b*-PCL diblock copolymers is to terminate the polymerization of CL when the conversion of CL is less than 70%. Kinetic plot in Figure 2.1 is empirically helpful to estimate the termination time in order to get expected MW of PEG-*b*-PCL diblock copolymer. It was also found that rate of polymerization of CL is highly depends on the amount of $Sn(Oct)_2$, temperature and CL concentration.

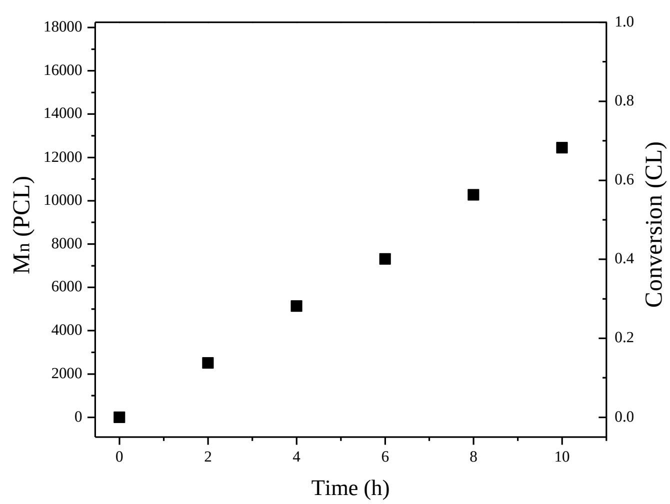

Figure 2.1: The growing of number average molecular weight (M_n) of PCL towards reaction time (t) at a constant feeding ratio ([CL]:[PEG]=160).

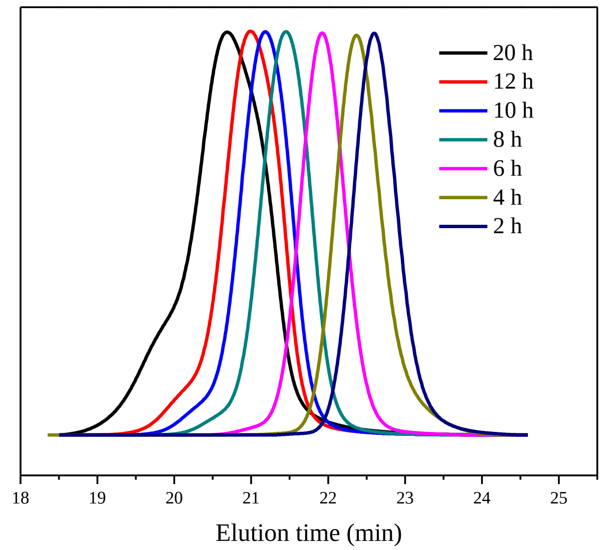

Figure 2.2: GPC traces for the MeO-PEG$_{45}$-*b*-PCL diblock copolymers obtained from different reaction time.

2.2.2 Polymerization kinetic of butylene oxide (BO)

The kinetic of BO polymerization was studied just like the CL polymerization. Synthesis of MeO-PEG$_{45}$-*b*-PBO$_n$-OH diblock copolymer were accomplished by anionic polymerization of 1,2-butylene oxide (BO) with MeO-PEG$_{45}$-OH as a macroinitiator[30-33]. Excess Potassium naphthalenide was used to deprotonate the PEG-OH and to remove moisture in the reaction system. 18-Crown-6-ether was added to trap the potassium ions, increase the rate of polymerization and reduce the side reactions[34-35]. A series of BO polymerization were running at the same initial feeding ratio ([BO]:[PEG]= 30) with different termination times. The increase of M_n of PBO as a function of reaction time was plotted in Figure 2.3. The MW of PBO is almost linearly increasing with time and then it stops growing anymore when the conversion of the BO reaches about 40%. Excess Potassium naphthalenide was used to remove the moisture in the reaction system but the naphthalenide anion was proved to compete initiating the polymerization of BO with

PEG to form the PBO homopolymer. The low MW naphthalene terminated PBO polymer side products were easily washed away during the process of purification of MeO-PEG$_{45}$-*b*-PBO-OH diblock copolymer. GPC traces for the purified MeO-PEG$_{45}$-*b*-PBO$_n$-OH diblock copolymers shows that all the polymers were narrow dispersed (Figure 2.4). According to the polymerization kinetic of BO in Figure 2.3, we are able to make MeO-PEG$_{45}$-*b*-PBO$_n$-OH (n= 6, 9) diblock copolymers with controlled PBO length when we terminating the BO polymerization at certain reaction times.

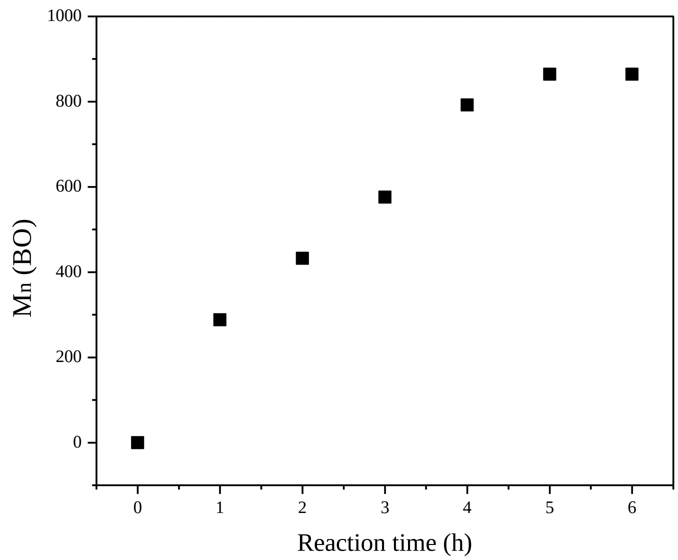

Figure 2.3: The growing of number average molecular weight (M_n) of MeO-PEG$_{45}$-*b*-PBO$_n$ towards reaction time (t) at a constant feeding ratio ([BO]:[PEG]=30).

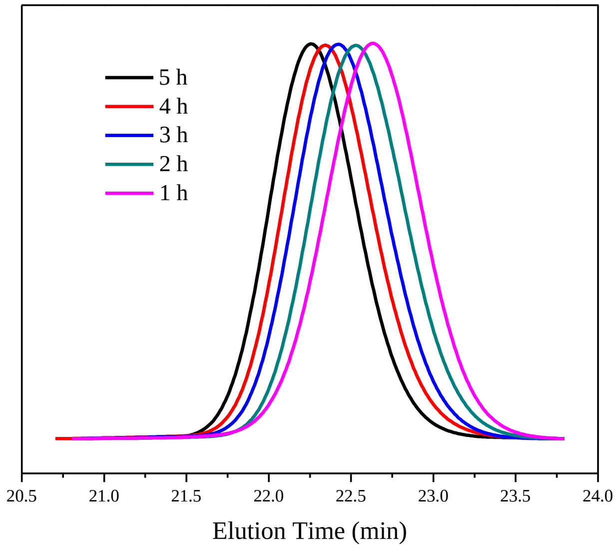

Figure 2.4: GPC traces for the MeO-PEG$_{45}$-*b*-PBO$_n$ diblock copolymers obtained from different reaction times.

2.2.3 Synthesis and characterization of MeO-PEG$_{45}$-*b*-PBO$_n$-*b*-PCL$_{60}$ (n = 0, 6, 9) block copolymers

The block copolymers of MeO-PEG$_{45}$-*b*-PBO$_n$-*b*-PCL$_{60\pm2}$ (n = 0, 6, 9) were synthesized as shown in Scheme 2.2. Molecular weights of the polymers were determined by GPC and ^{1}H NMR analysis (Table 2.1, Figures 2.5-2.8) and the molecular weight distribution was evaluated by GPC (Figure 2.9-2.11). Amphiphilic block copolymer MeO-PEG$_{45}$-*b*-PCL$_{60}$ (PDI = 1.08) was synthesized utilizing methoxy terminated poly (ethylene glycol) as the macroinitiator for the controlled ring-opening polymerization (ROP) of ε-caprolactone (CL) in the presence of stannous octoate (Sn(Oct)$_2$) as a catalyst[14, 21]. The labeled ^{1}H NMR spectrum is shown in Figure 2.5. The degree of polymerization (DP) of CL was evaluated to be 60 by comparing the integration of signals at 3.62 ppm for CH_2 of PEG (labeled b) and triplet at 2.30 ppm for CH_2 of PCL (labeled d). Copolymer was synthesized by terminating the reaction at only moderate CL conversion (36.0 (3.0) %) to ensure narrow molecular weight distributions.

The triblock copolymer of MeO-PEG_{45}-*b*-PBO_9-PCL_{60} (PDI = 1.10) was analogously synthesized by ROP of CL with MeO-PEG_{45}-*b*-PBO_9-OH as macroinitiator and $Sn(Oct)_2$ as catalyst. Synthesis of MeO-PEG_{45}-*b*-PBO_9 (PDI = 1.08) was accomplished by anionic polymerization of 1,2 butylene oxide (BO) with PEG as a macroinitiator[30-33]. The DP of the PBO was determined by comparing the integration of signals at 3.62 ppm for CH_2 of PEG (labeled b) and triplet at 0.93 ppm for CH_3 of BO methyl group (labeled e) (Figures 2.6-2.8). GPC traces from Figures 2.9-2.11 demonstrate that for all the polymers are unimodal and narrow dispersed.

Scheme 2.2: Synthesis of MeO-PEG_{45}-*b*-PCL_{60} and MeO-PEG_{45}-*b*-PBO_9-*b*-PCL_{60} block copolymers

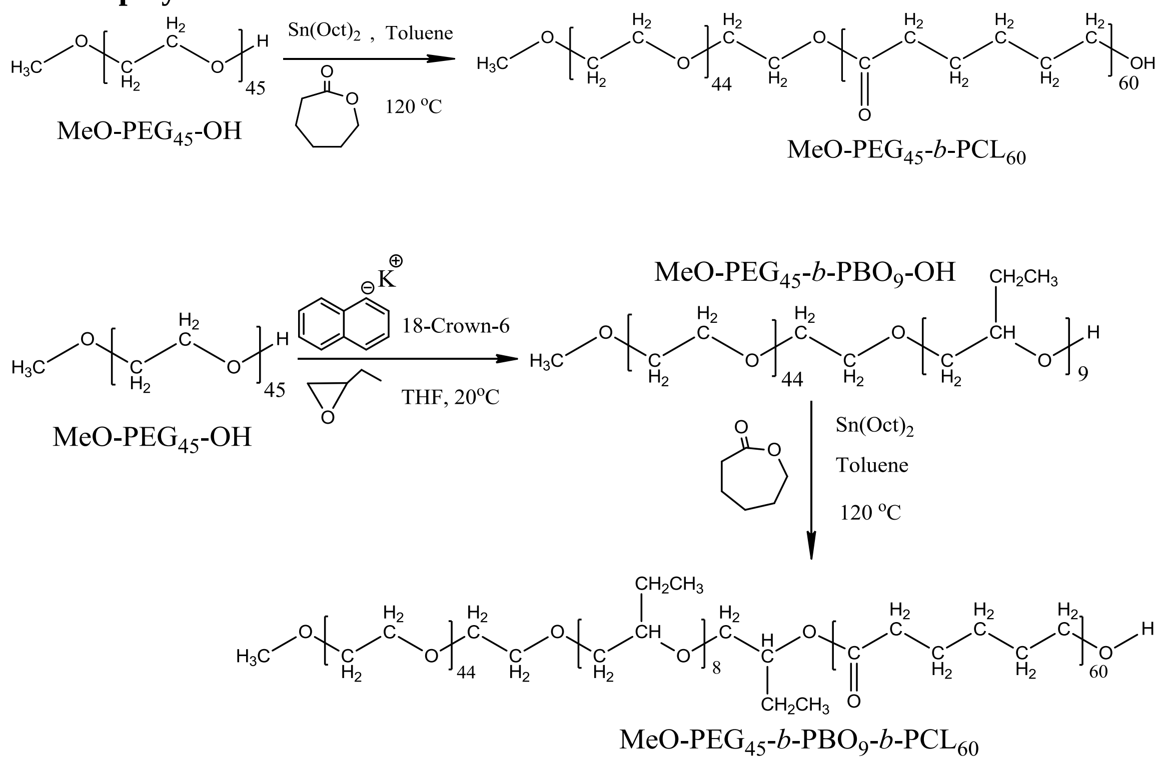

Table 2.1: Synthetic results for MeO-PEG$_{45}$-*b*-PCL$_{60}$ and MeO-PEG$_{45}$-*b*-PBO$_9$-*b*-PCL$_{60}$ block copolymers.

Sample	Mn(theory)[a]	Mn(nmr)[b]	W(PEG)[c]	PDI[d]
MeO-PEG$_{45}$-*b*-PBO$_9$	2830	2650	0.76	1.08
MeO-PEG$_{45}$-*b*-PBO$_9$-*b*-PCL$_{60}$	9260	9610	0.21	1.10
MeO-PEG$_{45}$-*b*-PCL$_{60}$	8600	9080	0.22	1.08

a) Number average molecular weight of block copolymers based on a standard conversion of 36.0(3.0)% for each monomer polymerization. b) Number average molecular weight of block copolymers determined by integration of ^{1}H NMR resonances unique to each segment. c) Weight fraction of PEG in the block copolymers based on the Mn from ^{1}H NMR. d) Polydispersity (M_w/M_n) evaluated by GPC.

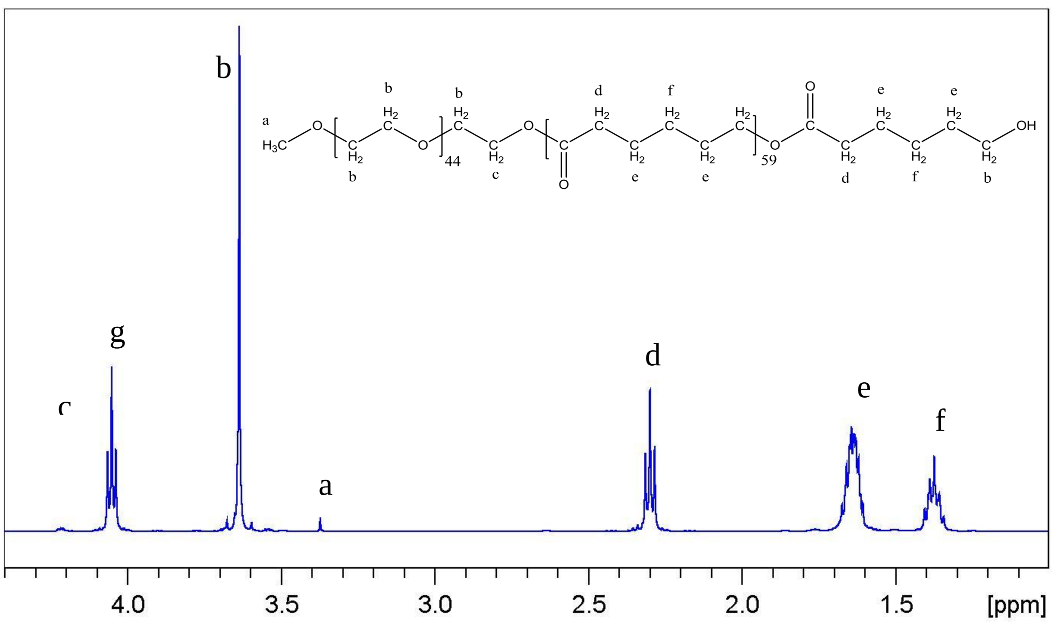

Figure 2.5: ^{1}H NMR spectrum of MeO-PEG$_{45}$-*b*-PCL$_{60}$ diblcok copolymer in $CDCl_3$ and peak assignments.

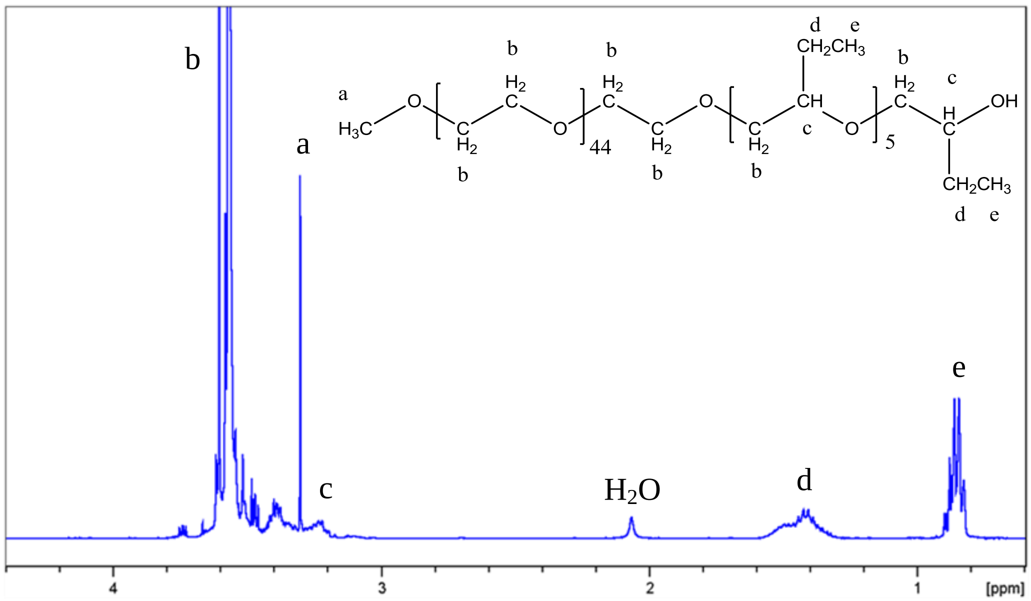

Figure 2.6: [1] H NMR spectrum of MeO-PEG$_{45}$-*b*-PBO$_{6}$ diblock copolymer in CDCl$_{3}$ and peak assignments.

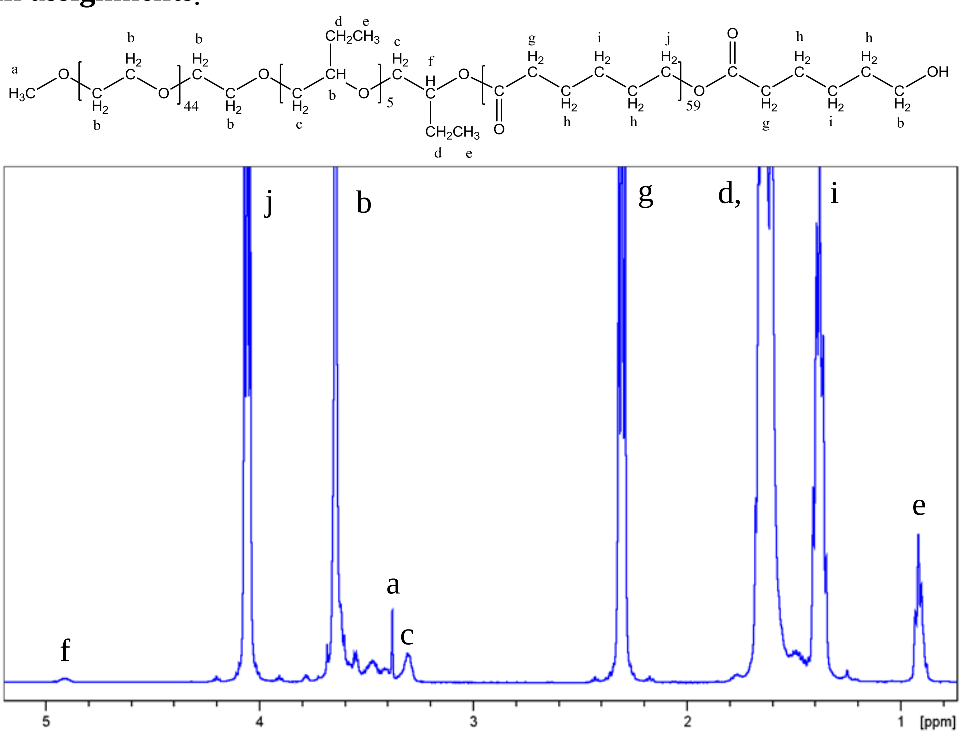

Figure 2.7: [1] H NMR spectrum of MeO-PEG$_{45}$-*b*-PBO$_{6}$-*b*-PCL$_{60}$ triblock copolymer in CDCl$_{3}$ and peak assignments.

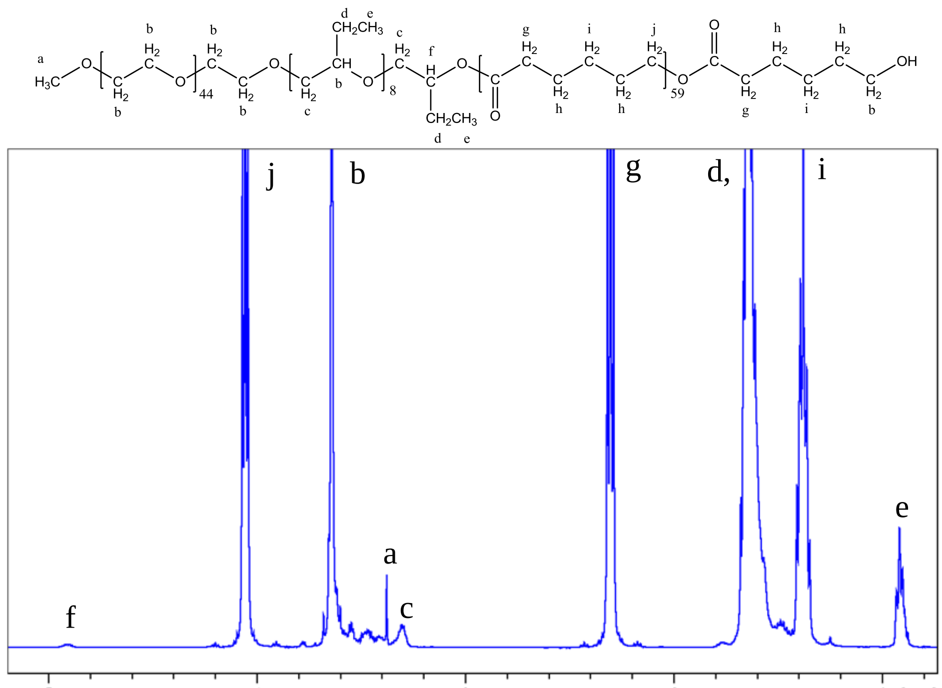

Figure 2.8: ^{1}H NMR spectrum of MeO-PEG$_{45}$-*b*-PBO$_9$-*b*-PCL$_{60}$ triblock copolymer in CDCl$_3$ and peak assignments.

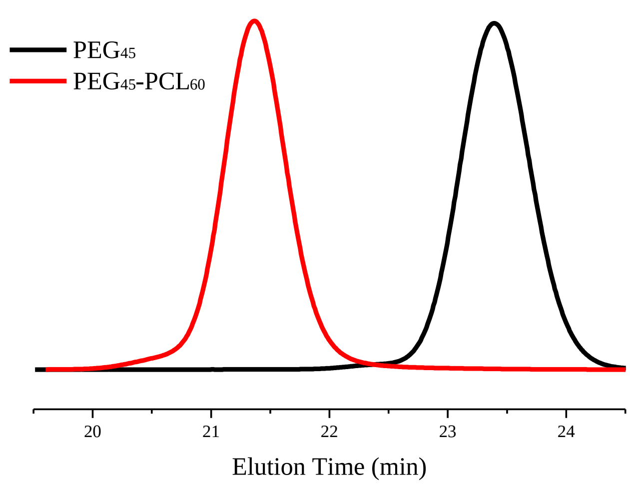

Figure 2.9: GPC traces for MeO-PEG$_{45}$ homopolymer (PDI = 1.06) and MeO-PEG$_{45}$-*b*-PCL$_{60}$ diblock copolymer (PDI=1.08).

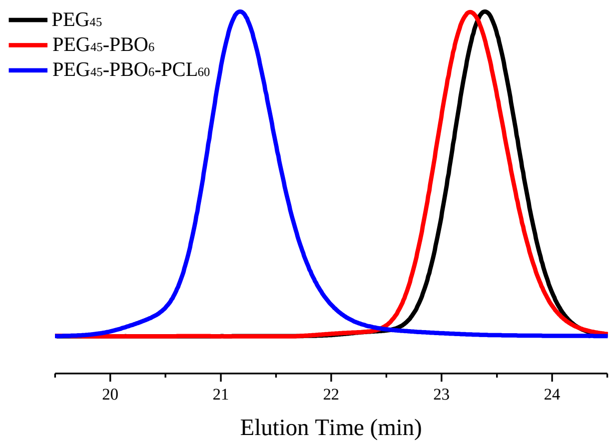

Figure 2.10: GPC traces for MeO-PEG$_{45}$ homopolymer (PDI=1.06), MeO-PEG$_{45}$-*b*-PBO$_9$ (PDI=1.08) and MeO-PEG$_{45}$-*b*-PBO$_6$-*b*-PCL$_{60}$ (PDI = 1.09) block copolymers.

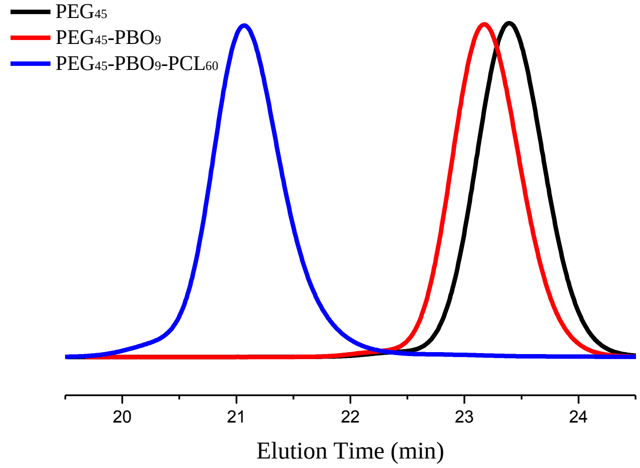

Figure 2.11: GPC traces for MeO-PEG$_{45}$ homopolymer (PDI = 1.06), MeO-PEG$_{45}$-*b*-PBO$_9$ (PDI=1.08) and MeO-PEG$_{45}$-*b*-PBO$_9$-*b*-PCL$_{60}$ (PDI = 1.10) block copolymers.

2.2.4 Formation and characterization of micelles from MeO-PEG$_{45}$-*b*-PBO$_n$-*b*-PCL$_{60}$ (n = 0, 6, 9) block copolymers

Samples of 1.0 mg/mL of PEG$_{45}$-*b*-PBO$_n$-*b*-PCL$_{60\pm2}$ (n = 0, 6, 9) block copolymer micelles were prepared by adding a stock solution of polymer in acetone to water under vigorous stirring[24,36]. Results from dynamic light scattering (DLS) studies for these micelle solutions are shown in Figure 2.12 and Table 2.2. These three low polydispersity block copolymers readily self assemble in aqueous media into well defined narrowly size dispersed 20 $\pm$ 2 nm micelles by the nano-precipitation method[24, 36-38] (pH = 6.8, T = 25 ℃). The slightly larger average size for the triblock copolymer from the DLS is consistent with the larger hydrophobic-hydrophilic ratio. TEM images of the micelles from diblock and triblock copolymers revealed only spherically shaped particles with average sizes comparable to those obtained by DLS (Figure 2.12). Neither DLS nor TEM observations produced evidence for larger particles such as filomicelles[6-8] and polymerosomes[9-11] even at concentrations of polymer higher than the 1.0 mg/ml used in this study. Selective formation of spherical micelles probably results from the strong self assembling property of the PCL hydrophobic core. Both the di and triblock copolymer micelles have similar size and narrow size distributions, which justifies comparing results of acid catalyzed hydrolysis studies. The micelle dispersions formed by slowly adding acetone solutions of polymer to water and the reverse are indistinguishable by DLS. The residual acetone in the micelle suspensions is removed by dialysis against water. The hydrodynamic diameters of the micelles are highly dependent on the conditions and are observed to change from ~20 $\pm$ 2 nm at pH = 6.8, T = 25 ℃ to 30 $\pm$ 2 nm at pH = 7.4, T = 37 ℃ (Table 2.2). The 30 $\pm$ 2 nm micelles form stable dispersions of particles with a mass of 2.0 $\pm$0.5 $\times 10^6$ Da evaluated by Debye plots[39] from light scattering measurements.

Table 2.2: Hydrodynamic diameters for the micelles from MeO-PEG$_{45}$-*b*-PBO$_n$-*b*-PCL$_{60}$ (n = 0, 6, 9) block copolymers at different temperatures and pH.

Micelle Sample	(pH = 6.8, 25℃)	(pH = 7.4, 37℃)
MeO-PEG$_{45}$-*b*-PCL$_{60}$	20 nm	29 nm
MeO-PEG$_{45}$-*b*-PBO$_6$-*b*-PCL$_{60}$	21 nm	31 nm
MeO-PEG$_{45}$-*b*-PBO$_9$-*b*-PCL$_{60}$	22 nm	32 nm

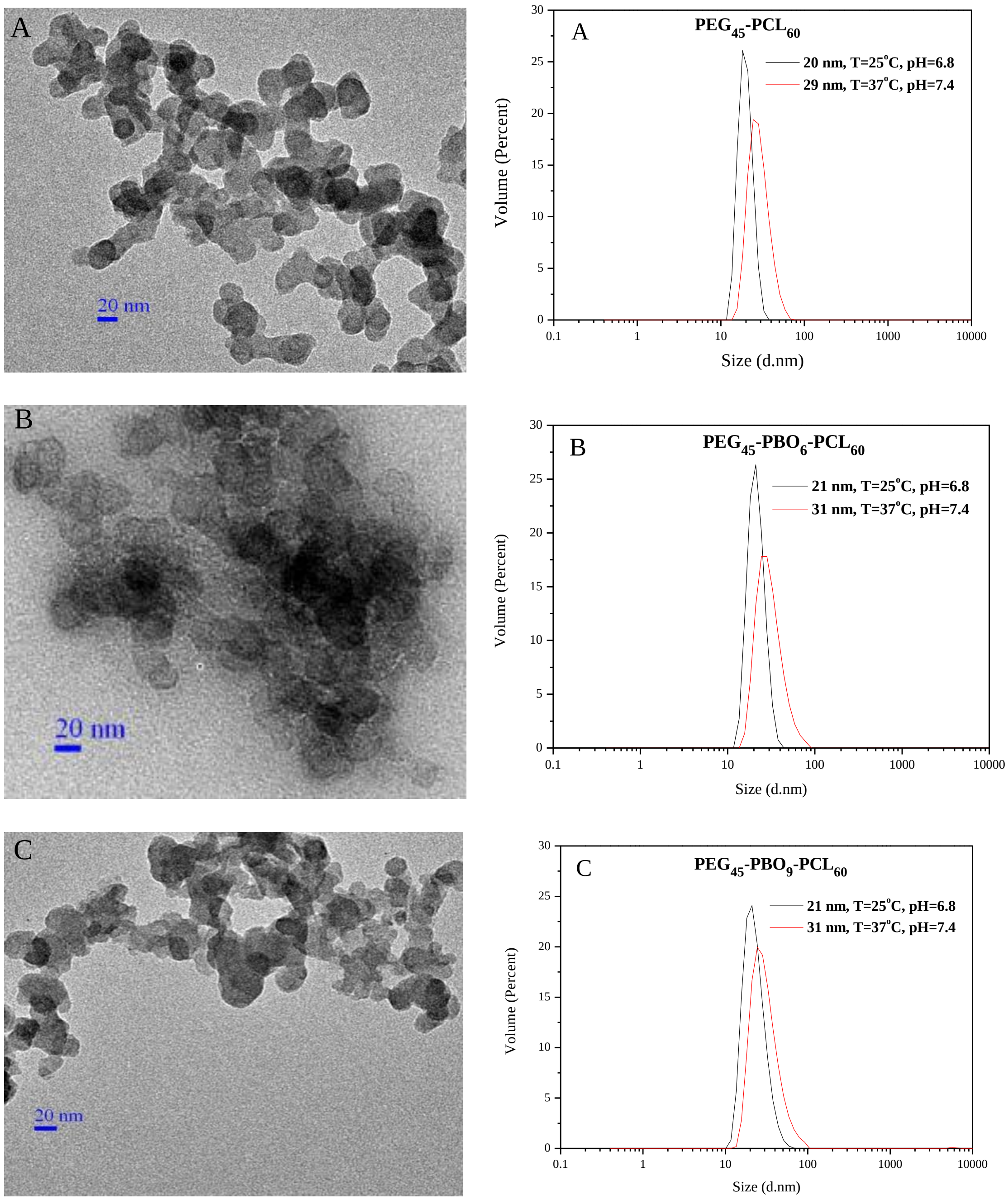

Figure 2.12: TEM and DLS results for micelles from (A) MeO-PEG$_{45}$-*b*-PCL$_{60}$; (B) MeO-PEG$_{45}$-*b*-PBO$_{6}$-*b*-PCL$_{60}$; (C) MeO-PEG$_{45}$-*b*-PBO$_{9}$-*b*-PCL$_{60}$.

2.2.5 Stability of micelles from MeO-PEG$_{45}$-*b*-PBO$_n$-*b*-PCL$_{60}$ (n = 0, 6, 9) block copolymers stored in water for extended periods of time

Dispersions of spherical micelles generated from MeO-PEG$_{45}$-*b*-PBO$_n$-*b*-PCL$_{60}$ (n= 0, 6, 9) block copolymers in HPLC grade water with an initial pH of 6.8 were stored in sealed vials for periods of months at ambient laboratory temperature of 20 ± 2 ℃. Dispersions of PEG$_{45}$-*b*-PCL$_{60}$ diblock copolymer micelles in water over a period of two months showed a slow decrease in the solution pH from 6.8 to 4.5, an increase in the mean micelle hydrodynamic diameter from 20 to 25 nm, and visible white precipitate that are indicative of partial micelle degradation. Increase in the aqueous solution acidity is associated with generation of carboxylic acid groups from ester hydrolysis. Aqueous dispersions of micelles generated from triblock copolymers of PEG$_{45}$-*b*-PBO$_n$-*b*-PCL$_{60}$ (n = 6, 9) manifested constant pH (6.8), stable particle hydrodynamic diameters and no visible precipitation over periods of at least six months and thus are substantially more hydrolytically stable than micelles generated from PEG$_{45}$-*b*-PCL$_{60}$ diblock copolymers.

2.2.6 ^{1}H NMR of micelles from MeO-PEG$_{45}$-*b*-PBO$_n$-*b*-PCL$_{60}$ (n = 0, 6, 9) block copolymers

^{1}H NMR spectra for the 30 ± 2 nm micelles in aqueous PBS buffer dispersions (pH=7.4) are also similar to homogeneous solutions of molecules where the hydrogen resonances for the polymer chains in the micelle dispersions are broadened compared to water soluble small molecules, but all of the resonances are readily observed and fully assigned (Figures 2.13). The line width for the resonance of the more mobile exterior shell PEG units (5.4 Hz) is smaller than the value for the less exposed and less mobile

CH_2 groups for the PCL segment in the micelle core (~10 Hz). The relatively small micelle diameter (30 ± 2 nm) and thermal motions of the polymer chains within the micelles are sufficient to give substantial averaging of the local dipolar magnetic interactions[40]. NMR is usually applied to solution species rather than dispersions of particles in fluid media, but there are precedents where NMR has been used effectively to study dispersions of small particles like liposomes and vesicles[41-43].

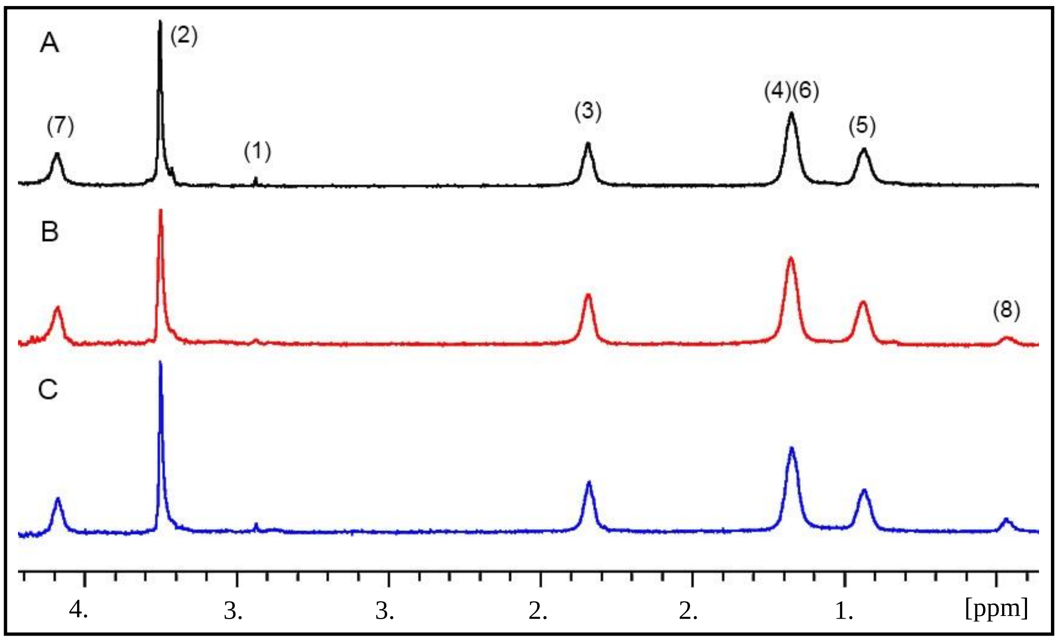

Figure 2.13: Water suppressed ^{1}H NMR spectra of micelles in aqueous PBS buffer at T=37 ^{o}C from PEG$_{45}$-*b*-PBO$_n$-*b*-PCL$_{60}$ (n=0,6,9). ^{1}H NMR assignments for micelle peaks:CH_3(1)O-[CH_2CH_2(2)O]$_{45}$[$CH_2CH(CH_2CH_3$(8))O]$_n$[C(O)CH_2(3)CH_2(4)CH_2(5) CH_2(6)CH_2(7)-O]$_{60}$-OH; δ(1) =3.45 ppm; δ(2) = 3.76 ppm; δ(3) = 2.35 ppm; δ(4,6)= 1.70 ppm ; δ(5) = 1.45 ppm ; δ(7) = 4.12 ppm ; δ(8) = 0.98 ppm.

2.2.7 GPC traces for the products from acid catalyzed degradation of MeO-PEG$_{45}$-*b*-PBO$_n$-*b*-PCL$_{60}$ (n = 0, 9) block copolymers micelles

The hydrolytic degradation of MeO-PEG$_{45}$-*b*-PBO$_n$-*b*-PCL$_{60}$ (n = 0, 9) block copolymer micelles was evaluated in aqueous HCl (pH = 0) at 25 ^oC by terminating the hydrolysis with NaOH at 3.0 h time intervals and extracting the polymeric materials with CH_2Cl_2 for ^1H NMR and GPC studies. GPC traces for the polymer products from degradation of MeO-PEG$_{45}$-*b*-PCL$_{60}$ micelles in water at a series of time intervals are shown in Figure 2.14 (A and B). The GPC results clearly show that the MeO-PEG$_{45}$-*b*-PCL$_{60}$ diblock copolymer is cleaved into two individual polymer units with the low molecular weight peak occurring preciously at the same position as the pure PEG block shown in Figure 2.9. The average molecular weight decreased and the width increased regularly for the MeO-PEG$_{45}$-*b*-PCL$_{60}$ diblock copolymer GPC peak as the relative intensity of peak for PEG increased with the time of degradation.

The ^1H NMR chemical shift of the unique CH_2 group that is connected to the hydrophilic-hydrophobic interface ester group (Scheme 2.3) occurs at 4.23 ppm in the PEG-b-PCL block copolymer and shifts to 3.62 ppm when the interface ester group hydrolyzes and the PEG segment cleaves off. The peak intensity of this special CH_2 group relative to the intensity of the end methyl group of PEG, which is set as constant, was monitored by the time evolution of the ^1H NMR (Figure 2.15). The ^1H NMR peak intensity of the CH_2 group decreases with time as hydrolysis proceeds.

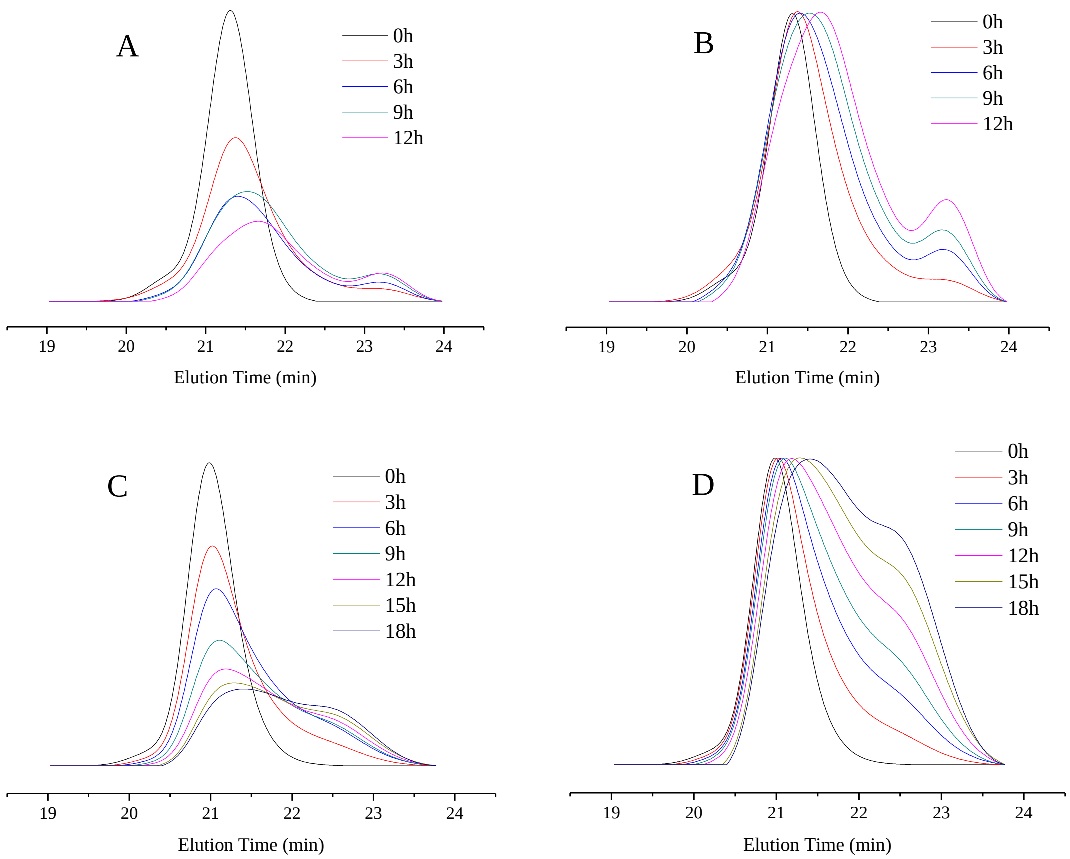

Figure 2.14: GPC traces for degradation products of MeO-PEG$_{45}$-*b*-PCL$_{60}$ micelles before normalization of block copolymer peak (A), after normalization (B), MeO-PEG$_{45}$-*b*-PBO$_9$-*b*-PCL$_{60}$ micelles before normalization (C), after normalization (D).

Scheme 2.3: Hydrolysis of the interface ester groups in spherical micelles

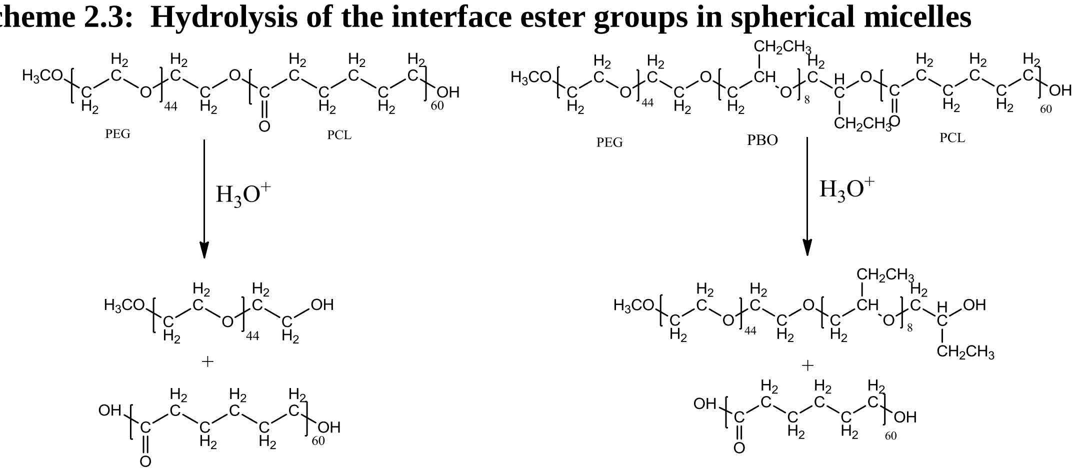

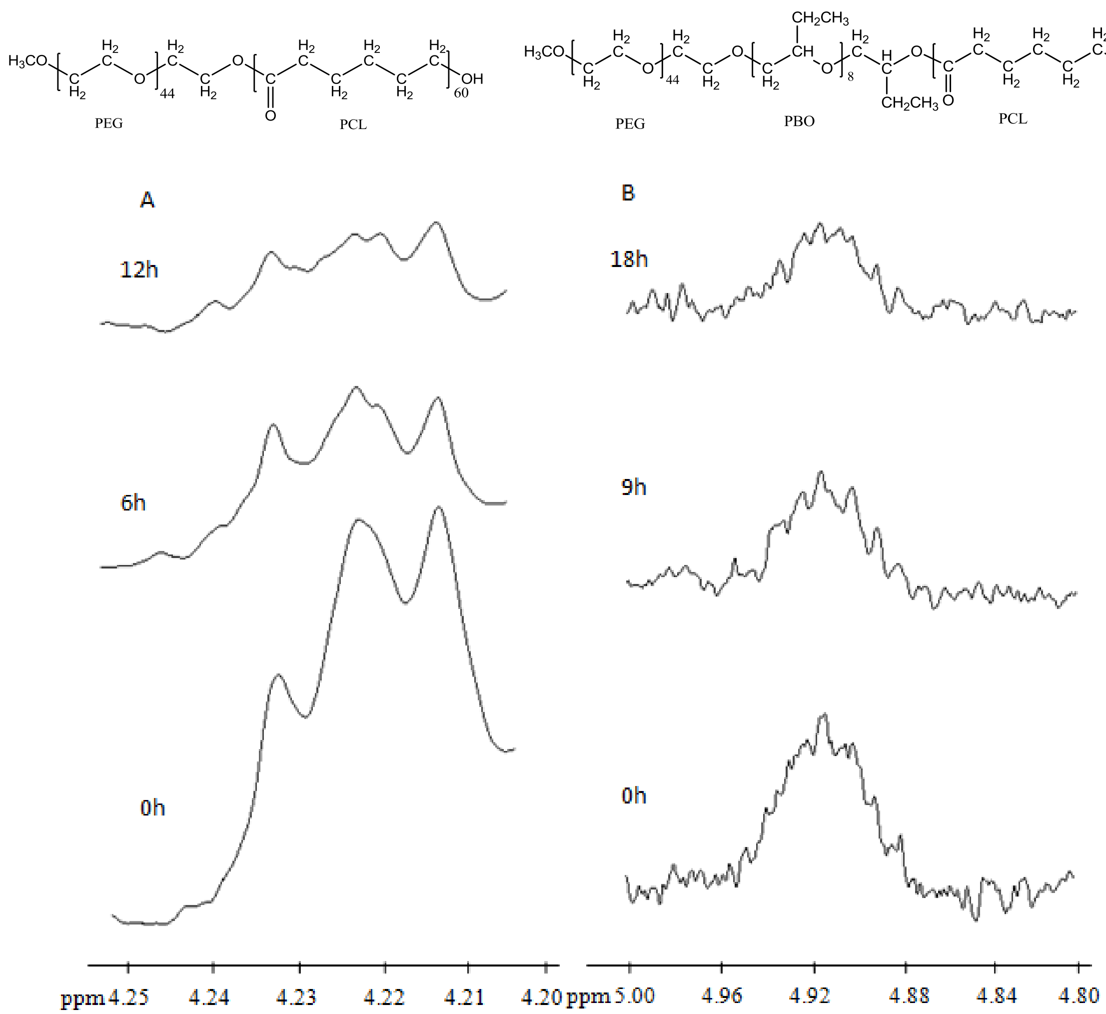

Figure 2.15: [1]H NMR time evolution of CH_2/CH group bonded to ester group at the junction of PEG-PCL (A), PEGPBO-PCL (B). The intensity of end methyl group of PEG is used as a control.

Results from DLS and TEM studies show that diblock copolymers of MeO-PEG$_{45}$-*b*-PCL$_{60}$ self-assemble into narrowly size distributed micelles with a core-shell structure. The hydrophilic corona permits relatively facile access of water to the junction the hydrophilic and hydrophobic polymer segments. The ester group at the hydrophilic-hydrophobic interface is exposed to the aqueous solution for hydrolysis. The initial event for acid catalyzed ester hydrolysis is observed to occur exclusively at the unique interface ester group as shown by appearance of the PEG homopolymer segment on the GPC traces and a decrease of ^1H NMR peak intensity of the CH_2 group that connects to ester group at the junction of the PEG-PCL on ^1H NMR traces. These observations are in agreement with the results of previous hydrolytic degradation studies of PEG-*b*-PCL which concluded that an initial stage of interfacial erosion was followed by bulk degradation in the micellar core[27, 44-46].

Short segments of hydrophobic and hydrolytically stable PBO were inserted between the PEG and PCL blocks as a strategy to tune access of water to the interface ester linkage and thus alter the rate of hydrolysis and ultimately the micelle stability. The working hypothesis is that water can only freely reach the PEG-PBO junction in the triblock copolymer micelles and thus access by water to the ester group at the PBO-PCL interface will be retarded by the insulating PBO segment.

The GPC and ^1H NMR results for the interface ester hydrolysis of the MeO-PEG_{45}-*b*-PBO_9-*b*-PCL_{60} triblock copolymer micelles (Figures 2.14 (C and D), 2.15) are analogous with those for the MeO-PEG_{45}-*b*-PCL_{60} diblock copolymer micelles. The GPC results show that the MeO-PEG_{45}-*b*-PBO_9-*b*-PCL_{60} triblock copolymer micelle is cleaved into two individual polymer units with the low molecular weight peak occurring at the same position as the MeO-PEG_{45}-*b*-PBO_9 block shown in Figure 2.11. The average molecular weight decreased and the width of the distribution increased regularly for the MeO-PEG_{45}-*b*-PBO_9-*b*-PCL_{60} triblock copolymer GPC peak as the relative peak intensity of MeO-PEG_{45}-*b*-PBO_9 increased with the time of hydrolysis.

The time evolution of the ^1H NMR for the triblock copolymer micelle ester hydrolysis products is shown in Figure 2.15 (B). The ^1H NMR intensity of the unique CH group (Scheme 2.3) bonded to the ester group at the PEGPBO-PCL junction decreases with time relative to the end methyl group of PEG as hydrolysis proceeds, which is very similar to results for the MeO-PEG$_{45}$-*b*-PCL$_{60}$ diblock copolymer. However, the rate of the disappearance of the CH ^{1}H NMR resonance resulting from the interface ester hydrolysis for the triblock copolymer micelle proceeds slowly relative to that of the diblock copolymer micelle.

2.2.8 Kinetic comparison of acid catalyzed hydrolysis of ester group at junctions of PEG-PCL and PEGPBO-PCL

Quantitative comparison of the rate for acid catalyzed (pH = 0) hydrolysis of the ester group at the PEG-PCL and PEGPBO-PCL junctions were obtained by following the time evolution of the ^{1}H NMR. First order kinetic plots for the intact di and triblock copolymers as a function of time are shown in Figure 2.16. The kinetic plots demonstrate that the rate of interface ester hydrolysis for the MeO-PEG$_{45}$-*b*-PCL$_{60}$ diblock copolymer micelles (0.11 h^{-1}) is faster than that of the MeO-PEG$_{45}$-*b*-PBO$_9$-*b*-PCL$_{60}$ triblock copolymer micelles (0.041 h^{-1}). The half life of the interface ester for diblock copolymer micelles is 6.3 h compared to a 16.9 h half life for triblock copolymer micelles. Insertion of a short hydrophobic PBO segment between PEG and PCL is thus observed to provide increased kinetic stability for the MeO-PEG-*b*-PBO-*b*-PCL triblock copolymer micelles relative to the MeO-PEG-*b*-PCL diblock copolymer micelles.

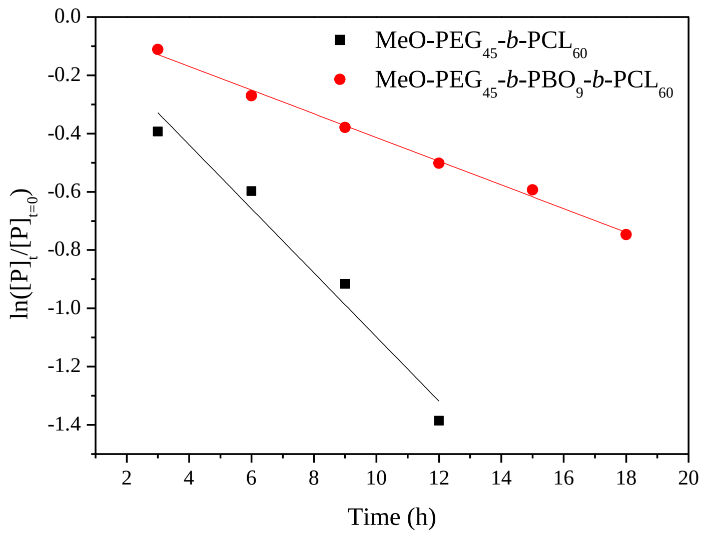

Figure 2.16: First order kinetic plots for the acid catalyzed hydrolysis of interface ester groups that occur at the PEG-PCL and PEGPBO-PCL junctions. $[P]_t$ is defined as the relative molar concentration of the intact block copolymer at time t.

2.2.9 Kinetics of acid catalyzed ester hydrolysis for micelles generated from PEG_{45}-*b*-PBO_n-*b*-PCL_{60} (n = 0, 6, 9) block copolymers

^{1}H NMR was used to follow changes of the micelle compositions and appearance of water soluble species during the acid catalyzed hydrolysis of MeO-PEG_{45}-*b*-PBO_n-*b*-PCL_{60} (n = 0, 6, 9) micelle dispersions (pH = 0.3, 37 ℃). The hydrogen resonances for the polymer chains in the micelle dispersions are broadened compared to water soluble small molecules generated from the acid catalyzed hydrolysis, but all of the resonances are readily observed and assigned (Figures 2.17-2.18). ^{1}H NMR for dispersions of micelles from MeO-PEG_{45}-*b*-PBO_9-*b*-PCL_{60} at time zero and after 25 hours of reaction in 0.5 M aqueous HCl at 37 ℃ shows the appearance of MeO-PEG_{45}-*b*-PBO_9-OH and 6-hydroxycaproic acid ($HO(CH_2)_5CO_2H$) (Figure 2.17).

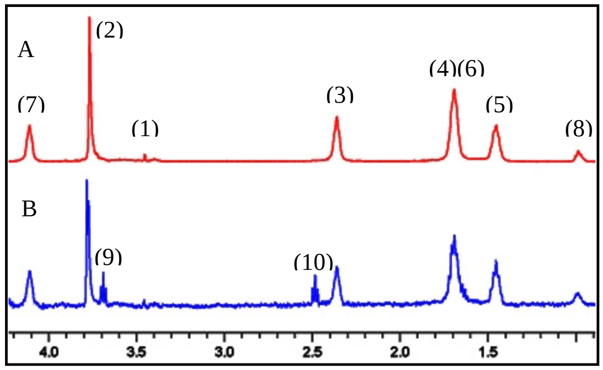

Figure 2.17: Comparison of ^{1}H NMR for PEG$_{45}$-*b*-PBO$_9$-*b*-PCL$_{60}$ micelle (0.75 mg/mL) (A) before the acid catalyzed degradation (B) after addition of HCl at a concentration of 0.5 M (pH = 0.3), T=37 ℃ and a reaction time of 25 hours. ^{1}H NMR peak assignments for PEG$_{45}$-*b*-PBO$_9$-*b*-PCL$_{60}$ micelle in water: CH_3(1)O-[CH_2CH_2(2)-O]$_{45}$[CH_2CH(CH_2CH_3(8))-O]$_9$[C(O)CH_2(3)CH_2(4)CH_2(5)CH_2(6)CH_2(7) -O]$_{60}$-OH, the chemical shifts in ppm for each assignment are as follow: δ(1)=3.45; δ(2)=3.76; δ(3)=2.35; δ(4,6)=1.70; δ(5)=1.45; δ(7)=4.12; δ(8)=0.98; (9) -*CH_2*-OH hydrogens from 6-hydroxycaproic acid (δ=3.68); (10) -*CH_2*-COOH hydrogens from 6-hydroxycaproic acid (δ=2.47).

Time evolution of the ^{1}H NMR spectra during the acid catalyzed ester hydrolysis for dispersions of micelles generated from MeO-PEG$_{45}$-*b*-PCL$_{60}$ and MeO-PEG$_{45}$-*b*-PBO$_9$-*b*-PCL$_{60}$ at pH = 0.3 and T = 37 ℃ is shown in Figure 2.18. Prior studies of hydrolysis reactions of related micelles were reported to give the first hydrolysis event in the vicinity of the interface ester, which results in detaching a hydrophilic polymer from the corona and subsequent hydrolysis of polyester PCL core[27, 44, 46-47]. The results of the current study corroborate this sequence of hydrolysis events and provide quantitative details on the micelle and solution compositions as a function of time and the rates for the interface ester hydrolysis (Figures 2.17-2.22). The initial acid catalyzed ester hydrolysis event in each of the micelles is shown to occur exclusively at the interface ester group that joins the hydrophilic PEG$_{45}$ and the hydrophobic polyester PCL$_{60}$ blocks as evidenced by appearance in the ^{1}H NMR resonances of only MeO-PEG$_{45}$-OH, and MeO-PEG$_{45}$-*b*-PBO$_9$-OH water soluble fragments (Figure 2.18, peaks 2 and 7). ^{1}H NMR observations of the CH$_2$ and CH groups attached to the interface ester groups in the di and triblock copolymers also show that the initial hydrolysis events selectively occur at the junction of PEG and PCL segment[48].

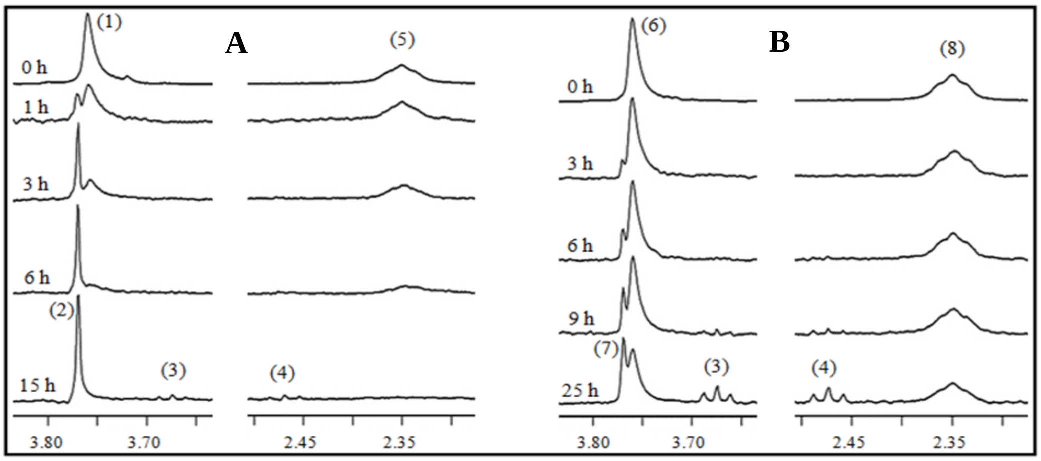

Figure 2.18: ^{1}H NMR for acid catalyzed degradation of block copolymer micelles (0.75 mg/mL) from (A) PEG$_{45}$-*b*-PCL$_{60}$ during a reaction time of 15 hours (B) PEG$_{45}$-*b*-PBO$_9$-*b*-PCL$_{60}$ during a reaction time of 25 hours with HCl concentration of 0.5 M (pH=0.3), T = 37 ℃. ^{1}H NMR peak assignments (in ppm): (1) PEG$_{45}$ segment in PEG$_{45}$-*b*-PCL$_{60}$ micelle (δ=3.76); (2) PEG$_{45}$ segment in aqueous solution after shedding from the PEG$_{45}$-*b*-PCL$_{60}$ micelle (δ=3.77); (3) -*CH$_2$*-OH hydrogens from 6-hydroxycaproic acid (δ=3.68); (4) -*CH$_2$*-COOH hydrogens from 6-hydroxycaproic acid (δ=2.47); (5) Ester -*CH$_2$*-C(O)O- hydrogens of PEG$_{45}$-*b*-PCL$_{60}$ micelles (δ=2.35); (6) PEG$_{45}$-*b*-PBO$_9$ segment in PEG$_{45}$-*b*-PBO$_9$-*b*-PCL$_{60}$ micelles (δ=3.76); (7) PEG$_{45}$-*b*-PBO$_9$ segment in aqueous solution after shedding from the PEG$_{45}$-*b*-PBO$_9$-*b*-PCL$_{60}$ micelles (δ=3.77); (8) Ester -*CH$_2$*-C(O)O- hydrogens of PEG$_{45}$-*b*-PBO$_9$-*b*-PCL$_{60}$ micelles(δ=2.35).

Hydrolysis and shedding of the MeO-PEG$_{45}$-OH block into solution from the diblock MeO-PEG$_{45}$-*b*-PCL$_{60}$ copolymer micelle is much faster than the shedding of the MeO-PEG$_{45}$-*b*-PBO$_n$-OH unit by the triblock MeO-PEG$_{45}$-*b*-PBO$_n$-*b*-PCL$_{60}$ (n = 6, 9) copolymer micelles (Figures 2.18, 2.19). Dissociation of the hydrophilic MeO-PEG$_{45}$-OH corona from MeO-PEG$_{45}$-*b*-PCL$_{60}$ diblock copolymer micelles destabilizes the micelle dispersions. Particle precipitation begins to occur for MeO-PEG$_{45}$-*b*-PCL$_{60}$ diblock copolymer micelles after 4 hours of the hydrolytic degradation reaction which contrasts with the absence of precipitation over periods of days for the MeO-PEG$_{45}$-*b*-PBO$_n$-*b*-PCL$_{60}$ (n = 6, 9) triblock copolymer micelles (pH = 0.3, 37 ℃). A much larger fraction of the PEG units is retained in the micelles generated from the triblock copolymers of MeO-PEG$_{45}$-*b*-PBO$_n$-*b*-PCL$_{60}$ (n = 6, 9) as a function of time during acid catalyzed hydrolysis than for micelles generated from MeO-PEG$_{45}$-*b*-PCL$_{60}$ diblock copolymers at the same conditions (Figure 2.19). Changing the length of the PBO block from 6 to 9 units does not have a large effect on hydrolytic stability of the micelles (Figure 2.19).

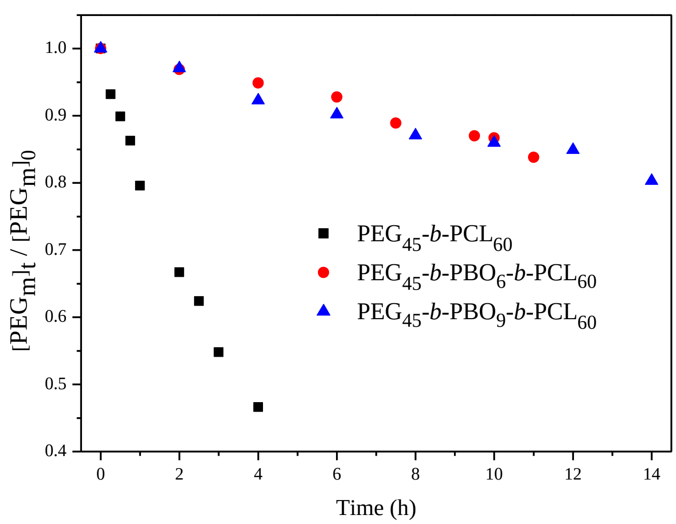

Figure 2.19: Fraction of the PEG units retained in the micelle as a function of time during the acid catalyzed hydrolysis of the interface esters for micelles from PEG$_{45}$-*b*-PBO$_n$-*b*-PCL$_{60}$ (n = 0, 6, 9) at pH = 0.3 and T=37 ℃. [PEG$_m$] is defined as the concentration of the PEG segment that remains in the micelle.

The HO-PCL$_{60}$-CO_2H homo-polymer chains that are produced by hydrolysis of the interface ester group are shown experimentally to remain in the hydrophobic PCL micelle core by the constant ^1H NMR areas for the micelle PCL CH_2 resonances (δ = 2.35 ppm) during the early reaction period. Subsequent slow acid catalyzed hydrolysis of the PCL_{60} segments exclusively produce 6-hydroxycaproic acid ($HO(CH_2)_5CO_2H$) which suggests that the ester hydrolysis gradually advances inward from the terminal PCL ester groups on the surface of the micelle core. The rates of 6-hydroxycaproic acid formation by micelles from MeO-PEG_{45}-*b*-PBO_n-*b*-PCL_{60} (n = 6, 9) are comparable (Figure 2.20). Relatively little 6-hydroxycaproic acid is seen in the PEG_{45}-*b*-PCL_{60} diblock copolymer micelle dispersions because of the early precipitation. The compositions of the micelles are changing regularly as the interface ester hydrolysis and shedding of the corona occurs. Integration of the ^{1}H NMR shows that the ratio of the PEG (δ = 3.76 ppm) to that of PCL (δ = 2.35 ppm) segments in the micelles decreases regularly as the water soluble fragments (MeO-PEG_{45}-*b*-PBO_n-OH (n = 0, 6, 9)) escape into aqueous solution and the PCL homo-polymer remains in the hydrophobic core (Figure 2.18). The di and triblock copolymer micelles can lose about 40-50% of the hydrophilic corona PEG and PEG-PBO units before observable turbidity occurs followed by micelle precipitation.

Detachment of MeO-PEG_{45}-*b*-PBO_n-OH (n = 0, 6, 9) from the micelle corona and retention of HO-PCL_{60}-CO_2H polymer units in the core results in an increasing rate of PCL hydrolysis. The appearance of 6-hydroxycaproic acid became detectable by ^{1}H NMR when more than 10 % of the MeO-PEG-*b*-PBO_n-OH (n = 6, 9) from was dissociated from the micelles and the rate for release of 6-hydroxycaproic acid into solution accelerated as additional PEG units were shed from the micelles (Figures 2.19, 2.20).

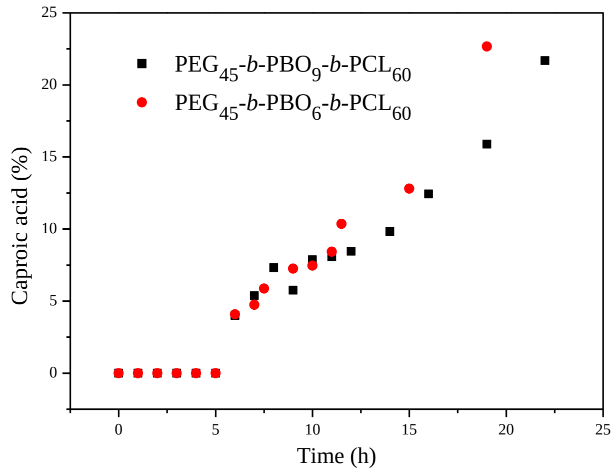

Figure 2.20: Fraction of ε-caprolactone (CL) units in PCL segments that have been converted to 6-hydroxycaproic acid as a function of time in the acid catalyzed hydrolysis of PEG_{45}-*b*-PBO_n-*b*-PCL_{60} (n = 6, 9) triblock copolymer micelles at pH=0.3 and T=37 ℃.

The GPC traces for the products from acid catalyzed hydrolysis of micelles generated from MeO-PEG_{45}-*b*-PBO_6-*b*-PCL_{60} that were freeze dried and dissolved in DMF are shown in Figure5. The changes in the GPC traces with time show that the MeO-PEG_{45}-*b*-PBO_6-*b*-PCL_{60} triblock copolymer concentration decreases as MeO-PEG_{45}-*b*-PBO_6 segment that result from hydrolysis increase. The 6-hydroxycaproic acid GPC peak begins to appear after about 10-15 % of the corona is shed and then increases regularly with time. There are no PCL oligomers other than 6-hydroxycaproic acid observed in the GPC traces during a period of 23 hours of reaction time (Figure 2.21). The GPC results shown in Figure 2.21 are fully consistent with the species observed in the ^1H NMR (Figure 2.18).

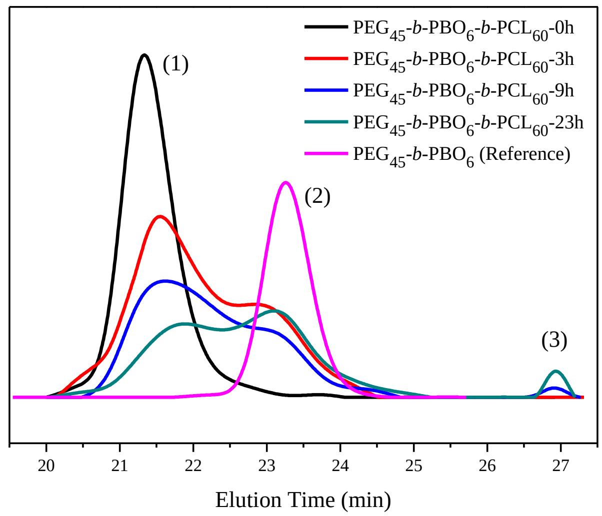

Figure 2.21: GPC traces for PEG$_{45}$-*b*-PBO$_6$-*b*-PCL$_{60}$ micelles as a function of time in 0.5 M aqueous HCl (pH = 0.3; 37 ℃); GPC peak assignments: (1) PEG$_{45}$-*b*-PBO$_6$-*b*-PCL$_{60}$; (2) PEG$_{45}$-*b*-PBO$_6$ used as an external reference; (3) 6-hydroxycaproic acid.

Acid catalyzed hydrolysis of the interface ester groups in dispersions of micelles generated from MeO-PEG$_{45}$-*b*-PBO$_n$-*b*-PCL$_{60}$ (n = 0, 6, 9) results in severing PEG segments (PEG$_{45}$, PEG$_{45}$-*b*-PBO$_n$ (n = 6, 9)) which enter the aqueous solution. Integration of the ^{1}H NMR for the broadened micelle PEG$_{45}$ resonances (δ = 3.76 ppm) as a function of time is used to evaluate the kinetics for hydrolysis of the interface ester groups for micelle dispersions from MeO-PEG$_{45}$-*b*-PBO$_n$-*b*-PCL$_{60}$ (n = 0, 6, 9) (pH = 0.3 and T = 37℃). Linear first order rate plots are obtained for hydrolysis of the interface ester groups in all three block copolymer micelles (Figure 2.22). The rate at which the interface ester is hydrolyzed and PEG$_{45}$ units enter solution for the diblock polymer micelle is 12 times faster than the near equal rates of hydrolysis for the PEG$_{45}$-*b*-PBO$_n$-*b*-PCL$_{60}$ (n = 6, 9) triblock polymer micelles (Figure 2.22).

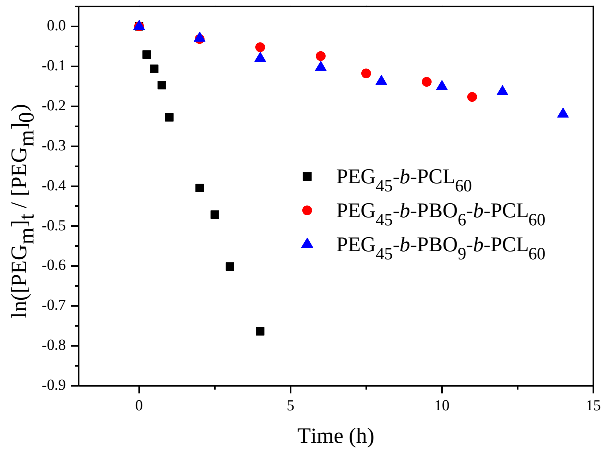

Figure 2.22: First order rate plots for hydrolysis of the interface ester and PEG_{45} segments entering solution at pH = 0.3 and T = 37 ℃: PEG_{45}-*b*-PCL_{60} diblock polymer micelle (slope = - 0.18 h^{-1}); PEG_{45}-*b*-PBO_n-*b*-PCL_{60} (n = 6, 9) triblock polymer micelle (slope = - 0.015 h^{-1}). [PEG_m] is defined as the concentration of the PEG segment that remains in the micelle.

2.3 Summary

Kinetics of polymerization of caprolactone and 1,2-butylene oxide were studied, followed by the synthesis of a set of narrow polydispersity MeO-PEG_{45}-*b*-PBO_n-*b*-PCL_{60} (n = 0, 6, 9) block copolymers for comparative studies of micelle formation and relative stability in aqueous media. Block copolymers that were characterized by ^{1}H NMR and GPC were self-assembled in water by nano-precipitation from organic solvents. DLS results indicate that both polymers form near quantitative yields of micelles that are shown to be spherical by TEM. Insertion of a relatively short hydrophobic PBO chain between the hydrolyzable hydrophobic polyester (PCL) core and the non-hydrolyzable hydrophilic (PEG) corona was designed to move the water-micelle interface away from the PCL core and increase the barrier for water to reach the PCL esters (Scheme 2.1). Micelles generated from triblock copolymers of MeO-PEG_{45}-*b*-PBO_n-*b*-PCL_{60} (n = 6, 9) thus are substantially more hydrolytically stable than micelles generated from MeO-

PEG_{45}-*b*-PCL_{60} diblock copolymers in aqueous solution at room temperature. ^{1}H NMR and GPC were used to evaluate the micelle and solution compositions, determine the kinetics of diblock and triblock copolymer micelle degradation and advance the mechanistic understanding for the acid catalyzed micelle degradation processes. The initial step in acid catalyzed degradation involves the selective hydrolysis of the interface ester groups that connect the hydrophobic PCL segment to the hydrophilic PEG and PEG-*b*-PBO blocks. Subsequent slow acid catalyzed hydrolysis of the PCL_{60} core exclusively generate 6-hydroxycaproic acid which indicates that the ester hydrolysis gradually advances inward from the terminal PCL ester groups at the junction of PEG-PCL or PEGPBO-PCL. Cleavage of the hydrophilic MeO-PEG_{45}-OH corona from MeO-PEG_{45}-*b*-PCL_{60} diblock copolymer micelles destabilizes the micelle dispersions. The di and triblock copolymer micelle solutions become cloudy followed the micelle precipitation after about 40-50% of hydrophilic PEG or PEG-PBO corona is shed. Linear first order rate plots for hydrolysis of the interface ester groups in all three block copolymer micelles from MeO-PEG_{45}-*b*-PBO_{n}-*b*-PCL_{60} (n =0, 6, 9). The rate at which the PEG_{45} units enter solution and interface ester group is hydrolyzed for the MeO-PEG_{45}-*b*-PCL_{60} micelle is much faster than the near equal rates of hydrolysis for the MeO-PEG_{45}-*b*-PBO_{n}-*b*-PCL_{60} (n = 6, 9) triblock polymer micelles. The observed substantial decrease in the rate of acid catalyzed interfacial ester hydrolysis represents an experimental fulfillment of obtaining an increased barrier for water to reach the interfacial ester position in triblock MeO-PEG_{45}-*b*-$PBO_{6,9}$-*b*-PCL_{60} compared to MeO-PEG_{45}-*b*-PCL_{60} diblock copolymer micelles. These robust and easily prepared triblock copolymer micelles have potential utility in applications on drug delivery systems.

2.4 Experimental Section

2.4.1 Materials

Methoxy poly (ethylene glycol) (PEG, Mn = 2000, PDI = 1.06, Sigma Aldrich) was purified by precipitation from petroleum ether prior to use. ε-Caprolactone (CL) (99%, TCI America) and 1,2-butylene Oxide (BO) (Sigma Aldrich) were dried over CaH_2 and distilled prior to use. Phosphate buffered saline tablet, 18-Crown-6-ether and Stannous Octoate ($Sn(Oct)_2$) were used as received from Sigma Aldrich. Potassium naphthalenide THF solution (0.89 M) was prepared by mixing of naphthalene (3.0 g), potassium (0.92 g) and THF (26 mL) in a flask. Concentrated hydrochloric acid (12 M, Fisher scientific) was used as received. SnakeSkin Dialysis tubing (10K MWCO, 35mm dry I.D., 35 feet) was used for dialysis of aqueous media containing polymer micelles. Deuterated solvents were purchased from Cambridge Isotope Laboratories, Inc.. Acetone, toluene, petroleum ether, dichloromethane and methanol were use as received from J.T. Baker and dimethylformamide (DMF, HPLC grade, 99.7% +, Alfa Aesar) was used as the GPC eluent.

2.4.2 Analytical techniques

^{1}H NMR spectra were obtained using Bruker 500 MHz spectrometer with $CDCl_3$ and D_2O as NMR solvent media. ^{1}H NMR data were analyzed by using the Bruker Topspin 2.1 software. Water suppressed ^{1}H NMR spectra of block copolymer micelles in buffer solutions containing 10% of D_2O were acquired using presaturation of water with 50 dB attenuation. The ^{1}H NMR covered a spectral window of -5.0 ppm to 15.0 ppm. The excitation relaxation delay was set to 5 s. Each NMR spectrum was collected from accumulation of 24 scans.

Gel permeation chromatography (GPC) measurements were carried out using a Shimadzu LC-20AV liquid chromatography system equipped with three linear PolarGel-M 300×7.5 mm columns, a RID-10A differential refractive index detector and a SPD-20AV UV/VIS detector. Data were analyzed by Shimadzu LCsolution software. DMF was used as the eluent at a flow rate of 1.0 mL/min at 50 ℃. Molecular weight calibrations were based on narrow peak width polystyrene standards from Polymer Laboratories.

Dynamic Light Scattering (DLS). Hydrodynamic diameters of micelles were measured by a Zetasizer Nano ZS (Malvern Instruments, Westborough, MA) at 25 ℃/ 37 ℃, using 1 cm polystyrene sample cuvettes. The mean diameters were obtained by use of the DTS software using the volume measurements.

Transmission Electron Microscope (TEM). Micelle morphology was evaluated by JOEL JEM-1400 TEM operating at an acceleration voltage of 80 kV. One drop of the micelle solution (1.0 mg/mL) was placed on the ultrathin carbon type-A 400 mesh copper grid (Ted Pella Inc., Redding, CA), and the droplet was then blotted and allowed to evaporate under ambient conditions overnight before analysis[49-50]. The average diameters of the spherical micelles were evaluated by Digital Micrograph software (Gatan Inc.).

2.4.3 Procedures for MeO-PEG$_{45}$-*b*-PBO$_n$-*b*-PCL$_{60}$ (n = 0, 6, 9) block copolymer synthesis and micelle formation

Synthesis of MeO-PEG$_{45}$-*b*-PBO$_n$-OH (n = 6, 9) diblock copolymers: Dried MeO-PEG$_{45}$-OH (8.0 g, 4.0 mmol) and 18-Crown-6-ether (1.5 g, 5.7 mmol) were dissolved in 80 mL of anhydrous THF in a 250 mL dry flask under inert atmosphere. Potassium naphthalenide (9.0 mL, 0.89 M in THF) was added into the solution via syringe. After stirring the mixture for 15 mins while the dark green color persisted, BO (10 mL, 0.12 mol) was added into the reaction mixture via syringe. The solution was stirred at room temperature for 40 min to make 6 BO units and 1 h to make 9 BO units, and the reaction was terminated by the adding of HCl (0.80 mL, 12 M) drop by drop and the green solution became colorless again. The undissolved inorganic salt was removed by filtration and the MeO-PEG-*b*-PBO-OH block copolymer was precipitated from petroleum ether. The white precipitates were recovered by filtration, redissolved in toluene and precipitated from the petroleum ether again. The precipitates were collected and dried under vacuum at 40 ℃ for 48 h.

Synthesis of MeO-PEG$_{45}$-*b*-PBO$_n$-*b*-PCL$_{60}$-OH (n = 0, 6, 9) block copolymers: Dried MeO-PEG$_{45}$-*b*-PBO$_9$-OH (0.90 g, 0.34 mmol) was dissolved in dry toluene (16 mL) in a 50 mL dry flask under inert atmosphere. Caprolactone (6.0 mL, 0.054mol) and Sn(Oct)$_2$ (0.02 g) were added into the solution via syringe. The reaction mixture was gently refluxed under nitrogen atmosphere at 120 ℃. After stirring the solution for 5 h, excess cold methanol was poured into the solution to terminate and precipitate the product. The white precipitate was collected by filtration, redissolved in dichloromethane and precipitated from the methanol again. The precipitate was collected and dried under vacuum at 40 ℃ for 48 h. The other two block copolymers were prepared according to the same procedure and feeding ratios.

Formation of MeO-PEG$_{45}$-*b*-PBO$_n$-*b*-PCL$_{60}$ (n = 0, 6, 9) block copolymer micelles: The nano-precipitation method[24, 36-38] was used to form the block copolymer micelles. A stock solution of the MeO-PEG$_{45}$-*b*-PBO$_n$-*b*-PCL$_{60}$ (n = 0, 6, 9) block copolymer (10 mg/mL) was prepared in acetone. An aliquot of the polymer stock solution (0.80 mL) was added to stirring HPLC grade water (8.0 mL) at the rate of 0.2 mL/min which resulted in formation of the block copolymer micelles (1.0 mg/mL). The micelle suspension was transferred into dialysis bags (MWCO: 10,000 Da) and dialyzed against HPLC grade water for 36 hours. ^{1}H NMR confirmed the acetone was completely removed after the dialysis.

2.4.4 Acid catalyzed degradation of MeO-PEG$_{45}$-*b*-PBO$_n$-*b*-PCL$_{60}$ (n = 0, 9) block copolymers micelles

Degradation of MeO-PEG$_{45}$-*b*-PBO$_n$-*b*-PCL$_{60}$ (n = 0, 9) block copolymer micelles at pH=0: The hydrolytic degradation of MeO-PEG$_{45}$-*b*-PCL$_{60}$ and MeO-PEG$_{45}$-*b*-PBO$_9$-*b*-PCL$_{60}$ micelles was studied in HCl (pH = 0), at 25 ^{o}C. The acid catalyzed degradation experiment was done in a series of vials. In each 5 mL vial, 0.7 mL micelle suspension (1.0 mg/mL) was added. Subsequently, 0.7 mL of HCl (2 M) solution was added into the vials. The reactions were terminated by adding 1.4 mL of NaOH (1 M) solution every 3 h. The final degradation products were extracted from water solution by CH_2Cl_2 for ^{1}H NMR and GPC evaluation.

^{1}H NMR for micelles from MeO-PEG$_{45}$-*b*-PBO$_n$-*b*-PCL$_{60}$ (n = 0, 6, 9) block copolymers (0.714 mg/mL): PBS buffer solution (0.70 mL, pH = 7.4) was evaporated to dryness by air in a vial. A micelle suspension (0.50 mL, 1.0 mg/mL) and D_2O (0.10 mL) was added into the vial to redissolve the PBS salts. A solution of micelle with dissolved PBS salt was transferred into a NMR tube and the solution was heated to 37 ℃ in the NMR instrument. Water solvent suppressed NMR was used in this experiment.

^{1}H NMR for HCl catalyzed hydrolytic degradation of micelles from PEG_{45}-*b*-PBO_n-*b*-PCL_{60} (n = 0, 6, 9) block copolymers (0.75 mg/mL): The HCl catalyzed degradation of micelles from PEG_{45}-*b*-PBO_n-*b*-PCL_{60} (n = 0, 6, 9) block copolymers were studied at HCl concentration of 0.5 M (pH = 0.3) and T = 37 ℃**.** A micelle suspension (0.60 mL, 1.0 mg/mL) and D_2O (0.10 mL) was added into a NMR tube and the solution was heated to 37 ^oC in the NMR instrument. Concentrated HCl solution (0.10 mL, 4 M) was then quickly added into the NMR tube to catalyze the hydrolysis of PEG_{45}-*b*-PBO_n-*b*-PCL_{60} (n = 0, 6, 9) micelles. The acid catalyzed degradation of micelle was followed by ^{1}H NMR at 37 ℃ and the water solvent suppressed NMR was used in this experiment.

GPC for HCl catalyzed hydrolytic degradation of PEG_{45}-*b*-PBO_6-*b*-PCL_{60} triblock copolymer micelles (0.75 mg/mL): GPC traces for the acid catalyzed degradation of PEG_{45}-*b*-PBO_6-*b*-PCL_{60} micelle were studied at HCl concentration of 0.5 M (pH = 0.3) and T = 37 ℃. A micelle suspension of PEG_{45}-*b*-PBO_6-*b*-PCL_{60} (0.60 mL, 1.0 mg/mL) and H_2O (0.10 mL) was added into a vial. The micelle solution was first warmed to 37 ℃ in the water bath and then HCl solution (0.10 mL, 4 M) was added into the vial. The reactions were terminated at different times by dipping the vials into liquid N_2. Degradation products were collected by freeze drying method and redissolved in DMF for GPC studies.

2.5 References

(1) Kang, N.; Perron, M.-È.; Prud'homme, R. E.; Zhang, Y.; Gaucher, G.; Leroux, J.-C. *Nano. Letters.* 2005, 5, 315-319.

(2) Hayward, R. C.; Pochan, D. J. *Macromolecules* 2010, 43, 3577-3584.

(3) Cameron, N. S.; Corbierre, M. K.; Eisenberg, A. *Can. J. Chem.* 1999, 77, 1311-1326.

(4) Discher, B. M.; Won, Y.-Y.; Ege, D. S.; Lee, J. C.-M.; Bates, F. S.; Discher, D. E.; Hammer, D. A. *Science* 1999, 284, 1143-1146.

(5) Zhang, X.; Cheng, J.; Wang, Q.; Zhong, Z.; Zhuo, R. *Macromolecules* 2010, 43, 6671-6677.

(6) Cai, S.; Vijayan, K.; Cheng, D.; Lima, E.; Discher, D. *Pharm. Res.* 2007, 24, 2099-2109.

(7) Christian, D. A.; Cai, S.; Garbuzenko, O. B.; Harada, T.; Zajac, A. L.; Minko, T.; Discher, D. E. *Mol. Pharmaceutics* 2009, 6, 1343-1352.

(8) Shuvaev, V. V.; Ilies, M. A.; Simone, E.; Zaitsev, S.; Kim, Y.; Cai, S. S.; Mahmud, A.; Dziubla, T.; Muro, S.; Discher, D. E.; Muzykantov, V. R. *Acs Nano* 2011, 5, 6991-6999.

(9) Pang, Z.; Lu, W.; Gao, H.; Hu, K.; Chen, J.; Zhang, C.; Gao, X.; Jiang, X.; Zhu, C. *J. Controlled Release* 2008, 128, 120-127.

(10) Hvasanov, D.; Wiedenmann, J.; Braet, F.; Thordarson, P. *Chem. Commun.* 2011, 47, 6314-6316.

(11) Christian, D. A.; Cai, S.; Bowen, D. M.; Kim, Y.; Pajerowski, J. D.; Discher, D. E. *Eur. J. Pharm. Biopharm.* 2009, 71, 463-474.

(12) Benahmed, A.; Ranger, M.; Leroux, J.-C. *Pharm. Res.* 2001, 18, 323-328.

(13) Studer, P.; Limal, D.; Breton, P.; Riess, G. *Bioconjugate Chem.* 2004, 16, 223-229.

(14) Master, A. M.; Rodriguez, M. E.; Kenney, M. E.; Oleinick, N. L.; Gupta, A. S. *J. Pharm. Sci.* 2010, 99, 2386-2398.

(15) Kagaya, H.; Oba, M.; Miura, Y.; Koyama, H.; Ishii, T.; Shimada, T.; Takato, T.; Kataoka, K.; Miyata, T. *Gene Ther* 2011.

(16) Rameez, S.; Alosta, H.; Palmer, A. F. *Bioconjugate Chem.* 2008, 19, 1025-1032.

(17) Jette, K.; Law, D.; Schmitt, E.; Kwon, G. *Pharm. Res.* 2004, 21, 1184-1191.

(18) Forrest, M. L.; Zhao, A.; Won, C.-Y.; Malick, A. W.; Kwon, G. S. *J. Controlled Release* 2006, 116, 139-149.

(19) Gan, Z.; Jim, T. F.; Li, M.; Yuer, Z.; Wang, S.; Wu, C. *Macromolecules* 1999, 32, 590-594.

(20) Nie, T.; Zhao, Y.; Xie, Z.; Wu, C. *Macromolecules* 2003, 36, 8825-8829.

(21) Meier, M. A. R.; Aerts, S. N. H.; Staal, B. B. P.; Rasa, M.; Schubert, U. S. *Macromol. Rapid Commun.* 2005, 26, 1918-1924.

(22) Cuong, N.-V.; Jiang, J.-L.; Li, Y.-L.; Chen, J.-R.; Jwo, S.-C.; Hsieh, M.-F. *Cancers* 2010, 3, 61-78.

(23) Ge, H.; Hu, Y.; Jiang, X.; Cheng, D.; Yuan, Y.; Bi, H.; Yang, C. *J. Pharm. Sci.* 2002, 91, 1463-1473.

(24) Chung, T. W.; Cho, K. Y.; Lee, H.-C.; Nah, J. W.; Yeo, J. H.; Akaike, T.; Cho, C. S. *Polymer* 2004, 45, 1591-1597.

(25) Cuong, N.-V.; Hsieh, M.-F.; Chen, Y.-T.; Liau, I. *J. Appl. Polym. Sci.* 2010, 117, 3694-3703.

(26) Ahmed, F.; Discher, D. E. *J. Controlled Release* 2004, 96, 37-53.

(27) Shen, C.; Guo, S.; Lu, C. *Polym. Adv. Technol.* 2008, 19, 66-72.

(28) Carstens, M. G.; van Nostrum, C. F.; Verrijk, R.; de Leede, L. G. J.; Crommelin, D. J. A.; Hennink, W. E. *J. Pharm. Sci.* 2008, 97, 506-518.

(29) Shen, C.; Guo, S.; Lu, C. *Polym. Degrad. Stab.* 2007, 92, 1891-1898.

(30) Nagasaki, Y.; Kutsuna, T.; Iijima, M.; Kato, M.; Kataoka, K.; Kitano, S.; Kadoma, Y. *Bioconjugate Chem.* 1995, 6, 231-233.

(31) Park, S.-J.; Kang, S.-G.; Fryd, M.; Saven, J. G.; Park, S.-J. *J. Am. Chem. Soc.* 2010, 132, 9931-9933.

(32) Ding, J.; Price, C.; Booth, C. *Eur. Polym. J.* 1991, 27, 891-894.

(33) Wu, J.; Thio, Y. S.; Bates, F. S. *J. Polym. Sci., Part B: Polym. Phys.* 2005, 43, 1950-1965.

(34) Ding, J.; Heatley, F.; Price, C.; Booth, C. *Eur. Polym. J.* 1991, 27, 895-899.

(35) Ding, J.; Price, C.; Booth, C. *Eur. Polym. J.* 1991, 27, 891-894.

(36) Giacomelli, C.; Borsali, R. *Macromol. Symp.* 2006, 245-246, 147-153.

(37) Schubert, S.; Delaney, J. J. T.; Schubert, U. S. *Soft Matter* 2011, 7, 1581-1588.

(38) Lassalle, V.; Ferreira, M. L. *Macromol. Biosci.* 2007, 7, 767-783.

(39) Bajaj, H.; Sharma, V. K.; Kalonia, D. S. *Biophys. J* . 2004, 87, 4048-4055.

(40) Furó, I. *Journal of Molecular Liquids* 2005, 117, 117-137.

(41) Dorovska-Taran, V.; Wick, R.; Walde, P. *Anal. Biochem.* 1996, 240, 37-47.

(42) Geng, D.; Chura, J.; Roberts, M. F. *J. Biol. Chem.* 1998, 273, 12195-12202.

(43) Yang, H.; Roberts, M. F. *Protein Sci.* 2003, 12, 2087-2098.

(44) Hu, Y.; Zhang, L.; Cao, Y.; Ge, H.; Jiang, X.; Yang, C. *Biomacromolecules* 2004, 5, 1756-1762.

(45) Jiang, Z.; Zhu, Z.; Liu, C.; Hu, Y.; Wu, W.; Jiang, X. *Polymer* 2008, 49, 5513-5519.

(46) Zweers, M. L. T.; Engbers, G. H. M.; Grijpma, D. W.; Feijen, J. *J. Controlled Release* 2004, 100, 347-356.

(47) Jiang, Z.; Zhu, Z.; Liu, C.; Hu, Y.; Wu, W.; Jiang, X. *Polymer* 2008, 49, 5513-5519.

(48) Zhu, X.; Fryd, M.; Tran, B. D.; Ilies, M. A.; Wayland, B. B. *Macromolecules* 2012, 45, 660-665.

(49) Fairley, N.; Hoang, B.; Allen, C. *Biomacromolecules* 2008, 9, 2283-2291.

(50) Luo, L.; Tam, J.; Maysinger, D.; Eisenberg, A. *Bioconjugate Chem.* 2002, 13, 1259-1265.

CHAPTER 3:

ENZYME CATALYZED DEGRADATION OF MICELLES FROM PEG-*b*-PCL AND BLOCK JUNCTION MODIFIED PEG-*b*-PBO-*b*-PCL

3.1 Introduction

Amphiphilic block copolymer micelles with hydrophilic corona and hydrophobic cores[1-10] provide a broad platform for development of drug and gene delivery vehicles[11-18] that function through their capability for loading, transport and release of lipophilic substances incorporated in the hydrophobic core. The efficiency observed for micelle deliver therapeutics to the desired site is currently limited by processes that prematurely degrade the micelle[19-23] and this issue is stimulating increased effort in evaluating how micelles respond to the conditions encountered in the digestive and circulatory systems[22, 24-30]. One central objective for our research is to identify and utilize polymer structural features that influence the hydrolytic stability of micelles toward acid, base and enzyme catalyzed hydrolysis of the polyester cores which subsequently trigger micelle degradation and drug release. It is well recognized that the initial acid catalyzed hydrolysis event in block copolymer micelles from poly (ethylene glycol) (PEG) block poly (ε-caprolactone) (PCL) (PEG-*b*-PCL) occurs in the vicinity of the PCL interface ester group[24-26] that attaches the polyester (PCL) block in the hydrophobic micelle core to the non-degradable hydrophilic PEG segment. This mechanistic feature suggested that moving the block copolymer hydrophilic-hydrophobic junction away from the PCL interface ester group could inhibit water reaching the site of hydrolysis and provide a strategy for tuning the micelle hydrolytic stability[31]. In the previous chapter (Chapter 2), an initial test for this general strategy was made by preparing a set of triblock copolymers (PEG-*b*-PBO-*b*-PCL) formed by inserting a short hydrophobic non-hydrolyzable poly (1,2-butylene oxide) (PBO) segment between the PEG and PCL blocks as an approach to increase the barrier for water to reach the interface ester at the surface of the PCL core[31]. It turned out that the acid catalyzed hydrolysis of the interface ester groups occurs substantially slower in the triblock copolymer micelles when compared to micelles of the parent diblock copolymer. The initial results from the test demonstrate that triblock copolymer micelles may have potential application of drug loaded micelles in acidic medium such as stomach.

PEG-*b*-PCL diblock copolymer micelles are also widely used to transfer lipophilic drugs though the blood stream to target cancer cells and then control release the drugs. Studies of cell specific drug delivery from polymer micelles that have appended functionalities such as proteins[32], antibodies[33] and sugars[34] have reported remarkable successes, but the fraction of drug that reaches the target site is small even when the target selectivity is high because of in vivo micelle instability[35]. Drug loaded block copolymer micelles introduced into the blood systems encounter a wide range of conditions, enzymes and other substances that can promote micelle degradation and premature release of therapeutics. This chapter reports on comparative studies of lipase enzyme catalyzed hydrolysis and degradation of micelles from diblock PEG-*b*-PCL and triblock PEG-*b*-PBO-*b*-PCL copolymers. Lipase enzymes from *P. cepacia*, *C. rugosa* and *P. fluorescens* are highly effective catalysts for degradation of block copolymer micelles, but porcine liver esterase enzyme does not catalyze PCL hydrolysis. ^{1}H NMR, GPC and DLS studies were used to evaluate the micelle and solution compositions, determine the kinetics of diblock and triblock copolymer micelle degradation and advance the mechanistic understanding for both the acid and lipase catalyzed processes.

The initial step in acid catalyzed degradation involves the selective hydrolysis of the interface ester groups that connect the hydrophobic PCL segment to the hydrophilic PEG and PEG-*b*-PBO blocks. Lipase catalyzed micelle degradations are distinctly different from acid catalysis and involve strong enzyme-micelle binding with complete sequential degradation[36-37] of the enzyme bound micelles.

3.2 Results and Discussion

3.2.1 DLS of MeO-PEG$_{45}$-*b*-PBO$_{n}$-*b*-PCL$_{60}$ (n = 0, 6, 9) block copolymer micelles during the lipase catalyzed PCL core hydrolysis and micelle degradation

Dynamic light scattering (DLS) measurements were taken at 15 minute intervals during the *P.cepacia* lipase catalyzed MeO-PEG$_{45}$-*b*-PBO$_{n}$-*b*-PCL$_{60}$ (n= 0, 6, 9) micelle degradation at the same conditions (pH=7.40, T=37 ^{o}C and E= 2.86 U/mL) used for the following ^{1}H NMR and GPC studies. The DLS results show that the average hydrodynamic diameters for micelles from the diblock and triblock copolymers are quite similar in value and effectively remain unchanged at 30 $\pm$4 nm during the entire time for the degradation processes to proceed to completion (Figure 3.1). Constancy of the micelle hydrodynamic diameter determined by DLS during lipase catalyzed degradations of MeO-PEG$_{m}$-*b*-PCL$_{n}$ micelles has been previously reported by both Wu[37] and Jiang[25].

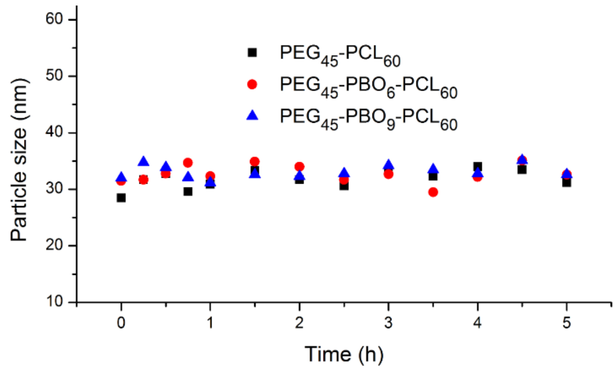

Figure 3.1: DLS of *P. cepacia* catalyzed MeO-PEG$_{45}$-*b*-PBO$_n$-*b*-PCL$_{60}$ (n= 0, 6, 9) micelles in aqueous PBS buffer solution (pH = 7.4) at T = 37 ℃.

3.2.2 ^{1}H NMR for MeO-PEG$_{45}$-*b*-PBO$_n$-*b*-PCL$_{60}$ (n = 0, 6, 9) block copolymer micelles during the lipase catalyzed hydrolysis of the PCL polyester core

Micelles from block copolymers MeO-PEG$_m$-*b*-PCL$_n$ with PCL polyester cores experience fast degradation catalyzed by lipase enzymes[25, 28, 36, 38]. Addition of *P. cepacia*[39-40] lipase to dispersions of micelles from MeO-PEG$_{45}$-*b*-PBO$_n$-*b*-PCL$_{60}$ (n = 0, 6, 9) in aqueous PBS buffer (pH = 7.4) at 37 ℃ results in micelle degradations that are readily followed by ^{1}H NMR (Figures 3.2, 3.3). Decline in the intensities for the broadened micelle ^{1}H NMR resonances as the degradation proceeds is accompanied by appearance of sharp resonances for water soluble MeO-PEG$_{45}$-*b*-PBO$_9$-*b*-PCL$_n$ (n ≤ 6) fragments (δ = 3.77 ppm) and a set of small PCL$_n$ (n ≤ 6) oligomers (δ ~ 2.25, 2.46, 3.67 ppm) that result from lipase catalyzed hydrolysis of MeO-PEG$_{45}$-*b*-PBO$_9$-*b*-PCL$_{60}$ block copolymer chains in the micelle (Figures 3.2, 3.3). ^{1}H NMR provides a convenient and effective technique to obtain detailed information that defines both the composition of the micelle and the products from polymer hydrolysis simultaneously as the process proceeds. The quantitative distribution of PCL oligomers is also provided by high resolution LC-

MS spectrum (Figure 3.4) and the LC-MS result is fully consistent with ^{1}H NMR. The ratio (R) of the areas of the CH_2 groups attached to an ester carbon (-CH_2-C(O)-O-,δ ~ 2.46 ppm) to that for terminal -CH_2-CO_2H (δ = 2.25 ppm) gives the average number of caprolactone units (n) in the PCL oligomers (n = R +1). An average chain length of 2.8 for the PCL oligomers was determined by ^{1}H NMR during the initial time interval of the lipase catalyzed MeO-PEG$_{45}$-*b*-PBO$_{9}$-*b*-PCL$_{60}$ micelle degradation (Figure 3.2). The 6-hydroxycaproic acid is not observed during the early portion of the enzyme catalyzed PCL hydrolysis, but it slowly accumulates from subsequent hydrolysis of the PCL oligomers in solution (Figures 3.3A, 3.13). Preferential cleavage of the PCL polymer chain into trimer units may reflect the positioning of the polyester substrate in the enzyme active catalytic center and adjacent hydrophobic and water accessible regions of the enzyme.

A constant ratio of 1.48 ± 0.07 is observed for the integrated areas of the micelle peaks for the MeO-PEG$_{45}$-PBO$_{9}$ segment (δ = 3.76 ppm) and one of the PCL CH_2 resonances (δ = 2.35 ppm) as the degradation proceeds (Figure 3.3). The micelles are shown to be composed primarily of intact MeO-PEG$_{45}$-*b*-PBO$_{9}$-*b*-PCL$_{60}$ block copolymers throughout the entire micelle degradation process by the close agreement between the observed constant ratio of 1.48 with the theoretical value of 1.50 (90/60) for MeO-PEG$_{45}$-*b*-PBO$_{9}$-*b*-PCL$_{60}$ triblock copolymers (Figures 3.2, 3.3).

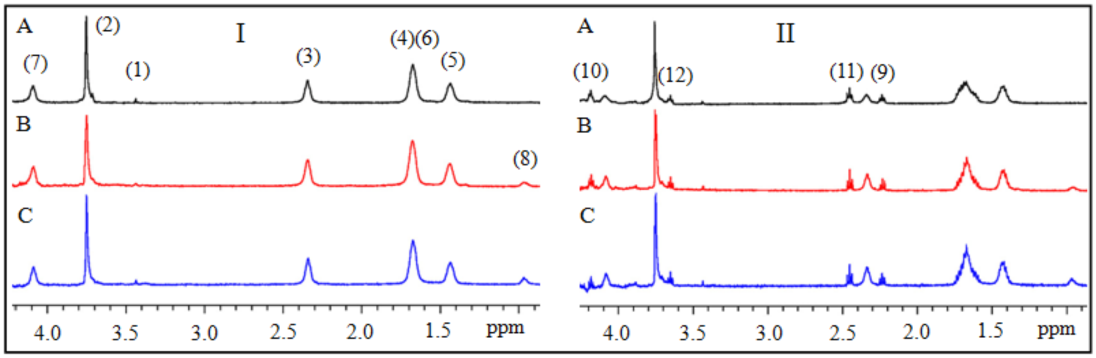

Figure 3.2: I) ^{1}H NMR (500 MHz) of micelles (0.714 mg/mL) from (A) MeO-PEG$_{45}$-*b*-PCL$_{60}$; (B) MeO-PEG$_{45}$-*b*-PBO$_6$-*b*-PCL$_{60}$; (C) PEG$_{45}$-*b*-PBO$_9$-*b*-PCL$_{60}$ in aqueous PBS buffer (pH=7.4) at T=37 ℃. ^{1}H NMR assignments for micelle peaks (chemical shifts in ppm): CH_3(1)O-[CH_2CH_2(2)-O]$_{45}$-[$CH_2CH(CH_2CH_3$(8))-O]$_n$-[C(O)CH_2(3)-CH_2(4)-CH_2(5)CH_2(6)CH_2(7)-O]$_{60}$-OH (n = 0, 6, 9); (δ(1)=3.45; δ(2)=3.76; δ(3)=2.35; δ(4,6)=1.70; δ(5)=1.45; δ(7)=4.12; δ(8)=0.98). II) ^{1}H NMR assignments for diagnostic hydrogens of water soluble PCL oligomers generated by *P. cepacia* lipase catalyzed hydrolysis of PEG$_{45}$-*b*-PBO$_n$-*b*-PCL$_{60}$ block copolymer micelles at T=37℃,pH=7.4, lipase activity of 2.86 U/mL and reaction time t =1.5 h: HOC(O)CH_2(9)(CH_2)$_3CH_2$(10)O[C(O)CH_2(11)(CH_2)$_3CH_2$(10)O]$_m$-C(O)CH_2(11) (CH_2)$_3CH_2$(12)OH. (δ(9)~2.25; δ(10)~4.19; δ(11)~2.46; δ(12)~3.67).

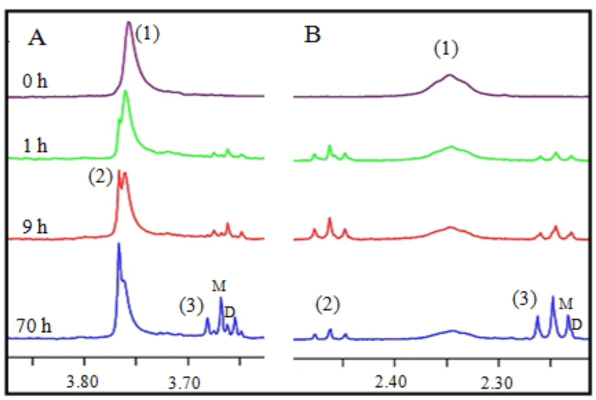

Figure 3.3: ^{1}H NMR (500 MHz) of MeO-PEG$_{45}$-*b*-PBO$_9$-*b*-PCL$_{60}$ block copolymer micelles (0.714 mg/mL) in aqueous PBS buffer (pH = 7.4) at T = 37 ℃ and *P. cepacia* lipase activity of 2.86 U/mL for a series of reaction times during a 70 hours time period. (M = HO(CH_2)$_5$-CO_2H; D = HO(CH_2)$_5$-C(O)O(CH_2)$_5$-CO_2H) (A) PEG segment in the micelle (1A, δ=3.76 ppm) and water soluble PEG fragment from hydrolysis (PEG$_{45}$-PCL$_n$ (n=0-6)) (2A, δ=3.77 ppm) and the -*CH_2*OH terminal groups for the PCL oligomers (3A, δ~3.67 ppm). (B) Ester -*CH_2*-C(O)-O-hydrogens in PEG-*b*-PCL diblock copolymer micelles (1B, δ=2.35 ppm) and ester-*CH_2*-C(O)-O- (2B, δ~2.46 ppm) and terminal *CH_2*CO_2H (3B, δ~2.25 ppm) for water soluble PCL oligomers.

3.2.3 ^{1}H NMR in $CDCl_3$ of the ester CH_2 that joins the PEG_{45} and PCL segments in the hydrolysis products (MeO-PEG_{45}-*b*-PCL_n)

GPC traces were obtained for DMF solutions containing the constituents of the *P.cepacia* catalyzed degradation of MeO-PEG_{45}-*b*-PCL_{60} block copolymer micelles and the eluent from the GPC column for the fraction containing the PEG_{45} segment (Figure 3.8, peak 2) was collected and examined by ^{1}H NMR (Figure 3.4). The vast majority of MeO-PEG_{45} units were observed by ^{1}H NMR to have several PCL units attached (MeO-PEG_{45}-*b*-PCL_n ($n \leq 6$)) which is shown by ^{1}H NMR that the unique -CH_2O-C(O)- (δ=4.23 ppm) unit in the ester group that bridges the PCL and PEG segments. ^{1}H NMR of the PCL terminal CH_2OH shows that *P. cepacia* hydrolyzes the PCL chains into a series of PCL oligomers (PCL_n (n=1-6)) with the dimer and trimer units being dominant (Figures 3.2, 3.3). The quantitative distribution of PCL oligomers is also given by high resolution LC-MS spectrum (Figure 3.5).

The PEG_{45} unit thus has at least one attached caprolactone unit at the time immediately following the initial phase of the lipase enzyme hydrolysis. This lipase enzyme behavior is in direct contrast with acid-catalyzed PEG_{45}-*b*-PCL_{60} micelle degradation process where the rate determining step hydrolysis event occurs at the ester group that binds together the PEG and PCL blocks. The junction ester CH_2 group for the triblock copolymers MeO-PEG_{45}-*b*-$PBO_{6,9}$-*b*-PCL_{60} remains attached to the PEG_{45}-*b*-$PBO_{6,9}$- showing that the lipase catalyzed avoids the junction ester CH_2 which is the dominant site previously for acid catalyzed hydrolysis during the period for micelle degradation.

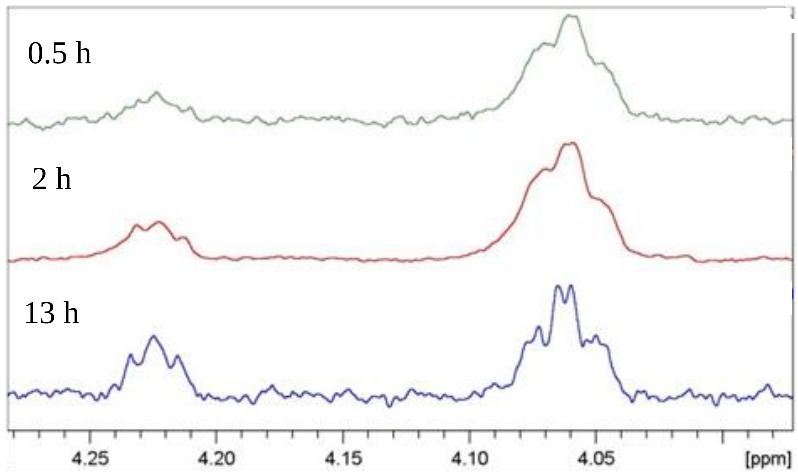

Figure 3.4: [1]H NMR in $CDCl_3$ for the specific unique CH_2 that joins the PEG_{45} and PCL_n segments (-*CH₂*O-C(O)-, δ=4.23 ppm) for the hydrolysis products MeO-PEG_{45}-*b*-PCL_n(n=1-6) separated by GPC.

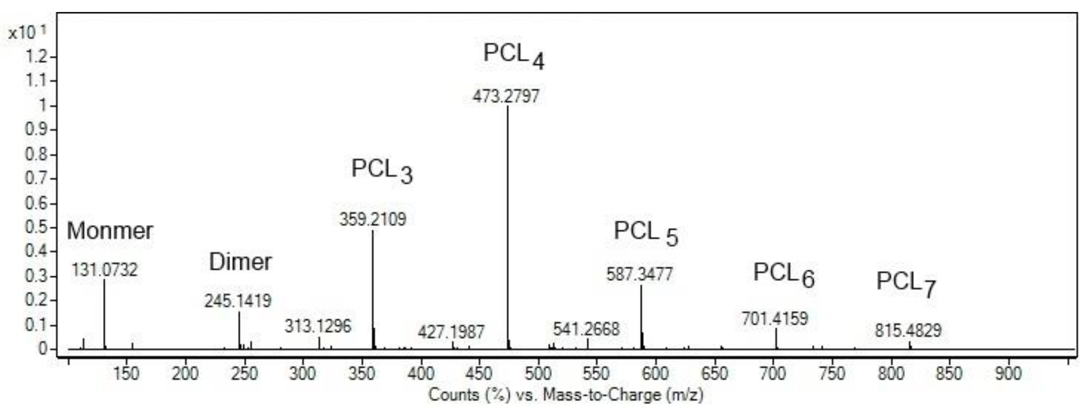

Figure 3.5: LC-MS spectrum of micelle degradation products (PCL_n) separated by GPC.

3.2.4 Absence of esterase enzyme catalyzed degradation of MeO-PEG_{45}-*b*-PBO_n-*b*-PCL_{60} (n = 0, 6, 9) Micelles

Esterase type hydrolase enzymes do not promote degradation of micelles from MeO-PEG_{45}-*b*-PBO_n-*b*-PCL_{60} (n = 0, 6, 9). Addition of the *porcine liver* esterase at an activity of 2.86 U/mL to micelles from MeO-PEG_{45}-*b*-PBO_n-*b*-PCL_{60} (n = 0, 6, 9) in aqueous

PBS did not produce observable micelle degradation over a period of 2 days at 37 ^{o}C. Dispersions of micelles from MeO-PEG$_{45}$-*b*-PCL$_{60}$ with *porcine liver* esterase even at the very high activity of 21 U/mL did not produce any observed micelle degradation or PCL hydrolysis over a period of days. Absence of esterase catalysis for the micelles with polyester cores illustrates the specific need for lipase enzymes to catalyze the micelle hydrolytic degradation. Both esterase and lipase enzymes are capable of catalyzing the hydrolysis of water soluble esters[41-44], but lipase enzymes have the exclusive property of being highly activated through binding with assemblies of ester substrates such as membranes and vesicles dispersed in water by a process called enzyme interfacial activation[45-46].

3.2.5 Number of micelles per enzyme molecule and the number of lipase enzyme hydrolysis events

One micelle of MeO-PEG$_{45}$-*b*-PBO$_{9}$-*b*-PCL$_{60}$ with a hydrodynamic diameter of 32 nm has an estimated average micelle particle mass of $2.2(4)10^{6}$ Da and contain ~ 220 triblock copolymer chains. Pure lipase from *P. cepacia* has an activity of 5800 units (U) per mg of enzyme[47]. A dispersion of 0.50 mg of MeO-PEG$_{45}$-*b*-PBO$_{9}$-*b*-PCL$_{60}$ micelles and a *P. cepacia* activity of 2.0 U in 0.70mL of aqueous PBS contains ~23 micelle particles and 5×10^{3} MeO-PEG$_{45}$-*b*-PBO$_{9}$-*b*-PCL$_{60}$ polymer chains per lipase enzyme molecule. Approximately 20% of the micelles and component triblock copolymers degrade during the first 15 minutes of reaction time (Figure 3.5) which corresponds to approximately 22,000 hydrolysis events per enzyme. In this representative lipase catalyzed micelle degradation reaction each enzyme molecule on average fully degrades ~4.6 micelles during the first 15 minutes of reaction time. The lipase catalyzed micelle degradation and polyester hydrolysis ultimately proceed to completion by consuming 23 micelles and 5×10^3 MeO-PEG$_{45}$-*b*-PBO$_9$-*b*-PCL$_{60}$ polymer chains per lipase enzyme molecule. Full hydrolytic degradation of MeO-PEG$_{45}$-*b*-PBO$_9$-*b*-PCL$_{60}$ produces one MeO-PEG$_{45}$-*b*-PBO$_9$ fragment and 60 molecules of 6-hydroxycaproic acid ($HO(CH_2)_5CO_2H$) which is 13.4×10^3 lipase hydrolysis events per micelle and a total of $\sim3.1\times10^5$ catalyzed hydrolysis events per enzyme molecule to complete the process. Comparable parameters for the *P. cepacia* lipase catalyzed hydrolytic degradation are also obtained for each of the PEG$_{45}$-*b*-PCL$_{60}$ and MeO-PEG$_{45}$-*b*-PBO$_6$-*b*-PCL$_{60}$ micelle degradation processes.

3.2.6 Kinetics for lipase enzymes catalyzed degradation of MeO-PEG$_{45}$-*b*-PBO$_n$-*b*-PCL$_{60}$ (n = 0, 6, 9) block copolymer micelles by ^{1}H NMR

Kinetics for degradation of the diblock and triblock copolymer micelles of MeO-PEG$_{45}$-*b*-PBO$_n$-*b*-PCL$_{60}$ (n = 0, 6, 9) are conveniently followed by observing the decrease in the ^{1}H NMR intensities for one of the CH_2 resonances from the PCL polymer segments in the micelles (Figure 3.2, δ=2.35 ppm). Representative results for the decrease in the ^{1}H NMR integrated intensity for the micelle ester CH_2 groups as a function of time are plotted in Figure 3.6. Comparable kinetic results are obtained from analysis of the time dependence for the intensity of each of the micelle ^{1}H NMR peaks. The ^{1}H NMR kinetic results directly measure the rate at which the copolymer micelles degrade at two specific lipase enzyme activities (0.714 U/mL and 2.86 U/mL) at 37 ℃ in aqueous PBS (pH = 7.4). Kinetic plots of lipase catalyzed hydrolysis of micelles at the lower enzyme activity (0.714 U/mL) shows that ~ 80% of MeO-PEG$_{45}$-*b*-PBO$_6$-*b*-PCL$_{60}$ triblock copolymer micelles remain intact after 5 hours of reaction time compared to ~ 50% of the MeO-PEG$_{45}$-*b*-PCL$_{60}$ diblock copolymer micelles (Figure 3.6). At higher lipase activity (2.86 U/mL) about 65% of the triblock copolymer micelles and 35% of the diblock copolymer micelles persist after 5 hours of reaction (Figure 3.6). The relative rates of degradation for the two triblock copolymer (MeO-PEG$_{45}$-*b*-PBO$_6$-*b*-PCL$_{60}$, MeO-PEG$_{45}$-*b*-PBO$_9$-*b*-PCL$_{60}$) micelles are almost equal and both significantly slower than the MeO-PEG$_{45}$-*b*-PCL$_{60}$ diblock copolymer micelle degradation (Figure 3.6).

Parallel reactions with *P. fluorescens* and *C. rugosa* lipase with the micelle of MeO-PEG$_{45}$-*b*-PCL$_{60}$ gave closely related micelle degradation as that observed for *P. cepacia* lipase (Figure 3.7). However, the average number of caprolactone units (n) in the PCL oligomers (n = R +1) for cepacia, fluorescens and rugosa is 3.2, 3.0 and 1.4. The different length of PCL oligmers cleaved from the PCL$_{60}$ segment may indicate that lipase active centers are different. Proteinase K and Phosphalipase A$_2$ both doesn't catalyze the degradation of MeO-PEG$_{45}$-*b*-PCL$_{60}$ micelles.

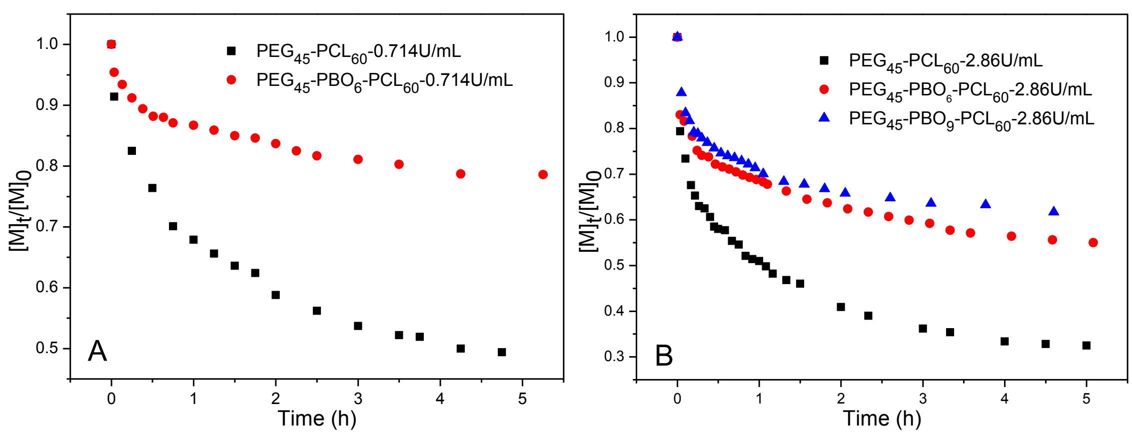

Figure 3.6: Kinetic plots from [1]H NMR for degradation of micelles from MeO-PEG$_{45}$-*b*-PBO$_n$-*b*-PCL$_{60}$ (n = 0, 6, 9) block copolymers in aqueous PBS (pH = 7.4) at 37 ℃ catalyzed by *P. cepacia* lipase at an activity of (A) 0.714 U/mL (B) 2.86 U/mL; [M] is defined as the concentration of micelles.

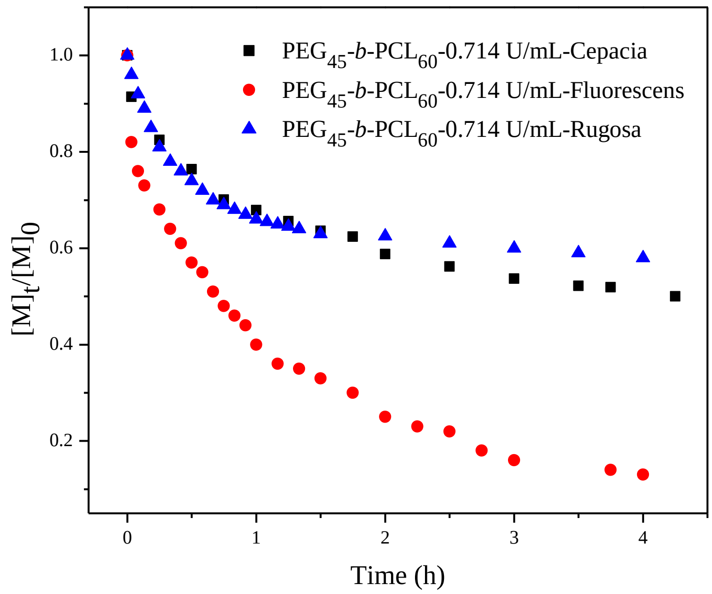

Figure 3.7: Kinetic plots for MeO-PEG$_{45}$-*b*-PCL$_{60}$ diblock copolymer micelle degradation catalyzed by *P. cepacia*, *P. fluorescens*, and *C. rugosa* lipases in aqueous PBS (pH = 7.4) at E= 0.714 U/mL and T= 37 ℃

3.2.7 GPC observations during the lipase catalyzed MeO-PEG$_{45}$-*b*-PBO$_n$-*b*-PCL$_{60}$ (n = 0, 6, 9) block copolymer micelle degradation

GPC traces at a series of reaction times during the lipase catalyzed MeO-PEG$_{45}$-*b*-PBO$_n$-*b*-PCL$_{60}$ (n = 0, 6, 9) block copolymer micelle degradation at a lipase activity of 2.86 U/mL after freeze drying and dissolving in DMF are shown in Figure 3.8. GPC traces obtained by this procedure using DMF as the solvent reflect the constituents of the entire sample consisting of the lipase, residual unreacted diblock or triblock copolymers (MeO-PEG$_{45}$-*b*-PBO$_n$-*b*-PCL$_{60}$), and all of the MeO-PEG$_{45}$-*b*-PBO$_n$-*b*-PCL$_m$ and a set of PCL$_m$ (n = 0, 6, 9 and m ≤ 6) fragments produced in the hydrolytic degradation.

The GPC trace corresponding to MeO-PEG$_{45}$-*b*-PBO$_9$-*b*-PCL$_{60}$ decreases in area as the reaction proceeds, but the position and width are unchanged (Figure 3.8A). The decrease in the triblock copolymer observed in the GPC as the micelle degrades is accompanied by appearance of new peaks in the GPC corresponding to MeO-PEG$_{45}$-*b*-PBO$_9$-*b*-PCL$_m$ ($m \leq 6$) and a set of relatively small PCL oligomers (PCL$_m$, $m \leq 6$) (Figure 3.8A). Figure 3.8B shows that the lipase catalyzed hydrolysis of the diblock and triblock copolymer micelles produce the same set of PCL$_m$ ($m \leq 6$) oligomers, and at the same reaction conditions and times the diblock copolymer micelle reacts away faster than the two triblock copolymer micelles based upon the relative peak intensity between intact diblock and triblock copolymers and the newly formed polymer fragments (Figure 3.8B).

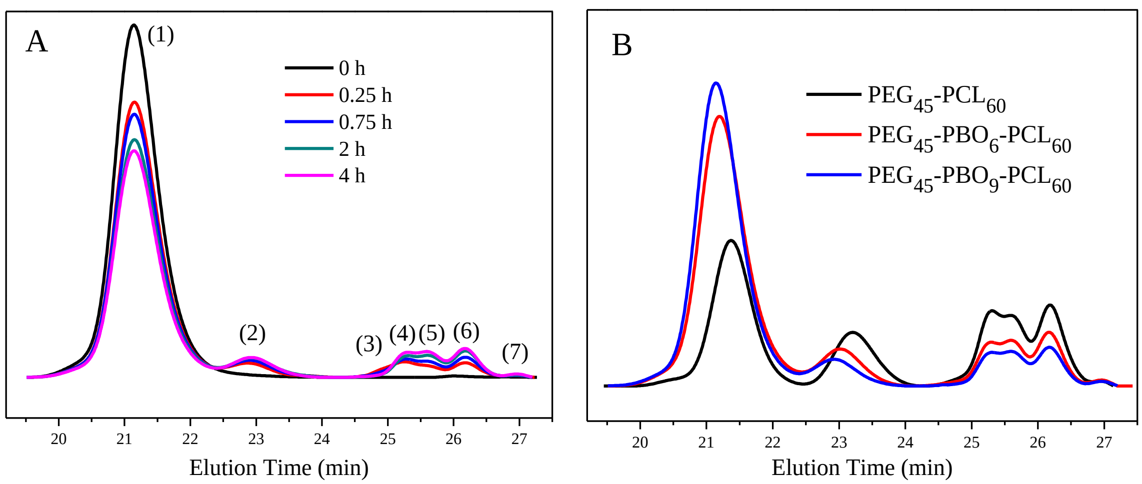

Figure 3.8: (A) GPC traces for DMF solutions that contain all the products from the *P. cepacia* lipase catalyzed hydrolytic degradation of MeO-PEG$_{45}$-*b*-PBO$_9$-*b*-PCL$_{60}$ micelles at an activity of 2.86 U/mL in aqueous PBS (pH = 7.4) at 37 °C; (1) PEG$_{45}$-*b*-PBO$_9$-*b*-PCL$_{60}$; (2) PEG$_{45}$-*b*-PBO$_9$-*b*-PCL$_{(1-6)}$; (3) PCL$_{(5-6)}$; (4) PCL$_4$; (5) PCL$_3$; (6) HO(CH$_2$)$_5$-C(O)O(CH$_2$)$_5$-CO$_2$H; (7) HO(CH$_2$)$_5$-CO$_2$H. (B) GPC traces for DMF solutions that contain all the products from the *P. cepacia* lipase catalyzed hydrolytic degradation of MeO-PEG$_{45}$-*b*-PBO$_n$-*b*-PCL$_{60}$ (n = 0, 6, 9) micelles in aqueous PBS (pH = 7.4) at 37 ^{o}C and at a constant reaction time of 4.0 hours.

GPC traces for *P. fluorescens* lipase catalyzed degradation of MeO-PEG$_{45}$-*b*-PBO$_{0,9}$-*b*-PCL$_{60}$ micelles resulted in effectively the same distribution of water soluble hydrolysis products as those observed for the *P. cepacia* lipase catalysis (Figures 3.8, 3.9). ^{1}H NMR and GPC results for *P. fluorescens* and *P. cepacia* lipase catalyzed hydrolytic degradation of diblock and triblock copolymer micelles demonstrate that these two lipase enzymes have closely related binding and catalytic reactions with the micelles and constituent block copolymers.

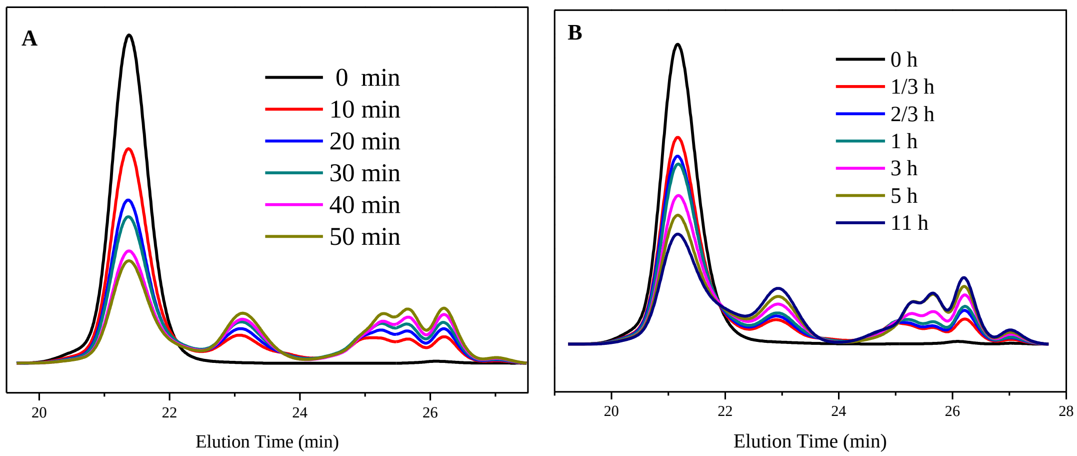

Figure 3.9: GPC traces for all the products from the *P. fluorescens* lipase catalyzed hydrolytic degradation of block copolymer micelles at 37°C, pH=7.4 and lipase activity of 3.0 U/mL. A) MeO-PEG$_{45}$-*b*-PCL$_{60}$ B) MeO-PEG$_{45}$-*b*-PBO$_9$-*b*-PCL$_{60}$.

3.2.8 Kinetics of *P. fluorescens* and *P. cepacia* lipase catalyzed hydrolysis of micelles from MeO-PEG$_{45}$-*b*-PBO$_n$-*b*-PCL$_{60}$ (n = 0, 6, 9) evaluated by GPC

The samples for GPC studies are obtained by freeze drying the aqueous PBS solutions used in the *P. fluorescens* and *P. cepacia* lipase catalyzed MeO-PEG$_{45}$-*b*-PBO$_n$-*b*-PCL$_{60}$ (n = 0, 6, 9) micelle degradations at a series of reaction times and then dissolving the entire sample in DMF to record the GPC traces (Figures 3.10-3.11). The DMF solutions for GPC analysis thus contain all of the constituents that are present during the enzyme catalyzed polymer micelle degradations which include the residual unreacted diblock MeO-PEG$_{45}$-*b*-PCL$_{60}$ or triblock copolymers MeO-PEG$_{45}$-*b*-PBO$_{6,9}$-*b*-PCL$_{60}$, enzyme, and all of the PEG and PCL units produced in the hydrolysis of the polymers. Kinetic measurements for the diblock and triblock copolymer hydrolytic degradation from observing the decrease in the intact block copolymer GPC intensity as a function of time are shown in Figures 3.10-3.11. The kinetic results obtained by GPC in Figure 3.9 shows that rate of *P. fluorescens* lipase catalyzed degradation of micelle from MeO-PEG$_{45}$-*b*-PBO$_9$-*b*-PCL$_{60}$ is much slower than that of MeO-PEG$_{45}$-*b*-PCL$_{60}$ micelle. Kinetic results from GPC for *P. cepacia* lipase catalyzed MeO-PEG$_{45}$-*b*-PBO$_n$-*b*-PCL$_{60}$ (n = 0, 6, 9) micelle degradations are almost identical to kinetic plots that are obtained by NMR (Figures 3.6, 3.11).

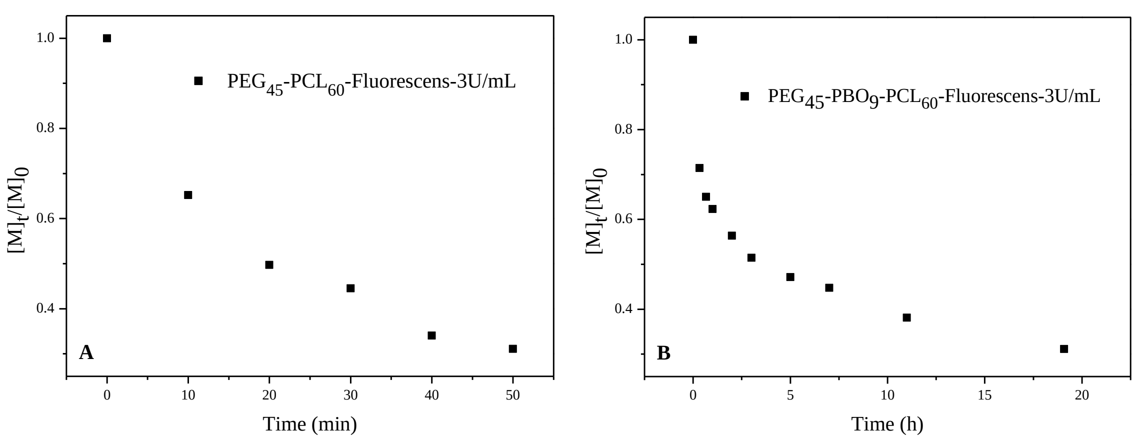

Figure 3.10: GPC kinetic plots for and *P. fluorescens* catalyzed degradation of block copolymer micelles (0.8 mg/mL) in aqueous PBS buffer (pH=7.4) at T=37 ^{o}C and enzyme activity of 3.0 U/mL; A) MeO-PEG$_{45}$-*b*-PCL$_{60}$ and B) MeO-PEG$_{45}$-*b*-PBO$_9$-*b*-PCL$_{60}$.

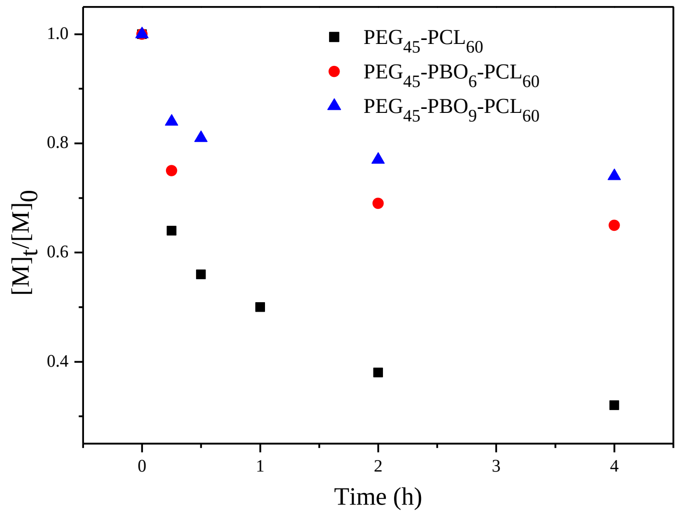

Figure 3.11: GPC kinetic plots for *P. cepacia* catalyzed degradation of MeO-PEG$_{45}$-*b*-PBO$_n$-*b*-PCL$_{60}$ (n = 0, 6, 9) block copolymer micelles in aqueous PBS buffer (pH=7.4) at T=37 ^{o}C and enzyme activity of 2.86 U/mL.

3.2.9 Equivalence of the kinetics for lipase catalyzed micelle degradation obtained by ^{1}H NMR and GPC

Kinetic analysis of the results from GPC and ^{1}H NMR provide complementary information on the rates at which the molecular block copolymer hydrolyzes and the micelle polymer assemblies degrade. The rate plot for hydrolytic fragmentation of the MeO-PEG$_{45}$-*b*-PCL$_{60}$ diblock and MeO-PEG$_{45}$-*b*-PBO$_9$-*b*-PCL$_{60}$ observed by GPC nearly superimposes on the rate plots for micelle degradation measured by ^{1}H NMR (Figure 3.12). Equivalence of the relative rates for block copolymer hydrolytic degradation by GPC and micelle degradation by ^{1}H NMR establishes the direct relationship between the quantities of micelles and intact block copolymers.

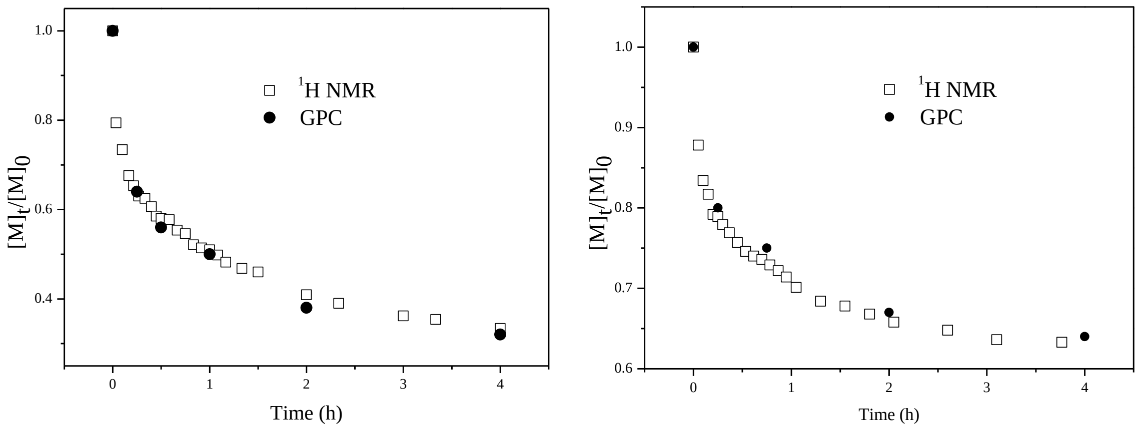

Figure 3.12: ^{1}H NMR and GPC kinetic plots for micelles from A) MeO-PEG$_{45}$-*b*-PCL$_{60}$, B) MeO-PEG$_{45}$-*b*-PBO$_9$-*b*-PCL$_{60}$ micelle degradation in aqueous PBS buffer (pH=7.4) at T=37 ^{o}C and *P. cepacia* activity of 2.86 U/mL.

3.2.10 ^{1}H NMR and GPC for lipase catalyzed degradation of MeO-PEG$_{45}$-*b*-PBO$_n$-*b*-PCL$_{60}$ (n= 0,9) micelles at reaction time ~70 h

The ^{1}H NMR after ~70 hours of reaction time at the high lipase activity shows that there is still about 35% of the triblock MeO-PEG$_{45}$-*b*-PBO$_9$-*b*-PCL$_{60}$ micelle (2.35 ppm) remaining while all of the MeO-PEG$_{45}$-*b*-PCL$_{60}$ micelles have been fully degraded into MeO-PEG$_{45}$OH, HO$(CH_2)_5$-C(O)O$(CH_2)_5$-CO_2H and 6-hydroxycaproic acid (HO$(CH_2)_5CO_2$H) (Figures 3.13). The relative rates of degradation for the two triblock copolymer (MeO-PEG$_{45}$-*b*-PBO$_n$-*b*-PCL$_{60}$, n = 6, 9) micelles are almost equal and both significantly slower than the MeO-PEG$_{45}$-*b*-PCL$_{60}$ diblock copolymer micelle degradation (Figure 3.6B). GPC traces for the two samples that reacted for ~70 hours demonstrate that *P. cepacia* lipase converts all of the MeO-PEG$_{45}$-*b*-PCL$_{60}$ into MeO-PEG$_{45}$OH, HO$(CH_2)_5$-C(O)O$(CH_2)_5$-CO_2H and 6-hydroxycaproic acid, during a time in which a substantial fraction of the triblock polymer MeO-PEG$_{45}$-*b*-PBO$_9$-*b*-PCL$_{60}$ remains intact (Figure 3.14, peak 1).

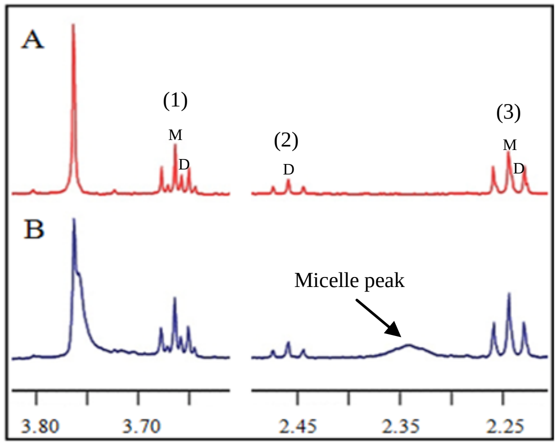

Figure 3.13: [1]H NMR for *P. cepacia* lipase catalyzed degradation of block copolymer micelles from (A) MeO-PEG$_{45}$-*b*-PCL$_{60}$ at an activity of 0.714 U/mL for 74 hours (B) MeO-PEG$_{45}$-*b*-PBO$_{9}$-*b*-PCL$_{60}$ at an activity of 2.86 U/mL for 70 hours (pH = 7.40, T = 37 ℃). [1]H NMR assignments for water soluble HO(CH$_2$)$_5$-C(O)O(CH$_2$)$_5$-CO$_2$H (D) and HO(CH$_2$)$_5$-CO$_2$H (M) degradation products: (1) terminal -*CH$_2$*-OH from both monomer and dimer; (2) -*CH$_2$*-C(O)O- from dimer; (3) terminal -*CH$_2$*-COOH from both monomer and dimer.

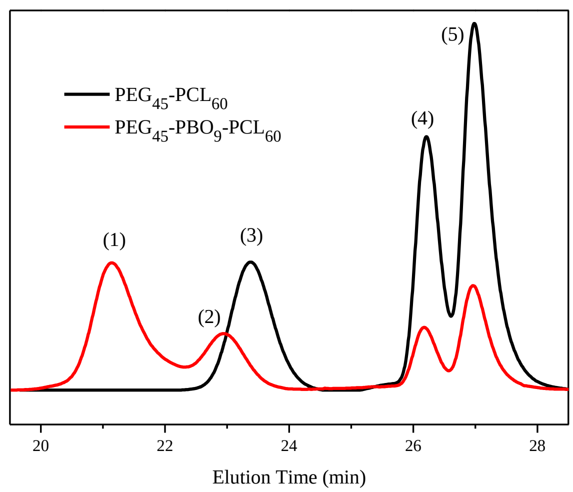

Figure 3.14: GPC traces for *P. cepacia* lipase catalyzed degradation of block copolymer micelles from MeO-PEG$_{45}$-*b*-PCL$_{60}$ at an activity of 0.714 U/mL for 74 hours (black curve) and MeO-PEG$_{45}$-*b*-PBO$_{9}$-*b*-PCL$_{60}$ at an activity of 2.86 U/mL for 70 hours (red curve) (pH =7.40, T= 37 ℃). GPC peak assignments: (1) PEG$_{45}$-*b*-PBO$_{9}$-*b*-PCL$_{60}$; (2) PEG$_{45}$-*b*-PBO$_{9}$-*b*-PCL$_{1\text{-}2}$; (3) PEG$_{45}$-*b*-PCL$_{1\text{-}2}$; (4) HO(CH$_2$)$_5$-C(O)O(CH$_2$)$_5$-CO$_2$H (Dimer); (5) HO(CH$_2$)$_5$-CO$_2$H (Monomer).

3.2.11 Inhibition of lipase enzyme by MeO-PEG$_{45}$-*b*-PBO$_n$-*b*-PCL$_{60}$ initial degradation products (n=0,6,9)

As lipase catalyzed degradation of the MeO-PEG$_{45}$-*b*-PCL$_{60}$, MeO-PEG$_{45}$-*b*-PBO$_6$-*b*-PCL$_{60}$ and MeO-PEG$_{45}$-*b*-PBO$_9$-*b*-PCL$_{60}$ block copolymer micelles proceed the reactions slow down very much with conversion than would be expected based on the initial rates (Figure 3.6). The shape of the relative micelle concentration versus time plots indicates that the enzyme activity is decreasing with time which could occur either by the enzyme protein being irreversibly denatured or through one or more of the reaction products inhibiting the enzyme-micelle reactions. The enzyme catalysis is at no time fully quenched as evidenced by slow micelle degradation and hydrolysis of the water soluble PCL oligomers continuing for days which ultimately produces 6-hydroxycaproic acid (Figures 3.13-3.14). Product inhibition of the lipase enzyme catalytic degradation of the block copolymer micelles could occur either by the reaction products binding in the lipase Ser-His-Asp triad[48-49] hydrolase active center and inhibiting the polyester in the micelle from entering the catalytic center or through formation of a new micelle from the reaction products that competes for enzyme binding[50].

Several of the reaction products including MeO-PEG$_{45}$-OH, 6-hydroxycaproic acid and MeO-PEG$_{45}$-*b*-PCL$_6$-OH were independently prepared and evaluated as inhibitors of lipase catalytic micelle degradation. The rate for *P. cepacia* lipase enzyme catalyzed MeO-PEG$_{45}$-*b*-PCL$_{60}$ micelle degradation was unchanged by addition of the MeO-PEG$_{45}$-OH and 6-hydroxycaproic acid, but PEG$_{45}$-*b*-PCL$_6$ (0.714mg/mL) was observed to have a strong inhibitory effect on both the *P. cepacia* and *P. fluorescens* catalyzed degradation of MeO-PEG$_{45}$-*b*-PCL$_{60}$ micelles (Figure 3.15). The magnitude of the observed inhibitory effect of MeO-PEG_{45}-*b*-PCL_6 is sufficient to explain the product inhibition of the micelle degradation. The MeO-PEG_{45}-*b*-PCL_6 product fragment quenches the initial fast reaction observed for all of the lipase enzyme- micelle systems and totally blocks the *P. cepacia* lipase catalyzed MeO-PEG_{45}-*b*-PCL_{60} micelle degradation during the first hour of reaction (Figure 3.15), and subsequently the micelle degradation occurs slowly. The PCL units in PEG_{45}-*b*-PCL_6 function as an ester substrate for *P. cepacia* lipase and the large PEG probably has binding interactions with the enzyme protein that block the catalytic site by retarding the PCL hydrolosis and movement out of the active center. Slow hydrolysis of MeO-PEG_{45}-*b*-PCL_6 ultimately produces MeO-PEG_{45}-OH and HO-$CH_2(CH_2)_4CH_2$-CO_2H which clears the lipase catalytic center for entrance of the micelle MeO-PEG_{45}-*b*-PCL_{60} polymers for hydrolysis and subsequent micelle degradation. Hydrolytic degradation of the MeO-PEG_{45}-*b*-$PBO_{6,9}$-*b*-PCL_{60} triblock copolymer micelles produce MeO-PEG_{45}-*b*-$PBO_{6,9}$-*b*-PCL_n ($n \leq 6$) fragments that have an inhibiting effect that is even larger than PEG_{45}-*b*-PCL_6. Larger enzyme inhibition is a major contributing factor for the MeO-PEG_{45}-*b*-PBO_6-*b*-PCL_{60} and MeO-PEG_{45}-*b*-PBO_9-*b*-PCL_{60} triblock copolymer micelles having substantially slower degradation than the diblock MeO-PEG_{45}-*b*-PCL_{60} micelles (Figure 3.6).

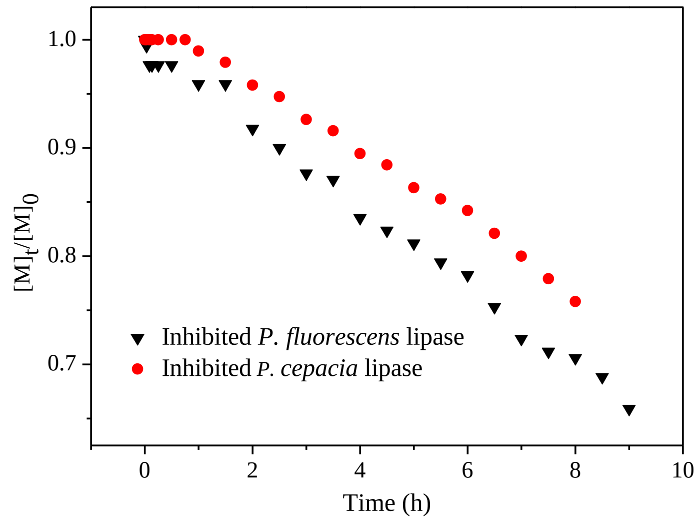

Figure 3.15: Inhibition of *P. cepacia* and *P. fluorescence* lipase (0.714 U/mL) catalyzed degration of MeO-PEG$_{45}$-*b*-PCL$_{60}$ by MeO-PEG$_{45}$-*b*-PCL$_{6}$ (0.714 mg/mL) in aqueous PBS buffer (pH=7.4) at T=37 ^{o}C.

3.2.12 Comparison of acid and lipase catalyzed PCL ester hydrolysis in MeO-PEG$_{45}$-*b*-PBO$_n$-*b*-PCL$_{60}$ (n = 0, 6, 9) block copolymer micelles

The importance of amphiphilic block copolymer micelles in the transport and release of therapeutics[11-16] has stimulated studies of acid[24-26], base[25, 27] and enzyme[25, 36-38] catalyzed hydrolysis of polyester micelle cores that trigger drug release. Acid and lipase catalyzed hydrolysis of ester groups from the PCL polyester segment in MeO-PEG$_{45}$-*b*-PBO$_n$-*b*-PCL$_{60}$ (n = 0, 6, 9) block copolymer micelles occur by distinctly different pathways and produce different products. In the acid catalyzed process the total number of micelles remains constant while the composition of each micelle changes, but in the lipase catalyzed process the micelles are fully degraded sequentially so that the number of micelle particles decreases while the composition of the remaining micelles is constant.

The initial event in acid catalyzed micelle ester hydrolysis occurs exclusively at the interface ester that joins the PCL_{60} polyester hydrophobic block with the more hydrophilic PEG_{45} and PEG_{45}-PBO_n (n = 6, 9) segments. Hydrolysis of the interface ester cleaves the block copolymer into PCL_{60} chains that are retained in the micelle core and water soluble PEG_{45} or PEG_{45}-PBO_n fragments enter the aqueous solution. There is a second phase of the hydrolysis in which 6-hydroxycaproic acid ($HO(CH_2)_5CO_2H$) is the exclusive observed product that most probably results from hydrolysis of the terminal ester groups of HO-PCL_n-CO_2H chains. As the micelles shed the water soluble PEG containing units in the acid catalyzed hydrolysis process, the composition of the micelles changes, but the number of micelle particles remains constant. Decrease in the ratio of PEG units in the corona to the PCL units in the core destabilizes the micelle dispersions, and micelle aggregation and precipitation occurs when about half of the corona is lost. The micelles are not fully degraded in solution by the acid catalyzed ester hydrolysis but rather form precipitates that subsequently are further degraded by slow heterogeneous hydrolysis. Lipase catalyzed micelle PCL ester hydrolysis is distinctly different from the acid catalyzed process. The initial step in lipase catalyzed process is the strong lipase-micelle binding that activates both the enzyme and the polyester core. Subsequent fast lipase catalyzed ester hydrolysis fully degrades the micelles to a set of small water soluble HO-PCL_m-CO_2H oligomers and one water soluble MeO-PEG_{45}-*b*-PCL_m-OH or MeO-PEG_{45}-*b*-PBO_n-*b*- PCL_m-OH ($m \leq 6$, n = 6, 9) fragments. The initial water soluble degradation products slowly hydrolyze into 6-hydroxycaproic acid ($HO(CH_2)_5CO_2H$) and MeO-PEG_{45}-OH or MeO-PEG_{45}-*b*-PBO_n-OH over a period of days. Observations that both the composition of the micelles from ^{1}H NMR and size of the micelles by DLS remain unchanged throughout the entire degradation process provides complementary direct evidence that the micelle particles react away sequentially[27, 36-37].

3.3 Summary

Enzyme catalyzed degradation of micelles from MeO-PEG_{45}-*b*-PBO_n-*b*-PCL_{60} (n=0,6,9) at different conditions were studied in this chapter to understand the kinetic and mechanistic differences between diblock and triblock copolymer micelles. ^{1}H NMR, GPC and DLS studies were used to evaluate the micelle and solution compositions, determine the kinetics of diblock and triblock copolymer micelle degradation and advance the mechanistic understanding for both the acid and lipase catalyzed processes.

The DLS results indicated that the average hydrodynamic diameters for micelles from the diblock and triblock copolymers are almost identical in value and effectively stay unchanged at 30 $\pm$4 nm during the entire period for the degradation processes to proceed to completion. ^{1}H NMR resonances for the micelles as the degradation proceeds is accompanied by appearance of sharp resonances for water soluble MeO-PEG_{45}-*b*-PBO_n-*b*-PCL_m (n= 0,6,9, m $\leq$ 6) fragments and a set of small PCL_m (m $\leq$ 6) oligomers that result from lipase catalyzed hydrolysis of MeO-PEG_{45}-*b*-PBO_n-*b*-PCL_{60} (n= 0,6,9, m $\leq$ 6) block copolymer chains in the micelle. The 6-hydroxycaproic acid monomer and MeO-PEG_{45}-OH is difficult to observe during the early portion of the lipase catalyzed micelle degradation, but they slowly accumulate from subsequent hydrolysis of the MeO-PEG_{45}-*b*-PBO_n-*b*-PCL_m fragments and PCL_m (m $\leq$ 6) oligomers. The average number of caprolactone units (n) in the PCL oligomers for cepacia, fluorescens and rugosa is 3.2, 3.2 and 1.4 respectively. ^{1}H NMR integration of the micelles indicates that the micelles compose primarily of intact MeO-PEG_{45}-*b*-PBO_n-*b*-PCL_{60} block copolymers throughout the entire micelle degradation process. The GPC traces of lipase catalyzed micelle degradation of demonstrates that the decrease in the concentrations of MeO-PEG_{45}-*b*-PBO_n-*b*-PCL_{60} block copolymers as the micelle degrades is accompanied by appearance of new peaks in the GPC corresponding to MeO-PEG_{45}-*b*-PBO_n-*b*-PCL_m ($m \leq 6$) and a set of relatively small PCL oligomers (PCL_m, $m \leq 6$). Near equivalence of the micelle degradation kinetics and relative rates for block copolymer hydrolytic degradation by GPC and ^{1}H NMR establishes the direct relationship between the quantities of micelles and intact block copolymers. Observations that both the composition of the micelles from ^{1}H NMR and size of the micelles by DLS remain the same during the entire degradation process provide complementary direct evidence that the micelle particles react away sequentially.

The initial acid catalyzed micelle ester hydrolysis occurs exclusively at the interface ester that joins the PCL_{60} polyester hydrophobic block with the more hydrophilic MeO-PEG_{45} and MeO-PEG_{45}-PBO_n (n = 6, 9) segments, but the initial lipase catalyzed micelle degradation products is MeO-PEG_{45} with several PCL units on it.

Both esterase and lipase enzymes are capable of catalyzing the hydrolysis of water soluble esters, but lipase enzymes have the exclusive property of being highly activated through binding with assemblies of ester substrates such as membranes and vesicles dispersed in water by a process called enzyme interfacial activation. ^{1}H NMR and GPC results for *P. fluorescens* and *P. cepacia* lipase catalyzed hydrolytic degradation of micelles from MeO-PEG_{45}-*b*-PBO_n-*b*-PCL_{60} (n=0,6,9) demonstrate that these two lipase enzymes have closely related binding and catalytic reactions with the micelles and constituent block copolymers.

MeO-PEG$_{45}$-OH and 6-hydroxycaproic acid were proved to have no effects on reduce the rate of lipase catalyzed MeO-PEG$_{45}$-*b*-PCL$_{60}$ micelle degradation, but PEG$_{45}$-*b*-PCL$_{6}$ was observed to have a strong inhibitory effect on both the *P. cepacia* and *P. fluorescens* catalyzed degradation of MeO-PEG$_{45}$-*b*-PCL$_{60}$ micelles. The significant inhibitory effect of MeO-PEG$_{45}$-*b*-PCL$_{6}$ is sufficient to explain the product inhibition of the micelle degradation. Product inhibition of the lipase enzyme catalytic degradation of the block copolymer micelles could occur by the MeO-PEG$_{45}$-*b*-PCL$_{6}$ binding in the lipase Ser-His-Asp triad active center and inhibiting the polyester in the micelle core from entering the catalytic center.

Insertion of a relatively short hydrophobic PBO chain between the hydrolyzable hydrophobic polyester (PCL) core and the non-hydrolyzable hydrophilic (PEG) corona was designed to move the water-micelle interface away from the PCL core and increase the barrier for PCL ester hydrolysis. Kinetic plots at two enzyme concentrations for the lipase catalyzed hydrolysis of the block copolymer micelles show that substantially more MeO-PEG$_{45}$-*b*-PBO$_{6,9}$-*b*-PCL$_{60}$ triblock copolymer micelles compared to micelles from the MeO-PEG$_{45}$-*b*-PCL$_{60}$ diblock copolymer remain intact after 5 hours of reaction time. Micelles from the MeO-PEG$_{45}$-*b*-PBO$_{n}$-*b*-PCL$_{60}$ (n = 6, 9) react slower and persist intact much longer in the presence of lipase enzymes than micelles generated from the parent diblock copolymer (MeO-PEG$_{45}$-*b*-PCL$_{60}$). Larger enzyme inhibition is a major contributing factor for the MeO-PEG$_{45}$-*b*-PBO$_{6}$-*b*-PCL$_{60}$ and MeO-PEG$_{45}$-*b*-PBO$_{9}$-*b*-

PCL_{60} triblock copolymer micelles having substantially slower degradation than the diblock MeO-PEG_{45}-*b*-PCL_{60} micelles.

Therefore, the strategy of inserting of a relatively short hydrophobic PBO chain between the hydrolyzable hydrophobic polyester (PCL) core and the non-hydrolyzable hydrophilic (PEG) corona was observed substantial decrease in the rate of catalyzed interfacial ester hydrolysis represents an experimental fulfillment of obtaining an increased barrier for water to reach the interfacial ester position in triblock PEG_{45}-*b*-PBO_n-*b*-PCL_{60} (n = 6, 9) compared to PEG_{45}-*b*-PCL_{60} diblock copolymer micelles. The same strategy doesn't have significant effects on slowing the lipase enzyme catalyzed degradation of MeO-PEG-*b*-PCL micelles.

3.4 Experimental Section

3.4.1 Materials

Methoxy poly (ethylene glycol) (PEG, Mn = 2000, Mw/Mn = 1.06, Sigma Aldrich) was purified by precipitating from petroleum ether prior to use. ε-Caprolactone (CL) (99%, TCI America) and 1,2-butylene Oxide (BO) (Sigma Aldrich) were dried over CaH_2 and distilled prior to use. Phosphate buffered saline tablet, 18-Crown-6-ether and Stannous Octoate ($Sn(Oct)_2$) were used as received from Sigma Aldrich. Potassium naphthalenide THF solution (0.89 M) was prepared by mixing of naphthalene (3.0 g), potassium (0.92 g) and THF (26 mL) in a flask. Concentrated hydrochloric acid (12 M, Fisher scientific) Lipase from *P. cepacia* (37.8 U/mg), Lipase from *P. fluorescens* (42 U/mg), *C. rugosa* (22.8 U/mg), esterase from porcine liver (≥15 U/mg), Proteinase K from Tritirachium album (≥ 30 U/mg) and Phospholipase A2 from honey bee venom (1956 U/mg) were used as received from Sigma Aldrich. SnakeSkin Dialysis tubing (10K MWCO, 35mm dry I.D., 35 feet) was used for dialysis. Acetone and methanol were use as received from J.T. Baker. Dimethylformamide (DMF, HPLC grade, 99.7% +, Alfa Aesar) was used as GPC eluent.

3.4.2 Analytical techniques

^{1}H NMR spectra were obtained using Bruker 500 MHz spectrometer with $CDCl_3$ and D_2O as NMR solvent media. ^{1}H NMR data were analyzed by using the Bruker Topspin 2.1 software. Water suppressed ^{1}H NMR spectra of block copolymer micelles in buffer solutions containing 10% of D_2O were acquired using presaturation of water with 50 dB attenuation. The ^{1}H NMR covered a spectral window of -5.0 ppm to 15.0 ppm. The excitation relaxation delay was set to 5 s. Each NMR spectrum was collected from accumulation of 24 scans.

Gel permeation chromatography (GPC) measurements were carried out using a Shimadzu LC-20AV liquid chromatography system equipped with three linear PolarGel-M 300×7.5 mm columns, a RID-10A differential refractive index detector and a SPD-20AV UV/VIS detector. Data were analyzed by Shimadzu LCsolution software. DMF was used as the eluent at a flow rate of 1.0 mL/min at 50 ℃. Molecular weight calibrations were based on narrow peak width polystyrene standards from Polymer Laboratories.

Dynamic Light Scattering (DLS). Hydrodynamic diameters of micelles were measured by a Zetasizer Nano ZS (Malvern Instruments, Westborough, MA) at 25 ℃/

37 ℃, using 1 cm polystyrene sample cuvettes. The mean diameters were obtained by use of the DTS software using the volume measurements.

3.4.3 DLS for lipase catalyzed degradation of MeO-PEG$_{45}$-*b*-PBO$_n$-*b*-PCL$_{60}$ (n = 0, 6, 9) block copolymer micelle

DLS of a MeO-PEG$_{45}$-*b*-PBO$_n$-*b*-PCL$_{60}$ (n = 0, 6, 9) micelle sample during the *P. cepacia* lipase catalyzed degradation was observed at a lipase activity of 2.86 U/mL, pH = 7.4 and T = 37 ℃ in PBS buffer solution using a 1 cm polystyrene cuvette. The micelle suspension of MeO-PEG$_{45}$-*b*-PBO$_n$-*b*-PCL$_{60}$ (n = 0, 6, 9) (0.714 mL, 1.0 mg/mL) was added into the cuvette to redissolve the air dried PBS salts. The micelle dispersion in the PBS salt solution was warmed to 37 ℃ in the water bath and *P. cepacia* lipase water solution (0.286 mL, 0.265 mg/mL) was then added into the cuvette quickly. The hydrodynamic diameter of the particles was monitored by DLS at 37 ℃ every 15 minutes.

3.4.4 ^{1}H NMR for lipase enzyme catalyzed hydrolysis and degradation of micelles from MeO-PEG$_{45}$-*b*-PBO$_n$-*b*-PCL$_{60}$ (n = 0, 6, 9) block copolymers

The *P. cepacia* lipase catalyzed degradation of micelles from MeO-PEG$_{45}$-*b*-PBO$_n$-*b*-PCL$_{60}$ (n = 0, 6, 9) block copolymers were studied at two lipase activities (0.714 and 2.86 U/mL), pH=7.4 and T=37 ℃**.** PBS buffer solution (0.70 mL, pH = 7.4) was evaporated to dryness by air in a vial. A micelle suspension (0.50 mL, 1.0 mg/mL) and D_2O (0.10 mL) was added into the vial to redissolve the PBS salts. A solution of micelle with dissolved PBS salt was transferred into a NMR tube and the solution was heated to 37 ℃ in the NMR instrument. *P. cepacia* lipase water solution (0.10 mL, 0.132 mg/mL or 0.530 mg/mL) was added into the NMR tube quickly to catalyze the hydrolysis of MeO-

PEG_{45}-*b*-PBO_n-*b*-PCL_{60} (n = 0, 6, 9) micelle. The degradation of micelle was followed by ^1H NMR at 37 ℃. Water solvent suppressed NMR was used in this experiment.

3.4.5 GPC tracesfor lipase enzyme catalyzed hydrolysis and degradation of micelles from MeO-PEG_{45}-*b*-PBO_n-*b*-PCL_{60} (n = 0, 6, 9) block copolymers

GPC traces for the *P. cepacia* lipase catalyzed degradation of MeO-PEG_{45}-*b*-PBO_n-*b*-PCL_{60} (n = 0, 6, 9) were studied at lipase activity of 2.86 U/mL, pH = 7.4 and T = 37 ℃. The experiments were done in a series of vials for different degradation times. PBS buffer solution (1.0 mL, pH = 7.4) was predried by air in each 5 mL vial. A micelle suspension of MeO-PEG_{45}-*b*-PBO_n-*b*-PCL_{60} (n = 0, 6, 9) (0.714 mL, 1.0 mg/mL) was added into the vial to redissolve the PBS salts. The solution of micelle with dissolved PBS salt was warmed to 37 ℃ in the water bath. Subsequently, *P. cepacia* lipase water solution (0.286 mL, 0.265 mg/mL) was added into the vials. The reactions were terminated at different times by dipping the vials into liquid N_2. Degradation products were collected by freeze drying method and redissolved in DMF for GPC studies.

3.4.6 ^1H NMR for lipase catalyzed degradation of MeO-PEG_{45}-*b*-PCL_{60} block copolymer micelles at the presence of MeO-PEG_{45}-*b*-PCL_6 inhibitor

MeO-PEG_{45}-*b*-PCL_6 diblock copolymer was prepared followed the same procedure as making MeO-PEG_{45}-*b*-PCL_{60} diblock copolymer. The lipase catalyzed degradation of PEG_{45}-*b*-PCL_{60} micelle inhibited by MeO-PEG_{45}-*b*-PCL_6 was studied at lipase activity of 0.714 U/mL, pH=7.4 and T=37 ^oC. PBS buffer solution (0.70 mL, pH=7.4) was predried by air in a vial. A micelle suspension of MeO-PEG_{45}-*b*-PCL_{60} (0.50 mL, 1.0 mg/mL) and D_2O (0.10 mL) was added into the vial to redissolve the PBS salts. A solution of micelle with dissolved PBS salt was transferred into the NMR tube and the solution was heated to 37 ^{o}C in the NMR instrument. Stock aqueous solution (0.10 mL) that contains *P. cepacia* lipase (0.132 mg/mL) and MeO-PEG$_{45}$-*b*-PCL$_{6}$ (5.0 mg/mL) was added into the NMR tube quickly to catalyze the hydrolysis of MeO-PEG$_{45}$-*b*-PCL$_{60}$ micelle. The degradation of micelle was followed by ^{1}H NMR at 37 ^{o}C. DMF was introduced into the NMR tube as internal reference. Water solvent suppressed NMR was used in this experiment.

3.5 References

(1) Tyrrell, Z. L.; Shen, Y.; Radosz, M. *Prog. Polym. Sci.* 2010, 35, 1128-1143.

(2) Zhang, Q.; Remsen, E. E.; Wooley, K. L. *J. Am. Chem. Soc.* 2000, 122, 3642-3651.

(3) Hickey, R. J.; Haynes, A. S.; Kikkawa, J. M.; Park, S.-J. *J. Am. Chem. Soc.* 2011, 133, 1517-1525.

(4) Zhu, W.; Nese, A.; Matyjaszewski, K. *J. Polym. Sci., Part A: Polym. Chem.* 2011, 49, 1942-1952.

(5) Lee, H.-i.; Wu, W.; Oh, J. K.; Mueller, L.; Sherwood, G.; Peteanu, L.; Kowalewski, T.; Matyjaszewski, K. *Angew. Chem. Int. Ed.* 2007, 46, 2453-2457.

(6) Discher, B. M.; Won, Y.-Y.; Ege, D. S.; Lee, J. C.-M.; Bates, F. S.; Discher, D. E.; Hammer, D. A. *Science* 1999, 284, 1143-1146.

(7) Zhang, X.; Cheng, J.; Wang, Q.; Zhong, Z.; Zhuo, R. *Macromolecules* 2010, 43, 6671-6677.

(8) Geng, Y.; Discher, D. E. *J. Am. Chem. Soc.* 2005, 127, 12780-12781.

(9) Mai, Y.; Eisenberg, A. *Chem. Soc. Rev.* 2012, 41, 5969-5985.

(10) Rajagopal, K.; Mahmud, A.; Christian, D. A.; Pajerowski, J. D.; Brown, A. E. X.; Loverde, S. M.; Discher, D. E. *Macromolecules* 2010, 43, 9736-9746.

(11) Langer, R.; Tirrell, D. A. *Nature* 2004, 428, 487-492.

(12) Elsabahy, M.; Wooley, K. L. *Chem. Soc. Rev.* 2012, 41, 2545-2561.

(13) Endres, T. K.; Beck-Broichsitter, M.; Samsonova, O.; Renette, T.; Kissel, T. H. *Biomaterials* 2011, 32, 7721-7731.

(14) Zhu, Z.; Li, Y.; Li, X.; Li, R.; Jia, Z.; Liu, B.; Guo, W.; Wu, W.; Jiang, X. *J. Controlled Release* 2010, 142, 438-446.

(15) Aliabadi, H. M.; Mahmud, A.; Sharifabadi, A. D.; Lavasanifar, A. *J. Controlled Release* 2005, 104, 301-311.

(16) Kataoka, K.; Harada, A.; Nagasaki, Y. *Adv. Drug Deliv. Rev.* 2001, 47, 113-131.

(17) Ensign, L. M.; Schneider, C.; Suk, J. S.; Cone, R.; Hanes, J. *Adv. Mater.* 2012, 24, 3887-3894.

(18) Shuvaev, V. V.; Ilies, M. A.; Simone, E.; Zaitsev, S.; Kim, Y.; Cai, S.; Mahmud, A.; Dziubla, T.; Muro, S.; Discher, D. E.; Muzykantov, V. R. *ACS Nano* 2011, 5, 6991-6999.

(19) Bae, Y. H.; Yin, H. *J. Controlled Release* 2008, 131, 2-4.

(20) Read, E. S.; Armes, S. P. *Chem. Commun.* 2007, 3021-3035.

(21) Xiong, J.; Meng, F.; Wang, C.; Cheng, R.; Liu, Z.; Zhong, Z. *J. Mater. Chem.* 2011, 21, 5786-5794.

(22) Samarajeewa, S.; Shrestha, R.; Li, Y.; Wooley, K. L. *J. Am. Chem. Soc.* 2011, 134, 1235-1242.

(23) Howard, M. D.; Lu, X.; Rinehart, J. J.; Jay, M.; Dziubla, T. D. *Langmuir* 2012, 28, 12030-12037.

(24) Hu, Y.; Zhang, L.; Cao, Y.; Ge, H.; Jiang, X.; Yang, C. *Biomacromolecules* 2004, 5, 1756-1762.

(25) Jiang, Z.; Zhu, Z.; Liu, C.; Hu, Y.; Wu, W.; Jiang, X. *Polymer* 2008, 49, 5513-5519.

(26) Shen, C.; Guo, S.; Lu, C. *Polym. Adv. Technol.* 2008, 19, 66-72.

(27) Hu, Y.; Jiang, Z.; Chen, R.; Wu, W.; Jiang, X. *Biomacromolecules* 2010, 11, 481-488.

(28) Nie, T.; Zhao, Y.; Xie, Z.; Wu, C. *Macromolecules* 2003, 36, 8825-8829.

(29) Li, S.; Garreau, H.; Pauvert, B.; McGrath, J.; Toniolo, A.; Vert, M. *Biomacromolecules* 2002, 3, 525-530.

(30) D'Addio, S. M.; Saad, W.; Ansell, S. M.; Squiers, J. J.; Adamson, D. H.; Herrera-Alonso, M.; Wohl, A. R.; Hoye, T. R.; Macosko, C. W.; Mayer, L. D.; Vauthier, C.; Prud'homme, R. K. *J. Controlled Release* 2012, 162, 208-217.

(31) Zhu, X.; Fryd, M.; Tran, B. D.; Ilies, M. A.; Wayland, B. B. *Macromolecules* 2012, 45, 660-665.

(32) Giacomelli, F. C.; Stepanek, P.; Schmidt, V.; Jager, E.; Jager, A.; Giacomelli, C. *Nanoscale* 2012, 4, 4504-4514.

(33) Noh, T.; Kook, Y. H.; Park, C.; Youn, H.; Kim, H.; Oh, E. T.; Choi, E. K.; Park, H. J.; Kim, C. *J. Polym. Sci., Part A: Polym. Chem.* 2008, 46, 7321-7331.

(34) Nagasaki, Y.; Yasugi, K.; Yamamoto, Y.; Harada, A.; Kataoka, K. *Biomacromolecules* 2001, 2, 1067-1070.

(35) Dobrovolskaia, M. A.; McNeil, S. E. *Nat. Nanotechnol.* 2007, 2, 469-478.

(36) Lam, H.; Gong, X.; Wu, C. *J. Phys. Chem. B* 2007, 111, 1531-1535.

(37) Gan, Z.; Jim, T. F.; Li, M.; Yuer, Z.; Wang, S.; Wu, C. *Macromolecules* 1999, 32, 590-594.

(38) Carstens, M. G.; van Nostrum, C. F.; Verrijk, R.; de Leede, L. G. J.; Crommelin, D. J. A.; Hennink, W. E. *J. Pharm. Sci.* 2008, 97, 506-518.

(39) Kim, K. K.; Song, H. K.; Shin, D. H.; Hwang, K. Y.; Suh, S. W. *Structure* 1997, 5, 173-185.

(40) Schrag, J. D.; Li, Y.; Cygler, M.; Lang, D.; Burgdorf, T.; Hecht, H.-J.; Schmid, R.; Schomburg, D.; Rydel, T. J.; Oliver, J. D.; Strickland, L. C.; Dunaway, C. M.; Larson, S. B.; Day, J.; McPherson, A. *Structure* 1997, 5, 187-202.

(41) Bornscheuer, U. T. *FEMS Microbiol. Rev* 2002, 26, 73-81.

(42) Chahinian, H.; Nini, L.; Boitard, E.; Dubès, J.-P.; Comeau, L.-C.; Sarda, L. *Lipids* 2002, 37, 653-662.

(43) Chahinian, H.; Fantini, J.; Garmy, N.; Manco, G.; Sarda, L. *Biochim. Biophys. Acta* 2010, 1801, 1195-1204.

(44) Berg, O. G.; Gelb, M. H.; Tsai, M.-D.; Jain, M. K. *Chem. Rev.* 2001, 101, 2613-2654.

(45) Schmid, R. D.; Verger, R. *Angew. Chem. Int. Ed.* 1998, 37, 1608-1633.

(46) Berg, O. G.; Gelb, M. H.; Tsai, M.-D.; Jain, M. K. *Chemical Reviews* 2001, 101, 2613-2654.

(47) Bornscheuer, U.; Reif, O.-W.; Lausch, R.; Freitag, R.; Scheper, T.; Kolisis, F. N.; Menge, U. *Biochim. Biophys. Acta* 1994, 1201, 55-60.

(48) Takano, Y.; Houk, K. N. *J. Phys. Chem. A* 2004, 108, 11740-11751.

(49) Torre, O.; Alfonso, I.; Gotor, V. *Chem. Commun.* 2004, 1724-1725.

(50) Berg, O. G.; Yu, B. Z.; Rogers, J.; Jain, M. K. *Biochemistry* 1991, 30, 7283-7297.

CHAPTER 4:

KINETIC AND MECHANISTIC STUDIES OF LIPASE-MICELLE BINDING AND CATALYTIC DEGRADATION: ENZYME INTERFACIAL ACTIVATION

4.1 Introduction

Carboxyl ester hydrolases are categorized as either esterases or lipases where both have activity with water soluble esters, but only lipases have the capability to catalyze the hydrolysis of lipid ester groups in water insoluble aggregates like membranes and vesicles[1-3]. Lipases can be distinguished from esterases by the phenomenon of interfacial activation, which is the unique characteristic of the lipase. The water soluble lipases were found to first bind to the oil-water interfaces and activate specifically at the interface through a conformation change followed by the substrates catalytic hydrolysis[4] (Figure 4.1).

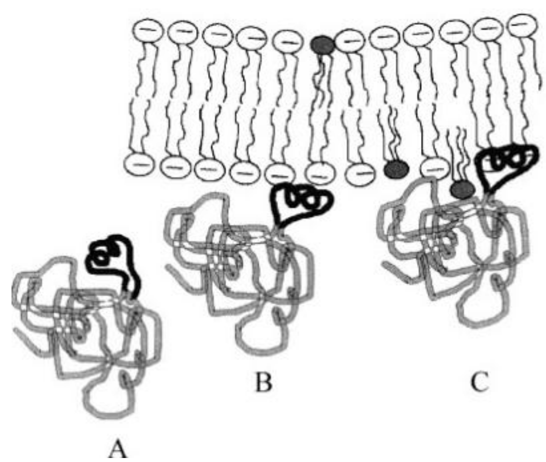

Figure 4.1: Schematic demonstration of the process of lipase interfacial activation: free lipase in solution (A); lipase activates at oil-water interface (B); catalytic substrate hydrolysis (C).

P. cepacia lipase is the main lipase that was selected for our micelle degradation studies with following reasons: i) it remains its activity in solution for a long time; ii) its structure and properties had been well studied; iii) it is commercially available and has high water solubility. The molecular weight *P. cepacia* lipase was reported at 34.1 K Da[5] and the isoelectric point of the *P. cepacia* lipase was determined to be 5.1[6]. The isoelectric point is the pH at which a particular molecule or surface carries no net electrical charge. At a pH below 5.1, the lipase carries a net positive charge and at the pH above 5.1, the lipase carries a net negative charge. The pure lipase has a esterase activity of 5800 U/mg[5]. The lipase activity of commercial lipase is directly related to the concentration of the lipase. 1 U of activity of lipase corresponds to the amount of lipase which liberates 1 μmol oleic acid per minute at pH = 8.0 and T = 40 ℃ using triolein as substrate (Fluka No. 62314).

In the 3D-structures of the *P. cepacia* lipase with an opened conformation[7] (Figure 4.2), the active site pocket, which contains the catalytic Ser-His-Asp triad active center[8-9] is buried under an helical loop (lid) which prevents access of the substrate. When the lipase binds to the hydrophilic-hydrophobic interface of the substrates, the lid has to move away and expose the active site to the substrate molecule (Figure 4.1). It was suggested that the movement of the lid was triggered by the interfacial binding of the lipase to hydrophilic-hydrophobic interface and was related the interfacial activation of the lipase[10].

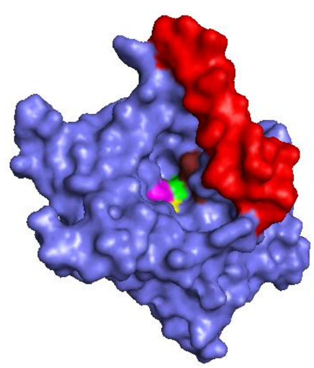

Figure 4.2: 3D structure of *P. cepacia* lipase with an opened conformation plotted by PyMOL, the Ser-His-Asp triad active site is highlighted in red yellow and green, the lid structure is in red color.

Aggregates of synthetic polyesters in aqueous suspensions[11], thin films[12], crystals[13] and nanoparticles[14] can also function as substrates for lipase enzymes. Poly (ethylene glycol) (PEG) block poly (ε-caprolactone) (PCL)[15-18] are prototypical amphiphilic block copolymers[19-20] that self-assemble into core-shell micelles[21-24] in water where the hydrolytically non-degradable hydrophilic segment (PEG) forms the exterior corona and the core contains the hydrolytically degradable hydrophobic block (PCL). Block copolymer micelles have a variety of biomedical applications[25-27], and are particularly prominent as drug and gene delivery vehicles[28-30] that function through their capability for loading, transport and release of lipophilic substances incorporated in the hydrophobic core. Development of strategies for selective release of micelle transported therapeutics motivates a growing effort to explore the mechanistic origins of micelle degradation[17,31-35].

Several lipase enzymes have been observed to catalyze polyester hydrolysis and degradation of micelles derived from water insoluble PEG-*b*-PCL block copolymers[15-16, 36-37]. Techniques previously applied in studying micelle degradations have typically utilized bulk properties of the system such as changes in light scattering[15-16, 38] that do not directly identify and quantify the micelle composition and concentration. This chapter mainly focuses on advancing mechanistic understanding of the *P. cepacia* lipase[7-8] catalyzed PEG_{45}-*b*-PCL_{60} micelle degradation primarily through using ^1H NMR observations of micelle dispersions. Application of ^1H NMR provides a comprehensive direct experiment to evaluate relative micelle concentrations, composition, and degradation kinetics, as well as identification and quantification of the water soluble hydrolysis products. Complementary GPC studies give the relative concentrations of intact block copolymers in the micelles and the products from lipase catalyzed polyester hydrolysis. The small spherical micelle particles dispersed in aqueous media are treated as pseudo-molecules that conform to the law of mass action in equilibrium and rate expressions for the lipase-micelle reaction system. Analysis and simulation of the concentration versus time profiles for *P. cepacia* lipase catalyzed PEG_{45}-*b*-PCL_{60} micelle degradation show that the process conforms to a Michaelis-Menten mechanism ($E + M \rightleftharpoons EM \rightarrow P + E$) with enzyme-micelle complex product inhibition ($EM + P \rightleftharpoons EMP$). A new model for lipase catalyzed micelle degradation is proposed based on analysis and interpretation of the experimental results. Formation and tight binding of the lipase enzyme-micelle complex, activation of lipase catalysis and sequential micelle degradation are characteristics of PEG_{45}-*b*-PCL_{60} micelle degradation which parallel features of enzyme interfacial activation[39-42] associated with native lipase catalyzed lipid membrane hydrolysis[43-48].

4.2 Results and Discussion

4.2.1 ^{1}H NMR for MeO-PEG_{45}-*b*-PCL_{60} diblock copolymer micelles

Narrowly size dispersed 30 $\pm$ 1 nm (pH = 7.4, T = 37 ^{o}C) spherical micelles were prepared from diblock copolymer (PDI = 1.08) which has a much lower polydispersity than MeO-PEG-*b*-PCL diblock copolymers used in prior micelle degradation studies[15-16]. The 30 $\pm$ 1 nm micelles form stable dispersions of particles with a mass of 2.0 $\pm 0.5 \times 10^6$ Da evaluated by Debye plots[49] from light scattering measurements. ^{1}H NMR spectra for the 30(1) nm micelles in aqueous PBS buffer dispersions are also similar to homogeneous solutions of molecules where the hydrogen resonances for the polymer chains in the micelle dispersions are broadened compared to water soluble small molecules, but all of the resonances are readily observed and fully assigned (Figure 4.3). The line width for the resonance of the more mobile exterior shell PEG units (5.4 Hz) is smaller than the value for the less exposed and less mobile CH_2 groups for the PCL segment in the micelle core (~10 Hz). The relatively small micelle diameter (30 nm) and thermal motions of the polymer chains within the micelles are sufficient to give substantial averaging of the local dipolar magnetic interactions[50]. NMR is usually applied to solution species rather than dispersions of particles in fluid media, but there are precedents where NMR has been used effectively to study dispersions of small particles like liposomes and vesicles[51-53].

^{1}H NMR of the terminal -CH_2OH (3.67 ppm) of the PCL oligomers shows that *P. cepacia* catalyzes the hydrolysis the PCL chains into a series of PCL fragments PCL_n (n = 1-6) (Figure 4.4) in which 6-hydroxycaproic acid ($HO(CH_2)_5CO_2H$) is effectively absent during the first hour of the PCL hydrolysis. Subsequent hydrolysis of the PCL oligomers which proceed in solution even after the micelles have fully reacted away produces 6-hydroxycaproic acid as the final product of hydrolysis of the PCL_{60} segment (Figure 4.4). ^{1}H NMR spectra that demonstrates the whole process of lipase catalyzed degradation of MeO-PEG_{45}-*b*-PCL_{60} micelles are stacked in Figure 4.5. The fast initial micelle degradation happens within the first hour. Then it takes about 38 hours to hydrolyze rest of the micelles into water soluble products (MeO-PEG-PCL_{0-6}, PCL_{0-6}) due to the lipase product inhibition. Eventually, these water soluble products will be hydrolyzed into MeO-PEG-OH and $HO(CH_2)_5CO_2H$ (6-hydroxycaproic acid, monomer).

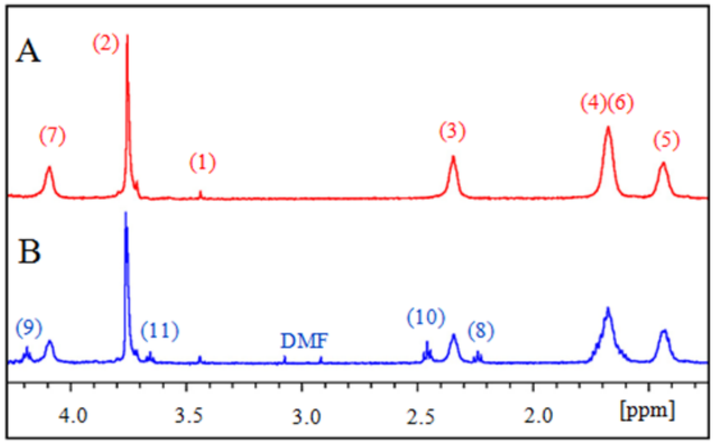

Figure 4.3: ^{1}H NMR (500 MHz) of MeO-PEG$_{45}$-*b*-PCL$_{60}$ block copolymer micelles (0.714 mg/mL) with PBS buffer (pH = 7.4;T = 37 ℃) : (A) ^{1}H NMR assignments for micelle peaks:CH$_3$(1)O-[CH$_2$CH$_2$(2)-O-]$_{45}$[C(O) CH$_2$(3)CH$_2$(4)CH$_2$(5)CH$_2$(6)CH$_2$(7)-O]$_{60}$C(O)(CH$_2$)$_5$OH. (B) Micelle with *P. cepacia* lipase at an activity of 0.714 U/mL, and a reaction time of 1.0 hour. ^{1}H NMR assignments for diagnostic hydrogens in PCL oligomers: HOC(O)CH$_2$(8) (CH$_2$)$_3$CH$_2$(9) O[C(O)CH$_2$(10) (CH$_2$)$_3$CH$_2$(9) O]$_n$C(O)CH$_2$(10) (CH$_2$)$_3$ CH$_2$(11)OH, the chemical shifts in ppm for each assignment are as follow: δ(1)=3.45; δ(2)=3.76; δ(3)=2.35; δ(4,6)=1.70; δ(5)=1.45; δ(7)=4.10; δ(8)~2.25; δ(9)~4.19; δ(10)~2.46; δ(11)~3.67.

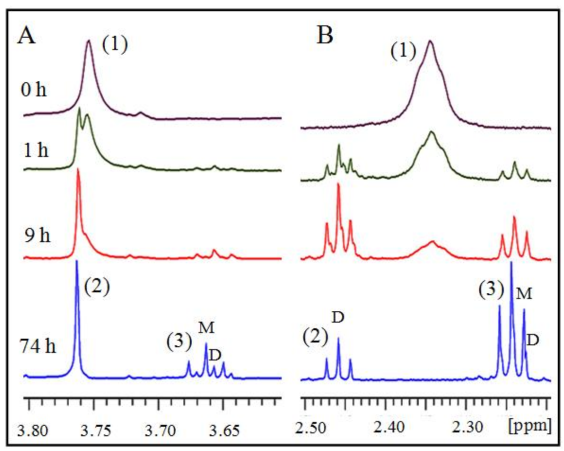

Figure 4.4: ^{1}H NMR (500 MHz) of MeO-PEG$_{45}$-*b*-PCL$_{60}$ block copolymer micelles (0.714 mg/mL) in PBS buffer(pH=7.4) at T=37 ℃ with *P. cepacia* lipase at an activity of 0.714 U/mL at a series of reaction times (M= HO(CH$_2$)$_5$-CO$_2$H; D=HO(CH$_2$)$_5$-C(O)O(CH$_2$)$_5$-CO$_2$H); (A) PEG segment in the micelle (1A) and water soluble PEG fragment from hydrolysis (PEG$_{45}$-PCL$_n$ (n=0-6)) (2A) and the -*CH$_2$*OH terminal groups for the PCL oligomers (3A). (B) Ester -*CH$_2$*-C(O)-O-hydrogens of PEG-*b*-PCL diblock copolymer micelles (1B) and ester-*CH$_2$*-C(O)-O- (2B) and terminal *CH$_2$*CO$_2$H (3B) for water soluble PCL oligomers.

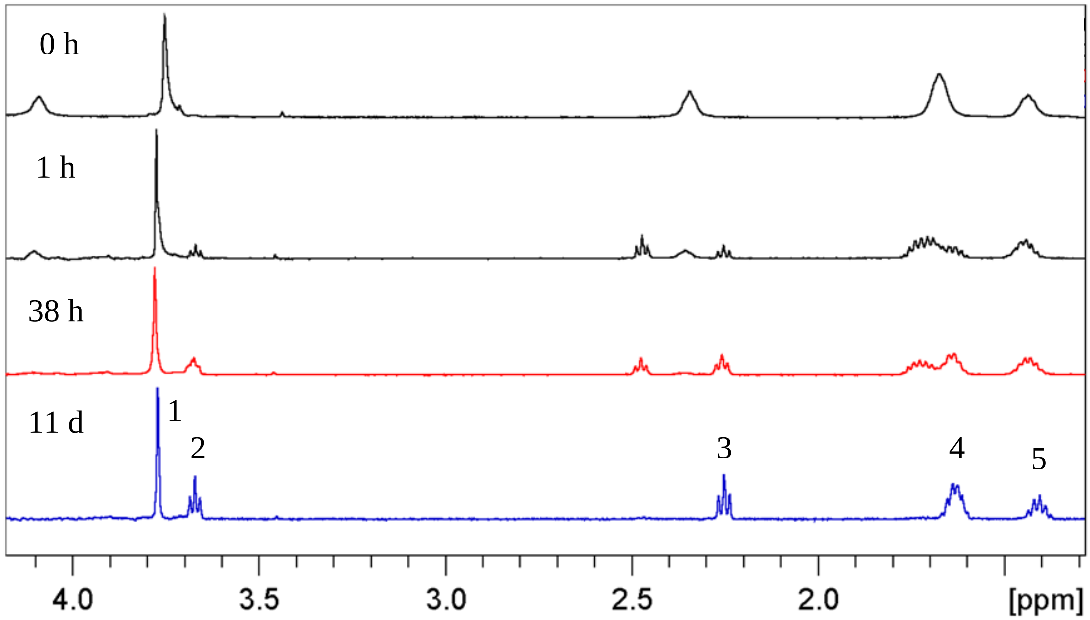

Figure 4.5: ^{1}H MNR of lipase catalyzed degradation of MeO-PEG$_{45}$-*b*-PCL$_{60}$ block copolymer micelles over 11 days at lipase activity of 2.86 U/mL, pH=7.4 and T=37 ^{o}C. Peak assignment for the degradation products (11 days): MeO-PEG$_{45}$-OH(1), HO-CH$_2$(2)CH$_2$(4)CH$_2$(5)CH$_2$(4)CH$_2$(3)-COOH.

4.2.2 GPC traces for lipase catalyzed degradation of MeO-PEG$_{45}$-*b*-PCL$_{60}$ diblock copolymer micelles

GPC observations of lipase catalyzed micelle degradation GPC traces at a series of reaction times for *P. cepacia* lipase catalyzed MeO-PEG$_{45}$-*b*-PCL$_{60}$ micelle degradation that are obtained after freeze drying the PBS reaction solution and dissolving in DMF are shown in Figure 4.6. The DMF solutions used for the GPC studies contain all of the constituents that are present during the enzyme catalyzed micelle degradation. GPC traces obtained by this procedure with DMF as the solvent reflect the constituents of the entire sample consisting of the enzyme, residual unreacted diblock MeO-PEG$_{45}$-*b*-PCL$_{60}$ and all of the MeO-PEG$_{45}$-*b*-PCL$_n$ and PCL$_n$ units produced in the hydrolysis of MeO-PEG$_{45}$-*b*-PCL$_{60}$ micelle. The GPC traces corresponding to the MeO-PEG$_{45}$-*b*-PCL$_{60}$

diblock copolymer decrease in area as the reaction proceeds, but the position and width are unchanged (Figure 4.6). Appearance of new peaks in the GPC corresponding to PEG_{45}-*b*-PCL_n ($n \leq 6$), a set of PCL_n ($n \leq 6$) oligomers and relatively little monomer ($HO(CH_2)_5$-CO_2H) (Figure 4.6) are in full agreement with the ^1H NMR observations (Figures 4.3-4.5).

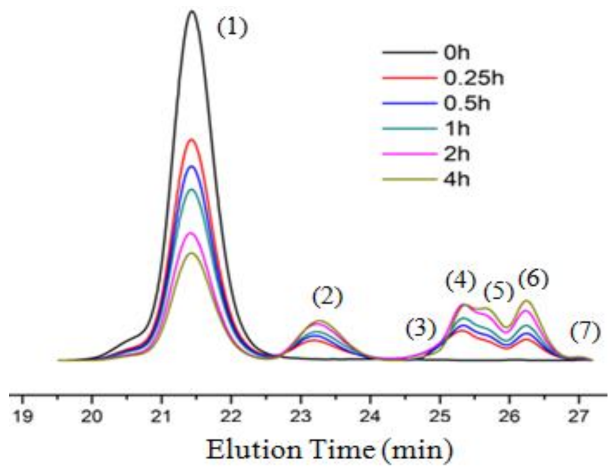

Figure 4.6: GPC traces for DMF solutions containing all the constituents from the *P. cepacia* lipase (2.86 U/mL) catalyzed hydrolysis of MeO-PEG_{45}-*b*-PCL_{60} and micelle degradation in water at 37 ^oC and pH =7.4. (1) PEG_{45}-*b*-PCL_{60}; (2) PEG_{45}-*b*-$PCL_{(1-6)}$; (3) $PCL_{(5-6)}$; (4) PCL_4; (5)PCL_3; (6) $HO(CH_2)_5$-C(O)O$(CH_2)_5$-CO_2H; (7) $HO(CH_2)_5$-CO_2H.

One micelle of MeO-PEG_{45}-*b*-PCL_{60} with a hydrodynamic diameter of 30 $\pm$ 1 nm in aqueous PBS buffer (pH = 7.4, T = 37℃) has an approximate micelle particle mass of 2.0 $\pm$ 0.5 $\times 10^6$ Da which is estimated by Debye plots from light scattering results and thus each micelle contains ~226 diblock copolymer chains. A sample that contains 1.00 mg/mL of PEG_{45}-*b*-PCL_{60} micelle particles has a concentration of 5.0 $\times 10^{-7}$ moles of particles per liter of solution. Pure lipase from *P. cepacia* (34.1 kDa) has 5800 units of activity (U) per mg of enzyme[5] and a solution that has 1.0 U/mL is 5.1 $\times 10^{-9}$ moles of lipase per liter of solution. A typical sample that is used as an example in this article

(Figures 4.3, 4.4) was prepared by dispersing of 0.50 mg of PEG_{45}-*b*-PCL_{60} micelles and combining with *P. cepacia* lipase to give 0.50 units of activity (0.50 U) in 0.70 mL of aqueous PBS which gives an enzyme concentration of 3.64×10^{-9} M (0.714 U/mL) and a micelle particle concentration of 3.57×10^{-7} M (0.714 mg/mL). The ratio of micelle particles to enzyme molecules for this sample is ~98 and all of the samples studied have micelle to enzyme ratios of 25 or larger.

4.2.3 Micelle composition and the water soluble hydrolysis products from ^{1}H NMR during the *P. cepacia* lipase catalyzed MeO-PEG_{45}-*b*-PCL_{60} diblock copolymer micelle degradation

Micelles from MeO-PEG_{45}-*b*-PCL_{60} diblock copolymers with PCL polyester cores are relatively stable with respect to ester hydrolysis in water, but lipase enzymes catalyze rapid micelle hydrolytic degradations[15-16, 36-37, 54]. Comparison of the micelle resonances for the PEG and PCL segments can be used to evaluate the average composition of the polymer chains in the micelles. If the enzyme exchanges between micelles and partially hydrolyzes polymer chains in a set of micelles then the ratio of PEG to PCL will increase as the degradation advances. The observed constant ratio for the integrated areas of the micelle peaks for the PEG_{45} (3.76 ppm) segment and one of the PCL CH_2 (2.35 ppm) resonances of 1.51 ± 0.05 as the degradation proceeds corresponds closely to the theoretical value of 1.50 (90/60) for intact MeO-PEG_{45}-*b*-PCL_{60} block copolymers. This ^{1}H NMR result provides a direct demonstration that the observed micelles are effectively composed of intact MeO-PEG_{45}-*b*-PCL_{60} block copolymers throughout the entire period of micelle degradation (Figures 4.3, 4.4A). This demonstrates that the enzyme entirely degrades one micelle at a time.

^{1}H NMR can also provide information on the distribution of hydrolysis products that enter aqueous solution. Each of the HO-PCL$_n$-CO$_2$H oligomers has one CH$_2$ group next to CO$_2$H and one next to OH and there are n-1 CH$_2$ groups adjacent to ester groups. The ratio (r) of the areas of CH$_2$ groups attached to an ester carbon (*CH$_2$*-C(O)-O-) (δ ~ 2.46 ppm) to that for terminal *CH$_2$*-CO$_2$H (δ ~ 2.25 ppm) provides an easy method to evaluate the average number of caprolactone units (n) in the PCL$_n$ oligomers (n = r + 1). An average chain length of 3.2 is observed for the PCL$_n$ oligomers that enter solution during the first hour of the lipase catalyzed micelle degradation. The value for n in PCL$_n$ subsequently decreases slowly over a period of days toward the value of unity for 6-hydroxycaproic acid (HO(CH$_2$)$_5$CO$_2$H) as the final hydrolysis product. An average PCL$_n$ oligomer chain length of 3.2 for the water soluble hydrolysis products early in the process indicates that there are ~19 hydrolysis events that occur within the micelle for each MeO-PEG$_{45}$-*b*-PCL$_{60}$ polymer chain that is degraded into water soluble fragments. Degradation of one MeO-PEG$_{45}$-*b*-PCL$_{60}$ micelle that is constructed from ~ 226 polymer chains thus involves ~ 4300 hydrolysis events within the micelle. The 20 water soluble fragments consisting of one MeO-PEG$_{45}$-PCL$_n$ and nineteen HO-PCL$_n$-CO$_2$H (n = 1-6) oligomers subsequently slowly hydrolyze through homogeneous catalysis by *P. cepacia* lipase. Full hydrolytic degradation of MeO-PEG$_{45}$-*b*-PCL$_{60}$ produces one MeO-PEG$_{45}$-OH fragment and 60 molecules of HO(CH$_2$)$_5$CO$_2$H (6-hydroxycaproic acid) which result from ~1.4×10^4 hydrolysis events per micelle and a total of ~1.4×10^6 *P. cepacia* lipase catalyzed hydrolysis events per enzyme molecule to complete the process for 98 micelles.

4.2.4 Kinetics for *P. cepacia* lipase catalyzed micelle degradation by ^{1}H NMR and MeO-PEG$_{45}$-*b*-PCL$_{60}$ diblock copolymer hydrolysis by GPC

Kinetics for degradation of the MeO-PEG$_{45}$-*b*-PCL$_{60}$ diblock copolymer micelles is conveniently followed by observing the decrease in the ^{1}H NMR intensities for one of the ^{1}H NMR resonances (2.35 ppm) for the micelles (Figure 4.3). Representative results for the decrease in the ^{1}H NMR integrated intensity for the micelle ester CH_2 groups reflects the change of micelle concentration as a function of time for two *P. cepacia* lipase concentrations are plotted in Figure 4.7. Dynamic light scattering (DLS) measurements during the *P. cepacia* lipase catalyzed PEG$_{45}$-*b*-PCL$_{60}$ micelle degradation at the same conditions (pH=7.4, T=37 ^{o}C and E=2.86 U/mL) as the ^{1}H NMR studies show that the average hydrodynamic diameter for micelles remains effectively unchanged at 30(2) nm during the entire degradation process (Figure 4.8).

Time dependence of the GPC traces for the unreacted MeO-PEG$_{45}$-*b*-PCL$_{60}$ diblock copolymers (Labeled 1, Figure 4.6) reflect the kinetics for hydrolysis of the diblock MeO-PEG$_{45}$-*b*-PCL$_{60}$ copolymer molecules. Kinetic analysis of the results from GPC and ^{1}H NMR provide complementary information on the rates at which the molecular block copolymer hydrolyzes and the micelle polymer assemblies degrade. Kinetic measurements for the diblock copolymer hydrolytic degradation from observing the decrease in the intact diblock copolymer GPC intensity as a function of time are shown in Figure 4.7. The rate plot for hydrolytic fragmentation of the MeO-PEG$_{45}$-*b*-PCL$_{60}$ diblock observed by GPC nearly superimposes on the rate plots for micelle degradation measured by ^{1}H NMR (Figure 4.7B). The fraction of block copolymer hydrolysis observed by GPC and the micelle degradation measured by ^{1}H NMR as a function of time are found to be equal. This set of observations establishes the direct relationship between the quantities of micelles and intact block copolymers which results from the micelles being sequentially degraded by hydrolysis of the PCL segment.

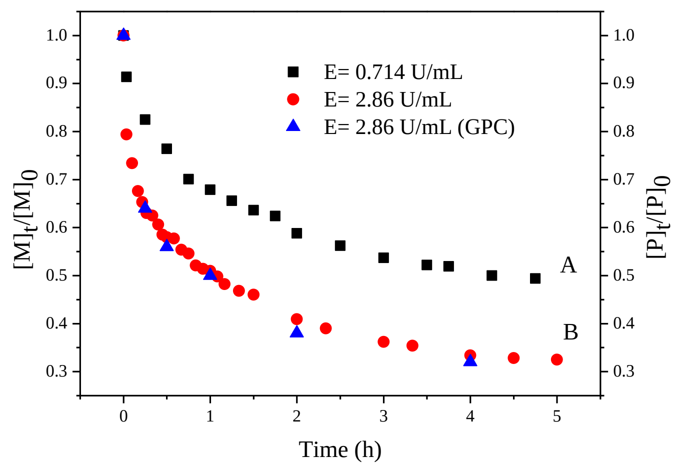

Figure 4.7: [1]H NMR kinetics of MeO-PEG$_{45}$-*b*-PCL$_{60}$ micelle degradation catalyzed by *P. cepacia* lipase at two lipase activities: E = 0.714 U/mL (A) and 2.86 U/mL (B) in PBS buffer where $[M]_t$ is the relative micelle concentration at time t (T=37 ^oC, pH=7.4). The triangles correspond to $[P]_t/[P]_0$ vs time from GPC measurements where [P] is the molar concentration of MeO-PEG$_{45}$-*b*-PCL$_{60}$ block copolymer. Superposition of the [1]H NMR and GPC kinetic plots demonstrate that $[P]_t = k\ [M]_t$ and $([P]_t/[P]_0) = ([M]_t/[M]_0)$.

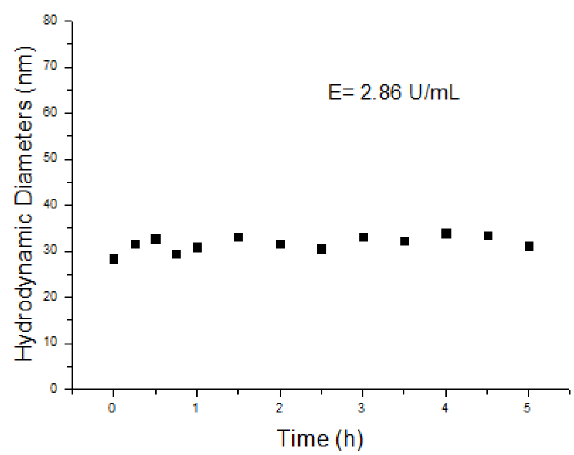

Figure 4.8: DLS of MeO-PEG$_{45}$-*b*-PCL$_{60}$ micelles in PBS buffer solution during *P. cepacia* lipase (E=2.86 U/mL) catalyzed degradation at 37 ^oC.

4.2.5 Product inhibition of lipase enzyme

As the *P. cepacia* lipase catalyzed micelle degradation proceeds the reaction slows down much faster than would be expected based on the initial rates (Figure 4.7) in a manner consistent with loss of enzyme activity. A decline in lipase activity could result from product inhibition[55-56] or changes in the protein[57]. Lipase product inhibition could result from competition for binding in the lipase Ser-His-Asp triad[58-59] catalytic center or through formation of a new micelle from the reaction products (MeO-PEG_{45}-*b*-PCL_n) that competes for enzyme binding[60]. Several of the reaction products including MeO-PEG_{45}-OH, $HO(CH_2)_5CO_2H$, $HO(CH_2)_5C(O)O(CH_2)_5CO_2H$ and MeO-PEG_{45}-*b*-PCL_6-OH were independently prepared and evaluated as potential inhibitors of lipase catalytic micelle degradation. The rate for *P. cepacia* lipase enzyme catalyzed MeO-PEG_{45}-*b*-PCL_{60} micelle degradation was unchanged by addition of the MeO-PEG_{45}-OH, $HO(CH_2)_5CO_2H$ and $HO(CH_2)_5C(O)O(CH_2)_5CO_2H$, but MeO-$PEG_{45}$-*b*-$PCL_6$ (0.714 mg/mL) was observed to have a strong inhibitory effect on the *P. cepacia* catalyzed micelle degradation (Figures 4.9, 4.10). The magnitude of the observed inhibitory effect of MeO-PEG_{45}-*b*-PCL_6 is sufficient to explain the product inhibition of the micelle degradation. The MeO-PEG_{45}-*b*-PCL_6 product fragment totally blocks the *P. cepacia* lipase catalyzed MeO-PEG_{45}-*b*-PCL_{60} micelle degradation during the first hour of reaction (Figure 4.9), and subsequently the micelle degradation occurs slowly. The PCL units in MeO-PEG_{45}-*b*-PCL_6 function as an ester substrate for binding with the *P. cepacia* lipase active center and the PEG segment may have interactions with the protein that retard the movement of the hydrolysis products out of the active center into the aqueous solution. Slow lipase catalyzed hydrolysis of MeO-PEG_{45}-*b*-PCL_6 ultimately produces

$MeO\text{-}PEG_{45}\text{-}OH$ and $HO\text{-}(CH_2)_5\text{-}CO_2H$ which clears the lipase catalytic center for entrance of the micelle MeO-PEG_{45}-*b*-PCL_{60} polymers for hydrolysis and subsequent micelle degradation.

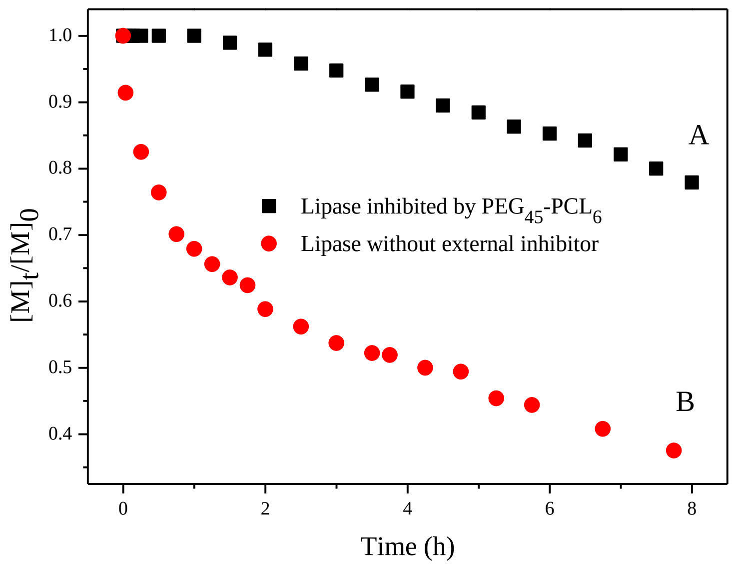

Figure 4.9: Kinetics of *P. cepacia* (0.714 U/mL) catalyzed degration of MeO-PEG_{45}-*b*-PCL_{60} (0.714 mg/mL) in PBS aqueous solution (pH =7.4) at T=37 ℃ A) with MeO-PEG_{45}-*b*-PCL_6 (0.714 mg/mL) inhibitor B) without inhibitor.

^1H NMR was used to study the hydrolysis of separately prepared MeO-PEG_{45}-*b*-PCL_6 inhibitor (4.0 mg/mL) at lipase activity of 2.86 U/mL, pH=7.4 and T=37 ^oC (Figure 4.10). The ^1H NMR spectra nearly remain the same over a period of 13 hours, which indicates that MeO-PEG_{45}-*b*-PCL_6 reacts with *P. cepacia* lipase very slow and makes it an inhibitor for lipase catalyzed degradation for MeO-PEG_{45}-*b*-PCL_{60} block copolymer micelles. However, MeO-PEG_{45}-*b*-PCL_6 diblock copolymer will be eventually fully hydrolyzed into MeO-PEG_{45}-OH and $HO(CH_2)_5CO_2H$ since it is also a substrate for the lipase.

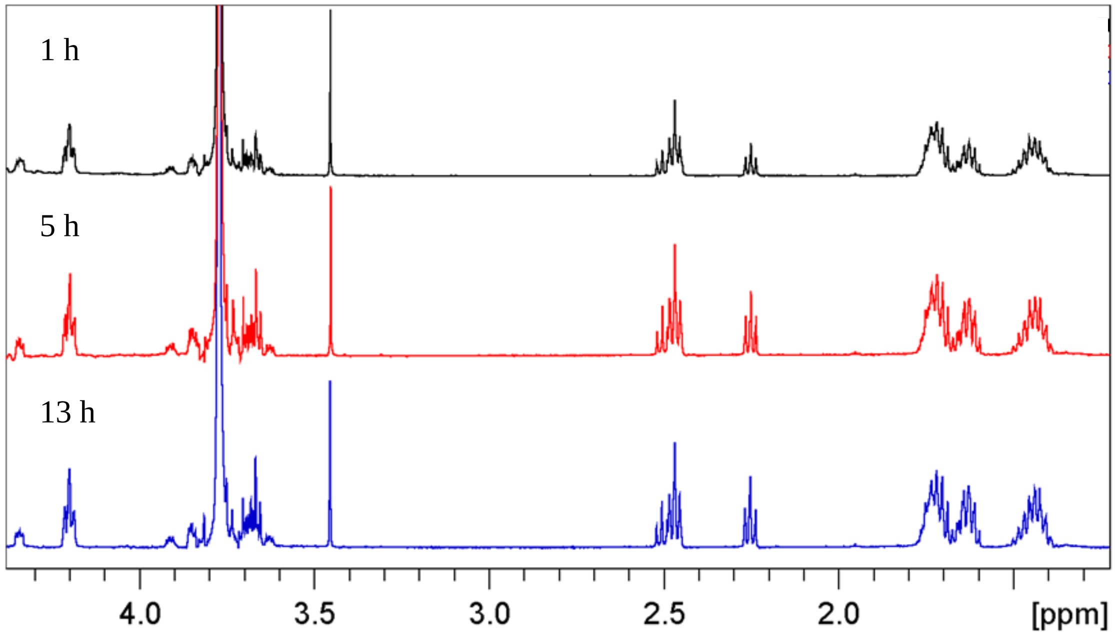

Figure 4.10: [1]H MNR of lipase catalyzed degradation of MeO-PEG$_{45}$-*b*-PCL$_6$ inhibitor (4.0 mg/mL) at lipase activity of 2.86 U/mL, pH=7.4 and T=37 ^{o}C.

4.2.6 *P. cepacia* lipase enzyme stability and reversible product inhibition

Micelles (0.714 mg/mL) from MeO-PEG$_{45}$-*b*-PCL$_{60}$ with *P. cepacia* lipase in aqueous PBS buffer (pH=7.4) at T=37 ℃ at an activity of 0.714 U/mL were reacted and the kinetics of micelle degradation followed by ^{1}H NMR for a period of 5 hours (Figure 4.11). The process continued to be observed for a period of 12 days until only the non-inhibiting reaction products of MeO-PEG$_{45}$-OH and $HO(CH_2)_5CO_2H$ and the enzyme remained in the system. A second addition of MeO-PEG$_{45}$-*b*-PCL$_{60}$ micelles (1.0 mg/mL, 0.5mL) was made to the solution and the kinetics of micelle degradation followed by ^{1}H NMR. The micelle degradation kinetics observed for the second addition of micelles was virtually identical to the kinetics for the initial micelle reaction (Figure 4.11). The superimposable micelle degradation kinetic plots for the two sequential additions of micelles indicate that the enzyme inhibition by the products of micelle hydrolytic degradation is fully reversible and that the *P. cepacia* lipase enzyme is not irreversibly deactivated at the reaction conditions during a period of more than 12 days. Full retention of activity in aqueous PBS buffer (pH = 7.4; T = 37 ℃) for extended time periods is an important factor in selecting *P. cepacia* lipase for the comprehensive mechanistic study of enzyme catalysis.

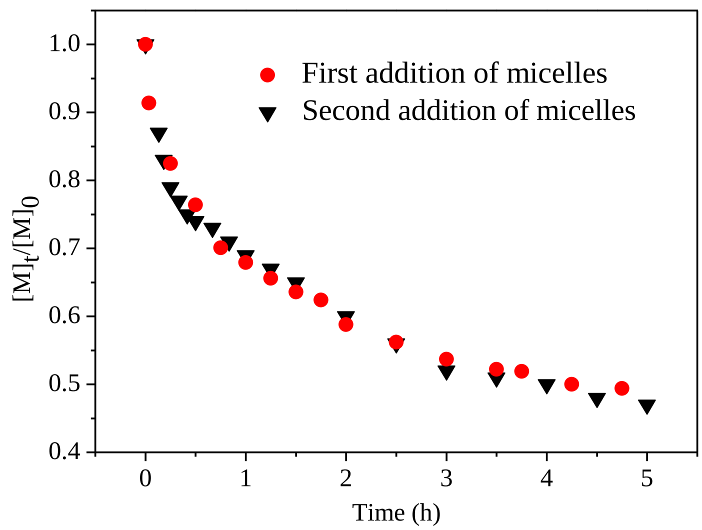

Figure 4.11: MeO-PEG$_{45}$-*b*-PCL$_{60}$ micelle degradation kinetic plots in aqueous PBS buffer (pH=7.4) at T=37 ^{o}C for two sequential additions of micelles (0.5 mL each) separated by 12 days during which all of the MeO-PEG$_{45}$-*b*-PCL$_{60}$ from the first addition of micelles was converted to MeO-PEG$_{45}$-OH and HO(CH$_2$)$_5$-CO$_2$H.

4.2.7 Rate law for lipase catalyzed micelle degradation

Kinetic data for the of *P. cepacia* lipase catalyzed MeO-PEG$_{45}$-*b*-PCL$_{60}$ micelle degradation were evaluated at a series of initial micelle and enzyme concentrations (Figures 4.12, 4.13). In analyzing and interpreting the kinetics of micelle degradation, the micelle particles are treated as if they were molecules. The fractional change in the relative micelle concentration as a function of time for three micelle concentrations at a fixed initial enzyme concentration (0.714 U/mL) is shown in Figure 4.12A. Plots of the change in the micelle concentration with time for the three micelle concentrations effectively superimpose which clearly shows that the rate of micelle degradation (-d[M]/dt) is independent of the micelle concentration (Figure 4.12B). Superposition of the three rate curves indicates that the process is zero order in the micelle concentration and that the inhibition is directly proportional to the concentration of the degraded micelles. Changing the enzyme concentration at a fixed initial micelle concentration (0.714 mg/mL) results in the series initial rates of micelle degradation (V_0) that are shown in Figure 4.13A. The near linear change in rate with initial enzyme concentration in the more dilute enzyme region (0.100 U/mL - 0.714 U/mL) demonstrates a first order rate dependence on initial enzyme concentration ($V_0 = 2.09 \times 10^{-10}\ E_0$). When the micelle particles are in excess over the number of enzyme molecules, the degradation is zero order in micelle concentration ([M]) and first order in the initial enzyme concentration ($[E_0]$) which is equivalent to first order in the enzyme-micelle complex [EM] ($-d[M]/dt = k[M]^0[E_o]^1 = k[M]^0[EM]^1$). The experimental rate law for lipase enzyme catalyzed micelle degradation corresponds to that expected for an enzyme interfacial activation mechanism[39]. Deviation of the enzyme kinetic behavior from strictly first order at the highest enzyme concentration (2.86 U/mL, Figure 4.13B) is tentatively ascribed to enzyme association[61] that reduces the effective enzyme activity. A large excess of micelles ([micelles]/[enzyme] > 25) guarantees that the process is not becoming zero order in enzyme as the concentration of enzyme increases.

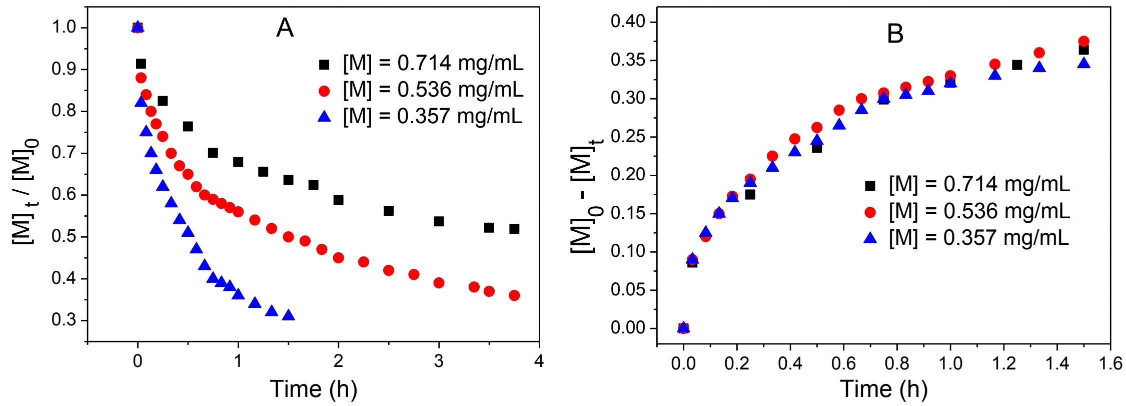

Figure 4.12: Effect of micelle concentration on the rate of *P. cepacia* lipase catalyzed diblock MeO-PEG$_{45}$-*b*-PCL$_{60}$ micelle degradation in aqueous PBS buffer (pH=7.4) at T=37 ℃ at an activity of 0.714 U/mL.

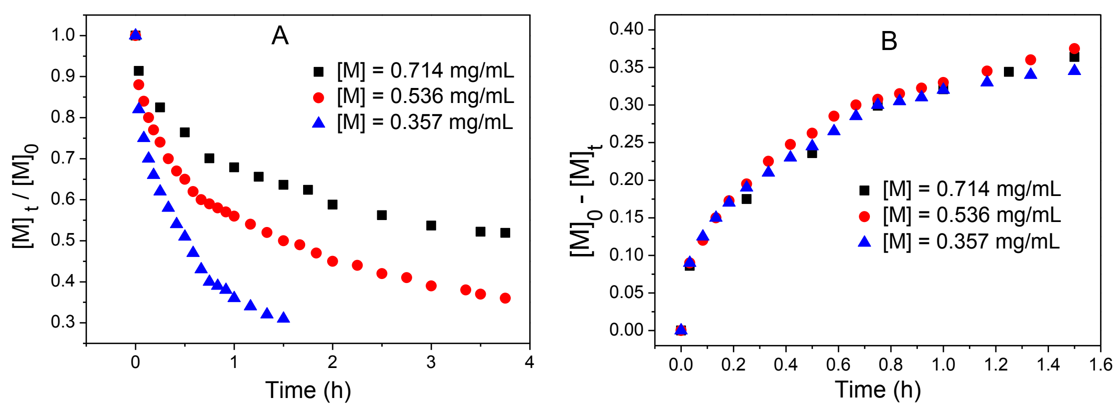

Figure 4.13: Effect of enzyme concentration on the rate of *P. cepacia* lipase catalyzed diblock MeO-PEG$_{45}$-*b*-PCL$_{60}$ micelle degradation in aqueous PBS buffer (pH=7.4) at T=37 ^{o}C at an activity of 0.714 U/mL. V_o is defined as the initial rate of micelle degradation (-d[M]/dt) determined by ^{1}H NMR at reaction time t =15 min.

4.2.8 Reactions involved in the P. cepacia lipase catalyzed MeO-PEG45-b-PCL60 micelle heterogeneous lipase and homogeneous esterase polyester ester hydrolysis reactions

An outline of the types of reactions that occur and contribute to the *P. cepacia* lipase hydrolytic degradation of MeO-PEG$_{45}$-*b*-PCL$_{60}$ micelles and subsequent ester hydrolysis of water soluble PCL_n fragments that ultimately form MeO-PEG_{45}-OH and ($HO(CH_2)_5$-CO_2H) over periods of days is given by equations 1- 4 and illustrated in scheme 4.1.

Scheme 4.1: Summary of the whole processes for lipase catalyzed degradation of MeO-PEG_{45}-*b*-PCL_{60} micelle.

$$(1) \quad E + M \underset{k_{-1}}{\overset{k_1}{\rightleftharpoons}} EM$$

$$(2) \quad EM \xrightarrow{k_2} P_I + E$$

$$(3) \quad EM + P_I \underset{k_{-3}}{\overset{k_3}{\rightleftharpoons}} EMP_I$$

$$(4) \quad P_I + E \xrightarrow{k_4} P_F + E$$

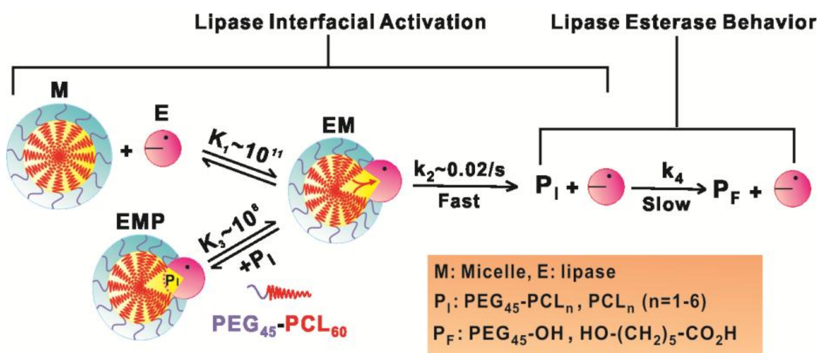

The four main steps identified in the lipase catalyzed micelle and constituent MeO-PEG_{45}-*b*-PCL_{60} block copolymer hydrolytic degradation are *1)* enzyme activation through tight binding with the micelle, *2)* rapid lipase catalyzed hydrolysis of the PCL_{60} polyester segments of MeO-PEG_{45}-*b*-PCL_{60} to form water soluble MeO-PEG_{45}-*b*-PCL_n and PCL_m oligomers and *3)* product inhibition by MeO-PEG_{45}-*b*-PCL_n ($n \leq 6$) and *4)* slow enzyme catalyzed hydrolysis of the water soluble PCL fragments to MeO-PEG_{45}-OH and ($HO(CH_2)_5$-CO_2H). Formation of the enzyme-micelle complex (EM) (eq 1) activates the lipase in a manner like that of the lipase-lipid membrane reactions[62-64] that involve enzyme interfacial activation[39]. The enzyme-micelle complex (EM) with the activated enzyme reacts with the polyester substrate from the micelle core to produce the hydrolysis products (P) (eq 2) accompanied by micelle degradation and regeneration of the free enzyme (E) that binds with another micelle. Product inhibition of the lipase catalyzed micelle degradation is depicted by equations 3 (Scheme 4.1). Partial hydrolysis of MeO-PEG_{45}-*b*-PCL_{60} chains in the micelles during degradation produces water soluble MeO-PEG_{45}-*b*-PCL_n ($n \leq 6$) where the PCL ester units are homogeneous substrates for the very slow esterase type hydrolysis catalyzed by *P. cepacia* lipase. The MeO-PEG_{45}-*b*-PCL_6 derivative was shown to inhibit the micelle degradation (Figure 4.9). *P. cepacia* lipase catalyzed micelle degradation is very much faster than hydrolysis of the water soluble products such that the MeO-PEG_{45}-*b*-PCL_n ($n \leq 6$) products accumulate. The ester units of MeO-PEG_{45}-*b*-PCL_n ($n \leq 6$) are proposed to dock in the enzyme Ser-His-Asp triad catalytic center[58-59]and produce an equilibrium with an adduct of the enzyme-micelle where the catalysis center is occupied by a product molecule. This is represented by the product P binding with the enzyme-micelle complex (EM) to form an enzyme-micelle complex (EMP) that is inactive in micelle degradation (eq 3). The enzyme–micelle complex (EM) remains bound until the micelle fully degrades and so it is the EM complex that is inhibited by binding a product molecule (P) in the catalytic center (eq 3). The final step in the full hydrolytic degradation of the MeO-PEG_{45}-*b*-PCL_{60} micelles is the *P. cepacia* lipase catalyzed ester hydrolysis of the water soluble PCL containing fragments of MeO-PEG_{45}-*b*-PCL_{60} resulting from the micelle degradation. These esterase like soluble ester hydrolysis reactions catalyzed by *P. cepacia* lipase are extremely slow and require days to weeks to achieve full conversion to MeO-PEG$_{45}$-OH and HO(CH$_2$)$_5$-CO$_2$H.

4.2.9 Reaction scheme for lipase catalyzed micelle degradation and kinetic simulations

The three steps that have a dominant influence on the observed kinetics of lipase enzyme catalyzed micelle degradation are given by equations 1-3 shown in Scheme 4.2. The *P. cepacia* lipase catalyzed micelle degradation corresponds to the Michaelis-Menten mechanism (E + M $\rightleftharpoons$ EM → P + E) with product inhibition of the enzyme-micelle complex (EM + P $\rightleftharpoons$ EMP).

Scheme 4.2: Micelle degradation reaction scheme where M, E, EM, P, EMP are the micelle, enzyme, enzyme-micelle complex, hydrolysis product, and product inhibited enzyme-micelle complex respectively.

$$(1)\quad E + M \underset{k_{-1}}{\overset{k_1}{\rightleftharpoons}} EM$$

$$(2)\quad EM \xrightarrow{k_2} P + E$$

$$(3)\quad EM + P \underset{k_{-3}}{\overset{k_3}{\rightleftharpoons}} EMP$$

Reactions 1-3 in Scheme 4.2 were used in kinetic simulations of the *P. cepacia* lipase catalyzed micelle degradation using the program Dynafit[65]. Initial estimates k_1, k_{-1}, and k_2 for the kinetic simulations were based on the observed sequential micelle degradation requiring a large equilibrium constant and experimental estimates for the lower limit of k_2 ($k_2 > 0.017\ s^{-1}$) come from the rate of micelle degradation at the reaction time t = 15 min.

A relatively small range of rate constants k ($k_1 \sim 1\times10^7$ $M^{-1}s^{-1}$, $k_{-1} \sim 1\times10^{-4}$ s^{-1}, $k_2 \sim 0.02$ s^{-1}, $k_3 \sim 1.5\times10^4$ $M^{-1}s^{-1}$, $k_{-3} \sim 1.5\times10^{-4}$ s^{-1}, T = 310 K) are capable of producing reasonable fitting with the observed concentration versus time plots for lipase catalyzed micelle degradation (Figures 4.12-4.13). Using a single set of parameters ($K_1 = 1\times10^{11}$, $k_2 = 0.02$ s^{-1} and $K_3 = 1\times10^8$; T = 310K) gives satisfactory kinetic simulations for all of kinetic data sets in Figure 4.14(A-C). The requirements for the kinetic simulation place the $\Delta G_1^{\mathbf{0}}$ (310K) for *P. cepacia* lipase-PEG_{45}-*b*-PCL_{60} micelle complex formation at -15(1) $kcalmol^{-1}$ ($\Delta G_1^0 = -15(1)$ $kcalmol^{-1}$) which must result from the net binding from numerous small contributing interactions. The change in the micelle concentration with time in the absence of product inhibition based on K_1 and k_2 for equations 1 and 2 (scheme 4.2) is plotted in Figure 4.15 and illustrates both that the interfacilly activated lipase enzyme reacts rapidly and that the product inhibition has a profound effect on slowing the degradation. The kinetic simulations of the micelle degradation results requires a large equilibrium constant for lipase-micelle binding ($K_1 > 10^{11}$, T = 310 K) which is consistent with the lipase-micelle attachment remaining intact until the micelle is fully degraded[39, 60]. The large equilibrium constant for enzyme-micelle complex formation ($K_1 \sim 1\times10^{11}$) and the large ratio of micelle to enzyme concentration ($[M]/[E_0]$=25-700) ensures that effectively every enzyme molecule is complexed by a micelle. Under these conditions the process is first order in the initial enzyme concentration and independent of the micelle concentration.

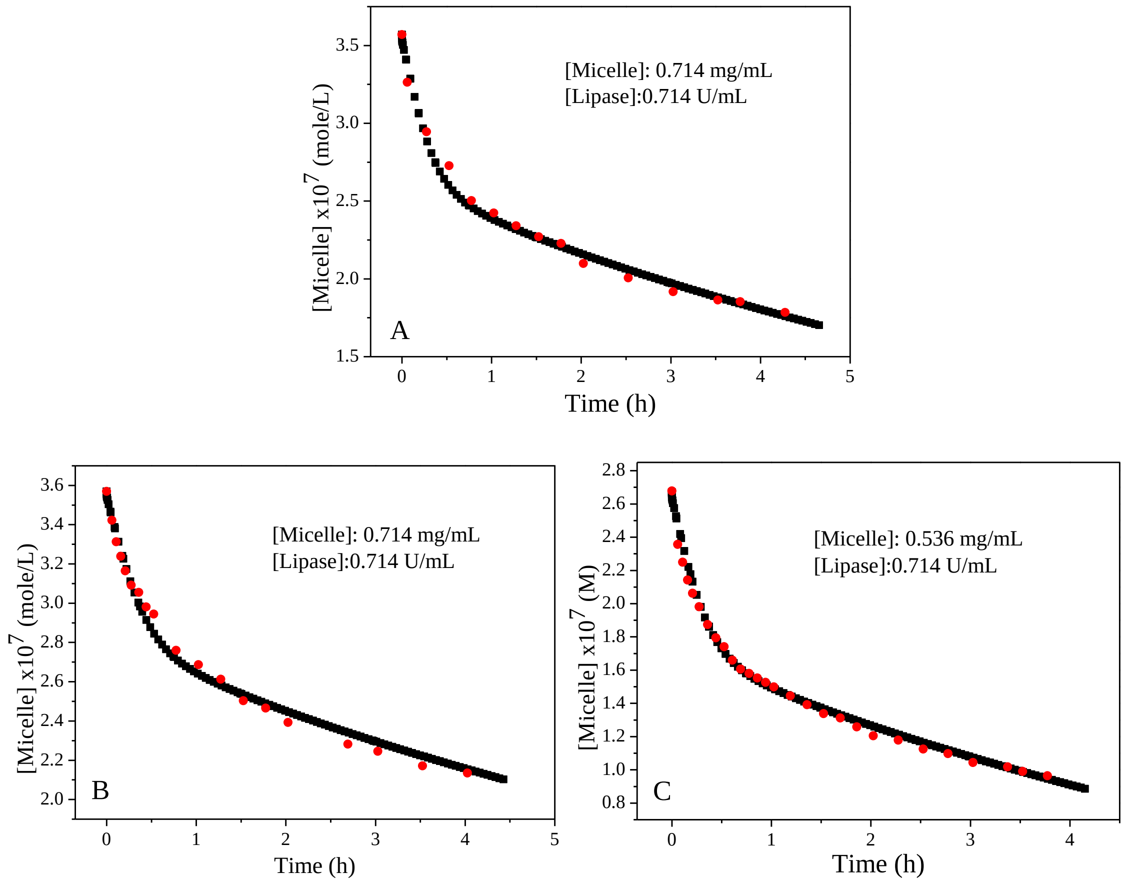

Figure 4.14: Simulations of experimental kinetics (A-C) for different lipase and micelle concentrations using eq. 1-3 and rate constant parameters: $k_1= 1\times10^6$, $k_{-1}= 1\times10^{-5}$, $k_2= 0.02$, $k_3= 1.5\times10^4$, $k_{-3}= 1.5\times10^{-4}$; A) 0.714 mg/mL micelle + 0.714 U/mL lipase; B) 0.714 mg/mL micelle + 0.476 U/mL lipase; C) 0.536 mg/mL micelle + 0.714 U/mL lipase; (Estimated absolute micelle and lipase concentrations in mole/L were used in the kinetic simulations).

The *P. cepacia* lipase catalyzed micelle degradation corresponds to the Michaelis-Menten mechanism ($E + M \rightleftharpoons EM \rightarrow P + E$) with product inhibition of the enzyme-micelle complex ($EM + P \rightleftharpoons EMP$). Simulations for the *P. cepacia* lipase catalyzed degradation kinetic for PEG$_{45}$-*b*-PCL$_{60}$ micelles (pH = 7.4, 310 K) require that K_1 (k_1/k_1) be greater than 10^{11} and that k_2 be ~ 0.02 s^{-1} in order to fit the experimental Micelle concentration versus profiles. The very large equilibrium constant to form the enzyme-micelle complex ($K_1 = k_1/k_{-1} = 10^{11}$) indicates that the enzyme will be an efficient degradation catalyst at nanomolar micelle concentrations. A K_1 of 10^{11} is also indicative of a near diffusion controlled forward rate constant ($k_1 > 10^7$) and Michaelis constant $K_m \sim 2 \times 10^{-9}$ ($K_m = (k_{-1} + k_2)/k_1 \sim k_2/k_1 \sim 2 \times 10^{-9}$). A k_{cat} of 0.02 s^{-1} ($k_2 = k_{cat}$) means that there would be ~ 0.02 micelles degraded per enzyme molecule per second in the absence of product inhibition of the enzyme activity. Without the product inhibition each enzyme would degrade one micelle in approximately 50 seconds and degradation of 98 micelles per enzyme would take ~ 82 minutes. The time required for the reaction in the absence of product inhibition is illustrated in Figure 4.15 which compares the experimental micelle concentration as a function of time with the calculated concentration using $k_2 = 0.02$ s^{-1} in the absence of product inhibition ($K_3 = 0$).

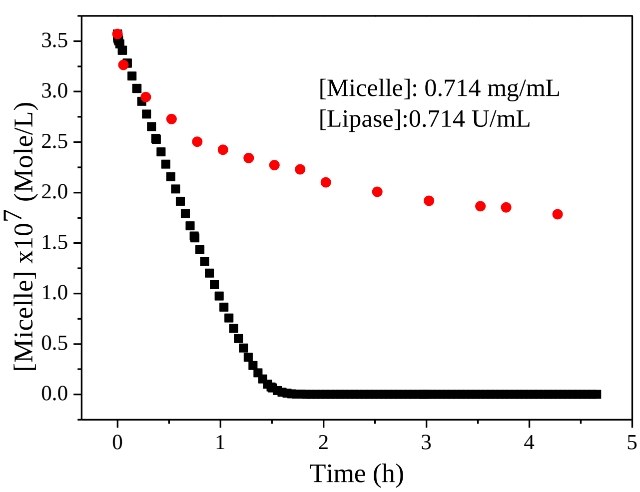

Figure 4.15: Simulated kinetics without inhibition using only eq.1-2 and rate constant parameters: $k_1 = 1\times10^6$, $k_{-1} = 1\times10^{-5}$, $k_2 = 0.02$; 0.714 mg/mL micelle + 0.714 U/mL lipase (Estimated absolute micelle and lipase concentrations in mole/L were used in the kinetic simulations).

The following computer program was used for the experimental kinetic simulation by Dynafit4.1:

```
[task]
data = progress
task = fit
model = 0.714 mg/mL +0.714U/mL

[mechanism]

E + M ---> EM        :    k1
EM ---> E + M       :    k-1
EM ---> P1 + E    :    k2
EM + P1 ---> EMP1   :    k3
EMP1 ---> EM + P1      :    k-3

[constants]

k1 = 1e6  ,  k-1 = 1e-5  ,  k2 = 0.02
k3 = 1.5e4    ,  k-3 = 1.5e-4

[concentrations]

M = 3.57e-7
E =3.97e-9

[data]
monitor EM
set M       | response M = 1

[output]

directory ./DynaFit/fit/lipase

;___________________________________________________________________________

[set:M]

t,s        conc

0          3.57E-7
120      3.26298E-7
900      2.94525E-7
1800    2.72748E-7
2700    2.50257E-7
```

3600	2.42403E-7
4500	2.34192E-7
5400	2.27052E-7
6300	2.22768E-7
7200	2.09916E-7
9000	2.00634E-7
10800	1.91709E-7
12600	1.86354E-7
13500	1.85283E-7
15300	1.785E-7

One micelle of MeO-PEG$_{45}$-*b*-PCL$_{60}$ with a hydrodynamic diameter of 30 ± 1 nm has an approximate micelle particle mass of 2.0 ± 0.5 × 10^6 Da that is estimated by light scattering and thus contains ~ 226 diblock copolymer chains. Each of the diblock polymer chains experiences ~ 19 hydrolysis events to produce water soluble PCL$_n$ oligomers with an average n of 3.2 and one MeO-PEG$_{45}$-*b*-PCL$_n$ fragment. The *P. cepacia* lipase thus binds a MeO-PEG$_{45}$-*b*-PCL$_{60}$ micelle and in ~ 50 s approximately 4300 ester hydrolysis events result in complete micelle degradation. A value for k_{cat} of 86 is obtained when k_2 is determined based upon ester hydrolysis events instead of micelle degradation.

4.2.10 Absence of esterase enzyme catalyzed degradation of micelles from MeO-PEG$_{45}$-*b*-PCL$_{60}$

Porcine liver esterase at an activity of 2.86 U/mL was added to micelles from MeO-PEG$_{45}$-*b*-PCL$_{60}$ in aqueous PBS and no observable micelle degradation occurred over a period of 2 days at 37 ℃. Dispersions of micelles from MeO-PEG$_{45}$-*b*-PCL$_{60}$ with *porcine liver* esterase even at very high activity (21 U/mL) did not produce any observed micelle degradation or PCL hydrolysis over a period of days. Absence of esterase catalysis for the micelles with polyester cores is consistent with the specific requirement to have lipase enzymes to catalyze the MeO-PEG$_{45}$-*b*-PCL$_{60}$ micelle hydrolytic degradation.

4.2.11 Kinetic effects of adding an esterase to the lipase catalyzed micelle degradation

Addition of a mixture of *P. cepacia* lipase (0.714U/mL) and large quantities of *porcine liver* esterase (11.0 U/mL, 22.0 U/mL) to micelles from MeO-PEG$_{45}$-*b*-PCL$_{60}$ results in substantial increases in the rate of micelle hydrolytic degradation compared with just having the lipase (Figure 4.16). The *porcine liver* esterase (11.0 U/mL, 22.0 U/mL) catalyzes hydrolysis of the initial PCL ester containing degradation products sufficiently fast so that only the non-inhibiting products MeO-PEG$_{45}$-OH and $HO(CH_2)_5CO_2H$ are observed. Reduction in the concentratration of the inhibitor product (P) by the esterase increases the enzyme-micelle complex concentration and thus increasing rates of micelle degradation (Figure 4.16).

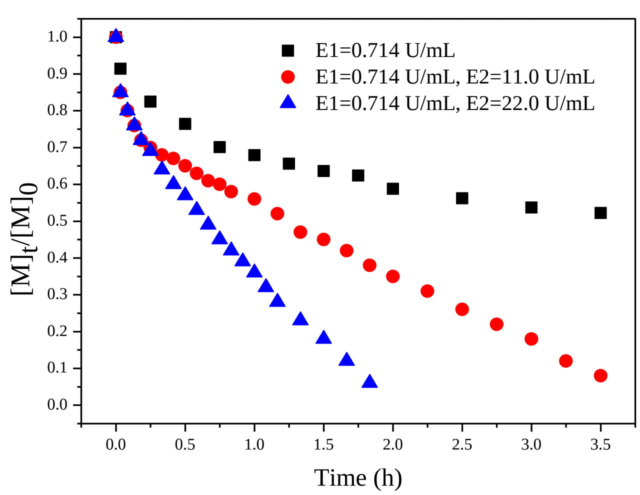

Figure 4.16: Effect of adding *porcine liver* esterase (E2) to the *P. cepacia* lipase (E1) catalyzed diblock MeO-PEG$_{45}$-*b*-PCL$_{60}$ micelle degradation in aqueous PBS buffer (pH=7.4) at T=37 ℃ at an activity of 0.714 U/mL.

4.2.12 Model of lipase enzyme catalyzed micelle degradation

Catalytic hydrolysis of lipid ester substrates assembled in bilayers, vesicles and micelles is an exclusive capability of lipase enzymes[43-48, 66]. Binding of the lipase with the lipid surface at the interface with water generally induces conformation changes that move a protein "lid" region[3, 67-69] to expose both a hydrophobic protein sequence and the adjacent Ser-His-Asp triad hydrolysis catalytic center to the lipid bilayer surface. This general mechanistic aspect of lipase catalysis is called "enzyme interfacial activation" and is a feature that distinguishes lipase from esterase substrate preferences[1-3]. A prominent pathway for lipase catalyzed lipid hydrolysis is the "scooting" mechanism[39, 60] which involves the tight binding and interfacial activation of the enzyme with a lipid assembly in membranes, vesicles and micelles. The enzyme is envisioned as migrating or scooting over the surface of the membrane or vesicle reacting with substrates at the surface.

Lipase-micelle tight binding with enzyme activation, rapid lipase catalyzed polyester hydrolysis of MeO-PEG$_{45}$-*b*-PCL$_{60}$ polymer chains associated sequential micelle degradation and absence of esterase-micelle reaction are features consistent with interfacial activation processes. Micelle-lipase binding is effectively irreversible because the hydrolytic degradation of the micelle is faster than the exchange of enzymes between micelles. These observed features of lipase catalyzed micelle degradation fulfill the criteria and mimic the behavior associated with the "scooting" mechanism for lipase-lipid membrane catalysis[60]. Relatively strong multiple site binding of the *P. cepacia* lipase enzyme molecules with the PEG-*b*-PCL block copolymer micelle (K_1(310 K) > 1×10^{11}, -

$\Delta G_1^0 > 15(1)$ kcalmol^{-1}) results in protein conformational changes[39] that activate the lipase enzyme and provide a favorable pathway for the polyester segments to enter the catalytic center. Lipase-micelle interactions must specifically cause the enzyme "lid" sequence to be pinned back to expose the micelle to a hydrophobic region of the protein and the adjacent open Ser-His-Asp triad catalytic center for ester hydrolysis[68, 70]. The exposed hydrophobic region most probably directs the hydrophobic PCL polyester units into the accessible active center for hydrolysis. Effectively all the PCL segments (~226) that comprise the core of a PEG_{45}-*b*-PCL_{60} block copolymer micelle are rapidly hydrolyzed into short water soluble oligomers. This behavior suggests that the hydrophobic enzyme region exposed by attachment to the micelle is extruding the PCL segments from the core into the active reaction center and clipping the polyester into relatively short water soluble HO-PCL_n-CO_2H oligomers that are continually expelled into the aqueous phase. The hydrophobic enzyme region called the "hydrophobic trench"[71] that is exposed to the micelle may locally disrupt the micelle structure in a manner such that one or more of the PCL segments may become directed away from the core toward the hydrophobic enzyme pocket and the triad hydrolysis catalytic center. The MeO-PEG_{45}-*b*-PCL_{60} polyester substrate is envisioned to enter the lipase catalytic center from the PCL end and produce hydrolysis events at intervals of 2-6 PCL units to form water soluble HO-PCL_n-CO_2H units that are drawn into the water phase to reopen the catalytic site. Reversible lipase enzyme inhibition occurs when products such as PEG_{45}-*b*-PCL_n are formed that are slower reacting substrates that compete for residing in the triad active center. The very fast initial rates of lipase catalyzed micelle degradation are triggered by strong enzyme-micelle complex formation which activates the lipase enzyme in a manner that parallels interfacial enzyme activation in lipase catalyzed lipid membrane hydrolysis. The micelle-protein binding sites that hold the lid in an open position which activates the lipase catalytic activity have not yet been identified. As a working model, we currently prefer to place the position for the enzyme-micelle binding near the water-micelle core interface to facilitate entrance of the PCL polyester segments and water into the reaction center and efficient transport of the water soluble hydrolysis products from the catalysis center into the bulk aqueous phase.

The evolving lipase enzyme-micelle reaction model builds on studies of lipase reactions with micelles[15-16, 38] and lipid[43, 47, 60] vesicles. The distinguishing features of this proposed model result from the availability of detailed compositional and kinetic information provided by the ^{1}H NMR and GPC observations and through the explicit use of interfacial activation as a unifying mechanistic feature of lipase enzyme catalysis. Mechanistic understanding of enzyme[15-16] and acid[17, 35] catalyzed polymer micelle degradation contribute to the design principles for block copolymer transport systems. Amphiphilic block copolymer micelles that mimic lipid vesicle-enzyme reactions may reveal unrecognized mechanistic aspects of native enzyme-substrate processes and provide a convenient approach to categorize the behavior of hydrolase enzymes.

4.3 Summary

Relatively small and uniformly sized block copolymer micelles from low polydispersity poly (ethylene glycol) (PEG) block poly (ε-caprolactone) (PCL) (MeO-PEG_{45}-*b*-PCL_{60}) give ^{1}H NMR spectra useful for direct micelle characterization and kinetic-mechanistic studies. *P. cepacia* lipase catalyzed MeO-PEG_{45}-*b*-PCL_{60} micelle degradations were followed by ^{1}H NMR and GPC to obtain simultaneous evaluation of the micelle composition, degradation kinetics and appearance of the water soluble hydrolysis products. GPC traces for the fraction of block copolymer hydrolysis by and ^{1}H NMR measurement of the micelle degradation as a function of time are found to be equal. This set of observations establishes the direct relationship between the quantities of micelles and intact block copolymers which results from the micelles being sequentially degraded by hydrolysis of the PCL segment. Initial micelle degradation products MeO-PEG_{45}-*b*-PCL_{6} was observed to have strong inhibitory effect on lipase catalyzed degradation of micelle from MeO-PEG_{45}-*b*-PCL_{60}. MeO-PEG_{45}-*b*-PCL_{6} inhibitor is also the lipase substrate and slow lipase catalyzed hydrolysis of MeO-PEG_{45}-*b*-PCL_{6} ultimately produces MeO-PEG_{45}-OH and HO-$(CH_2)_5$-CO_2H which clears the lipase catalytic center for entrance of the micelle MeO-PEG_{45}-*b*-PCL_{60} polymers for hydrolysis and subsequent micelle degradation. Kinetic studies of lipase catalyzed degradation of MeO-PEG_{45}-*b*-PCL_{60} micelles at different micelle and lipase concentrations demonstrates that the degradation is zero order in micelle concentration ([M]) and first order in the initial enzyme concentration ($[E_0]$) which is equivalent to first order in the enzyme-micelle complex [EM] when the micelle concentration is excess.

Analysis and simulation of the concentration versus time profiles for *P. cepacia* lipase catalyzed MeO-PEG_{45}-*b*-PCL_{60} micelle degradation show that the process conforms to a Michaelis-Menten mechanism ($E + M \rightleftharpoons EM \rightarrow P + E$) with enzyme-micelle complex product inhibition ($EM + P \rightleftharpoons EMP$). Formation and tight binding of the lipase enzyme-micelle complex, activation of lipase catalysis and sequential micelle degradation are characteristics of MeO-PEG_{45}-*b*-PCL_{60} micelle degradation which parallel features of enzyme interfacial activation associated with lipase catalyzed hydrolysis of lipids in membranes.

Kinetic results of lipase catalyzed degradation MeO-PEG-*b*-PCL micelles in Chapters 3 and 4 indicate the rate determinate step during the reaction is the step that forming the lipase-micelle complex. Therefore, in order to prepare stable polymer micelles that could deliver drugs to the target site without significantly preleasing under the lipase medium, we have to make a micelle that doesn't form the lipase-micelle complex. In the next two chapters, we will discuss the reaction between lipases and micelles with charged coronas.

4.4 Experimental

4.4.1 Materials

Methoxy poly (ethylene glycol) (PEG, Mn = 2000, Mw/Mn = 1.06, Sigma Aldrich) was purified by precipitation from petroleum ether prior to use. ε-Caprolactone (CL) (99%, TCI America) was dried over CaH_2 and distilled under vacuum prior to use. Stannous Octoate ($Sn(Oct)_2$) was used as received from Sigma Aldrich. Lipase from *P.*

cepacia (37.8 U/mg), esterase from porcine liver (17 U/mg) were used as received from Sigma Aldrich. SnakeSkin Dialysis tubing (10K MWCO, 35mm dry I.D., 35 feet) was used for dialysis of aqueous media containing polymer micelles. Acetone, toluene, dichloromethane and methanol were use as received from J.T. Baker and dimethylformamide (DMF, HPLC grade, 99.7% +, Alfa Aesar) was used as the GPC eluent.

4.4.2 Analytical techniques

^{1}H NMR spectra were obtained using Bruker 500 MHz spectrometer with $CDCl_3$ and D_2O as NMR solvent media. ^{1}H NMR data were analyzed by using the Bruker Topspin 2.1 software. Water suppressed ^{1}H NMR spectra of block copolymer micelles in buffer solutions containing 10% of D_2O were acquired using presaturation of water with 50 dB attenuation. The ^{1}H NMR covered a spectral window of -5.0 ppm to 15.0 ppm. The excitation relaxation delay was set to 5 s. Each NMR spectrum was collected from accumulation of 24 scans.

Gel permeation chromatography (GPC) measurements were carried out using a Shimadzu LC-20AV liquid chromatography system equipped with three linear PolarGel-M 300×7.5 mm columns, a RID-10A differential refractive index detector and a SPD-20AV UV/VIS detector. Data were analyzed by Shimadzu LCsolution software. DMF was used as the eluent at a flow rate of 1.0 mL/min at 50 ℃. Molecular weight calibrations were based on narrow peak width polystyrene standards from Polymer Laboratories.

Dynamic Light Scattering (DLS). Hydrodynamic diameters of micelles were measured by a Zetasizer Nano ZS (Malvern Instruments, Westborough, MA) at 25 ℃/ 37 ℃, using 1 cm polystyrene sample cuvettes. The mean diameters were obtained by use of the DTS software using the volume measurements.

Transmission Electron Microscope (TEM). Micelle morphology was evaluated by JOEL JEM-1400 TEM operating at an acceleration voltage of 80 kV. One drop of the micelle solution (1.0 mg/mL) was placed on the ultrathin carbon type-A 400 mesh copper grid (Ted Pella Inc., Redding, CA), and the droplet was then blotted and allowed to evaporate under ambient conditions overnight before analysis[72-73]. The average diameters of the spherical micelles were evaluated by Digital Micrograph software (Gatan Inc.).

4.4.3 Preparation and characterization of MeO-PEG$_{45}$-*b*-PCL$_{60}$ micelles

The nano-precipitation method was used to prepare the PEG$_{45}$-*b*-PCL$_{60}$ micelles. A stock solution of the MeO-PEG$_{45}$-*b*-PCL$_{60}$ block copolymer (10 mg/mL) was prepared in acetone. An aliquot of the polymer stock solution (0.8 mL) was added to stirring HPLC grade water (8 mL) at the rate of 0.2 mL/min which resulted in formation of the block copolymer micelles (1.0 mg/mL). The micelle suspension was transferred into dialysis bags (MWCO: 10,000 Da) and dialyzed against HPLC grade water for 36 hours. ^{1}H NMR confirmed the acetone was completely removed after the dialysis. PBS buffer solution (1.0 mL, pH=7.4) was evaporated to dryness by air in a vial. A MeO-PEG$_{45}$-*b*-PCL$_{60}$ micelle suspension (1.0 mL, 1.0 mg/mL) was added into the vial to redissolve the PBS salts. A final solution of micelle with dissolved PBS salt (pH=7.4) was transferred into a polystyrene cuvette. The sizes of the micelles were determined by dynamic light scattering (DLS) at 37 ^{o}C. The hydrodynamic diameter of the MeO-PEG$_{45}$-*b*-PCL$_{60}$ block copolymer micelles in aqueous suspension were found to be 30 nm (37 ^{o}C, pH = 7.4) (Figure 4.17). The shape of the micelles was characterized by TEM (Figure 4.18).

The molecular weight of micelle particles is determined by measuring the micelle sample at different concentrations and applying the Rayleigh equation using Malvern's Zetasizer Nano ZS instrument. The instrument measure the Intensity of scattered light (KC/R_{θ}) of various concentrations (C) (0.25, 0.50, 0.75, 1.0 mg/mL) of the micelle sample. This is compared with the scattering produced from a water standard. The plot of (KC/R_{θ}) vs C is called Debye plot. The weight average molecular weight is determined from the intercept at zero concentration. $KC/R_{\theta} = 1/Mw$ for $C \rightarrow 0$. The Weight average molecular weight of micelle was measured as $2.0 \pm 0.5 \times 10^{6}$ Da.

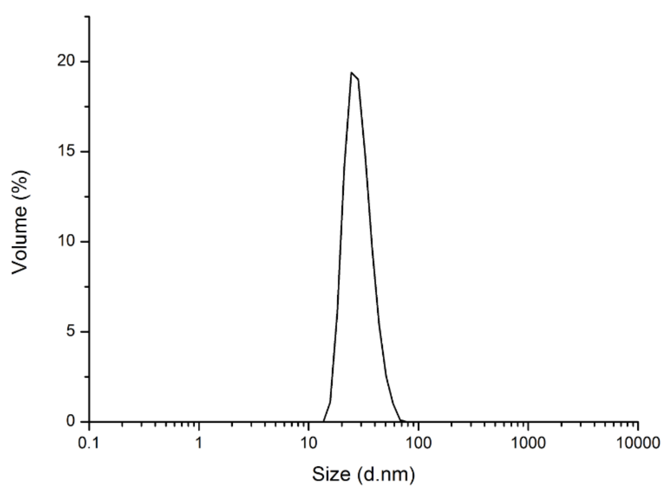

Figure 4.17: Hydrodynamic diameter distribution of MeO-PEG$_{45}$-*b*-PCL$_{60}$ micelles (30 nm, 37 ^{o}C, pH=7.4) after dialyzed in water determined by DLS.

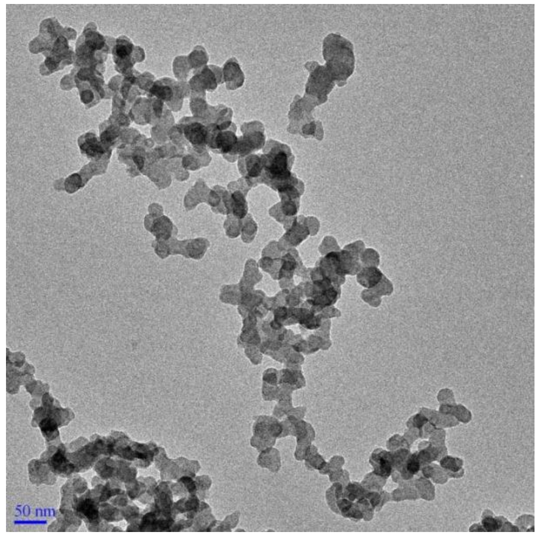

Figure 4.18: TEM image for PEG_{45}-*b*-PCL_{60} micelles obtained from dialysis in water at 25 °C.

4.4.4 ^{1}H NMR for lipase enzyme catalyzed hydrolysis and degradation of MeO-PEG_{45}-*b*-PCL_{60} block copolymer micelles:

The lipase catalyzed degradation of MeO-PEG_{45}-*b*-PCL_{60} micelles were studied at two lipase activities (0.714 and 2.86 U/mL), pH=7.4 and T=37 °C**.** PBS buffer solution (0.70 mL, pH=7.4) was evaporated to dryness by air in a vial. A MeO-PEG_{45}-*b*-PCL_{60} micelle suspension (0.50 mL, 1.0 mg/mL) and D_2O (0.10 mL) were added into the vial to redissolve the PBS salts. A solution of micelle with dissolved PBS salt was transferred into a NMR tube and the solution was heated to 37 °C in the NMR instrument. *P. cepacia* lipase water solution (0.10 mL, 0.132 mg/mL or 0.530 mg/mL) was added into the NMR tube quickly to catalyze the hydrolysis of MeO-PEG_{45}-*b*-PCL_{60} micelle. The degradation of micelle was followed by ^{1}H NMR at 37 °C. DMF was introduced into the NMR tube as internal reference. Water solvent suppressed NMR was used in this experiment.

4.4.5 GPC for lipase catalyzed degradation of MeO-PEG$_{45}$-*b*-PCL$_{60}$ block copolymer micelle:

GPC traces for the lipase catalyzed degradation of MeO-PEG$_{45}$-*b*-PCL$_{60}$ micelles were studied at lipase activity of 2.86 U/mL, pH=7.4 and T=37 ^{o}C. The experiments were done in a series of vials for different degradation times. PBS buffer solution (1.0 mL, pH=7.4) was predried by air in each 5 mL vial. A micelle suspension of MeO-PEG$_{45}$-*b*-PCL$_{60}$ (0.714 mL, 1.0 mg/mL) was added into the vial to redissolve the PBS salts. The solution of micelle with dissolved PBS salt was warmed to 37 ^{o}C in the water bath. Subsequently, *P. cepacia* lipase water solution (0.286 mL, 0.265 mg/mL) was added into the vials. The reactions were terminated at different times by dipping the vials into liquid N_2. Degradation products were collected by freeze drying method and redissolved in DMF for GPC studies.

4.4.6 ^{1}H NMR for lipase catalyzed degradation of MeO-PEG$_{45}$-*b*-PCL$_{60}$ block copolymer micelles at the presence of PEG$_{45}$-*b*-PCL$_{6}$ inhibitor:

MeO-PEG$_{45}$-*b*-PCL$_{6}$ diblock copolymer was prepared followed the same procedure as making MeO-PEG$_{45}$-*b*-PCL$_{60}$ diblock copolymer. The lipase catalyzed degradation of PEG$_{45}$-*b*-PCL$_{60}$ micelle inhibited by MeO-PEG$_{45}$-*b*-PCL$_{6}$ was studied at lipase activity of 0.714 U/mL, pH=7.4 and T=37 ^{o}C. PBS buffer solution (0.70 mL, pH=7.4) was predried by air in a vial. A micelle suspension of MeO-PEG$_{45}$-*b*-PCL$_{60}$ (0.50 mL, 1.0 mg/mL) and D_2O (0.10 mL) was added into the vial to redissolve the PBS salts. A solution of micelle with dissolved PBS salt was transferred into the NMR tube and the solution was heated to 37 ^{o}C in the NMR instrument. Stock aqueous solution (0.10 mL) that contains *P. cepacia* lipase (0.132 mg/mL) and MeO-PEG$_{45}$-*b*-PCL$_{6}$ (5.0 mg/mL) was added into the NMR tube quickly to catalyze the hydrolysis of MeO-PEG$_{45}$-*b*-PCL$_{60}$ micelle. The degradation of micelle was followed by ^{1}H NMR at 37 ^{o}C. DMF was introduced into the NMR tube as internal reference. Water solvent suppressed NMR was used in this experiment.

4.5 References

(1) Bornscheuer, U. T. *FEMS Microbiol. Rev* 2002, 26, 73-81.

(2) Chahinian, H.; Nini, L.; Boitard, E.; Dubès, J.-P.; Comeau, L.-C.; Sarda, L. *Lipids* 2002, 37, 653-662.

(3) Chahinian, H.; Fantini, J.; Garmy, N.; Manco, G.; Sarda, L. *Biochim. Biophys. Acta* 2010, 1801, 1195-1204.

(4) Heitz, F.; Van Mau, N. *Biochim. Biophys. Acta* 2002, 1597, 1-11.

(5) Bornscheuer, U.; Reif, O.-W.; Lausch, R.; Freitag, R.; Scheper, T.; Kolisis, F. N.; Menge, U. *Biochim. Biophys. Acta* 1994, 1201, 55-60.

(6) Sugihara, A.; Ueshima, M.; Shimada, Y.; Tsunasawa, S.; Tominaga, Y. *J. Biochem.* 1992, 112, 598-603.

(7) Schrag, J. D.; Li, Y.; Cygler, M.; Lang, D.; Burgdorf, T.; Hecht, H.-J.; Schmid, R.; Schomburg, D.; Rydel, T. J.; Oliver, J. D.; Strickland, L. C.; Dunaway, C. M.; Larson, S. B.; Day, J.; McPherson, A. *Structure* 1997, 5, 187-202.

(8) Kim, K. K.; Song, H. K.; Shin, D. H.; Hwang, K. Y.; Suh, S. W. *Structure* 1997, 5, 173-185.

(9) Schrag, J. D.; Li, Y. G.; Cygler, M.; Lang, D. M.; Burgdorf, T.; Hecht, H. J.; Schmid, R.; Schomburg, D.; Rydel, T. J.; Oliver, J. D.; Strickland, L. C.; Dunaway, C. M.; Larson, S. B.; Day, J.; McPherson, A. *Structure* 1997, 5, 187-202.

(10) Chahiniana, H.; Sarda, L. *Protein Pept. Lett.* 2009, 16, 1149-1161.

(11) Lemoine, D.; Francois, C.; Kedzierewicz, F.; Preat, V.; Hoffman, M.; Maincent, P. *Biomaterials* 1996, 17, 2191-2197.

(12) Peng, H.; Ling, J.; Liu, J.; Zhu, N.; Ni, X.; Shen, Z. *Polym. Degrad. Stab.* 2010, 95, 643-650.

(13) Iwata, T.; Doi, Y. *Polym. Int.* 2002, 51, 852-858.

(14) Gan, Z.; Fung, J. T.; Jing, X.; Wu, C.; Kuliche, W. K. *Polymer* 1999, 40, 1961-1967.

(15) Gan, Z.; Jim, T. F.; Li, M.; Yuer, Z.; Wang, S.; Wu, C. *Macromolecules* 1999, 32, 590-594.

(16) Jiang, Z.; Zhu, Z.; Liu, C.; Hu, Y.; Wu, W.; Jiang, X. *Polymer* 2008, 49, 5513-5519.

(17) Zhu, X.; Fryd, M.; Tran, B. D.; Ilies, M. A.; Wayland, B. B. *Macromolecules* 2012, 45, 660-665.

(18) Shen, C.; Guo, S.; Lu, C. *Polym. Degrad. Stab.* 2007, 92, 1891-1898.

(19) Tyrrell, Z. L.; Shen, Y.; Radosz, M. *Prog. Polym. Sci.* 2010, 35, 1128-1143.

(20) Zhang, Q.; Remsen, E. E.; Wooley, K. L. *J. Am. Chem. Soc.* 2000, 122, 3642-3651.

(21) Hickey, R. J.; Haynes, A. S.; Kikkawa, J. M.; Park, S.-J. *J. Am. Chem. Soc.* 2011, 133, 1517-1525.

(22) Zhu, W.; Nese, A.; Matyjaszewski, K. *J. Polym. Sci., Part A: Polym. Chem.* 2011, 49, 1942-1952.

(23) Bronich, T. K.; Keifer, P. A.; Shlyakhtenko, L. S.; Kabanov, A. V. *J. Am. Chem. Soc.* 2005, 127, 8236-8237.

(24) Lee, H.-i.; Wu, W.; Oh, J. K.; Mueller, L.; Sherwood, G.; Peteanu, L.; Kowalewski, T.; Matyjaszewski, K. *Angew. Chem. Int. Ed.* 2007, 46, 2453-2457.

(25) Deng, C.; Jiang, Y.; Cheng, R.; Meng, F.; Zhong, Z. *Nano Today* 2012, 7, 467-480.

(26) Langer, R.; Tirrell, D. A. *Nature* 2004, 428, 487-492.

(27) Elsabahy, M.; Wooley, K. L. *Chem. Soc. Rev.* 2012, 41, 2545-2561.

(28) Endres, T. K.; Beck-Broichsitter, M.; Samsonova, O.; Renette, T.; Kissel, T. H. *Biomaterials* 2011, 32, 7721-7731.

(29) Zhu, Z.; Li, Y.; Li, X.; Li, R.; Jia, Z.; Liu, B.; Guo, W.; Wu, W.; Jiang, X. *J. Controlled Release* 2010, 142, 438-446.

(30) Yang, R.; Meng, F.; Ma, S.; Huang, F.; Liu, H.; Zhong, Z. *Biomacromolecules* 2011, 12, 3047-3055.

(31) Samarajeewa, S.; Shrestha, R.; Li, Y.; Wooley, K. L. *J. Am. Chem. Soc.* 2011, 134, 1235-1242.

(32) Bae, Y. H.; Yin, H. *J. Controlled Release* 2008, 131, 2-4.

(33) Read, E. S.; Armes, S. P. *Chem. Commun.* 2007, 3021-3035.

(34) Xiong, J.; Meng, F.; Wang, C.; Cheng, R.; Liu, Z.; Zhong, Z. *J. Mater. Chem.* 2011, 21, 5786-5794.

(35) Shen, C.; Guo, S.; Lu, C. *Polym. Adv. Technol.* 2008, 19, 66-72.

(36) Lam, H.; Gong, X.; Wu, C. *J. Phys. Chem. B* 2007, 111, 1531-1535.

(37) Carstens, M. G.; van Nostrum, C. F.; Verrijk, R.; de Leede, L. G. J.; Crommelin, D. J. A.; Hennink, W. E. *J. Pharm. Sci.* 2008, 97, 506-518.

(38) Hu, Y.; Jiang, Z.; Chen, R.; Wu, W.; Jiang, X. *Biomacromolecules* 2010, 11, 481-488.

(39) Berg, O. G.; Gelb, M. H.; Tsai, M.-D.; Jain, M. K. *Chem. Rev.* 2001, 101, 2613-2654.

(40) van Tilbeurgh, H.; Egloff, M.-P.; Martinez, C.; Rugani, N.; Verger, R.; Cambillau, C. *Nature* 1993, 362, 814-820.

(41) Schmid, R. D.; Verger, R. *Angew. Chem. Int. Ed.* 1998, 37, 1608-1633.

(42) Sörensen, M. H.; Ng, J. B. S.; Bergström, L.; Alberius, P. C. A. *J. Colloid Interface Sci.* 2010, 343, 359-365.

(43) Andresen, T. L.; Jensen, S. S.; Jørgensen, K. *Prog. Lipid Res.* 2005, 44, 68-97.

(44) Tong, Y.; Li, N.; Liu, H.; Ge, A.; Osawa, M.; Ye, S. *Angew. Chem. Int. Ed.* 2010, 49, 2319-2323.

(45) Wu, H.; Yu, L.; Tong, Y.; Ge, A.; Yau, S.; Osawa, M.; Ye, S. *Biochim. Biophys. Acta*.

(46) Arouri, A.; Mouritsen, O. G. *Eur. J. Pharm. Sci.* 2012, 45, 408-420.

(47) Halperin, A.; Mouritsen, O. *Europhys. Lett.* 2005, 34, 967-971.

(48) Hoyrup, P.; Callisen, T. H.; Jensen, M. O.; Halperin, A.; Mouritsen, O. G. *Phys. Chem. Chem. Phys.* 2004, 6, 1608-1615.

(49) Bajaj, H.; Sharma, V. K.; Kalonia, D. S. *Biophys. J* . 2004, 87, 4048-4055.

(50) Furó, I. *Journal of Molecular Liquids* 2005, 117, 117-137.

(51) Dorovska-Taran, V.; Wick, R.; Walde, P. *Anal. Biochem.* 1996, 240, 37-47.

(52) Geng, D.; Chura, J.; Roberts, M. F. *J. Biol. Chem.* 1998, 273, 12195-12202.

(53) Yang, H.; Roberts, M. F. *Protein Sci.* 2003, 12, 2087-2098.

(54) Nie, T.; Zhao, Y.; Xie, Z.; Wu, C. *Macromolecules* 2003, 36, 8825-8829.

(55) Constantinou-Kokotou, V.; Magrioti, V.; Verger, R. *Chem. Eur. J.* 2004, 10, 1133-1140.

(56) Bertrand, T.; Augé, F.; Houtmann, J.; Rak, A.; Vallée, F.; Mikol, V.; Berne, P. F.; Michot, N.; Cheuret, D.; Hoornaert, C.; Mathieu, M. *J. Mol. Biol.* 2010, 396, 663-673.

(57) Tsou, C. L. *Biochim. Biophys. Acta* 1995, 1253, 151-162.

(58) Takano, Y.; Houk, K. N. *J. Phys. Chem. A* 2004, 108, 11740-11751.

(59) Torre, O.; Alfonso, I.; Gotor, V. *Chem. Commun.* 2004, 1724-1725.

(60) Berg, O. G.; Yu, B. Z.; Rogers, J.; Jain, M. K. *Biochemistry* 1991, 30, 7283-7297.

(61) Ali, M. H.; Imperiali, B. *Bioorg. Med. Chem.* 2005, 13, 5013-5020.

(62) Andresen, T. L.; Jensen, S. S.; Jørgensen, K. *Progress in Lipid Research* 2005, 44, 68-97.

(63) Halperin, A.; Mouritsen, O. *European Biophysics Journal* 2005, 34, 967-971.

(64) Hoyrup, P.; Callisen, T. H.; Jensen, M. O.; Halperin, A.; Mouritsen, O. G. *Physical Chemistry Chemical Physics* 2004, 6, 1608-1615.

(65) Kuzmič, P. *Anal. Biochem.* 1996, 237, 260-273.

(66) Cajal, Y.; Berg, O. G.; Jain, M. K. *Biochemistry* 2004, 43, 9256-9264.

(67) Barbe, S.; Lafaquière, V.; Guieysse, D.; Monsan, P.; Remaud-Siméon, M.; André, I. *Proteins: Structure, Function, and Bioinformatics* 2009, 77, 509-523.

(68) Ranaldi, S.; Belle, V. r.; Woudstra, M.; Bourgeas, R.; Guigliarelli, B.; Roche, P.; Vezin, H.; Carrière, F. r.; Fournel, A. *Biochemistry* 2010, 49, 2140-2149.

(69) Rehm, S.; Trodler, P.; Pleiss, J. *Protein Sci.* 2010, 19, 2122-2130.

(70) Yin, D.; Kazlauskas, R. J. *Chem. Eur. J.* 2012, 18, 8130-8139.

(71) Schulz, T.; Pleiss, J.; Uuml; Rgen; Schmid, R. D. *Protein Sci.* 2000, 9, 1053-1062.

(72) Fairley, N.; Hoang, B.; Allen, C. *Biomacromolecules* 2008, 9, 2283-2291.

(73) Luo, L.; Tam, J.; Maysinger, D.; Eisenberg, A. *Bioconjugate Chem.* 2002, 13, 1259-1265.

CHAPTER 5:

DESIGN AND SYNTHESIS OF PCL-*b*-PEG MICELLES WITH CHARGED CORONA: INCREASE STABILITY OF MICELLE AQUEOUS DISPERSIONS

5.1 Introduction

Amphiphilic block copolymers that self-assemble into core-shell micelles with hydrophilic corona and hydrophobic cores[1-9] provide a broad platform for development of drug delivery vehicles that encapsulate hydrophobic therapeutics that have been properly loaded into the micelle core[10-12]. Block copolymers from poly (ε-caprolactone) and poly (ethylene glycol) (PCL-*b*-PEG)[13-15] are typical amphiphilic block copolymers that self assemble into micelles in water where the hydrolytically stable hydrophilic PEG segment forms the exterior corona and the core contains the hydrophobic degradable PCL block. Micelles derived from the basic PCL-*b*-PEG block copolymer unit are among the top candidates for application as transport and delivery systems and serve as a prototypical system to use in the development of general strategies to optimize the target micelle properties of core loading, dispersion stability and selective degradation for drug release. Chapters 2-4 have addressed issues of acid and enzyme catalyzed PCL-*b*-PEG-OMe block copolymer micelle degradation that are important issues in drug transport, circulation time and selective release. Inserting a short hydrophobic non-hydrolyzable poly (1,2-butylene oxide) (PBO) segment between the PEG and PCL blocks as an approach to increase the barrier for water to reach the interface ester at the surface of the PCL core and thus increase the micelle stability at acidic aqueous medium. However, the PCL-*b*-PBO-*b*-PEG-OMe micelle doesn't significantly reduce the rate of lipase enzyme catalyzed degradation of micelle from PCL-*b*-PEG-OMe.

An essential feature for micelle application on drug delivery system is that the aqueous dispersions must be stable toward both precipitation and dissolution over the range of conditions such as concentrations of ions and pH encountered in the specific application. The loading content in the hydrophobic core depends on the size of the hydrophobic PCL block that can be supported in the dispersion by the hydrophilic corona. The capacity of a micelle to store a hydrophobic substance is proportional to the size of the core[1, 16-20] which in block copolymer micelles is related to the length of the hydrophobic polymer segment. The general approach to increase the loading capacity for a micelle carrier is simply to increase the volume of the hydrophobic core which is limited by the capability of the hydrophilic corona to maintain a stable aqueous dispersion of the insoluble hydrophobic core.

The PEG segment of PCL-*b*-PEG diblock copolymer micelles typically has an uncharged end group such as methoxide ($-OCH_3$)[14, 21-24] and allyl ($-CH_2CH{=}CH$)[12, 25] which yields micelles where the corona is terminated by a neutral group. The working hypothesis is that the stability of aqueous dispersions of micelles can be increased by placing ionic end groups on PEG which gives electrically charged corona that both increase interactions of the micelle with the aqueous environment and inhibit aggregation of micelles through electrostatic repulsions. This chapter reports on initial model studies that compare micelle dispersion stabilities of diblock copolymers of HO-PCL_n-*b*-PEG_{32}-$CH_2CH{=}CH$ and HO-PCL_n-*b*-PEG_{32}-RX (R= $-O(CH_2)_3S(CH_2)_2-$; X= $-CO_2H$, $-SO_3Na$; n=51,67,109). Thiol-ene click chemistry[26-28] of an allyl terminated block copolymer (HO-PCL_n-*b*-PEG_{32}-$CH_2CH{=}CH_2$) was used to introduce $-CO_2H$ and $-SO_3Na$ end groups on the PEG segment and produce micelles that have negatively charged groups at the end of the corona (Scheme 5.1). The general concept that micelles with ionic corona will increase the range of micelle dispersion stability is illustrated by the observation that HO-PCL_n-*b*-PEG_{32}-RX (X= $-CO_2Na$, $-SO_3Na$) give stable aqueous dispersions with much larger hydrophobic cores and higher ion concentration than micelles from HO-PCL_n-*b*-PEG_{32}-$CH_2CH=CH_2$ where a neutral allyl group terminates the corona.

Scheme 5. 1: Schematic demonstration of micelle corona charge modification.

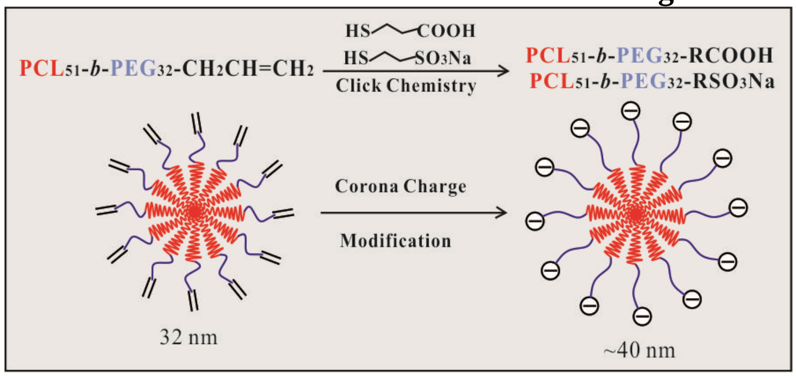

5.2 Results and Discussion

5.2.1 Synthesis of hydroxyl and allyl terminated polyethylene glycol (HO-PEG_{32}-$CH_2CH=CH_2$)

Low polydispersity (PDI) and high purity HO-PEG_{32}-$CH_2CH=CH_2$ was synthesized by anionic polymerization of ethylene oxide using allyl alcoholate ($CH_2=CHCH_2-O^-$) as an initiator[29-31] (Scheme 5.1). The allyl alcoholate was prepared by deprotonating allyl alcohol using potassium naphthalenide at reduced temperature (-5 ^oC) to avoid the formation of propenyl alcoholate isomer ($CH_3CH=CH-O^-$) that was reported by Riess[30]. The 18 crown 6 polyether was used both to coordinate the potassium ion which polymerization[32-33]. Methanol was used in place of dilute HCl acid to terminate the reaction in order to avoid placing a hydroxyl group at the terminal position to form HO-PEG_{32}-$CH_2CH_2CH_2OH$ by addition of H_2O.

Scheme 5.2: Synthesis of HO-PEG$_{32}$-CH$_2$CH=CH$_2$ homopolymer.

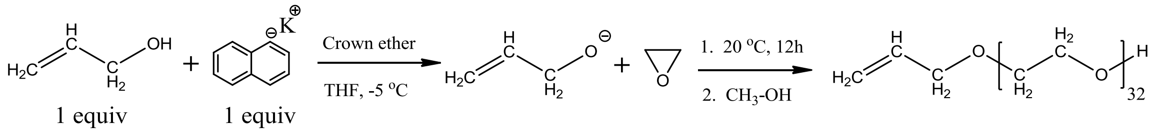

Relatively high quality HO-PEG$_n$-CH$_2$CH=CH$_2$ polymer product was indicated by the mono-modal GPC traces with narrow molecular weight distribution (PDI= 1.11) (Figure 5.5). The molecular weight of the highest concentration polymer observed in the MALDI mass spectrum is 1466 which corresponds to the PEG chain having a most probable length of 32 monomer units (HO-PEG$_{32}$-CH$_2$CH=CH$_2$) (Figure 5.1). The degree of polymerization (DP) of ethylene oxide obtained by comparing the ^{1}H NMR integration of signals at 3.6 ppm for CH$_2$ of PEG (labeled d) and two doublets at 5.2 ppm for CH$_2$ of the allyl end group (labeled a) is 35(2) which is in satisfactory agreement with the DP of 32 from the MALDI results (Figure 5.2).

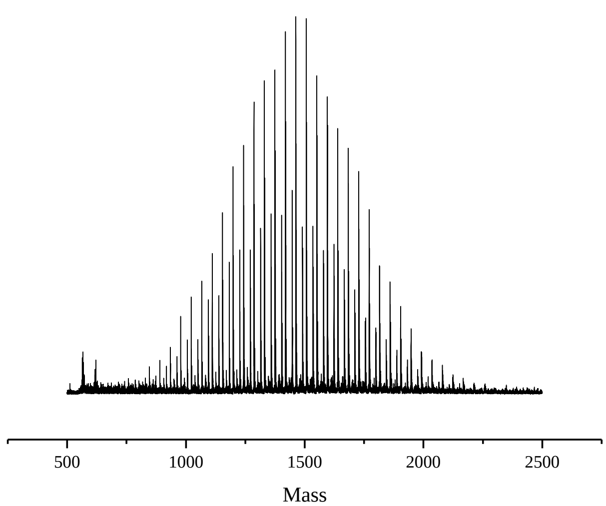

Figure 5.1: MALDI mass spectrum showing HO-PEG$_{32}$-CH$_2$CH=CH$_2$ as the most probable allyl terminated PEG polymer.

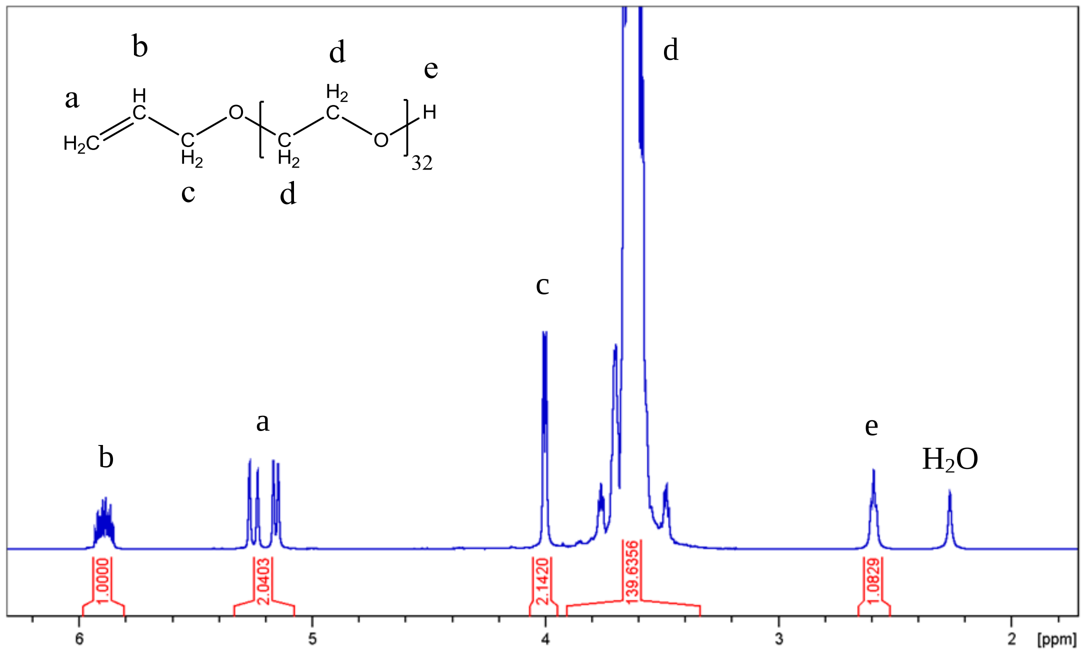

Figure 5.2: ^{1}H NMR for HO-PEG$_{32}$-CH$_2$CH=CH$_2$ in CDCl$_3$ and peak assignments.

5.2.2 Synthesis of HO-PCL$_n$-*b*-PEG$_{32}$-CH$_2$CH=CH$_2$ (n=51,67,109) diblock copolymers

Amphiphilic diblock copolymers from HO-PCL$_n$-*b*-PEG$_{32}$-CH$_2$CH=CH$_2$ (n= 51,67,109, PDI <1.10) were synthesized utilizing HO-PEG$_{32}$-CH$_2$CH=CH$_2$ as the macroinitiator for the ring-opening polymerization of ε-caprolactone (CL) in the presence of stannous octoate (Sn(Oct)$_2$) as a catalyst[34-35] (Scheme 5.2). An early termination strategy was used to prepare low polydispersity HO-PCL$_n$-*b*-PEG$_{32}$-CH$_2$CH=CH$_2$ (n= 51,67,109) diblock copolymers. The initial feeding ratio of CL to PEG is 160, but the CL polymerization was quenched in MeOH at reaction time of 3h, 4h, and 5.5h respectively before all the CL was polymerized. The NMR integration ratio CH$_2$ resonances from allyl group and PEG segment remains constant after the polymerization of CL indicating that allyl terminal group remains intact during the CL polymerization (Figure 5.3). The degree of polymerization (DP) of CL was evaluated by comparing the integration of signals at 3.62 ppm for CH_2 of PEG (labeled c) and a triplet at 2.30 ppm assigned to the CH_2 of PCL (labeled e)(Figures 5.3).

Scheme 5.3: Synthesis of HO-PCL$_n$-*b*-PEG$_{32}$-$CH_2CH=CH_2$ diblock copolymers (n=44,51,109).

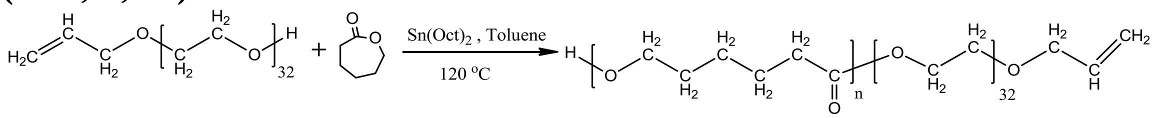

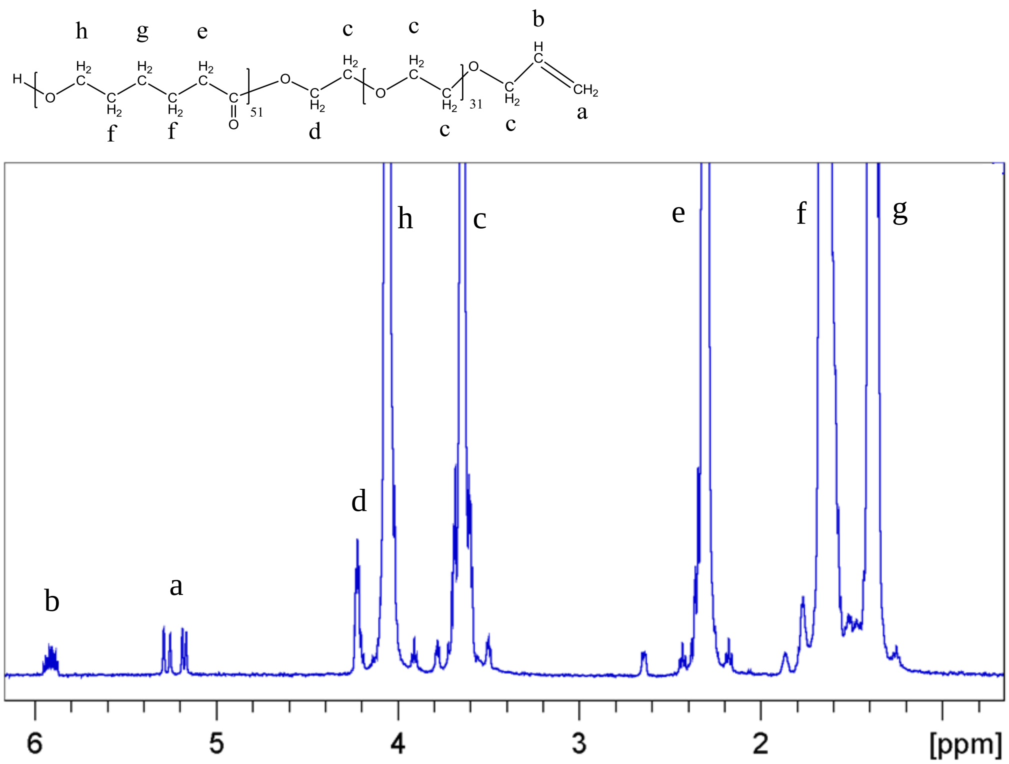

Figure 5.3: ^{1}H NMR for HO-PCL$_{51}$-*b*-PEG$_{32}$-$CH_2CH=CH_2$ diblock copolymer in $CDCl_3$ and peak assignments.

5.2.3 Synthesis of HO-PCL$_n$-*b*-PEG$_{32}$-RX (R=-O(CH$_2$)$_3$S(CH$_2$)$_2$-; X= CO$_2$H, SO$_3$Na; n=51,67,109) diblock copolymers by thiol-ene click chemistry

Negatively charged carboxylate (CO_2^-) and sulfonate(SO_3^-) terminal groups were placed onto end of the PEG segment by thiol-ene click chemistry of the HO-PCL$_{51}$-PEG$_{32}$-$CH_2CH{=}CH_2$ diblock copolymer[26-28](scheme 5.3). ^{1}H NMR of the HO-PCL$_{51}$-PEG$_{32}$-RX (X= CO_2Na, SO_3Na) diblock polymers shows that after the click coupling, all of the resonances associated with the allyl group (δ=5-6 ppm) entirely disappear and new peaks (δ= 2.5-3.4 ppm) appear that are associated with a -CH_2CH_2-S-CH_2CH_2- group (Figure 5.4). GPC traces for diblock copolymers of HO-PCL$_{51}$-*b*-PEG$_{32}$-$CH_2CH{=}CH_2$ and HO-PCL$_{51}$-*b*-PEG$_{32}$-RX (R= -O(CH$_2$)$_3$S(CH$_2$)$_2$-; X= CO_2Na; SO_3Na) are all mono-modal with low polydispersity (PDI < 1.10) (Figure 5.5). The combined results from the ^{1}H NMR and GPC of diblock copolymers (HO-PCL$_{51}$-*b*-PEG$_{32}$-RX, X=-CO_2H, -SO_3Na) demonstrates that the thiol-ene click chemistry method is an efficient method for introducing electronically charged groups at the end of the PEG segments.

Scheme 5.4: Synthesis of HO-PCL$_n$-*b*-PEG$_{32}$-RX (n=51,67,109, X=CO_2H, SO_3Na) diblock copolymers via click chemistry.

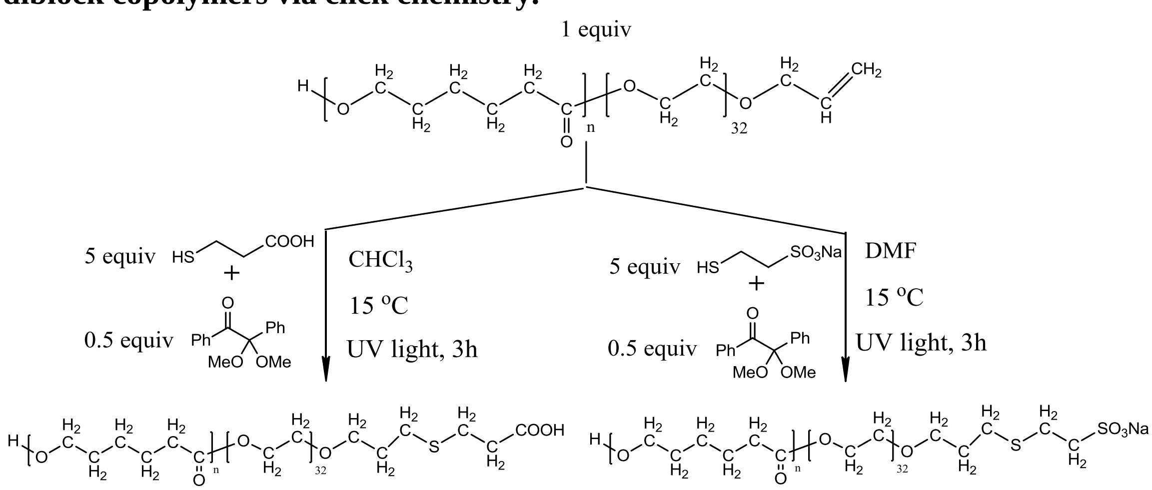

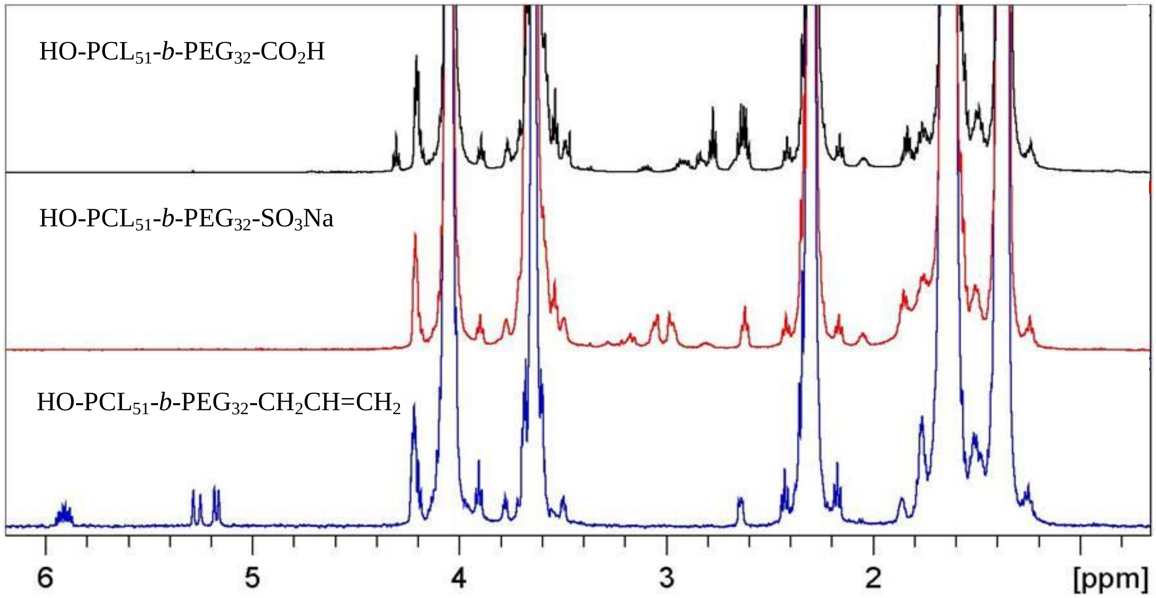

Figure 5.4: ^{1}H NMR for HO-PCL$_{51}$-*b*-PEG$_{32}$-RCOOH (A); HO-PCL$_{51}$-*b*-PEG$_{32}$-R SO$_3$Na (B); HO-PCL$_{51}$-*b*-PEG$_{32}$-CH$_2$CH=CH$_2$ (C) diblock copolymers in CDCl$_3$ (R= -O(CH$_2$)$_3$S(CH$_2$)$_2$-).

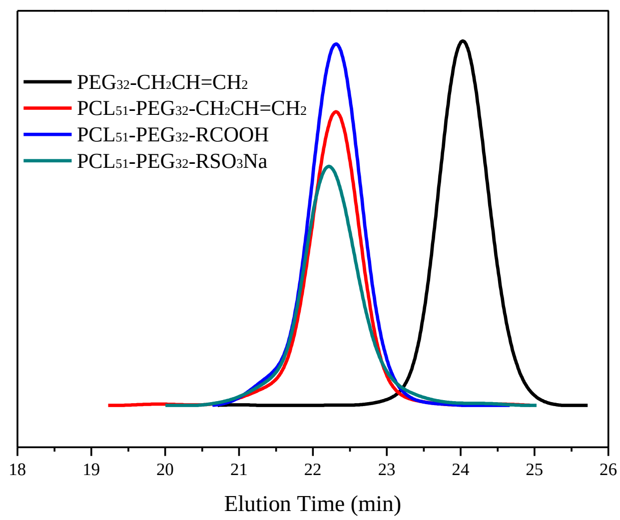

Figure 5.5: GPC traces for HO-PEG$_{32}$-CH$_2$CH=CH$_2$ homopolymer, HO-PCL$_{51}$-*b*-PEG$_{32}$-CH$_2$CH=CH$_2$ and HO-PCL$_{51}$-*b*-PEG$_{32}$-RX (R=-O(CH$_2$)$_3$S(CH$_2$)$_2$-, X= CO$_2$H, SO$_3$Na) diblock copolymers.

5.2.4 Formation and characterization of diblock copolymer micelles from PCL_n-*b*-PEG_{32}-$CH_2CH{=}CH_2$, $[PCL_n$-*b*-PEG_{32}-$RCO_2]^-Na^+$ and $[PCL_n$-*b*-PEG_{32}-$RSO_3]^-Na^+$

Micelles from PCL_n-*b*-PEG_{32}-$CH_2CH{=}CH_2$, $[PCL_n$-*b*-PEG_{32}-$RCO_2]^-Na^+$ and $[PCL_n$-*b*-PEG_{32}-$RSO_3]^-Na^+$ (n= 51,67,109) diblock copolymers were formed by the same nano precipitation method that was previously applied in forming micelles of MeO-PEG-*b*-PCL-OH diblock copolymers[36-39]. Stock solutions of the block copolymer in acetone acetone were added into water where self assemble into micelles with narrow size distribution. Hydrodynamic diameters of the micelles dispersed in PBS buffer were measured by DLS and the results are shown in Table 5.1 (pH=7.4; T= 37 ^oC). The micelle dispersions formed by slowly adding acetone solutions of polymer to water and those formed by the reverse process are indistinguishable by DLS. The hydrodynamic diameters evaluated by DLS regularly increase in going from micelles of PCL_n-*b*-PEG_{32}-$CH_2CH{=}CH_2$ to $[PCL_n$-*b*-PEG_{32}-$RCO_2]^-Na^+$ and finally $[PCL_n$-*b*-PEG_{32}-$RSO_3]^-Na^+$ at each value of n (n= 51,67,109) (Table 5.1). The possible reason for this behavior is that as the aqueous solubility of the terminal group increases the PEG corona stretches further out into the solution. DLS measurements also show that the hydrodynamic diameter of micelles is proportional to the length of the PCL segments with a fixed length of the PEG block. The cryo-TEM image of micelles from PCL_{51}-*b*-PEG_{32}-$CH_2CH{=}CH_2$ only resolves the PCL spherical core which has an average diameter of ~20 nm (Figure 5.6A) compared to the hydrodynamic diameter of ~ 32nm determined by DLS. The normal TEM image of $[PCL_{51}$-*b*-PEG_{32}-$RCO_2]^-Na^+$ micelles also indicates that the block copolymers only assemble into spherical micelles that aggregate together during the sample drying process (Figure 5.6B). The large hydrophobic to hydrophilic ratio of PCL_{109}-*b*-PEG_{32}-$CH_2CH{=}CH_2$ prohibited micelle formation, but micelles from [PCL_{109}-*b*-PEG_{32}-RCO_2]$^-$$Na^+$ and [PCL_{109}-*b*-PEG_{32}-RSO_3]$^-$$Na^+$ with negatively charged groups on the corona are very stable at pH=7.4. Block copolymer micelles that have electronically charged groups on the terminus of the corona increase the repulsion between micelles to enhance the micelles stability from high hydrophobic to hydrophilic ratio block copolymers.

Table 5.1: Effective hydrodynamic diameters from DLS and surface charges from Zeta potentials for diblock copolymer micelles.

Micelle Sample	Diameter (pH = 7.4, 37℃)	Zeta Potential (ζ, 25℃)
PCL_{51}-*b*-PEG_{32}-$CH_2CH{=}CH_2$	32 nm	-13 mV
[PCL_{51}-*b*-PEG_{32}-RCO_2]$^-$ Na^+	38 nm	-31 mV
[PCL_{51}-*b*-PEG_{32}-RSO_3]$^-$ Na^+	43 nm	-27 mV
PCL_{67}-*b*-PEG_{32}-$CH_2CH{=}CH_2$	37 nm	-5 mV
[PCL_{67}-*b*-PEG_{32}-RCO_2]$^-$ Na^+	50 nm	-30 mV
[PCL_{67}-*b*-PEG_{32}-RSO_3]$^-$ Na^+	53 nm	-28 mV
PCL_{109}-*b*-PEG_{32}-$CH_2CH{=}CH_2$	Precipitated	Precipitated
[PCL_{109}-*b*-PEG_{32}-RCO_2]$^-$ Na^+	84 nm	-35 mV
[PCL_{109}-*b*-PEG_{32}-RSO_3]$^-$ Na^+	90 nm	-26 mV

The measured zeta potentials (ζ) of all the polymer micelles in water at 25 ^oC are listed in Table 5.1. The PCL-*b*-PEG-$CH_2CH{=}CH_2$ micelles have a ζ of -10 ± 5 mV which is similar to the values that were previous measured for PCL-*b*-PEG-MeO micelles[17]. The measured zeta potentials for micelles from [PCL_n-*b*-PEG_{32}-RCO_2]$^-$$Na^+$ and [PCL_n-*b*-PEG_{32}-RSO_3]$^-$$Na^+$ are ~ -30 mV. Attaching negatively charged sulfonate

(SO_3^-) and carboxylate (CO_2^-) groups on the PEG corona as expected results in large negative Zeta potentials.

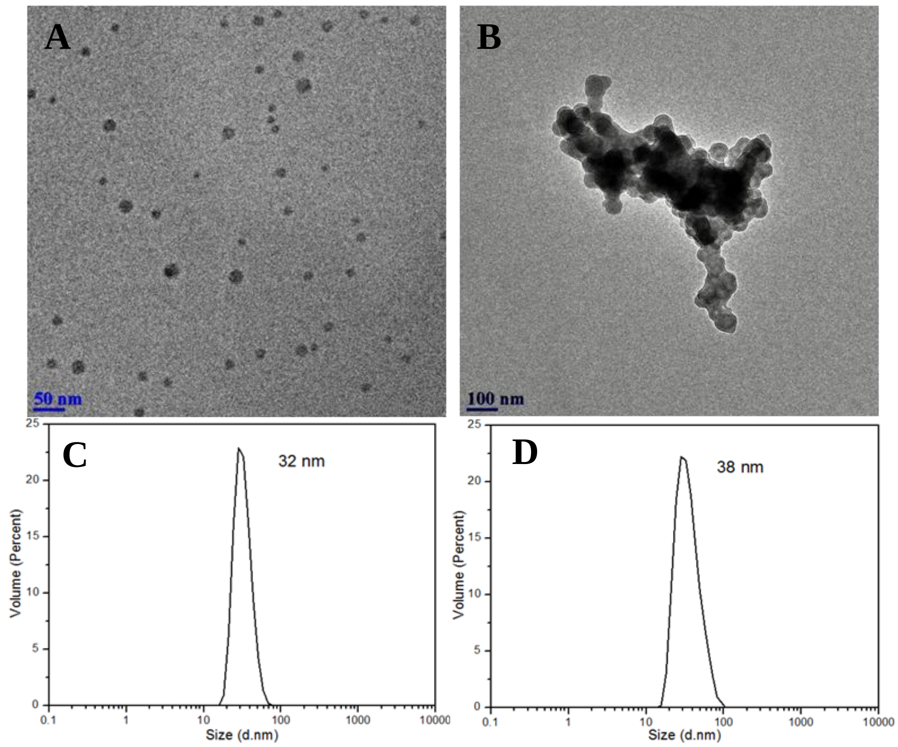

Figure 5.6: Cryo-TEM image for PCL_{51}-*b*-PEG_{32}-$CH_2CH{=}CH_2$ micelles (A); normal TEM image for $[PCL_{51}$-*b*-PEG_{32}-$RCO_2]^-Na^+$ micelles (B); size distribution of PCL_{51}-*b*-PEG_{32}-$CH_2CH{=}CH_2$ micelles (C) and $[PCL_{51}$-*b*-PEG_{32}-$RCO_2]^-Na^+$ (D).

5.2.5 Stability of diblock copolymer micelles formed from PCL_n-*b*-PEG_{32}-$CH_2CH{=}CH_2$, $[PCL_n$-*b*-PEG_{32}-$RCO_2]^-Na^+$ and $[PCL_n$-*b*-PEG_{32}-$RSO_3]^-Na^+$ (n= 51,67,109) at different pH

A series of nine block copolymer micelles with different terminal groups and varying PCL chain lengths (HO-PCL_n-*b*-PEG_{32}-$CH_2CH{=}CH_2$, [HO-PCL_n-*b*-PEG_{32}-$RCO_2]^-Na^+$ and [HO-PCL_n-*b*-PEG_{32}-$RSO_3]^-Na^+$ (n= 51,67,109)) were prepared and the aqueous dispersion stabilities were observed in several pH buffered solutions (pH = 4.0, 7.4 ,10.0) (Table 5.2) and over a range of NaCl solution concentrations (Tables 5.2, 5.3).

Table 5.2: Stabilities of micelle aqueous dispersions as a function of block copolymer composition and solutions buffered at a series of pH values ("S" indicates stable dispersion, "P" indicates micelle precipitation).

Buffer / End group	pH = 4.0 buffer	pH = 7.4 buffer	pH = 10.0 buffer
$-CH_2CH=CH_2$	PCL_{51}-*b*-PEG_{32} (***S***)	PCL_{51}-*b*-PEG_{32} (***S***)	PCL_{51}-*b*-PEG_{32} (***P***)
	PCL_{67}-*b*-PEG_{32} (***S***)	PCL_{67}-*b*-PEG_{32} (***S***)	PCL_{67}-*b*-PEG_{32} (***P***)
	PCL_{109}-*b*-PEG_{32} (***P***)	PCL_{109}-*b*-PEG_{32} (***P***)	PCL_{109}-*b*-PEG_{32} (***P***)
$-CO_2^-$	PCL_{51}-*b*-PEG_{32} (***S***)	PCL_{51}-*b*-PEG_{32} (***S***)	PCL_{51}-*b*-PEG_{32} (***S***)
	PCL_{67}-*b*-PEG_{32} (***S***)	PCL_{67}-*b*-PEG_{32} (***S***)	PCL_{67}-*b*-PEG_{32} (***S***)
	PCL_{109}-*b*-PEG_{32} (***P***)	PCL_{109}-*b*-PEG_{32} (***S***)	PCL_{109}-*b*-PEG_{32} (***S***)
$-SO_3^-$	PCL_{51}-*b*-PEG_{32} (***S***)	PCL_{51}-*b*-PEG_{32} (***S***)	PCL_{51}-*b*-PEG_{32} (***S***)
	PCL_{67}-*b*-PEG_{32} (***S***)	PCL_{67}-*b*-PEG_{32} (***S***)	PCL_{67}-*b*-PEG_{32} (***S***)
	PCL_{109}-*b*-PEG_{32} (***S***)	PCL_{109}-*b*-PEG_{32} (***S***)	PCL_{109}-*b*-PEG_{32} (***S***)

Footnote: pH=7.40 buffer solution obtained from dissolve PBS buffer saline tablet from Sigma Aldrich in water: 0.01 M phosphate buffer, 0.0027 M KCl and 0.137 M NaCl (pH 7.4, 25 ℃). pH = 4.0 buffer solution was purchased from Fisher Scientific (SB98-500): 0.05 M Potassium Acid Phthalate with 0.05% Formaldehyde. pH = 10.0 buffer solution was purchased from Fisher Scientific (SB116-500): Potassium Carbonate, Potassium Tetraborate, Potassium Hydroxide/Disodium EDTA Dihydrate.

Table 5.3: Stabilities for aqueous dispersions of micelle as a function of NaCl concentrations.

[NaCl] / Micelle	0.14 M	0.30 M	1.50 M
PCL_{51}-*b*-PEG_{32}-$CH_2CH=CH_2$	(***S***)	(***P***)	(***P***)
[HO-PCL_{51}-*b*-PEG_{32}-RSO_3]$^-$ Na^+	(***S***)	(***S***)	(***S***)

5.3 Summary

Thiol-ene click reactions of HO-PCL_n-*b*-PEG_{32}-$CH_2CH=CH_2$ provide a convenient approach to form low polydispersity block copolymers terminated with -CO_2H and -SO_3Na groups (HO-PCL_n-*b*-PEG_{32}-RX (X= -CO_2H, -SO_3Na, R= -$O(CH_2)_3S(CH_2)_2$-; n=51,67,109). Carboxylate and sulfonate terminated HO-PCL_n-*b*-PEG_{32}-X block copolymers readily self-assemble into spherical micelles in water that manifest dispersion stabilities consistent with the general strategy of using charged groups placed at the end of the micelle corona to increase the stability of micelle aqueous dispersions. Micelles from $[PCL_n\text{-}b\text{-}PEG_{32}\text{-}RCO_2]^-Na^+$ and $[PCL_n\text{-}b\text{-}PEG_{32}\text{-}RSO_3]^-Na^+$ are observed to give stable aqueous dispersions with much larger hydrophobic cores and higher solution ion concentrations than micelles from PCL_n-*b*-PEG_{32}-$CH_2CH=CH_2$ where a neutral allyl group terminates the corona. Sulfonate terminated polymers produced stable micelle dispersions at all block copolymers and solution compositions studied, and are particularly unusual in giving stable micelle dispersions at highly acidic conditions. Negatively charged CO_2^- and SO_3^- groups on the corona terminus have attractive interactions with water and inter-particle electrostatic repulsions that inhibit aggregation both of which contribute to increasing the micelle dispersion stability relative to micelles with neutral groups terminating the corona. The favorable stability properties of block copolymer micelle dispersions associated with having charged groups at the corona terminus justifies considering the placement of electronically charged groups at the end of the hydrophilic polymer segment as a general design feature for block copolymer micelle drug and gene delivery systems. The lipase enzyme catalyzed degradation of these micelles with different core sizes and corona charged are critical issues that will be discussed in Chapter 6.

5.4 Experimental Section

5.4.1 Materials

Allyl alcohol (≥99%, Sigma Aldrich) was dried by 3 Å molecular sieves prior to use. Ethylene Oxide (99%, PFALTZ & BAUER. INC) and ε-caprolactone (CL) (99%, TCI America) were dried over CaH_2 and distilled prior to use. 18-crown-6-ether (18C6, ≥99%), stannous octoate ($Sn(Oct)_2$, ~95%), mercaptosuccinic acid (97%), sodium 2-mercaptoethanesulfonate(BioXtra, ≥98.0%), 2,2-Dimethoxy-2-phenylacetophenone (99%) and phosphate buffered saline (PBS, tablet) were used as received from Sigma Aldrich. Buffer solutions from pH=4 (SB98-500, 0.05 M Potassium Acid Phthalate) and pH=10(SB116-500, Potassium Carbonate/Potassium Tetraborate/Potassium Hydroxide) were purchased from Fisher Scientific. Potassium naphthalenide THF solution (1.0 M) was prepared by mixing of naphthalene (5.12 g), potassium (1.56 g) and THF (35 mL) in a flask. SnakeSkin Dialysis tubing (10K MWCO, 35mm dry I.D., 35 feet) was used for dialysis of aqueous media containing polymer micelles. Acetone, toluene, petroleum ether, dichloromethane and methanol were used as received from J.T. Baker and dimethylformamide (DMF, HPLC grade, 99.7%+, Alfa Aesar) was used as the GPC eluent.

5.4.2 Analytical techniques

^{1}H NMR spectra were obtained using Bruker 500 MHz spectrometer with $CDCl_3$ as NMR solvent media. NMR data were analyzed by using the Bruker Topspin 2.1 software.

Gel permeation chromatography (GPC) measurements were carried out using a Shimadzu LC-20AV liquid chromatography system equipped with three linear PolarGel-M 300×7.5 mm columns, a RID-10A differential refractive index detector and a SPD-20AV UV/VIS detector. Data were analyzed by Shimadzu LCsolution software. DMF was used as the eluent at a flow rate of 1.0 mL/min at 50 ℃. Molecular weight calibrations were based on narrow peak width polystyrene standards from Polymer Laboratories.

MALDI-TOF mass spectrum of HO-PEG-$CH_2CH{=}CH_2$: The HO-PEG-$CH_2CH{=}CH_2$sample was dissolved in H_2O (5.0 g/L), 2,5-Dihydroxybenzoic acid dissolved in water: Ethanol (9:1 vol:vol) solution (10.0 g/L) was used as a matrix. 2.0 uL of the matrix solution was mixed with 0.5 uL of the PEG solution, placed on a steal sample holder, and air dry. MALDI-TOF mass spectra were acquired using the reflectron mode on an UltraflexIII TOF-TOF mass spectrometer (Bruker Daltonik GmbH, Bremen, Germany). The serial instrument was equipped with a 337 nm, 50 Hz N_2 Laser used with a 33% attenuation level. The acceleration voltage was set to 19 kV, the pulsed extraction voltage to 17.15 kV, the extraction delay to 280 ns, and the reflector voltage to 20 kV. The achieved peak resolution was comprised between 10,000 and 30,000, depending on the peaks.

Dynamic light scattering (DLS) measurements were conducted by by a Zetasizer Nano ZS (Malvern Instruments, Westborough, MA). Hydrodynamic diameter and size distribution of micelles in PBS buffer solution were measured at 37 ^oC, using 1 cm polystyrene cuvettes. The mean diameter was obtained from the instrument's DTS software using the volume reading. The

Zeta potential (ζ) of the micelle samples in water was measured at 25 ^{o}C using the same instrument according to electrophoretic light scattering technology.

Transmission Electron Microscope (TEM). Micelle morphology was evaluated by JOEL JEM-1400 TEM operating at an acceleration voltage of 80 kV. One drop of the micelle solution (1.0 mg/mL) was placed on the ultrathin carbon type-A 400 mesh copper grid (Ted Pella Inc., Redding, CA), and the droplet was then blotted and allowed to evaporate under ambient conditions overnight before analysis. The average diameters of the spherical micelles were evaluated by DigitalMicrograph software (Gatan Inc.).

Cryogenic transmission electron microscopy (cryo-TEM). One drop of the micelle solution (1.0 mg/mL) was put on a quantifoil grid for Cryo-TEM (CF-MH-4C-25, Electron Microscopy Sciences). Most of the liquid was then removed with blotting paper, leaving aqueous thin film in the open holes of the grid. The aqueous thin film was instantly vitrified by rapid immersion into liquid ethane cooled by liquid nitrogen. The specimen was then transferred to the TEM instrument with a Gatan 626 cryo-transfer holder. The temperature was maintained at approximately -160 ^{o}C during cryo-TEM study. The transmission electron microscope was operated at an acceleration voltage of 120 kV. All images were recorded by a bottom mounted Ultrascan-1000 CCD camera system (Gatan Inc.). The average diameters of the spherical micelles were evaluated by Digital Micrograph software.

5.4.3 Synthesis of HO-PEG-$CH_2CH=CH_2$ homopolymer

Dried allyl alcohol (0.34 mL, 5 mmol), 18-crown-6-ether (1.98 g, 7.5 mmol) and THF (80 mL) were added into a vacuum dried 250 mL two necked flask sealed with a rubber stopper. The flask was placed into salt ice bath and potassium naphthalenide THF solution (5.0 mL, 1.0 M) was added into the flask by a syringe. The solution was stirred for 20 min until the solution became colorless. The CaH_2 dried EO (8.70 mL, 0.175 mol) was transfered into the flask through a dried cannula. The EO polymerization was first run at -5 ^{o}C for 30 min and then the temperature was increased to 20 ^{o}C. The reaction was terminated after 12 hours by adding an excess of MeOH into the solution. The solvents were evaporated, the resulting white solid dissolved in water and the HO-PEG-$CH_2CH{=}CH_2$ was extracted into CH_2Cl_2. The CH_2Cl_2 was evaporated and THF was added back to dissolve the HO-PEG-$CH_2CH{=}CH_2$ and the white HO-PEG-$CH_2CH{=}CH_2$ was precipitated out by adding the solution into excess petroleum ether. Redissolving the polymer in CH_2Cl_2 and precipitation using petroleum ether resulted in a white powder of HO-PEG-$CH_2CH{=}CH_2$ that was dried under vacuum for 48 hours.

5.4.4 Synthesis of HO-PCL$_{51}$-*b*-PEG$_{32}$-$CH_2CH{=}CH_2$ diblock copolymer

Dried HO-PEG$_{32}$-$CH_2CH{=}CH_2$ (0.73 g, 0.50 mmol) was dissolved in 22 mL of dry toluene in a 50 mL dry flask under a nitrogen inert atmosphere. A mixture of ε-caprolactone (CL) (9 mL, 0.080 mol) and $Sn(Oct)_2$ (0.03 g) was added into the PEG solution via a syringe. The reaction mixture was gently refluxed under nitrogen atmosphere at 120 ^{o}C. After stirring the solution for 3 hours, excess cold methanol was poured into the solution to terminate the reaction and precipitate the polymer product. The white solid precipitate (HO-PCL$_{51}$-*b*-PEG$_{32}$-$CH_2CH{=}CH_2$) was collected by filtration, redissolved in dichloromethane and precipitated by methanol. The precipitate was collected and dried under vacuum at 40 ℃ for 48 h.

5.4.5 Synthesis of HO-PCL_{51}-*b*-PEG_{32}-RCO_2H and HO-PCL_{51}-*b*-PEG_{32}-RSO_3Na diblock copolymers via thiol-ene click chemistry

Diblock copolymer of HO-PCL_{51}-*b*-PEG_{32}-$CH_2CH=CH_2$ (0.36 g, 0.050 mmol), 3-Mercaptopropionic acid (0.0218 mL, 0.25 mmol) and 2,2-Dimethoxy-2-phenylacetophenone (6.4 mg 0.025 mmol) were dissolved in 5 mL of CH_3Cl in a 25 mL flask. The solution was bubbled with N_2 for 15 min. The reaction solution was stirred in a UV reactor (3500 Å) at 15 ^oC for 3h. The product was precipitated out by pouring the reaction solution into excess cold methanol. The white precipitate (HO-PCL_{51}-*b*-PEG_{32}-RCO_2H) was collected by gravity filtration, washed by cold methanol several times and dried at 40 ^oC under vacuum for 48 hours.

Diblock copolymer of HO-PCL_{51}-*b*-PEG_{32}-$CH_2CH=CH_2$ (0.36 g, 0.050 mmol), Sodium 2-mercaptoethanesulfonate (41.0 mg, 0.25 mmol) and 2,2-Dimethoxy-2-phenylacetophenone (6.4 mg, 0.025 mmol) were dissolved in 5 mL of DMF in a 25 mL flask and N_2 bubbled through the solution for 15 min. The reaction solution was placed in a UV reactor (3500 Å) and stirred at 15 ^oC for 3h. The product was precipitated out by pouring the reaction solution into excess cold methanol. The white precipitate (HO-PCL_{51}-*b*-PEG_{32}-RSO_3Na) was collected by gravity filtration, washed by cold methanol several times and dried at 40 ^oC under vacuum for 48 hours.

5.4.6 Formation of PCL_{51}-*b*-PEG_{32}-$CH_2CH{=}CH_2$ diblock copolymer micelles via nano-precipitation method

A stock solution of the HO-PCL_{51}-*b*-PEG_{32}-$CH_2CH{=}CH_2$ diblock copolymer (10 mg/mL) was prepared in acetone. An aliquot of the polymer stock solution (0.80 mL) was added to stirring HPLC grade water (8.0 mL) at the rate of 0.2 mL/min which resulted in formation of the block copolymer micelles (1.0 mg/mL). The micelle suspension was then transferred into dialysis bags (MWCO: 10,000 Da) and dialyzed against HPLC grade water for 24 hours. ^{1}H NMR was used to confirm that the acetone was completely removed after the dialysis. Other micelles with different polymer compositions were formed using the same procedure.

5.5 References

(1) Tyrrell, Z. L.; Shen, Y.; Radosz, M. *Prog. Polym. Sci.* 2010, 35, 1128-1143.

(2) Zhang, Q.; Remsen, E. E.; Wooley, K. L. *J. Am. Chem. Soc.* 2000, 122, 3642-3651.

(3) Hickey, R. J.; Haynes, A. S.; Kikkawa, J. M.; Park, S.-J. *J. Am. Chem. Soc.* 2011, 133, 1517-1525.

(4) Zhu, W.; Nese, A.; Matyjaszewski, K. *J. Polym. Sci., Part A: Polym. Chem.* 2011, 49, 1942-1952.

(5) Lee, H.-i.; Wu, W.; Oh, J. K.; Mueller, L.; Sherwood, G.; Peteanu, L.; Kowalewski, T.; Matyjaszewski, K. *Angew. Chem. Int. Ed.* 2007, 46, 2453-2457.

(6) Discher, B. M.; Won, Y.-Y.; Ege, D. S.; Lee, J. C.-M.; Bates, F. S.; Discher, D. E.; Hammer, D. A. *Science* 1999, 284, 1143-1146.

(7) Geng, Y.; Discher, D. E. *J. Am. Chem. Soc.* 2005, 127, 12780-12781.

(8) Mai, Y.; Eisenberg, A. *Chem. Soc. Rev.* 2012, 41, 5969-5985.

(9) Rajagopal, K.; Mahmud, A.; Christian, D. A.; Pajerowski, J. D.; Brown, A. E. X.; Loverde, S. M.; Discher, D. E. *Macromolecules* 2010, 43, 9736-9746.

(10) Endres, T. K.; Beck-Broichsitter, M.; Samsonova, O.; Renette, T.; Kissel, T. H. *Biomaterials* 2011, 32, 7721-7731.

(11) Zhu, Z.; Li, Y.; Li, X.; Li, R.; Jia, Z.; Liu, B.; Guo, W.; Wu, W.; Jiang, X. *J. Controlled Release* 2010, 142, 438-446.

(12) Yang, R.; Meng, F.; Ma, S.; Huang, F.; Liu, H.; Zhong, Z. *Biomacromolecules* 2011, 12, 3047-3055.

(13) Gan, Z.; Jim, T. F.; Li, M.; Yuer, Z.; Wang, S.; Wu, C. *Macromolecules* 1999, 32, 590-594.

(14) Jiang, Z.; Zhu, Z.; Liu, C.; Hu, Y.; Wu, W.; Jiang, X. *Polymer* 2008, 49, 5513-5519.

(15) Zhu, X.; Fryd, M.; Tran, B. D.; Ilies, M. A.; Wayland, B. B. *Macromolecules* 2012, 45, 660-665.

(16) Elhasi, S.; Astaneh, R.; Lavasanifar, A. *Eur. J. Pharm. Biopharm.* 2007, 65, 406-413.

(17) Shi, B.; Fang, C.; You, M.; Zhang, Y.; Fu, S.; Pei, Y. *Colloid. Polym. Sci.* 2005, 283, 954-967.

(18) Letchford, K.; Liggins, R.; Burt, H. *J. Pharm. Sci.* 2008, 97, 1179-1190.

(19) Kim, S.; Shi, Y.; Kim, J. Y.; Park, K.; Cheng, J.-X. *Expet Opin Drug Deliv.* 2010, 7, 49-62.

(20) Shuai, X.; Ai, H.; Nasongkla, N.; Kim, S.; Gao, J. *J. Controlled Release* 2004, 98, 415-426.

(21) Zhang, X.; Cheng, J.; Wang, Q.; Zhong, Z.; Zhuo, R. *Macromolecules* 2010, 43, 6671-6677.

(22) Nie, T.; Zhao, Y.; Xie, Z.; Wu, C. *Macromolecules* 2003, 36, 8825-8829.

(23) Shen, C.; Guo, S.; Lu, C. *Polym. Adv. Technol.* 2008, 19, 66-72.

(24) Fairley, N.; Hoang, B.; Allen, C. *Biomacromolecules* 2008, 9, 2283-2291.

(25) Yang, X.; Deng, W.; Fu, L.; Blanco, E.; Gao, J.; Quan, D.; Shuai, X. *J. biomed. mater. res., Part A* 2008, 86A, 48-60.

(26) Hoyle, C. E.; Bowman, C. N. *Angew. Chem. Int. Ed.* 2010, 49, 1540-1573.

(27) Killops, K. L.; Campos, L. M.; Hawker, C. J. *J. Am. Chem. Soc.* 2008, 130, 5062-5064.

(28) Tucker-Schwartz, A. K.; Farrell, R. A.; Garrell, R. L. *J. Am. Chem. Soc.* 2011, 133, 11026-11029.

(29) Nagasaki, Y.; Kutsuna, T.; Iijima, M.; Kato, M.; Kataoka, K.; Kitano, S.; Kadoma, Y. *Bioconjugate Chem.* 1995, 6, 231-233.

(30) Studer, P.; Breton, P.; Riess, G. *Macromol. Chem. Phys.* 2005, 206, 2461-2469.

(31) Park, S.-J.; Kang, S.-G.; Fryd, M.; Saven, J. G.; Park, S.-J. *J. Am. Chem. Soc.* 2010, 132, 9931-9933.

(32) Ding, J.; Heatley, F.; Price, C.; Booth, C. *Eur. Polym. J.* 1991, 27, 895-899.

(33) Ding, J.; Price, C.; Booth, C. *Eur. Polym. J.* 1991, 27, 891-894.

(34) Master, A. M.; Rodriguez, M. E.; Kenney, M. E.; Oleinick, N. L.; Gupta, A. S. *J. Pharm. Sci.* 2010, 99, 2386-2398.

(35) Meier, M. A. R.; Aerts, S. N. H.; Staal, B. B. P.; Rasa, M.; Schubert, U. S. *Macromol. Rapid Commun.* 2005, 26, 1918-1924.

(36) Schubert, S.; Delaney, J. J. T.; Schubert, U. S. *Soft Matter* 2011, 7, 1581-1588.

(37) Chung, T. W.; Cho, K. Y.; Lee, H.-C.; Nah, J. W.; Yeo, J. H.; Akaike, T.; Cho, C. S. *Polymer* 2004, 45, 1591-1597.

(38) Giacomelli, C.; Borsali, R. *Macromol. Symp.* 2006, 245-246, 147-153.

(39) Lassalle, V.; Ferreira, M. L. *Macromol. Biosci.* 2007, 7, 767-783.

CHAPTER 6:

CHARGE SELECTIVE LIPASE ENZYME-BLOCK COPOLYMER MICELLE BINDING, INTERFACIAL ACTIVATION AND CATALYTIC DEGRADATION

6.1 Introduction

Catalytic hydrolysis of lipid ester substrates assembled in bilayers, vesicles and micelles is an exclusive capability of lipase enzymes[1-7]. Lipases are involved in diverse biological processes ranging from metabolism of triglycerides to inflammation[8] and cell signaling[9]. Activation of catalytic substrate hydrolysis through binding of an assembly of ester substrates with the lipase enzyme at the hydrophobic-water interface is a characteristic of interfacial activation and a classic distinguishing feature between lipase and esterase behavior[10-13].

Amphiphilic block copolymer micelles with hydrophilic corona and hydrophobic core have an array of biomedical applications[14-16] and in particular provide a broad platform for development of drug and gene delivery vehicles that function through their capability for loading, transport and release of lipophilic substances incorporated in the hydrophobic core[17-22]. Block copolymers of poly (ethylene glycol) (PEG) block poly (ε-caprolactone) (PCL) are prototypical amphiphilic block copolymers that self-assemble into core-shell micelles in water where the hydrolytically non-degradable hydrophilic PEG segment forms the exterior corona and the core contains the hydrolytically degradable polyester hydrophobic PCL block[23-27]. Micelles that self assemble from poly (caprolactone)-poly (ethylene glycol) block copolymers (HO-PCL-*b*-PEG) function as an intra-particle source of polyester substrates for *P. cepacia* lipase catalyzed hydrolysis of the PCL core and subsequent micelle degradation through an interfacial activation mechanism. Several lipase enzymes have been used to catalyze PCL ester hydrolysis and degradation of micelles derived from HO-PCL-*b*-PEG-OMe diblock copolymers[26, 28-32].

In Chapters 2-3, kinetic studies were reported for acid and lipase enzyme catalytic degradations of aqueous dispersions of di and triblock copolymer micelles from HO-PCL-*b*-PBO-*b*-PEG-OMe through ester hydrolysis of the PCL core[31]. The lipase catalyzed process proceeds through interfacial activation which occurs at several orders of magnitude faster than either acid or base catalyzed hydrolysis processes[32-33].

In Chapter 4, detailed kinetic and mechanistic studies were carried out for the *P. cepacia* lipase catalyzed hydrolytic degradation of micelles from the block copolymer HO-PCL_{60}-*b*- PEG_{45}-OMe where neutral methoxy groups terminate the micelle corona[31]. The kinetics of the lipase enzyme catalyzed micelle degradation involves three steps given by equations (1-3).

Scheme 6.1: Reaction scheme for lipase catalyzed degradation of micelle with product inhibition

$$(1) \quad E + M \underset{k_{-1}}{\overset{k_1}{\rightleftharpoons}} EM$$

$$(2) \quad EM \xrightarrow{k_2} P + E$$

$$(3) \quad EM + P \underset{k_{-3}}{\overset{k_3}{\rightleftharpoons}} EMP$$

The *P. cepacia* lipase catalyzed micelle degradation corresponds to a two step mechanism for the catalysis ($E+ M \rightleftharpoons E\text{-}M \rightarrow P + E$) and a third step for product inhibition of the enzyme-micelle complex ($EM + P \rightleftharpoons EMP$). A required feature for the process is relatively strong binding between the block copolymer micelle of HO-PCL_{60}-*b*-PEG_{45}-OMe with a hydrophobic region of the enzyme adjacent to the Ser-His-Asp triad catalytic center[34-35]. Micelle-lipase binding is effectively irreversible because the hydrolytic degradation of the micelle is faster than the exchange of enzymes between micelles. Interactions of the aqueous phase and the hydrophobic regions of the enzyme and micelle promotes the lipase-micelle binding that activates both the lipase and the micelle for catalytic ester hydrolysis by a mechanism called interfacial activation[13, 31] (eq 1,2). The micelle-protein binding sites are suggested to occur near the water-micelle core interface in order to facilitate entrance of water and the PCL polyester segments into the reaction center and efficient transport of the water soluble hydrolysis products from the catalysis center into the bulk aqueous phase. Reversible inhibition of the lipase enzyme catalyzed micelle degradation occurs from hydrolysis products, and the PEG segment with a few residual PCL units (HO-PCL$_{n\leq 6}$-*b*-PEG$_{45}$-OMe) has been demonstrated to be an effective inhibitor. The product inhibitors have PCL units that function as slowly reacting substrates which compete for residing in the triad active center of the enzyme-micelle complex. The very fast initial rates of lipase catalyzed micelle degradation are triggered by strong enzyme-micelle complex formation which activates the lipase enzyme catalysis in a manner that parallels interfacial enzyme activation in lipase catalyzed lipid membrane hydrolysis[1-2, 4-6, 36]. Scheme 6.2 summarizes the model for lipase catalyzed hydrolytic degradation of micelles of PCL-*b*-PEG diblock copolymers through an interfacial activation mechanism where the active lipase- micelle complex is inhibited by the reaction products.

Scheme 6.2: Reaction scheme for a product inhibited lipase catalyzed degradation of PCL-*b*-PEG diblock copolymer micelles through an interfacial activation mechanism.

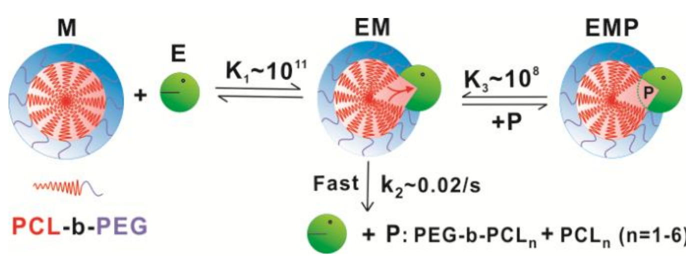

The original motivation for placing charged groups on the corona of HO-PCL-*b*-PEG-RX (R= $-O(CH_2)_3S(CH_2)_2-$, X= $-CO_2^-$,$-RSO_3^-$,$-NH_3^+$) block copolymer micelles was that when the micelle corona and lipase enzyme have the same charge there will be an increased barrier to reaction which could be used as a design feature to obtain selectivity for therapeutic transport and release. Thiol-ene "click" chemistry[37-39] of an allyl terminated block copolymer (HO-PCL_n-*b*-PEG_{32}-$CH_2CH=CH_2$) was used to introduce end groups on the PEG segment that are anionic ($-CO_2^-$,$-SO_3^-$) and a Michael addition[40-41] was used to place positive ($-NH_3^+$) corona charge. Block copolymers with charged PEG end groups self assemble into spherical micelles that have charged exteriors that are useful for probing the corona charge effects on micelle stability. This chapter discusses on the influence that the electronic charge on the micelle corona has on lipase enzyme catalyzed hydrolytic degradation of micelles formed from a series of HO-PCL_n-*b*-PEG_{32}-RX block copolymers. Kinetic studies detected the presence of two *P. cepacia* lipase isoforms that have opposite corona charge selectivity for catalyzing the degradation of micelles with positively and negatively charged corona.

6.2 Results and Discussion

6.2.1 Formation and properties of micelles from PCL_{51}-*b*-PEG_{32}-$CH_2CH=CH_2$, $[PCL_{51}$-*b*-PEG_{32}-$RCO_2]^-Na^+$, $[PCL_{51}$-*b*-PEG_{32}-$RSO_3]^-Na^+$ and $[PCL_{44}$-*b*-PEG_{32}-$RNH_3]^+Cl^-$

Micelles with a concentration of 1.0 mg/mL from PCL_{51}-*b*-PEG_{32}-$CH_2CH=CH_2$, $[PCL_{51}$-*b*-PEG_{32}-$RCO_2]^-Na^+$, $[PCL_{51}$-*b*-PEG_{32}-$RSO_3]^-Na^+$ and $[PCL_{51}$-*b*-PEG_{32}-

$RNH_3]^+Cl^-$ diblock copolymers are formed via the same nano-precipitation method that was previously applied for MeO-PEG-*b*-PCL-OH diblock copolymers[42-45]. Results from dynamic light scattering (DLS) studies for these micelle solutions are shown in Table 6.1. All the micelle solutions have uni-modal and narrow size distribution. Those micelles from the same parent PCL_n-*b*-PEG_{32}-$CH_2CH{=}CH_2$ but with different end groups have comparable sizes. The measured zeta potentials for all the micelles are consistent with the micelle corona charge. Both cryo-TEM and normal TEM images in the chapter 5 for the micelles indicate that the polymers selectively form spherical micelles.

Table 6.1: Effective hydrodynamic diameters from DLS and Zeta potentials for diblock copolymer micelles. (R= $-O(CH_2)_3S(CH_2)_2-$)

Micelle Sample	Diameter (pH = 7.4, 37℃)	Zeta Potential (ζ, 25℃)
PCL_{51}-*b*-PEG_{32}-$CH_2CH{=}CH_2$	32 nm	-13 mV
$[PCL_{51}$-*b*-PEG_{32}-$RCO_2]^-$ Na^+	38 nm	-31 mV
$[PCL_{51}$-*b*-PEG_{32}-$RSO_3]^-$ Na^+	43 nm	-27 mV
$[PCL_{44}$-*b*-PEG_{32}-$RNH_3]^+$ Cl^-	27 nm	+ 20 mV

6.2.2 ^{1}H NMR of lipase catalyzed degradation of PCL_{51}-*b*-PEG_{32}-$CH_2CH{=}CH_2$ micelles

Micelles from HO-PCL_{51}-*b*-PEG_{32}-$CH_2CH{=}CH_2$ diblock copolymers experience fast degradation catalyzed by lipase enzymes. Addition of *P. cepacia* lipase to HO-PCL_{51}-*b*-PEG_{32}-$CH_2CH{=}CH_2$ micelle dispersions in aqueous PBS buffer (pH = 7.4) at 37 ℃ results in micelle degradations that are readily followed by ^{1}H NMR (Figure 6.1). Decline in the intensities for the broadened micelle ^{1}H NMR resonances (δ = 2.36 ppm) as the degradation proceeds is accompanied by appearance of sharp resonances for water soluble HO-PCL_n-*b*-PEG_{32}-$CH_2CH=CH_2$ ($n \leq 6$) fragments (δ = 3.78 ppm) and a set of small PCL_n ($n \leq 6$) oligomers (δ ~ 2.27, 2.48, 3.70 ppm) that result from lipase catalyzed hydrolysis of HO-PCL_{51}-*b*-PEG_{32}-$CH_2CH=CH_2$ block copolymer chains in the micelle (Figure 6.1). The ratio (R) of the areas of the CH_2 groups attached to an ester carbon (-CH_2-C(O)-O-, δ ~ 2.48 ppm) to that for terminal -CH_2-CO_2H (δ = 2.27 ppm) gives the average number of caprolactone units (n) in the PCL oligomers (n = R +1). The average length (n) of PCL_n fragment from the initial step in the lipase catalyzed hydrolytic degradation of the allyl terminated micelle is 3.2-3.4 and a similar average PCL_n fragment length of 2.8-3.0 is observed for degradation of the CO_2H terminated micelle. ^{1}H NMR provides a PCL_n fragment convenient and effective technique to obtain detailed information that simultaneously defines the composition of the micelle and the products from polymer hydrolysis as the degradation process proceeds.

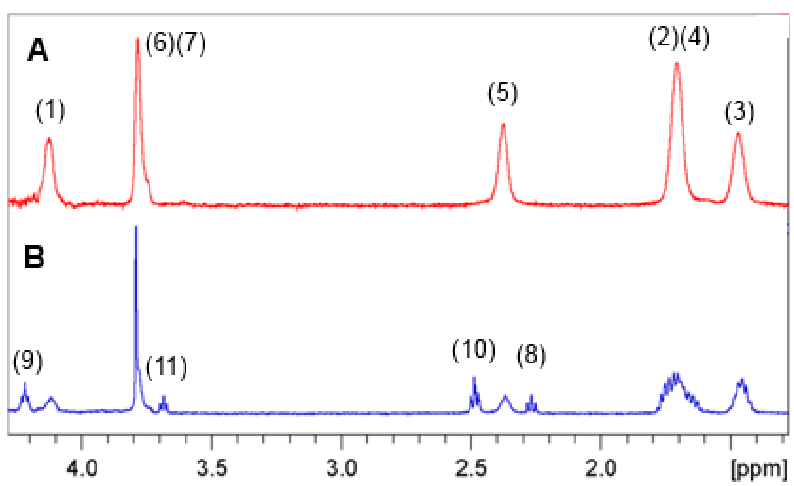

Figure 6.1: 500 MHz ^{1}H NMR of PCL_{51}-*b*-PEG_{32}-$CH_2CH=CH_2$ micelle in PBS buffer at 37 ^oC (A); micelle with *P. cepacia* lipase (1.0 U/mL) for 15 min (B). NMR peak assignments: (A): H-[O-CH_2(1)-CH_2(2)-CH_2(3)-CH_2(4)-CH_2(5)-C(O)]$_{51}$-*b*-[O-CH_2(6)-CH_2(7)]$_{32}$-O-$CH_2CH=CH_2$;(B)HOC(O)CH_2(8)$(CH_2)_3CH_2$(9)O-[C(O)CH_2(10) $(CH_2)_3CH_2$(9)O]$_m$-C(O)CH_2(10)$(CH_2)_3CH_2$(11)OH. Chemical shifts in ppm: δ(1) = 4.12, δ(2,4)=1.72, δ(3)=1.45, δ(5)= 2.36, δ(6,7)=3.78, δ(8)~2.27, δ(9)~4.22, δ(10)~2.48, δ(11)~3.70.

6.2.3 Kinetics of lipase catalyzed hydrolytic degradation of micelles that carry varying charges on the terminus of the block copolymer micelle corona

Kinetics of degradation of micelles catalyzed by commercially obtained lipase enzymes were measured at a series of conditions designed to study the effects of micelle corona charge. The change in the concentration with time for micelles from PCL_{51}-*b*-PEG_{32}-$CH_2CH=CH_2$, $[PCL_{51}$-*b*-PEG_{32}-$RCO_2]^-$ Na^+, $[PCL_{51}$-*b*-PEG_{32}-$RSO_3]^-$ Na^+ and $[PCL_{44}$-*b*-PEG_{32}-$RNH_3]^+$ Cl^- were conveniently followed by observing the decrease in the ^1H NMR intensities for the micelle ester CH_2 groups at 2.36 ppm (Figure 6.1). The concentration of micelles in each sample is 0.714 mg/mL and the lipase activity is 1.0 U/mL unless otherwise specified. The MW of the PCL_{51}-*b*-PEG_{32}-$CH_2CH=CH_2$ micelle is approximated to be $5.3 \pm 0.5 \times 10^6$ Da by a Debye plot[46] which gives an estimated micelle concentration of 1.35×10^{-7} M. The *P.cepacia* lipase concentration at an enzyme activity of 1.0 U/mL is ~ 5.1×10^{-9} M based on an activity of 5800 U/mg for the pure enzyme[47]. The commercial *P. cepacia* lipase is a mixture of protein and predominantly non-protein solids including including polysachharides and poly polypropylene glycol. A 29 mg/mL solution of commercial lipase has an $A_{280nm} \approx 0.2$. Assuming the protein component is mostly lipase (33.1 kD; $\varepsilon_{280nm(calculated)} = 35{,}000\ M^{-1}cm^{-1}$), the solid is thus only ~0.7% protein. We note that this number is quite close to the value (0.65%) one would obtain by comparing the stated activity of the commercial lipase (37.8 U/mg) with the literature value for purified lipase (5800 U/mg)[47]. The ratio of the micelle to enzyme molar concentrations is approximately 26 for the typical aqueous solution sample that contains 0.714 mg/mL of micelles and *P. cepacia* lipase activity of 1.0 U/mL. The initial micelle to enzyme molar ratio is always greater than 10 which ensures that the catalytic micelle degradation is zero order in the micelle concentration. The relative initial rate of micelle degradation ($V_0 \equiv \Delta[M]/10min$) is directly proportional to the initial enzyme concentration[31] ($(-d[M]/dt)_i = k[EM] = k[E_0]$) and V_0 measurements are regularly used to compare active enzyme or enzyme micelle complex concentrations.

Interpretations of the kinetics for each of the PCL_{51}-*b*-PEG_{32}-$CH_2CH=CH_2$, [PCL_{51}-*b*-PEG_{32}-RCO_2]$^-$ Na^+, [PCL_{51}-*b*-PEG_{32}-RSO_3]$^-$ Na^+ and [PCL_{44}-*b*-PEG_{32}-RNH_3]$^+$ Cl^- block copolymer micelle degradations catalyzed by commercial samples of *P. cepacia* lipase are based on results from detailed kinetic-mechanistic studies for the very closely related degradation of HO-PCL_{60}-*b*-PEG_{45}-OMe block copolymer micelles catalyzed by *P. cepacia* lipase[31] in chapter 3 and 4. The lipase enzyme catalysis involves an initial step of lipase-micelle complex formation which is sufficiently favorable so that when the micelle concentration is greater than the initial enzyme concentration then effectively the entire enzyme is bound in the complex ($E + M \rightleftharpoons E\text{-}M$) (eq 1). The enzyme-micelle complex in the subsequent step generates product ($E\text{-}M \rightarrow P + E$) (eq 2). The rate law for the lipase catalysis from eq 1,2 is first order in both the enzyme and micelle concentrations ($-d[M]/dt = k[EM] = k[E][M]$), but the excess of micelles over lipase for all of the kinetic studies is sufficiently large so that the rate of the catalytic process becomes zero order in the micelle concentration[31].The concentration of the EM is constant and equal to the initial enzyme concentration because of the strong lipase-micelle binding[31].

Each of the micelles has a large initial rate of lipase catalyzed degradation, but as the micelle degradation proceeds the reaction slows down much faster than would be expected based on the rate law and the initial rates in a manner consistent with loss of enzyme activity. A similar decline in effective lipase activity that occurs in the *P. cepacia* lipase catalyzed degradation of micelles from HO-PCL_{60}-*b*-PEG_{45}-OMe was shown to result from inhibition from products of the hydrolytic micelle degradation that compete for binding in the lipase Ser-His-Asp triad catalytic center[34-35]. Degradation products of the form HO-$PCL_{n\leq6}$-*b*-PEG_{45}-OMe were demonstrated to be efficient lipase catalyst inhibitors[31] and the closely related HO-$PCL_{n\leq6}$-*b*-PEG_{32}-$CH_2CH{=}CH_2$ and HO-$PCL_{n\leq6}$-*b*-PEG_{32}-RX (X= CO_2H, SO_3Na, NH_3Cl) degradation products from the micelles used in this study assumed also to function as lipase inhibitors.

Micelles derived from PCL_{51}-*b*-PEG_{32}-$CH_2CH{=}CH_2$ and $[PCL_{44}$-*b*-PEG_{32}-$RNH_3]^+$ Cl^- with effectively neutral or positively charged corona are catalytically degraded by commercial *P. cepacia* lipase effectively to completion, but micelles from $[PCL_{51}$-*b*-PEG_{32}-$RCO_2]^-$ Na^+ and $[PCL_{51}$-*b*-PEG_{32}-$RSO_3]^-$ Na^+ with negatively charged corona only react to partial conversion(Figure 6.2). The *P. cepacia* lipase enzyme that catalytically degrades micelles with negative corona exteriors become almost completely inhibited by the products of hydrolytic degradation during the first 60 minutes of reaction in which ~6.5 of the 26 micelles per enzyme are degraded into water soluble fragments. An average PCL_n oligomer chain length of 3.0 for the water soluble hydrolysis products early in the process indicates that there are ~17 hydrolysis events that occur within the micelle for each $[PCL_{51}$-*b*-PEG_{32}-$RCO_2]^-$ Na^+ polymer chain that is degraded into water soluble fragments. Degradation of one $[PCL_{51}$-*b*-PEG_{32}-$RCO_2]^-$ Na^+ micelle that is constructed from ~ 727 polymer chains thus involves ~ 1.2×10^4 hydrolysis events for each micelle degradation. During this time ~ 8.0×10^4 polyester hydrolysis events occur which produce 4700 [HO-$PCL_{n\leq6}$-*b*-PEG_{32}-$RCO_2]^-Na^+$ inhibitor molecules per enzyme.

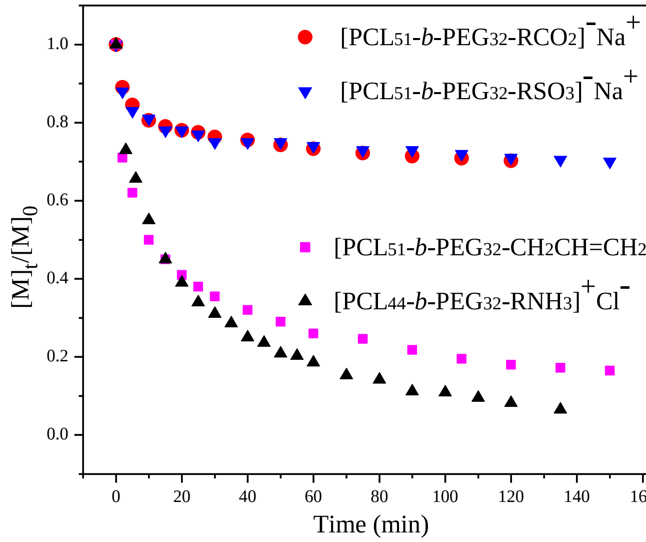

Figure 6.2: Kinetic plots for the commercial *P. cepacia* lipase (1.0 U/mL) catalyzed degradation of a series of block copolymer micelles from PCL_{51}-*b*-PEG_{32}-$CH_2CH{=}CH_2$, [PCL_{51}-*b*-PEG_{32}-RCO_2]$^-$ Na^+, [PCL_{51}-*b*-PEG_{32}-RSO_3]$^-$ Na^+ and [PCL_{44}-*b*-PEG_{32}-RNH_3]$^+$ Cl^- in aqueous PBS (pH = 7.4) at 37 ℃ using integration of the micelle ^{1}H NMR. The effective molar concentration of the micelles is defined as [M], (R= -$O(CH_2)_3S(CH_2)_2$-).

The initial rates of micelle degradation (V_o= -d[M]/dt) are approximated by the integrated ^{1}H NMR intensities for the micelle hydrogens at time zero (t=0) and at relatively short reaction time of 10 minutes (t = 10 min) which is dictated by the requirements of the NMR measurements. The relative initial rates (V_o) for the neutral corona micelle from PCL_{51}-*b*-PEG_{32}-$CH_2CH{=}CH_2$ (V_o = 6.0(.5) $\times 10^{-4}$ mg/mL/s) and the positively charged corona micelles from [PCL_{44}-*b*-PEG_{32}-RNH_3]$^+$$Cl^-$ (V_o = 5.2(.5) $\times 10^{-4}$ mg/mL/s) are substantially larger than the initial rates for micelles with negatively charged corona from [PCL_{51}-*b*-PEG_{32}-RCO_2]$^-$$Na^+$ and [PCL_{51}-*b*-PEG_{32}-RSO_3]$^-$ Na^+ (V_o = 2.3 (.2) $\times 10^{-4}$ mg/mL/s) (Figure 6.2). The earlier observed onset and sharper curvature of the micelle degradation rate plots clearly show that product inhibition of the degradation is more efficient for micelles with negatively charged corona than micelles with neutral and positively charged corona (Figure 6.2).

Kinetics of commercial *P. cepacia* lipase catalyzed degradation another set of micelles from PCL_{44}-*b*-PEG_{32}-$CH_2CH=CH_2$, [PCL_{44}-*b*-PEG_{32}-RCO_2]$^-$ Na^+ and [PCL_{44}-*b*-PEG_{32}-RNH_3]$^+$ Cl^- are shown in Figure 6.3. The general trend of the kinetic curves in Figure 6.3 is very similar to the results in Figure 6.2, which means that the result of charge selectivity of *P. cepacia* lipase is reproducible.

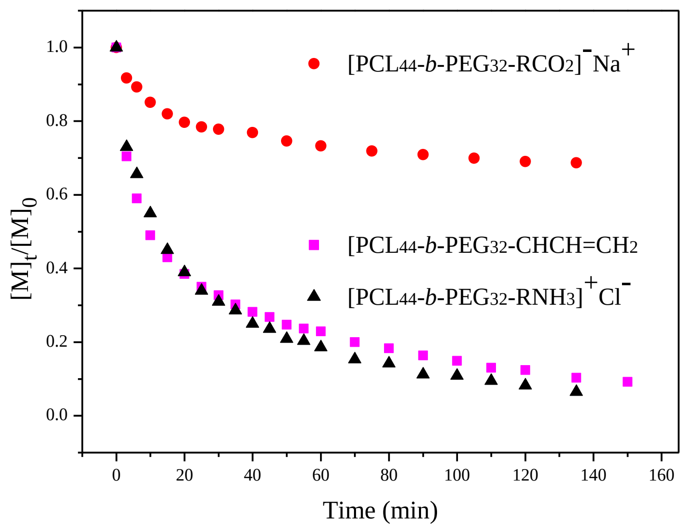

Figure 6.3: Kinetic plots for the commercial *P. cepacia* lipase catalyzed degradation of a series of block copolymer micelles from PCL_{44}-*b*-PEG_{32}-$CH_2CH=CH_2$, [PCL_{44}-*b*-PEG_{32}-RCO_2]$^-$ Na^+ and [PCL_{44}-*b*-PEG_{32}-RNH_3]$^+$ Cl^- in aqueous PBS (pH = 7.4) at E=1.0 U/mL and 37 ℃.

As discussed in the chapter 5, the size of the micelle is proportional to the length of PCL for a fixed length of PEG. The commercial *P. cepacia* lipase catalyzed degradation of micelles from [PCL_{44}-*b*-PEG_{32}-RCO_2]$^-$ Na^+ , [PCL_{51}-*b*-PEG_{32}-RCO_2]$^-$ Na^+ and [PCL_{67}-*b*-PEG_{32}-RCO_2]$^-$ Na^+ lipase activity of 1.0 U/mL, pH=7.4 and T= 37 ^oC were studied and the kinetic plots are shown in Figure 6.4. The measured relative initial rates for these three micelles are $V_o = 1.8 \times 10^{-4}$, 2.3×10^{-4} and 2.5×10^{-4} mg/mL/s respectively. The initial rate of micelle degradation is proportional to the enzyme concentration. The fastest degradation rate for [PCL_{67}-*b*-PEG_{32}-RCO_2]$^-$ Na^+ micelle might result from a higher

[E]/[M] ratio. With the same mass (0.5 mg) of polymer in each experiment, less number of micelles will be formed if the size the each micelle is bigger.

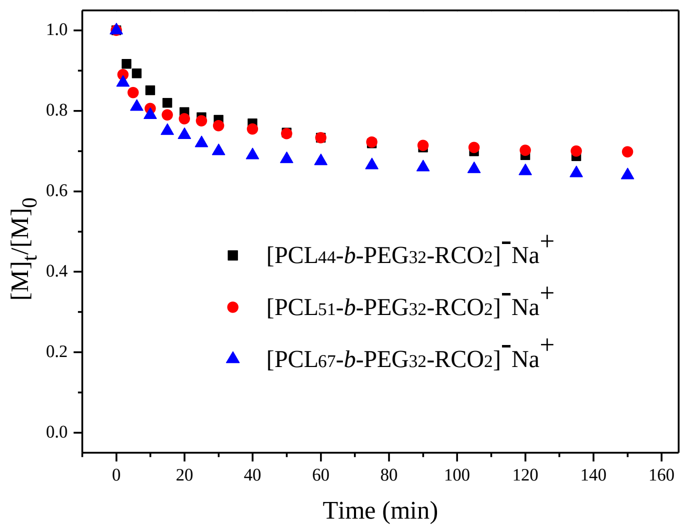

Figure 6.4: Kinetic plots for the commercial *P. cepacia* lipase catalyzed degradation of a series of block copolymer micelles from $[PCL_{44}$-*b*-PEG_{32}-$RCO_2]^-$ Na^+ $[PCL_{51}$-*b*-PEG_{32}-$RCO_2]^-$ Na^+ and $[PCL_{67}$-*b*-PEG_{32}-$RCO_2]^-$ Na^+in aqueous PBS (pH = 7.4) at E=1.0 U/mL and 37 ℃.

6.2.4 Kinetics for lipase catalyzed degradation of $[PCL_{51}$-*b*-PEG_{32}-$RCO_2]^-Na^+$, $[PCL_{51}$-*b*-PEG_{32}-$RNH_3]^+$ Cl^- and PCL_{51}-*b*-PEG_{32}-$CH_2CH{=}CH_2$ micelles by commercial *P. cepacia* lipase where the lipase component that degrades micelles from $[PCL_{51}$-*b*-PEG_{32}-$RCO_2]^-Na^+$ is fully product inhibited

One of the potential explanations for the more effective product inhibition and thus smaller conversions observed for micelles with negatively charged corona was that the products produced that have negatively charged groups might be very powerful inhibitors that efficiently deactivate all of the lipase enzymes present in the system. This possibility was examined by testing for the presence of residual active enzyme by adding micelles from $[PCL_{51}$-*b*-PEG_{32}-$RCO_2]^-Na^+$, PCL_{51}-*b*-PEG_{32}-$CH_2CH{=}CH_2$ and $[PCL_{44}$-*b*-PEG_{32}-$RNH_3]^+Cl^-$ to the aqueous system that is obtained after the reaction of micelles from

$[PCL_{51}$-b-PEG_{32}-$RCO_2]^-$ Na^+ with *P. cepacia* lipase for 10 hours (Figure 6.5-I). The results from this set of test experiments are shown in Figure 6.5-II.

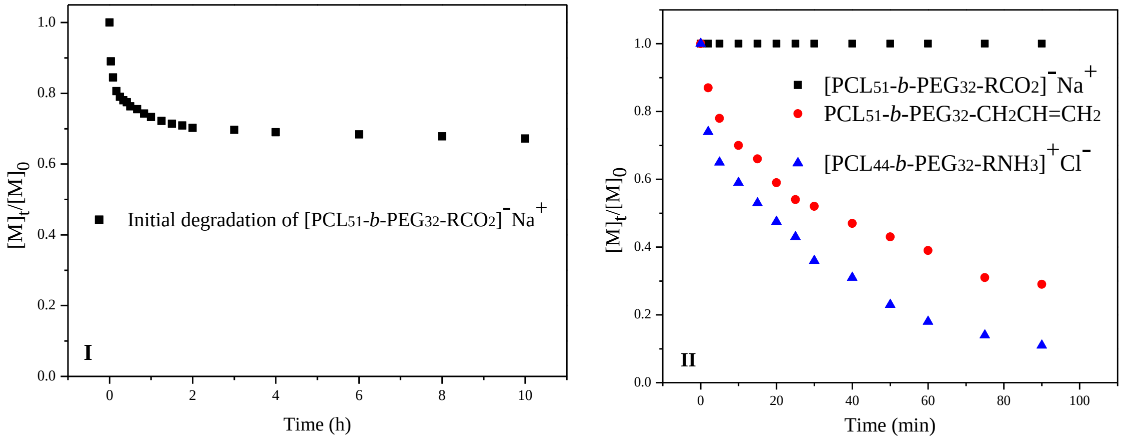

Figure 6.5: I) Kinetic plot of the degradation of $[PCL_{51}$-*b*-PEG_{32}-$RCO_2]^-Na^+$ micelles catalyzed by commercial *P. cepacia* lipase at pH=7.4, T= 37 ℃ and E=1.0 U/mL. II) Kinetic plots for the degradation of micelles from $[PCL_{51}$-*b*-PEG_{32}-$RCO_2]^-$ Na^+, PCL_{51}-*b*-PEG_{32}-$CH_2CH{=}CH_2$ and $[PCL_{44}$-*b*-PEG_{32}-$RNH_3]^+Cl^-$ that are added to the system described in part I after 10 hours of reaction of $[PCL_{51}$-*b*-PEG_{32}-$RCO_2]^-Na^+$ micelles catalyzed by commercial *P. cepacia* lipase at pH=7.4, T= 37 ℃ and E=1.0 U/mL.

The micelles from $[PCL_{51}$-b-PEG_{32}-$RCO_2]^-$ Na^+ with negative corona as expected do not react at a measureable rate, but contrary to the initial hypothesis both the micelles with neutral corona from PCL_{51}-b-PEG_{32}-$CH_2CH{=}CH_2$ (V_0 = 3.6(.2) $\times 10^{-4}$ mg/mL/s) and micelles with positively charged corona from $[PCL_{44}$-b-PEG_{32}-$RNH_3]^+Cl^-$ (V_0 = 4.9(.5) $\times 10^{-4}$ mg/mL/s) are catalytically degraded at substantial rates (Figure 6.5-II). Lipase enzymes must persist that can catalyze degradation of micelles with neutral and positively charged corona after the lipase catalyzed degradation of micelles from $[PCL_{51}$-b-PEG_{32}-$RCO_2]^-$ Na^+ with negative corona is fully inhibited. Several important conclusions can be immediately deduced from these unanticipated results. The commercially obtained *P. cepacia* lipase(s) that was thought to be a single lipase enzyme must actually contain at least two lipases L(I) and L(II). The more intriguing adventitious result is that the catalytic activity of the two different *P. cepacia* lipases L(I) and L(II) in the mixture manifest opposite high levels of selectivity for the charge on the micelle corona. Lipase enzyme L(I) catalyzes degradation of micelles with negatively charged corona at a much higher rate than micelles with positively charged corona and lipase L(II) is complementary to L(I) in having a large preference for catalyzing degradation of micelles with positively charged corona. The reactions of micelles with charged corona may actually be charge specific, but kinetic measurements by NMR are not sufficiently accurate to rule out much slower catalysis of micelle degradation with the opposite charge.

The measured relative initial rates for micelle degradation (V_o) were analyzed assuming the presence of only two lipases in the mixture in an effort to obtain additional information on the distribution and nature of the two lipases. One of the lipases present in the mixture L(I) binds and catalytically degrades the micelles from [PCL_{51}-*b*-PEG_{32}-RCO_2]$^-$ Na^+ and [PCL_{51}-*b*-PEG_{32}-RSO_3]$^-$ Na^+ which have negatively charged corona. The second lipase L(II) present does not catalyze at a measurable rate the degradation of micelles from [PCL_{51}-*b*-PEG_{32}-RCO_2]$^-$ Na^+ where the corona is negatively charged (Figure 6.5-I), but L(II) does catalyze the degradation of micelles with neutral and positively charged corona from PCL_{51}-*b*-PEG_{32}-$CH_2CH{=}CH_2$ (V_0 = 3.6(.2) × 10^{-4} mg/mL/s) and [PCL_{44}-*b*-PEG_{32}-RNH_3]$^+$$Cl^-$($V_0$ = 4.9(.4) × 10^{-4} mg/mL/s) respectively. The rate at which active lipase L(II) degrades the micelles from PCL_{51}-*b*-PEG_{32}-$CH_2CH{=}CH_2$ (V_0 = 3.6(.2) × 10^{-4} mg/mL/s) in the system where L(I) is product deactivated is ~ 0.60 (3.6/6.0) of the rate when both lipases are active in the initial enzyme mixture. The residual active lipase L(II) after L(I) is fully inhibited reacts with the micelle of $[PCL_{44}\text{-}b\text{-}PEG_{32}\text{-}RNH_3]^+Cl^-$ (V_0 = 4.9(.4) × 10^{-4} mg/mL/s) with a rate that approaches that of the initial lipase mixture (L(I)+ L(II)) (V_0 = 5.2(.4) × 10^{-4} mg/mL/s) and this result is interpreted as indicating that L(I) is ineffective in catalytic degradation of the micelle of $[PCL_{44}\text{-}b\text{-}PEG_{32}\text{-}RNH_3]^+Cl^-$ at a significant rate. Analysis of the relative initial rate estimates provide strong evidence that L(I) catalyzes degradation of micelles with negatively charged corona, L(II) catalyzes degradation of micelles with positively charged corona, and both enzymes L(I) and L(II) catalyze degradation of micelles with neutral corona (Scheme 6.3).

Scheme 6.3: Illustration of complementary micelle corona charge selective catalysis for two *P cepacia* lipase components.

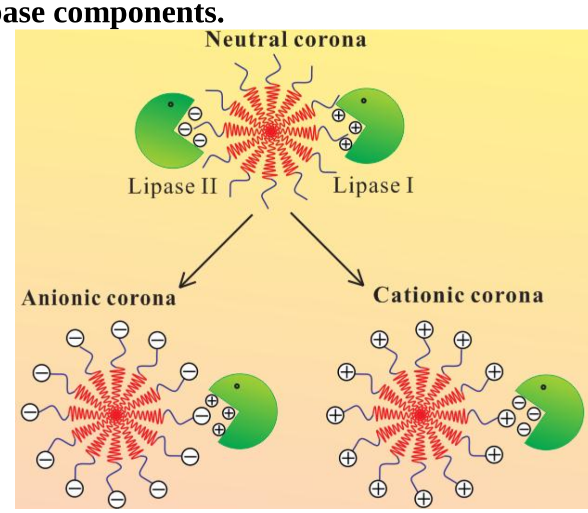

Besides, the inhibitor ($[PCL_{n\leq6}\text{-}b\text{-}PEG_{32}\text{-}RCO_2]^-$ Na^+) must have much stronger inhibitory effects on L(I) than L(II). Otherwise, the L(II) won't catalyze the degradation of the second addition of $PCL_{51}\text{-}b\text{-}PEG_{32}\text{-}CH_2CH{=}CH_2$, $[PCL_{44}\text{-}b\text{-}PEG_{32}\text{-}RNH_3]^+Cl^-$ so efficiently. This result could be an indication that the lipase (I) has a more positive hydrophobic trench and catalyst center that is subject to deactivation by anionic products.

So, the lipase not only is charge selective towards the micelle, but it is also selectively inhibited by the products with charged terminal groups.

6.2.5 Degradation kinetics for micelles from PCL_{51}-*b*-PEG_{32}-$CH_2CH=CH_2$ and $[PCL_{51}$-*b*-PEG_{32}-$RCO_2]^-Na^+$ catalyzed by commercial *P. cepacia* lipase at a series of enzyme activities

Kinetic curves for *P. cepacia* lipase catalyzed degradation of micelles from $[PCL_{51}$-*b*-PEG_{32}-$RCO_2]^-$ Na^+ and $[PCL_{51}$-*b*-PEG_{32}-$RSO_3]^-$ Na^+ also indicate that these micelle suspensions might contain defective micelles with only partial negatively charged corona or neutrally charged corona like PCL_{51}-*b*-PEG_{32}-$CH_2CH=CH_2$ (Figure 6.2). The primary objective of this set of experiments is to probe whether the defective micelle model as a possible origin for the lipase catalytic reactivity with micelles with different corona charges.

Kinetic plots of *P. cepacia* lipase catalyzed degradation of PCL_{51}-*b*-PEG_{32}-$CH_2CH=CH_2$ and $[PCL_{51}$-*b*-PEG_{32}-$RCO_2]^-Na^+$ micelles at a series of lipase concentrations indicates that rate of micelle degradation and initial rate for both PCL_{51}-*b*-PEG_{32}-$CH_2CH=CH_2$ and $[PCL_{51}$-*b*-PEG_{32}-$RCO_2]^-Na^+$ micelles are proportional to the lipase concentration (Figure 6.6). When the concentration of the commercial *P. cepacia* lipase increases the quantity of the proposed minority lipase L(I) component that reacts with negatively charged corona micelle ($[PCL_{51}$ -*b*-PEG_{32}-$RCO_2]^-Na^{+)}$ also increases. This is inconsistent with the defective micelle model because this model is based on a fixed ratio of defective to reactive micelles. These observations are fully consistent with the two lipase model. When the total concentration of lipase increases there will be a proportionate increase in the absolute quantity of the L (I) which produces a corresponding increase in the conversion of the micelles with negatively charged corona.

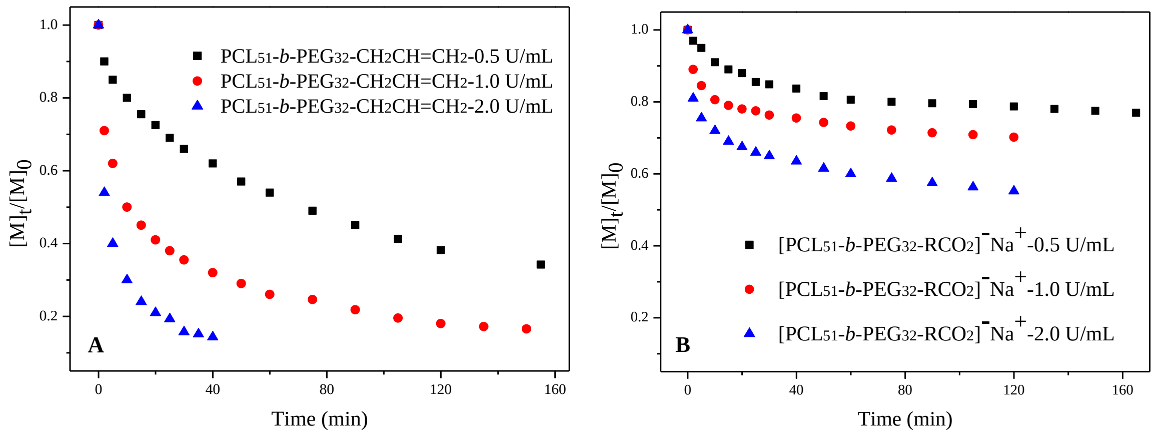

Figure 6.6: Kinetic plots for the degradation of (A) PCL$_{51}$-*b*-PEG$_{32}$-CH$_2$CH=CH$_2$ micelles (B) [PCL$_{51}$-*b*-PEG$_{32}$-RCO$_2$]$^-$Na$^+$ micelles at a lipase activity of 0.5, 1.0 and 2.0 U/mL, pH=7.4 and T=37 ^{o}C.

6.2.6 Kinetics of micelle degradation of [PCL$_{67}$-*b*-PEG$_{32}$-RCO$_2$]$^-$ Na$^+$ catalyzed by commercial *P. cepacia* lipase that is added sequentially in two equal aliquots at pH=7.4, T=37 ^{o}C

This experiment is used as another test for the two lipases model. Product inhibitors that totally shut down reaction with the negatively charged corona micelles formed in reacting with the first aliquot of commercial *P. cepacia* lipase partially inhibit the lipase in the subsequent addition of a second aliquot of commercial *P. cepacia* lipase .

Kinetics of [PCL$_{67}$-*b*-PEG$_{32}$-RCO$_2$]$^-$Na$^+$ micelle degradation catalyzed by lipase from sequential addition of two aliquots of commercial *P. cepacia* lipase are shown in Figure 6.7. Addition of second aliquot of lipase results in a much smaller initial rate of [PCL$_{67}$-*b*-PEG$_{32}$-RCO$_2$]$^-$Na$^+$ micelle degradation than the first addition (V$_0$ (1st) =2.5 $\times 10^{-4}$

mg/mL/s, V_0(2nd) =4.8 $\times 10^{-5}$ mg/mL/s). The catalytic micelle degradation is zero order in micelle therefore the lipase (I) in the second addition is partially deactivated by reaction products in solution from reactions of the first addition of lipase.

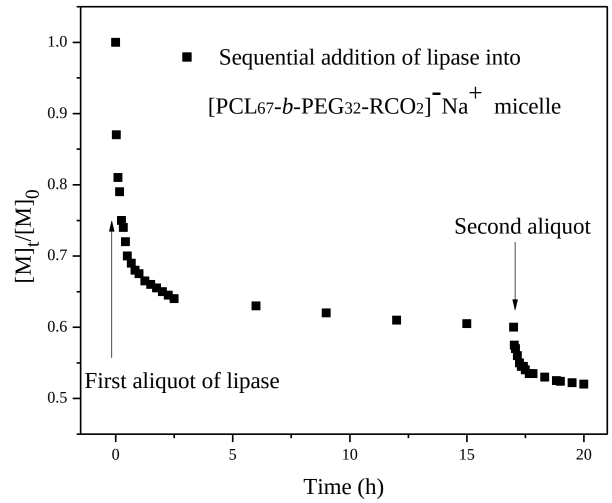

Figure 6.7: Kinetic plots for the degradation of $[PCL_{51}$-*b*-PEG_{32}-$RCO_2]^-Na^+$ micelles for 17 hours at a lipase activity of 1.0 U/mL, pH=7.4 and T=37 ^oC and then second aliquot of lipase was added into to the sample to keep degrading the micelles.

6.2.7 Kinetics of lipase catalyzed hydrolytic degradation of block copolymer micelles at a series of pH values using commercial *P. cepacia* lipase

Kinetics of *P. cepacia* lipase enzyme catalyzed degradation for the diblock copolymer micelles of PCL_{51}-*b*-PEG_{32}-$CH_2CH=CH_2$, $[PCL_{51}$-*b*-PEG_{32}-$RCO_2]^-Na^+$, $[PCL_{51}$-*b*-PEG_{32}-$RSO_3]^-$ Na^+ at constant temperature (T=37 ^oC) and lipase activity (E) equal to 1.0 U/mL are shown at pH of 7.4 in Figure 6.2 and at pH of 7.4 10.0, 7.4 and 4.0 in Figure 6.8. At the pH of 7.4 and more basic conditions the micelles from $[PCL_{51}$-*b*-PEG_{32}-$RCO_2]^-$ Na^+ and $[PCL_{51}$-*b*-PEG_{32}-$RSO_3]^-$ Na^+ both have negatively charged corona and thus exclusively react with the lipase L(I) which is distinctly different from micelles of PCL_{51}-*b*-PEG_{32}-$CH_2CH=CH_2$ which have neutral corona and react with both lipases L(I) and

L(II). When the pH is reduced to 4.0 the carboxylate anion polymer end groups become protonated to neutral carboxylic acid groups (-CO_2H) and the micelle reacts with both lipases L(I) and L(II) to closely emulate that of neutral corona micelle from PCL_{51}-*b*-PEG_{32}-$CH_2CH{=}CH_2$ at pH of 4.0 (Figure 6.8). Micelles from [PCL_{51}-*b*-PEG_{32}-RSO_3]$^-$ Na^+ retain a negatively charged corona at pH of 4.0 because of the much higher acidity of sulfonic acids and thus exclusively react with the lipase L(I). The observed pattern of *P. cepacia* lipase(s) degradation of micelles from PCL_{51}-*b*-PEG_{32}-$CH_2CH{=}CH_2$, [PCL_{51}-*b*-PEG_{32}-RCO_2]$^-$ Na^+ and [PCL_{51}-*b*-PEG_{32}-RSO_3]$^-$ Na^+ provide further confirmatory evidence that the commercial *P. cepacia* lipase(s) contains two lipase where one of the lipases (L(I)) catalyzes degradation of micelles with negatively charged corona, and both lipases L(I) and L(II) catalyze degradation of micelles with neutral corona (Figure 6.8).

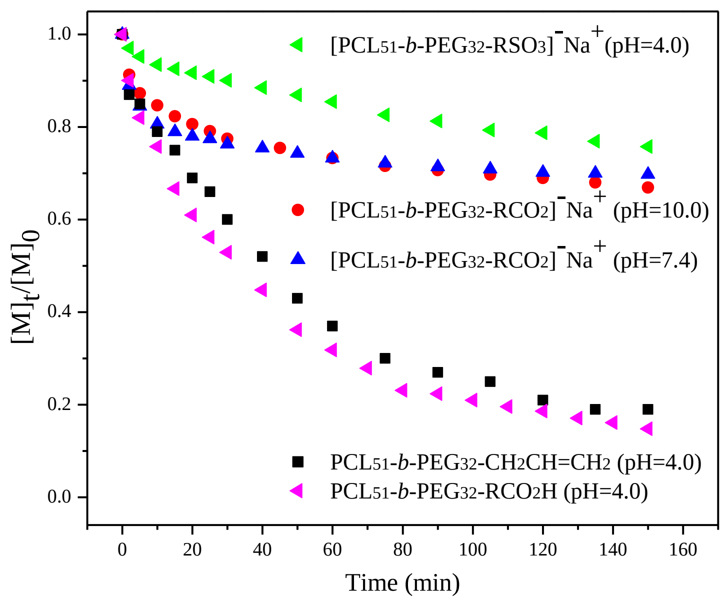

Figure 6.8: Kinetic plots of hydrolytic degradation of micelles from PCL_{51}-*b*-PEG_{32}-$CH_2CH{=}CH_2$, [PCL_{51}-*b*-PEG_{32}-RCO_2]$^-$ Na^+, [PCL_{51}-*b*-PEG_{32}-RSO_3]$^-$ Na^+ catalyzed by commercial *P. cepacia* lipase at a series of pH values (R= -$O(CH_2)_3S(CH_2)_2$ -)(T= 37 ℃, E=1.0 U/mL).

The kinetics of commercial *P. cepacia* lipase catalyzed degradation of $[PCL_{51}$-*b*-PEG_{32}-$RCO_2]^- Na^+$ micelle at pH = 7.4 and 10.0 (E=1.0 U/mL) over a long period of time were followed by ^1H NMR. The kinetic plots in Figure 6.9 demonstrate that the rate of micelle degradation is extremely fast at the beginning and then the rates rate reduces significantly due to the lipase products inhibition. During the slow reaction step, at more basic conditions, the base catalyzed hydrolysis of the lipase inhibitor ($[PCL_{n\leq6}$-*b*-PEG_{32}-$RCO_2]^- Na^+$) is faster and the inhibitory effects of the lipase becomes are less compared to less basic condition (pH=7.4). As a results, the rate of micelle degradation at pH=10 is faster than pH =7.4.

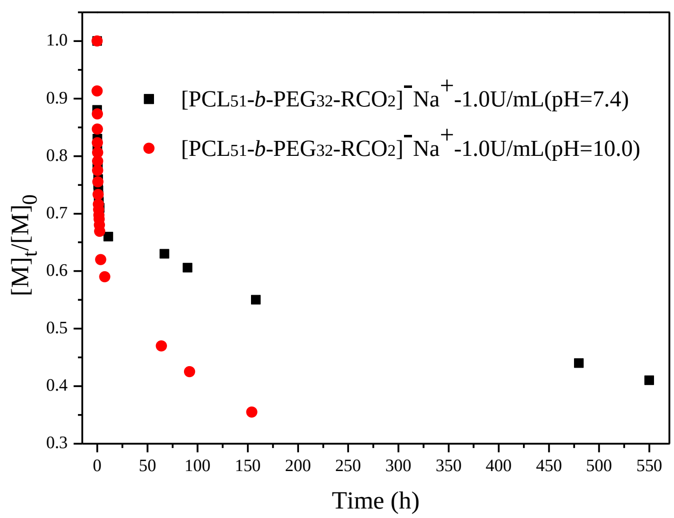

Figure 6.9: Comparison of kinetics for lipase catalyzed degradation of $[PCL_{51}$-*b*-PEG_{32}-$RCO_2]^- Na^+$ micelles at pH=7.4 and 10.

6.2.8 Kinetic simulation of lipase catalyzed degradation of block copolymer micelles with different corona charge

The three steps that have a dominant influence on the observed kinetics of lipase enzyme catalyzed micelle degradation are given by equations 1-3 shown in Scheme 6.1.

The *P. cepacia* lipase catalyzed micelle degradation corresponds to the Michaelis-Menten mechanism (E + M $\rightleftharpoons$ EM → P + E) with product inhibition of the enzyme-micelle complex (EM + P $\rightleftharpoons$ EMP).

Reactions 1-3 in Scheme 6.1 were used in kinetic simulations of the *P. cepacia* lipase catalyzed micelle degradation from PCL_{51}-*b*-PEG_{32}-CH_2CH=CH_2, [PCL_{51}-*b*-PEG_{32}-RCO_2]$^-$ Na^+ using the program Dynafit[48]. Initial estimates k_1, k_{-1}, and k_2 for the kinetic simulations were based on the observed sequential micelle degradation requiring a large equilibrium constant and experimental estimates for the lower limit of k_2 ($k_2 > 0.02$ s^{-1}) come from the rate of micelle degradation at the reaction time t = 10 min. A relatively small range of rate constants k (k_1~1×10^7 $M^{-1}s^{-1}$, k_{-1}~1×10^{-4} s^{-1}, k_2~0.03 s^{-1}, k_3(-CH_2CH=CH_2)~5.2×10^4 $M^{-1}s^{-1}$, k_3(-CO_2^-)~1.75×10^5 $M^{-1}s^{-1}$$k_{-3}$~$1.5\times10^{-4}$ s^{-1}, T = 310 K) are capable of producing reasonable fitting with the observed concentration versus time plots for lipase catalyzed micelle degradation (Figure 6.10). Using the same set of parameters $K_1 = 1\times10^{11}$, $k_2 = 0.03$ s^{-1} but different K_3 gives satisfactory kinetic simulations for all of kinetic data sets in Figure 6.10. The inhibition equlibrium constant K_3 for [PCL_{51}-*b*-PEG_{32}-RCO_2]$^-$ Na^+ micelle (13.3×10^8) is about 2.4 times larger than that for the PCL_{51}-*b*-PEG_{32}-CH_2CH=CH_2 micelle (3.47×10^8). The kinetic simulation results give direct evidence that the initial degradation products ([HO-PCL $_{n\leq6}$-*b*-PEG_{32}-RCO_2]$^-$$Na^+$) are strong inhibitors for the lipase (I).

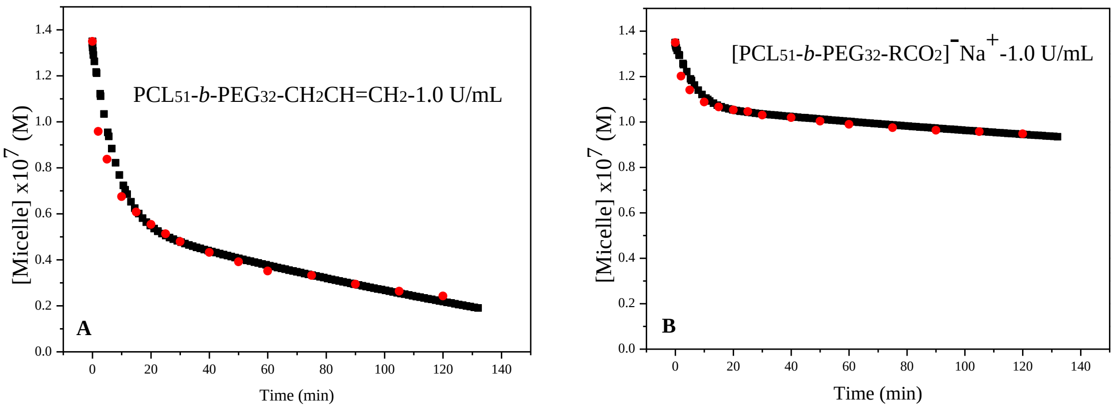

Figure 6.10: Simulations of experimental kinetics for micelles from A) PCL_{51}-*b*-PEG_{32}-$CH_2CH{=}CH_2$; B) [PCL_{51}-*b*-PEG_{32}-RCO_2]$^-$ Na^+ using rate constants : $k_1 = 1\times10^6$, $k_{-1} = 1\times10^{-5}$, $k_2 = 0.03$, $k_{-3} = 1.5\times10^{-4}$ and A) $k_3 = 5.2\times10^4$, B) $k_3 = 1.75\times10^5$. (Estimated absolute micelle and lipase concentrations in mole/L were used in the kinetic simulations)

The following computer program was used for the experimental kinetic simulation by Dynafit4.1:

```
[task]

data = progress
task = fit
model = lipase 1.0 U/mL for allyl micelle

[mechanism]

E + M ---> EM        :   k1
EM ---> E + M        :   k-1
EM ---> P1 + E       :   k2
EM + P1 ---> EMP1    :   k3
EMP1 ---> EM + P1    :   k-3

[constants]

k1 = 1e6  ,  k-1 = 1e-5  ,  k2 = 0.03
k3 = 5.2e4   ,  k-3 = 1.5e-4

[concentrations]

M = 1.35e-7
E =5.19e-9
```

```
[data]
monitor EM
set M       | response M = 1

[output]

directory ./DynaFit/fit/lipase

;___________________________________________________________________________

[set:M]

t,s      conc

0        1.35E-7
120      9.585E-8
300      8.37E-8
600      6.75E-8
900      6.075E-8
1200     5.535E-8
1500     5.13E-8
1800     4.7925E-8
2400     4.32E-8
3000     3.915E-8
3600     3.51E-8
4500     3.321E-8
5400     2.943E-8
6300     2.6325E-8
7200     2.43E-8
```

6.2.9 *P. cepacia, P. fluorescens* and *C. rugosa* lipase catalyzed degradation of $[PCL_{51}\text{-}b\text{-}PEG_{32}\text{-}RCO_2]^- Na^+$ micelle at T=37 ^oC, pH= 7.4 and E=1.0 U/mL

The purpose of this study is to examine whether or not other commercial *fluorescens* and *rugosa* lipases contain different charge selective lipase species like *cepacia* lipase.

Kinetics of degradation of $[PCL_{51}\text{-}b\text{-}PEG_{32}\text{-}RCO_2]^-Na^+$ micelles catalyzed by commercial lipases from *P. cepacia, P. fluorescens* and *C. rugosa* are shown in Figure 6.11. All the three lipases react with the $[PCL_{51}\text{-}b\text{-}PEG_{32}\text{-}RCO_2]^-Na^+$ micelle but with different rates which means that three lipases contains more than one lipase species that reacts with micelles with different corona charges and the ratio of each specie in the lipases is also different. V_o (*cepacia*) = 2.3×10^{-4} mg/mL/s, V_o (*fluorescens*) = 4.0×10^{-4} mg/mL/s, V_o (*Rugosa*) = 0.95×10^{-4} mg/mL/s. Figure 6.11 shows that the degradation of $[PCL_{51}$-*b*-PEG_{32}-$RCO_2]^-Na^+$ micelles catalyzed by *P. fluorescens* lipase is both faster and gives larger conversion than *C. rugosa and P. cepacia* lipases at the same lipase activity (E=1.0 U/mL). Figure 6.12 indicates that there are only small differences between the *P. fluorescens* lipase catalyzed degradation of micelles with neutral, negative and positive charged corona at the same conditions. The lipase component in commercial *P. fluorescens* lipase appears to be very effective in catalytic degradation of $[PCL_{51}$-*b*-PEG_{32}-$RCO_2]^-Na^+$ micelles which have negatively charged corona and products generated during the initial degradation has less inhibitory effects on this lipase component.

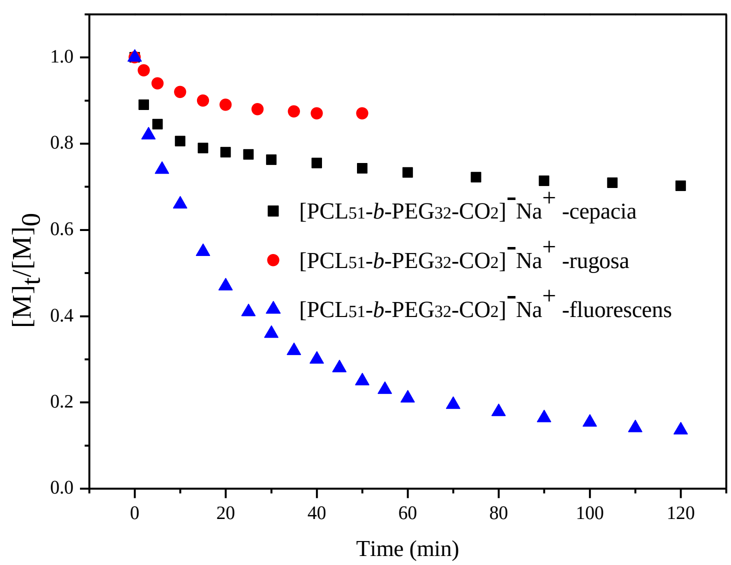

Figure 6.11: Kinetic plots for the degradation of $[PCL_{51}$-*b*-PEG_{32}-$RCO_2]^-Na^+$ micelles catalyzed by *P. cepacia, P. fluorescens and C. rugosa* lipase.

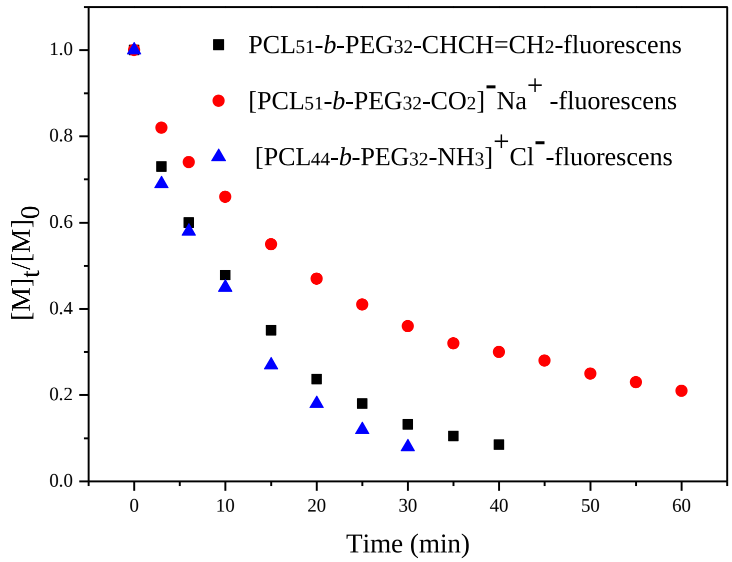

Figure 6.12: *P. fluorescens* catalyzes the degradation of micelles with different corona charges at E = 1.0 U/mL, pH=7.4 and T=37 ^{o}C.

6.2.10 Enrichment of the commercial *P. cepacia* lipase and degradation of neutral and negative corona micelles

The objectives of this set of experiments are to show that several lipase enzymes are present in commercial *P. cepacia lipase* and show that the pure lipases have distinctly different corona charge dependent reactivity.

The commercial *P. cepacia* lipase is a mixture of lipase (33.1 kD), other proteins (most obviously a ~ 45 kD protein that has no lipase activity; see below) (Figure 6.13), and non-protein solids. When 30 mg of commercial lipase is dissolved in 1 mL of 10 mM phosphate buffer, the A_{280nm} is ~0.2. If the absorption at 280 nm were entirely due to lipase (ε_{280nm} = 35000 $M^{-1}cm^{-1}$)[49], then the data suggest that only 0.6% of the total solid is lipase. Contaminant proteins (Figure 6.13) also contribute to the absorbance at 280 nm, so the true amount is even lower. This value agrees well with the fact that that the commercial material has activity of ~37.8 U/mg, whereas the purified lipase has a reported activity of 5800 U/mg in the same assay[47]. The resulting ratio (0.5%) is quite close to the value obtained by consideration of UV/vis absorbance.

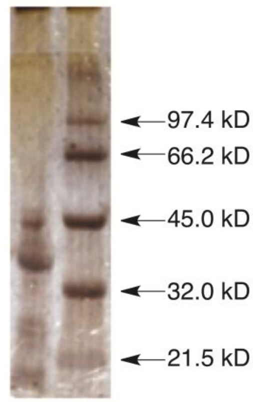

Figure 6.13: SDS-PAGE for the commercial *P. cepacia* lipase, lane 1: lipase sample, lane 2: protein markers.

Trituration with 1.5 M $(NH_4)_2SO_4$ in 10 mM phosphate buffer (pH=7) effectively removes many of the contaminant proteins and non-protein substances (Figure 6.15). The residual lipase pellet is dissolved in 0.1 M $(NH_4)_2SO_4$ in 10 mM phosphate buffer (pH= 7) for further purification by hydrophobic interaction chromatography.

The UV absorption trace from the hydrophobic interaction column showed that proteins eluted with broad overlapping peaks (Figure 6.14). The apparent lipase band always appeared by SDS-PAGE to include two barely resolved components, with a majority of a heavier species and a minority of a lighter species (Figure 6.15). Early fractions were relatively enriched in the lighter minority species, and later fractions were relatively enriched in the heavier majority species, but conditions were not found under which they were completely separated. These two proteins found in a commercial sample of *P. cepacia* lipase have sufficiently similar hydrophobicity and size that hydrophobic interaction chromatography and denaturing gel electrophoresis methods are ineffective in separating them.

There are precedents for multiple lipase isoforms, with the commercial lipase from eukaryotic *C. rugosa*[50] being one example. The multiplicity of lipases in fungi is attributable to distinct lipase genes in the organism (e.g. *lip1* through *lip7* in *C. rugosa*) and to variable glycosylation, proteolysis, or posttranslational modification. Among bacteria, *P. fluorescens* has several genes annotated as lipases in its genome[51]. The genome of *P. cepacia* contains only one apparent lipase gene[52], and so we speculate that the difference here will be due to a posttranslational modification. We note that about 40 amino acids are proteolyzed from the N terminus to afford the mature lipase characterized by X-ray crystallography[53-54], but sequence analysis predicts several favorable N-terminal cleavage sites that would yield slightly shorter or longer proteins [55].

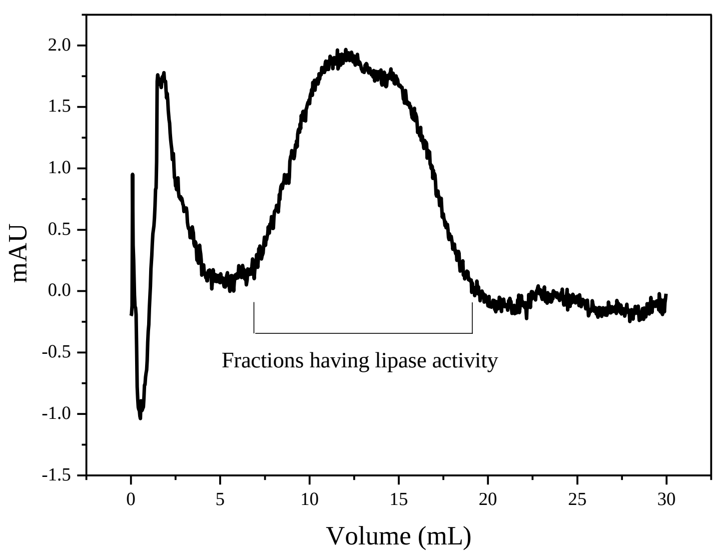

Figure 6.14: UV-vis trace for lipase fractions from the HiTrap Butyl-S Sepharose FF column.

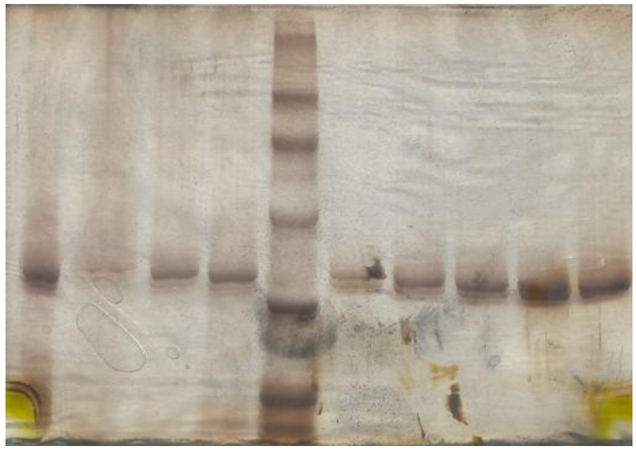

Figure 6.15: Electrophoretic analysis of the commercial and purified lipase from *P. cepacia.* SDS-PAGE, lanes: (1) commercial *P. cepacia* solution, (2) solution from 1.5 M $(NH_4)_2SO_4$ trituration, (3) residue from trituration dissolved in 0.1 M $(NH_4)_2SO_4$ (material loaded on column), (4) undissolved material from lane 3, (5) molecular weight markers (97.4, 66.2, 45.0, 32.0, and 21.5 kD), (6-10) column fractions at volume = 9, 11, 13, 15, 17 mL.

Degradation of PCL_{51}-*b*-PEG_{32}-$CH_2CH{=}CH_2$ and $[PCL_{51}$-*b*-PEG_{32}-$RCO_2]^-Na^+$ micelles by *P. cepacia* lipase from column fraction volume of 17 mL and the results are shown in Figure 6.16. The lipase activity of the column fractions was much higher than the standard lipase activity (1.0 U/ mL), so the lipase fraction was diluted before catalyzing the micelle degradation. Figure 6.16B shows that the *P. cepacia* lipase from the column fraction still catalyzes the degradation of $[PCL_{51}$-*b*-PEG_{32}-$RCO_2]^-Na^+$ micelle but the initial rate of the micelle gradation is significantly reduced after the column separation compared to the commercial lipase catalyzed degradation of the micelles (Figure 6.16A). The measured initial rates are $V_o(PCL_{51}$-*b*-PEG_{32}-$CH_2CH{=}CH_2) = 5.0 \times 10^{-4}$ mg/mL/s and V_o $([PCL_{51}$-*b*-PEG_{32}-$RCO_2]^-Na^+) = 0.60 \times 10^{-4}$ mg/mL/s.

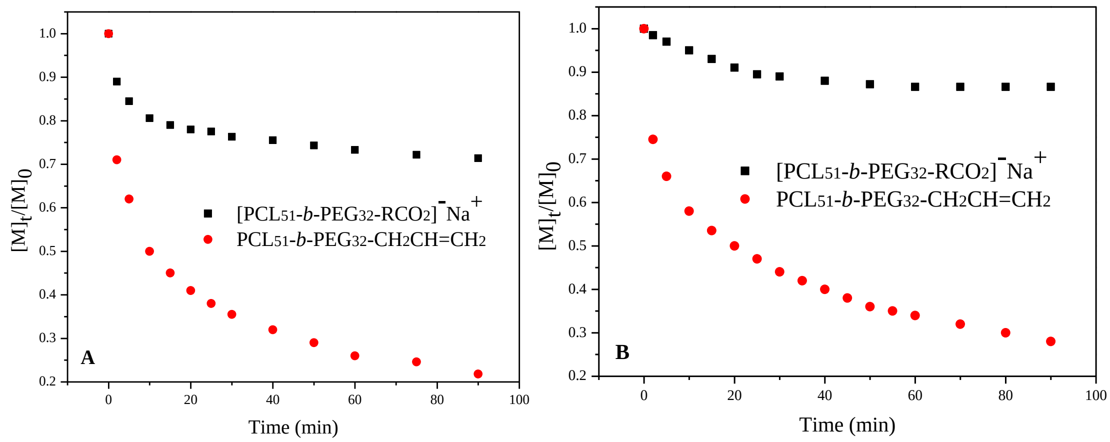

Figure 6.16: Kinetic plots for the degradation of PCL_{51}-*b*-PEG_{32}-$CH_2CH=CH_2$, $[PCL_{51}$-*b*-PEG_{32}-$RCO_2]^-$ Na^+ micelles catalyzed by commercial *P. cepacia* lipase at E=1.0 U/mL(A), by the column fraction (V=17 mL) at E ~ 0.9 U/mL(B), pH=7.4 and T=37 ^oC.

6.2.11 Separation of the commercial *P. cepacia* lipase through centrifuging

The commercial *P. cepacia* lipase contains two components. Lipase I selectively reacts with the micelle with negatively charged corona and Lipase II selectively reacts with micelle with positively charged corona. The objective of this experiment is to separate these two lipases though their selective binding with micelles with different charged. After the commercial *P. cepacia* lipase was added into the $[PCL_{109}$-*b*-PEG_{32}-$RCO_2]^-Na^+$ micelles with bigger cores, all the lipase I immediately binds with the micelle to form micelle-lipase I complex and while the lipase II remains in the solution. After centrifuging down the micelle-lipase I complex, we got Lipase II and some water soluble initial degradation products in the supernatant. The degradation of micelles from $[PCL_{44}$-*b*-PEG_{32}-$RNH_3]^+Cl^-$ and $[PCL_{51}$-*b*-PEG_{32}-$RCO_2]^-Na^+$ were catalyzed by supernatant solution obtained from the above method and the kinetic results are plotted in Figure 6.17. As was expected, there were no $[PCL_{51}$-*b*-PEG_{32}-$RCO_2]^-Na^+$ micelles degradation observing during the 1 hour of reaction. The lipase II solution obtained via centrifuging method catalyzed the degradation of $[PCL_{44}$-*b*-PEG_{32}-$RNH_3]^+Cl^-$ very efficiently but with obviously strong products inhibition. The initial rate of $[PCL_{44}$-*b*-PEG_{32}-$RNH_3]^+Cl^-$ was measured as 2.4 $\times 10^{-4}$ mg/mL/s for a calculated lipase activity of 0.57 U/mL. The actual lipase II activity should be less than this value after the purification. The kinetic results in this experiment further proved that the commercial *P. cepacia* lipase contains two components and each component reacts with micelles with different corona charges. The centrifuging method gives a potential method to fully separate the two lipase component but the separated lipases ether mixed with intact block copolymers or initial degradation products.

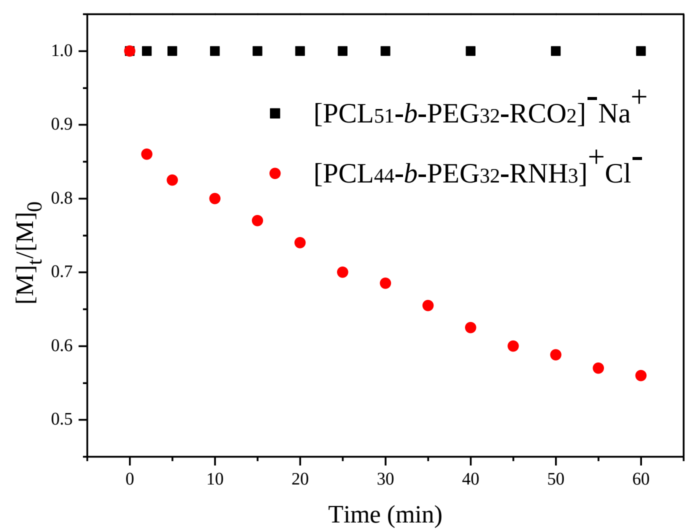

Figure 6.17: Kinetic plots of $[PCL_{44}$-*b*-PEG_{32}-$RNH_3]^+Cl^-$ and $[PCL_{51}$-*b*-PEG_{32}-$RCO_2]^-Na^+$ degradation catalyzed by lipase purified via centrifuging.

6.2.12 Analysis of initial rates of micelle degradation

Assume that commercial *P. cepacia* lipase has two and only two lipases.

Minority lipase (Lipase (I))= 1; Majority lipase (Lipase (II)) = 2;

[1] = molarity of 1; [2] = molarity of 2 ;

PCL_{51}-*b*-PEG_{32}-$CH_2CH{=}CH_2$ = micelle a ; $[PCL_{51}$-*b*-PEG_{32}-$RCO_2]^-Na^+$ = micelle b

Reaction solution1-commercial lipase catalyzed degradation of micelles

Figure 6.2 data:

V_0 (PCL_{51}-*b*-PEG_{32}-$CH_2CH{=}CH_2$) = 6.0 $\times 10^{-4}$ mg/mL/s ; relative rate = 6.0

V_0 ($[PCL_{51}$-*b*-PEG_{32}-$RCO_2]^-Na^+$) = 2.3 $\times 10^{-4}$ mg/mL/s ; relative rate = 2.3

V_0 ($[PCL_{51}$-*b*-PEG_{32}-$RSO_3]^- Na^+$) = 2.3 $\times 10^{-4}$ mg/mL/s ; relative rate = 2.3

V_0 ($[PCL_{51}$-*b*-PEG_{32}-$RNH_3]^+Cl^-$) = 5.2 $\times 10^{-4}$ mg/mL/s ; relative rate = 5.2

Figure 6.5 data:

V_0 (PCL_{51}-*b*-PEG_{32}-$CH_2CH{=}CH_2$) = 3.6 $\times 10^{-4}$ mg/mL/s ; relative rate = 3.6

When the molar concentration of micelle particles are in substantial excess over the number of enzyme molecules, the degradation is zero order in micelle concentration ([M]) and first order in the initial enzyme concentration ($[E_0]$) which is equivalent to first order in the enzyme-micelle complex [EM] ($-d[M]/dt = k [M]_0[E_0]^1 = k[M]^0[EM]^1$).

1) $[1]_1 k_{1a} + [2]_1 k_{2a} = 6.0$

2) $[1]_1 k_{1b} = 2.3$

3) $[2]_1 k_{2a} = 3.6$ 1 is fully deactivated $[1]_1 = 0$; and 2 is unchanged $[2]_1$

Therefore $[1]_1 k_{1a} = 2.4$ and $[1]_1 k_{1b} = 2.3$ and $k_{1a} \sim k_{1b}$ (The rates of Lipase I catalyzed degradation of micelles from PCL_{51}-*b*-PEG_{32}-$CH_2CH{=}CH_2$ and $[PCL_{51}$-*b*-PEG_{32}-$RCO_2]^-Na^+$ are almost the same. The reason is that it is the same lipase and the micelle cores are the also same.)

Figure 6.16 B, Reaction solution2-after the lipase enrichment:

V_0 (PCL_{51}-*b*-PEG_{32}-$CH_2CH{=}CH_2$) = 5.0 $\times 10^{-4}$ mg/mL/s

V_0 ([PCL_{51}-*b*-PEG_{32}-$RCO_2]^{-}Na^{+}$) = 0.60 $\times 10^{-4}$ mg/mL/s

4) $[1]_2\, k_{1a} + [2]_2\, k_{2a} = 5.0$

5) $[1]_2 k_{1b} = 0.6$

$k_{1a} \sim k_{1b}$ Therefore $[2]_2\, k_{2a} = 4.4$ and $[2]_2/[2]_1 = 1.22$; $[1]_2/[1]_1 = 0.26$

$[2]_2/[1]_2 = 4.7\ [2]_1/[1]_1$ Therefore, Ratio of Lipase I to Lipase II increases by a factor of 4.7 from lipase enrichment.

6.2.13 Model for Corona Charge Dependent Lipase Catalysis

Block copolymers of poly (ethylene glycol) (PEG) block poly (ε-caprolactone) (PCL) self-assemble into core-shell micelles in water where the hydrolytically non-degradable hydrophilic PEG segment forms the exterior corona and the core contains the hydrolytically degradable polyester hydrophobic PCL block. The micelle corona consists of the water soluble PEG segment which permits aqueous dispersions of micelles with water insoluble hydrophobic PCL cores. Lipases that catalyze hydrolysis of the assembly of polyester (PCL) segments in the micelle core must bind the micelle in the hydrophobic region which subsequently guides the polyester chain into the catalytic hydrolysis center. Binding of a hydrophobic region of the micelle with the hydrophobic trench[56] of the lipase enzyme is strong enough such that the polyester hydrolysis and micelle degradation occur much faster than exchange of the enzyme molecule between micelles.

The strong interaction between the dispersed micelle particles and the sparingly soluble lipase is aided by the hydrophobic effect from water that effectively pushes the hydrophobic sections of the enzyme and micelle together and out away from the aqueous phase. The two lipase enzymes found in a commercial sample of *P. cepacia* lipase have sufficiently similar hydrophobicity and size that hydrophobic interaction chromatography and denaturing gel electrophoresis methods are ineffective in separating the pair of lipases. However, the two lipase isoforms have highly selective micelle degradation catalysis associated with the electronic charge carried by the micelle corona, and the corona charge dependent catalysis is thus ascribed to electronic effects in the vicinity of the catalysis center and not bulk electronic effects of the entire enzyme molecule. The charged corona are distant from the water-hydrophobic interface where the polyester hydrolysis is thought to occur and so the corona charge effect is tentatively ascribed to a coulombic kinetic barrier to micelle-enzyme complex formation similar to that described as electrostatic steering[57]. This model further leads to expecting that the two *P.cepacia* lipases will have sites with opposite net charges that influence micelle-lipase complex formation. Scheme 6.3 illustrates the micelle corona charge dependent lipase catalyzed micelle degradation for the two observed complementary *P. cepacia* lipases. The larger equilibrium constant for product inhibition observed for the lipase that catalyzes degradation of negative corona micelles suggests that the active catalyst center and adjacent hydrophobic trench have one or more sites that exhibit stronger inhibitor-lipase binding than the lipase that reacts with positively charged or neutral corona micelles.

Several different types of posttranslational modifications might yield two electrostatically distinct lipase components originating from the same gene. Variable cleavage of the N-terminus, where numerous charged amino acids occur, might moderate bulk and/or local charge. The N-terminus in the crystal structures is somewhat distant from the active site [53-54], but a putative extension might reach towards the active site or might interact in the hydrophobic trench. Protein modifications like phosphorylation or glycosylation would also affect protein electrostatic properties and surfaces. Identifying the origin of the pair of *P.cepacia* lipases and comparison of the electronic charge distributions of the hydrophobic trench and catalyst centers are high priority continuing objectives.

6.3 Summary

Poly (caprolactone)-poly (ethylene glycol) block copolymers (HO-PCL-*b*-PEG-X) self assemble into micelles where the PEG-X (X= $-CH_2CH=CH_2$, $-RCO_2^-$, $-RSO_3^-$, $-RNH_3^+$, R=$-O(CH_2)_3S(CH_2)_2-$) segment is the corona and the PCL block is the polyester core. Aqueous dispersions of these micelles function as substrates for lipase enzymes catalyzed hydrolysis of the polyester (PCL) core and micelle degradation through an interfacial activation process. An allyl terminated PEG block copolymer (HO-PCL-*b*-PEG-$CH_2CH=CH_2$) is substituted to give a set of micelles that differ in having negatively charged ($-SO_3^-$, $-CO_2^-$) and positively charged ($-NH_3^+$) micelle corona. The charged and neutral corona micelle dispersions are observed to have corona charge dependent lipase binding and catalytic degradation by an interfacial activation pathway.

P. cepacia lipase from a commercial source was recognized to have two lipase components through observing different corona charge selective catalyzed micelle degradations. Both of the *P. cepacia* lipase components catalyze degradation of the micelles with neutral corona, but the lipase components are specific for either negatively or positively charged corona. The kinetic simulation and experimental kinetic results indicate that the initial degradation products ([HO-PCL $_{n\leq6}$-*b*-PEG$_{32}$-RCO$_2$]$^-$Na$^+$) are strong inhibitors for the lipase I that reacts with the micelle with negative corona. Lipase (I) was proved to catalyze the degradation of micelles with neutral or negative coronas at the same rate. Micelles from [PCL$_{51}$-*b*-PEG$_{32}$-RCO$_2$]$^-$ Na$^+$ that have negatively charged corona selectively at pH of 7.4 react with both lipase components at pH of 4.0 where the carboxylate groups are protonated.

A commercially obtained *P. cepacia* lipase sample was further shown to contain two lipases by partial resolution into portions enriched in one of the pair of lipases that have complementary corona charge dependent micelle degradation. Observation of corona charge selective lipase catalyzed micelle degradation suggests that strategies that incorporate variation of corona charge could be employed in designing block copolymer micelles for therapeutic substance delivery where transport is stabilized and lipase catalyzed micelle degradation providing selective release. Expanding investigations of corona charge dependent reactions of micelles and enzymes are directed toward revealing the origin for the observed pair of *P. cepacia* lipases, the enzyme structural features that result in charge dependent catalysis and whether or not these features have biological relevance.

6.4 Experimental

6.4.1 Materials

Allyl alcohol (≥99%, Sigma Aldrich) was dried by 3 Å molecular sieves prior to use. Ethylene Oxide (99%, PFALTZ & BAUER. INC) and ε-Caprolactone (CL) (99%, TCI America) were dried over CaH_2 and distilled prior to use. 18-Crown-6-ether (18C6, ≥99%), Stannous Octoate ($Sn(Oct)_2$, ~95%), Mercaptosuccinic acid (97%), Sodium 2-mercaptoethanesulfonate(BioXtra, ≥98.0%), 2,2-Dimethoxy-2-phenylacetophenone (99%), cysteamine hydrochloride (BioXtra), Azobisisobutyronitrile (AIBN, recrystallized, 99%), Ammonium sulfate(≥99%), Phosphate buffered saline (PBS, tablet), lipase from *P. cepacia* (37.8 U/mg, Lot # BCBD 7500V), lipase from *P. fluorescens* (42 U/mg) and Lipase from *C. rugosa* (22.8 U/mg) were used as received from Sigma Aldrich. Buffer solution (pH=4 and 10) were purchased from Fisher Scientific. Potassium naphthalenide THF solution (1.0 M) was prepared by mixing of naphthalene (5.12 g), potassium (1.56 g) and THF (35 mL) in a flask. SnakeSkin Dialysis tubing (10K MWCO, 35mm dry I.D., 35 feet) was used for dialysis of aqueous media containing polymer micelles. Acetone, toluene, petroleum ether, dichloromethane and methanol were use as received from J.T. Baker and dimethylformamide (DMF, HPLC grade, 99.7%+, Alfa Aesar) was used as the GPC eluent.

6.4.2 Analytical techniques

^{1}H NMR spectra were obtained using Bruker 500 MHz spectrometer with $CDCl_3$ as NMR solvent media. NMR data were analyzed by using the Bruker Topspin 2.1 software.

Water suppressed ^1H NMR spectra of block copolymer micelles in buffer solutions containing 10% of D_2O were acquired using presaturation of water with 50 dB attenuation. An arrayed experiment was used to monitor the kinetics of lipase catalyzed degradation of micelles, collecting spectra every 5, 10, 15 or 30 min, with a preacquisition delay. The ^1H NMR covered a spectral window of -5.0 ppm to 15.0 ppm. The excitation relaxation delay was set to 5 s. Each NMR spectrum was collected from accumulation of 24 scans.

Dynamic light scattering (DLS) measurements were conducted by by a Zetasizer Nano ZS (Malvern Instruments, Westborough, MA). Hydrodynamic diameter and size distribution of micelles in PBS buffer solution were measured at 37 ^oC, using 1 cm polystyrene cuvettes. The mean diameter was obtained from the instrument's DTS software using the volume reading. The Zeta potential (ζ) of the micelle samples in water was measured at 25 ^oC using the same instrument according to electrophoretic light scattering technology.

6.4.3 ^1H NMR for lipase catalyzed degradation of PCL_{51}-*b*-PEG_{32}-CH_2CH=CH_2 micelles at pH = 7.4, T = 37 ^oC and lipase activity of 1.0 U/mL

The *P. cepacia* lipase catalyzed degradation of block copolymer micelles from HO-PCL_{51}-*b*-PEG_{32}-CH_2CH=CH_2 were studied at pH=7.4, T=37 ℃ and lipase activity of 1.0 U/mL. PBS (0.70 mL, pH = 7.4) was evaporated to dryness by air in a vial. A micelle suspension (0.50 mL, 1.0 mg/mL) and D_2O (0.10 mL) was added into the vial to redissolve the PBS salts. A solution of micelle with dissolved PBS salt was transferred into a NMR tube and the solution was heated to 37 ℃ in the NMR instrument. *P. cepacia* lipase water solution (0.10 mL, 0.185 mg/mL) was added into the NMR tube quickly to catalyze the hydrolysis of micelle. The degradation of micelle was followed by ^{1}H NMR at 37 °C. Water solvent suppressed NMR was used in this experiment.

6.4.4 Enrichment of commercial *P. cepacia* lipase by hydrophobic column

A 30 mg portion of *P. cepacia* lipase (Sigma 62309, lot # BCBG7500) was suspended in 1.5 mL of 1.5 M $(NH_4)_2SO_4$ in 10 mM phosphate buffer (pH 7). The resulting cloudy suspension was centrifuged at 16000 g for 10 min. The supernatant was removed and the pellet was dissolved in 1.5 mL of 0.1 M $(NH_4)_2SO_4$ in 10 mM phosphate buffer (pH 7). The latter solution was centrifuged at 16000 g for 10 min; a small pellet was visible. The supernatant was loaded onto a 1 mL HiTrap Butyl-S Sepharose FF column (GE Heathcare Life Sciences) equilibrated with 0.1 M $(NH_4)_2SO_4$ in 10 mM phosphate buffer (pH 7) on an ÄKTA prime chromatography system (Amersham Biosciences). The column was washed with 5 mL of this buffer and protein was eluted with a 20 mL linear gradient from 0.1 M to 0 M of $(NH_4)_2SO_4$ in 10 mM phosphate buffer (pH 7) at a flow rate of 1.0 mL/min. Finally, the column was washed with 5 mL of 10 mM phosphate buffer (pH 7). The eluted fractions were collected every 1.0 mL.

6.4.5 Separation of the commercial through centrifuging

A commercial *P. cepacia* lipase stock solution (0.1mL, 0.37mg/mL) and 0.1 mL of D_2O were added into 0.5 mL $[PCL_{109}$-*b*-PEG_{32}-$RCO_2]^-Na^+$ micelle suspension with a average size ~84 nm. The activity of lipase in the reaction solution was 2.0 U/mL. Then the mixture was centrifuged at 16000 g for 20 min and 0.45 mL of supernatant was taken out for the micelle degradation.

The micelle suspensions (0.50 mL, 1.0 mg/mL) from $[PCL_{51}$-*b*-PEG_{32}-$RCO_2]^-Na^+$ and PCL_{51}-*b*-PEG_{32}-$CH_2CH{=}CH_2$ was added into the vial to redissolve the PBS salts. A solution of micelle with dissolved PBS salt was transferred into a NMR tube and the solution was heated to 37 ℃ in the NMR instrument. The supernatant obtained from the centrifuge (0.2 mL) was added into the NMR tube quickly to catalyze the hydrolysis of micelle. The degradation of micelle was followed by ^1H NMR at 37 ℃. Water solvent suppressed NMR was used in this experiment.

6.5 References

(1) Andresen, T. L.; Jensen, S. S.; Jørgensen, K. *Prog. Lipid Res.* 2005, 44, 68-97.

(2) Tong, Y.; Li, N.; Liu, H.; Ge, A.; Osawa, M.; Ye, S. *Angew. Chem. Int. Ed.* 2010, 49, 2319-2323.

(3) Wu, H.; Yu, L.; Tong, Y.; Ge, A.; Yau, S.; Osawa, M.; Ye, S. *Biochim. Biophys. Acta* 2012, 1828, 642-651.

(4) Arouri, A.; Mouritsen, O. G. *Eur. J. Pharm. Sci.* 2012, 45, 408-420.

(5) Halperin, A.; Mouritsen, O. *Europhys. Lett.* 2005, 34, 967-971.

(6) Hoyrup, P.; Callisen, T. H.; Jensen, M. O.; Halperin, A.; Mouritsen, O. G. *Phys. Chem. Chem. Phys.* 2004, 6, 1608-1615.

(7) Cajal, Y.; Berg, O. G.; Jain, M. K. *Biochemistry* 2004, 43, 9256-9264.

(8) Tjoelker, L. W.; Eberhardt, C.; Unger, J.; Trong, H. L.; Zimmerman, G. A.; McIntyre, T. M.; Stafforini, D. M.; Prescott, S. M.; Gray, P. W. *J. Biol. Chem.* 1995, 270, 25481-25487.

(9) Spiegel, S.; Foster, D.; Kolesnick, R. *Curr. Opin. Cell Biol.* 1996, 8, 159-167.

(10) Bornscheuer, U. T. *FEMS Microbiol. Rev* 2002, 26, 73-81.

(11) Chahinian, H.; Nini, L.; Boitard, E.; Dubès, J.-P.; Comeau, L.-C.; Sarda, L. *Lipids* 2002, 37, 653-662.

(12) Chahinian, H.; Fantini, J.; Garmy, N.; Manco, G.; Sarda, L. *Biochim. Biophys. Acta* 2010, 1801, 1195-1204.

(13) Berg, O. G.; Gelb, M. H.; Tsai, M.-D.; Jain, M. K. *Chem. Rev.* 2001, 101, 2613-2654.

(14) Deng, C.; Jiang, Y.; Cheng, R.; Meng, F.; Zhong, Z. *Nano Today* 2012, 7, 467-480.

(15) Langer, R.; Tirrell, D. A. *Nature* 2004, 428, 487-492.

(16) Elsabahy, M.; Wooley, K. L. *Chem. Soc. Rev.* 2012, 41, 2545-2561.

(17) Endres, T. K.; Beck-Broichsitter, M.; Samsonova, O.; Renette, T.; Kissel, T. H. *Biomaterials* 2011, 32, 7721-7731.

(18) Zhu, Z.; Li, Y.; Li, X.; Li, R.; Jia, Z.; Liu, B.; Guo, W.; Wu, W.; Jiang, X. *J. Controlled Release* 2010, 142, 438-446.

(19) Aliabadi, H. M.; Mahmud, A.; Sharifabadi, A. D.; Lavasanifar, A. *J. Controlled Release* 2005, 104, 301-311.

(20) Kataoka, K.; Harada, A.; Nagasaki, Y. *Adv. Drug Deliv. Rev.* 2001, 47, 113-131.

(21) Ensign, L. M.; Schneider, C.; Suk, J. S.; Cone, R.; Hanes, J. *Adv. Mater.* 2012, 24, 3887-3894.

(22) Shuvaev, V. V.; Ilies, M. A.; Simone, E.; Zaitsev, S.; Kim, Y.; Cai, S.; Mahmud, A.; Dziubla, T.; Muro, S.; Discher, D. E.; Muzykantov, V. R. *ACS Nano* 2011, 5, 6991-6999.

(23) Zhang, X.; Cheng, J.; Wang, Q.; Zhong, Z.; Zhuo, R. *Macromolecules* 2010, 43, 6671-6677.

(24) Nie, T.; Zhao, Y.; Xie, Z.; Wu, C. *Macromolecules* 2003, 36, 8825-8829.

(25) Shen, C.; Guo, S.; Lu, C. *Polym. Adv. Technol.* 2008, 19, 66-72.

(26) Jiang, Z.; Zhu, Z.; Liu, C.; Hu, Y.; Wu, W.; Jiang, X. *Polymer* 2008, 49, 5513-5519.

(27) Fairley, N.; Hoang, B.; Allen, C. *Biomacromolecules* 2008, 9, 2283-2291.

(28) Gan, Z.; Jim, T. F.; Li, M.; Yuer, Z.; Wang, S.; Wu, C. *Macromolecules* 1999, 32, 590-594.

(29) Lam, H.; Gong, X.; Wu, C. *J. Phys. Chem. B* 2007, 111, 1531-1535.

(30) Carstens, M. G.; van Nostrum, C. F.; Verrijk, R.; de Leede, L. G. J.; Crommelin, D. J. A.; Hennink, W. E. *J. Pharm. Sci.* 2008, 97, 506-518.

(31) Zhu, X.; Fryd, M.; Wayland, B. B. *Polym. Degrad. Stab.* 2013, 98, 1173-1181.

(32) Zhu, X.; Sharma, V. D.; Fryd, M.; Ilies, M. A.; Wayland, B. B. *Polymer* 2013, 54, 2879-2886.

(33) Zhu, X.; Fryd, M.; Tran, B. D.; Ilies, M. A.; Wayland, B. B. *Macromolecules* 2012, 45, 660-665.

(34) Takano, Y.; Houk, K. N. *J. Phys. Chem. A* 2004, 108, 11740-11751.

(35) Torre, O.; Alfonso, I.; Gotor, V. *Chem. Commun.* 2004, 1724-1725.

(36) Wu, H.; Yu, L.; Tong, Y.; Ge, A.; Yau, S.; Osawa, M.; Ye, S. *Biochim. Biophys. Acta*.

(37) Hoyle, C. E.; Bowman, C. N. *Angew. Chem. Int. Ed.* 2010, 49, 1540-1573.

(38) Killops, K. L.; Campos, L. M.; Hawker, C. J. *J. Am. Chem. Soc.* 2008, 130, 5062-5064.

(39) Tucker-Schwartz, A. K.; Farrell, R. A.; Garrell, R. L. *J. Am. Chem. Soc.* 2011, 133, 11026-11029.

(40) Yang, R.; Meng, F.; Ma, S.; Huang, F.; Liu, H.; Zhong, Z. *Biomacromolecules* 2011, 12, 3047-3055.

(41) Cammas, S.; Nagasaki, Y.; Kataoka, K. *Bioconjugate Chem.* 1995, 6, 226-230.

(42) Schubert, S.; Delaney, J. J. T.; Schubert, U. S. *Soft Matter* 2011, 7, 1581-1588.

(43) Chung, T. W.; Cho, K. Y.; Lee, H.-C.; Nah, J. W.; Yeo, J. H.; Akaike, T.; Cho, C. S. *Polymer* 2004, 45, 1591-1597.

(44) Giacomelli, C.; Borsali, R. *Macromol. Symp.* 2006, 245-246, 147-153.

(45) Lassalle, V.; Ferreira, M. L. *Macromol. Biosci.* 2007, 7, 767-783.

(46) Bajaj, H.; Sharma, V. K.; Kalonia, D. S. *Biophys. J* . 2004, 87, 4048-4055.

(47) Bornscheuer, U.; Reif, O.-W.; Lausch, R.; Freitag, R.; Scheper, T.; Kolisis, F. N.; Menge, U. *Biochim. Biophys. Acta* 1994, 1201, 55-60.

(48) Kuzmič, P. *Anal. Biochem.* 1996, 237, 260-273.

(49) Gill, S. C.; von Hippel, P. H. *Anal. Biochem.* 1989, 182, 319-326.

(50) Shaw, J. F.; Chang, C. H.; Wang, Y. J. *Biotechnology Letters* 1989, 11, 779-784.

(51) Winsor, G. L.; Lam, D. K. W.; Fleming, L.; Lo, R.; Whiteside, M. D.; Yu, N. Y.; Hancock, R. E. W.; Brinkman, F. S. L. *Nucleic Acids Research* 2011, 39, D596-D600.

(52) Winsor, G. L.; Khaira, B.; Van Rossum, T.; Lo, R.; Whiteside, M. D.; Brinkman, F. S. L. *Bioinformatics* 2008, 24, 2803-2804.

(53) Kim, K. K.; Song, H. K.; Shin, D. H.; Hwang, K. Y.; Suh, S. W. *Structure* 1997, 5, 173-185.

(54) Schrag, J. D.; Li, Y. G.; Cygler, M.; Lang, D. M.; Burgdorf, T.; Hecht, H. J.; Schmid, R.; Schomburg, D.; Rydel, T. J.; Oliver, J. D.; Strickland, L. C.; Dunaway, C. M.; Larson, S. B.; Day, J.; McPherson, A. *Structure* 1997, 5, 187-202.

(55) Petersen, T. N.; Brunak, S.; von Heijne, G.; Nielsen, H. *Nature Methods* 2011, 8, 785-786.

(56) Schulz, T.; Pleiss, J.; Schmid, R. D. *Protein Sci.* 2000, 9, 1053-1062.

(57) Hemsath, L.; Dvorsky, R.; Fiegen, D.; Carlier, M.-F.; Ahmadian, M. R. *Mol. Cell* 2005, 20, 313-324.

CHAPTER 7:

FUTURE STUDIES AND PERSPECTIVES

7.1 Introduction

Chapters 2-6 mainly focus on the design and synthesis of amphiphilic block copolymer for self assembly into micelles with modified hydrophilic-hydrophobic interface and corona charge to increase the micelle stability and to control acid and lipase enzyme catalyzed micelle degradation. The ultimate aim for this research is to design a polymer micelle that can load transport hydrophobic therapeutic drugs and transfer them to the targeted sites and then controlled release the drugs. The mechanistic and kinetic studies of acid and lipase catalyzed degradation of PCL-*b*-PEG block copolymer micelles with modified hydrophilic-hydrophobic interface and corona charge gives fundamental supports for making a micelle that can be utilized as a drug carrier for drug delivery system.

In this Chapter, I provide some suggestions for future works on this research project. The drug loading experiments for all the micelles used in the studies of Chapters 2-6 are missing. The future direction of this work should include the drug loading and in vitro drug releasing experiment for all the synthesized polymers. Besides, another strategy of inhibiting the fast lipase catalyzed degradation of PCL-*b*-PEG micelle through the PCL core cross linking should be tested. Finally, the interfacially cross linked [PCL-*b*-PMCL-*b*-PBO-*b*-PEG-$RSO_3]^{-}Na^{+}$ micelle with negatively charged corona should be prepared for drug loading and in vivo drug delivery test. Based upon our obtained results, we believe that this micelle might be ideal candidate for the drug delivery application.

7.2 Drug loading content of PCL_n-*b*-PEG_{45}-OMe (n= 27, 45, 60, 90) diblock copolymer micelles with different PCL length

In Chapter 5, DLS results of the PCL_n-*b*-PEG_{32}-CH_2-CH=CH_2 showed that the size of the micelles are proportional to the PCL length with a fixed length of PEG segment. For our future study, it is worth well to test if bigger PCL core could have more hydrophobic drug loading content (DLC%) since we already synthesized a set of PCL_n-*b*-PEG_{45}-OMe (n=27,45,60,90) diblock copolymer with different PCL length (Table 7.1). Though prior researchers had already studied this, their conclusions were not fully consistent with each other[1-6].

Table 7.1: Drug loading content (DLC%) of PCL_n-*b*-PEG_{45}-OMe (n= 27, 45, 60, 90) diblock copolymer micelles.

Micelle samples	Size(nm)(pH=7.4,T=37^{o}C)	DLC%
PCL_{27}-*b*-PEG_{45}-OMe	?	?
PCL_{45}-*b*-PEG_{45}-OMe	?	?
PCL_{60}-*b*-PEG_{45}-OMe	29	?
PCL_{90}-*b*-PEG_{45}-OMe	?	?

7.3 Acid and lipase catalyzed drug release of PCL_{60}-*b*-$PBO_{0,6}$-*b*-PEG_{45}-OMe block copolymer micelles

In Chapter 2, we have reported that strong acid catalyzed hydrolysis of interface ester groups for PCL_{60}-*b*-$PBO_{6,9}$-*b*-PEG_{45}-OMe triblock copolymer micelles were much slower when compared to micelles from parent PCL_{60}-*b*-PEG_{45}-OMe diblock copolymer. In other word, the triblock micelles are much stable than the diblock copolymer micelles at strong acid aqueous medium. In chapter 5, kinetic results from lipase enzyme catalyzed degradation of PCL_{60}-*b*-$PBO_{0,6,9}$-*b*-PEG_{45}-OMe block copolymer micelles indicates that rate of di and triblock micelles are very similar and the slower reaction obtained for the triblock copolymer micelles results from the stronger lipase products inhibition from the triblock micelle degradation.

In our future works, we will first compare the drug loading content (DLC%) between the micelles from PCL_{60}-*b*-PEG_{45}-OMe and PCL_{60}-*b*-PBO_6-*b*-PEG_{45}-OMe block copolymers (Table 7.2). These two micelles almost have the same PCL core size and they may load same amount of the drugs. However, the inserted short PBO segment may affect the loading capacity of the inner PCL core. So, it is very worth well to study the DLC of these two micelles.

Table 7.2: Drug loading content (DLC%) of PCL_{60}-*b*-$PBO_{0,6}$-*b*-PEG_{45}-OMe block copolymer micelles.

Micelle samples	Size(nm)(pH=7.4,T=37^oC)	DLC%
PCL_{60}-*b*-PEG_{45}-OMe	29	?
PCL_{60}-*b*-PBO_6-*b*-PEG_{45}-OMe	31	?

After both micelles from PCL_{60}-*b*-PEG_{45}-OMe and PCL_{60}-*b*-PBO_6-*b*-PEG_{45}-OMe block copolymers are loaded with drugs. Acid (pH=1.0) and *P. cepacia* lipase (E= 1.0 U/mL) will be used to catalyze the degradation of these micelles and then follow the drug releasing kinetics in vitro. We may expect to observe slow drug releases from the triblock micelle due to its higher stability at acid medium. Again, the slow drug release from the triblock at enzymatic medium may just result from the stronger lipase product inhibition.

7.4 Study the Drug loading content of PCL_n-*b*-PEG_{32}-OMe (n= 27, 45, 60, 90) diblock copolymer micelles with different PCL length

In Chapter 5, we found that the large hydrophobic to hydrophilic ratio of PCL_{109}-*b*-PEG_{32}-$CH_2CH=CH_2$ prohibited micelle formation, but micelles from [PCL_{109}-*b*-PEG_{32}-RCO_2]$^-$$Na^+$ and [PCL_{109}-*b*-PEG_{32}-RSO_3]$^-$$Na^+$ with negatively charged groups on the corona are very stable at pH=7.4. Block copolymer micelles that have electronically charged groups on the terminus of the corona increase the repulsion between micelles to enhance the micelles stability from high hydrophobic to hydrophilic ratio block copolymers. Stabilization of micelles with large hydrophobic segments permits increased loading of hydrophobic substances in the core which is a major objective for therapeutic transport systems.

Due to the time limit, we haven't tested the maximum length of PCL that PEG_{32}-RSO_3Na could stabilize in micelle suspensions. In our next step, we will synthesize PCL_{max}-*b*-PEG_{32}-RSO_3Na diblock copolymer that has the maximum PCL length to from stable micelles. The reason that we choose SO_3^- as a terminus group sulfonate anion end groups of PEG in [PCL_n-*b*-PEG_{32}-RSO_3]$^-$$Na^+$ block copolymers produce stable micelle dispersions at all of the compositions and conditions studied in Chapter 5. And the carboxylate terminated corona will be protanated at low pH medium. Then we will test drug loading content (DLC%) for micelle s from [PCL_n-*b*-PEG_{32}-RSO_3]$^-$$Na^+$ (n= 44,67,109, max) (Table 7.3).

Acid and lipase enzyme catalyzed drug releasing experiments for this set of micelles might not be worth well to try since they have vulnerable interface ester group like the methoxy terminated micelles for acid hydrolysis and the purified lipase (II) won't catalyze the degradation of the micelles with a negatively charged corona as proved in Chapter 6.

Table 7.3: Drug loading content (DLC%) of $[PCL_n\text{-}b\text{-}PEG_{32}\text{-}RSO_3]^-Na^+$ (n= 44,67,109, max) diblock copolymer micelles.

Micelle samples	Size(nm)(pH=7.4,T=37^{o}C)	DLC%
$[PCL_{44}\text{-}b\text{-}PEG_{32}\text{-}RSO_3]^-Na^+$	38	?
$[PCL_{67}\text{-}b\text{-}PEG_{32}\text{-}RSO_3]^-Na^+$	53	?
$[PCL_{109}\text{-}b\text{-}PEG_{32}\text{-}RSO_3]^-Na^+$	90	?
$[PCL_{max}\text{-}b\text{-}PEG_{32}\text{-}RSO_3]^-Na^+$	?	?

7.5 Design and synthesis a new set of core cross linkable PCL-*b*-PEG micelles to increase the micelles stability in enzymatic medium

7.5.1 Significance of preparing core cross linkable PCL-*b*-PEG micelles

The instability of PCL-*b*-PEG-OMe micelles in the presence of lipase enzymes limits the application to drug delivery (Chapters 3 and 4). Thought we reported in Chapter 6 that charge selective lipase-block copolymer micelle binding and catalytic degradation, it still couldn't ultimately solve the fast lipase catalyzed the degradation of the PCL-*b*-PEG micelles. In human body or blood streams, different lipases have different local/overall charges at the surface and they all react with the corona charged micelle differently though one of these lipases may not catalyze the degradation of corona charged micelle at not due to the charge repulsion. So, it is still top critical issue to design micelles that are stable in the lipase enzyme medium.

Preliminary kinetic results from the lipase catalyzed degradation of PCL-*b*-PEG-OMe micelles in Chapter 4 shows that lipase catalyzed degradation of PCL-*b*-PEG-OMe micelle is extremely fast at the beginning. The lipase is fully activated at the PEG and PCL interface after forming the tightly bound lipase-micelle complex followed by the extrusion of the PCL segments from the micelle core into the exposed lipase Ser-His-Asp triad active site and degradation of the micelle sequentially. The lipase enzyme catalyzed degradation of PCL-*b*-PEG micelle occurs through enzyme interfacial activation[7-10].

Based upon the mechanistic studies of lipase catalyzed degradation of PCL-*b*-PEG-OMe micelles, our working hypothesis to retard or inhibit the PCL chains in the micelle core from being extruded out into the lipase active catalyst center through cross linking the micelle core. The change in the rate of micelle hydrolysis as different regions of micelle core is cross linked will be evaluated and applied as a method for tuning the kinetics of enzyme catalyzed micelle degradation.

7.5.2 Design of core cross linkable PCL-*b*-PEG micelles

PEG and PCL are both FDA approved materials for implantable devices. Micelles formed by PCL-*b*-PEG diblock copolymers have already advanced to clinical trials[11]. The cross linking functional groups and agents introduced into the micelles should also be biocompatible and harmless toward human body.

We are planning to use α-methylene caprolactone (MCL) to substitute, partially or randomly substitute the CL units in the PEG-*b*-PCL diblock copolymer to make three different types of di and triblock copolymers: $PMCL_{60}$-*b*-PEG_{45}-OMe, PCL_{40}-*b*-$PMCL_{20}$-*b*-PEG_{45}-OMe and $PMCL_{20}$-*b*-PCL_{40}-*b*-PEG_{45}-OMe. MCL has a very similar structure to

CL but it has an additional C-C double bond that can be served as a cross linking agent through the radical initiated polymerization of the C-C double bonds. Whole core cross linked, interfacially cross linked and inner core cross linked micelles will be prepared by polymerizing the double bonds on PMCL segment after the block copolymers self assemble into micelles (Figure 7.1).

Besides, another whole core cross linkable block copolymer micelle from PCL_{40}-*co*-$PMCL_{20}$-*b*-PEG_{45}OMe will be prepared when CL units are randomly substituted by MCL. This type of whole core cross linked micelle should have less cross linking density compared to the cross linked $PMCL_{60}$-*b*-PEG_{45}-OMe micelle.

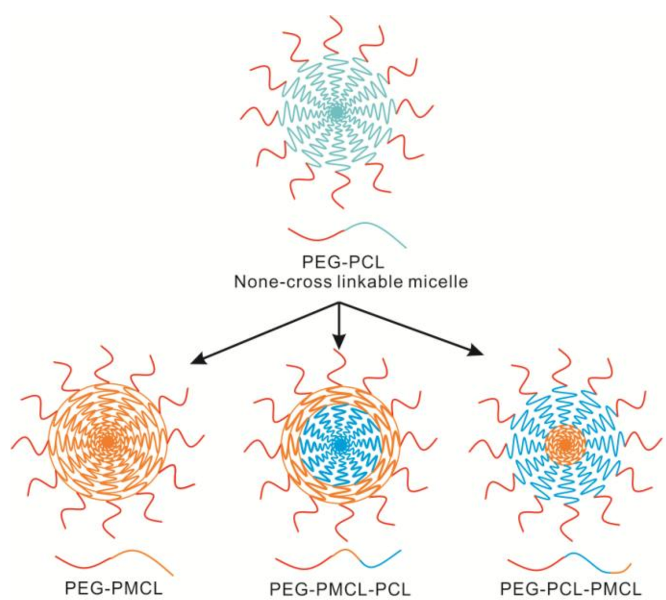

Whole core cross linked micelle Interfacially cross linked micelle Inner core cross linked micelle

Figure 7.1: Structures whole core cross linked, interfacially cross linked and inner core cross linked micelles by cross linking the PMCL layer.

Rate of lipase catalyzed degradation of three types of core cross linked micelles will be evaluated by both ^{1}H NMR and GPC. We hope the rate of the PEG-*b*-PCL diblock copolymer micelle could be tuned by cross linking different regions of micelle core.

7.5.3 Synthesis of $PMCL_{60}$-*b*-PEG_{45}-OMe, PCL_{40}-*b*-$PMCL_{20}$-*b*-PEG_{45}-OMe and $PMCL_{20}$-*b*-PCL_{40}-*b*-PEG_{45}-OMe block copolymers:

The MCL monomer is not commercial available. However, Takeda et al. had successfully synthesized MCL through a three-step reaction using caprolactone as starting material[12] (Scheme 7.1). The PCL_{40}-*b*-$PMCL_{20}$-*b*-PEG_{45}-OMe triblock copolymer can be synthesized by the ring opening polymerization of MCL and CL using MeO-PEG_{45}-OH as a macroinitiator and $Sn(Oct)_2$ as the catalyst. The polymerization of MCL was proved to be just like the polymerization of CL[13]. The $PMCL_{60}$-*b*-PEG_{45}-OMe and $PMCL_{20}$-*b*-PCL_{40}-*b*-PEG_{45}-OMe di/triblock copolymer can be prepared in the same way.

Scheme 7.1: Synthesis of α-methylene caprolactone (MCL) and PEG_{45}-*b*-$PMCL_{20}$-*b*-PCL_{40} triblock copolymer.

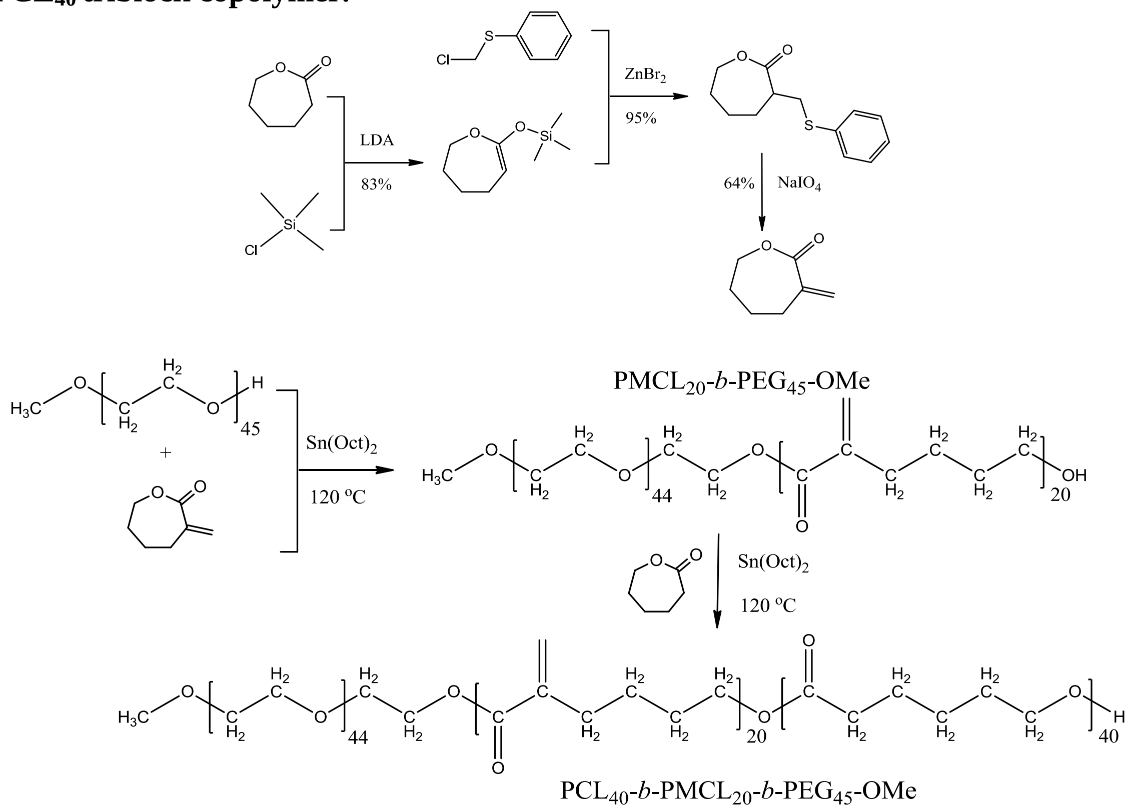

7.5.4 Formation of micelles from $PMCL_{60}$-*b*-PEG_{45}-OMe, PCL_{40}-*b*-$PMCL_{20}$-*b*-PEG_{45}-OMe and $PMCL_{20}$-*b*-PCL_{40}-*b*-PEG_{45}-OMe block copolymers and cross linking of the micelle cores

$PMCL_{60}$-*b*-PEG_{45}-OMe, PCL_{40}-*b*-$PMCL_{20}$-*b*-PEG_{45}-OMe and $PMCL_{20}$-*b*-PCL_{40}-*b*-PEG_{45}-OMe di and triblock copolymer micelles are formed by nano-precipitation method[14-17]. The polymer and 2-hydroxy-2-methylpropiophenone (Irgacure 1173, UV initiator) are dissolved in the acetone solution and then slowly adding the acetone solution into water to form the micelle. The micelles generated in this method all have a core loaded with the UV initiator[18]. The micelle solution was then irradiated under the UV light to cross the PMCL layers.

^{1}H NMR can be used to determine the degree of double bond cross linking. UV light might not penetrate deeply into the micelle core and some double bonds may remain in the micelle cores. An alternative method is to use low temperature hydrophobic thermal initiator such as lauroyl peroxide to thermal initiate the PMCL cross linking.

7.5.5 Rates of *P. cepacia* lipase catalyzed degradation of core cross linked $PMCL_{60}$-*b*-PEG_{45}-OMe, PCL_{40}-*b*-$PMCL_{20}$-*b*-PEG_{45}-OMe and $PMCL_{20}$-*b*-PCL_{40}-*b*-PEG_{45}-OMe block copolymer micelles determined by ^{1}H NMR and GPC

P. cepacia lipase was added into the three types of core cross linked micelles from block copolymers $PMCL_{60}$-*b*-PEG_{45}-OMe, PCL_{40}-*b*-$PMCL_{20}$-*b*-PEG_{45}-OMe and $PMCL_{20}$-*b*-PCL_{40}-*b*-PEG_{45}-OMe in aqueous PBS buffer (pH = 7.4) at 37 ℃ to catalyze the degradation of micelle core. The micelle degradation will be followed by ^{1}H NMR and the change of integrated intensity for the micelle ^{1}H NMR resonances reflects the change of micelle concentration as a function of time.

GPC will be used to detect the composition of lipase catalyzed degradation products and unreacted PMCL$_{60}$-*b*-PEG$_{45}$-OMe, PCL$_{40}$-*b*-PMCL$_{20}$-*b*-PEG$_{45}$-OMe and PMCL$_{20}$-*b*-PCL$_{40}$-*b*-PEG$_{45}$-OMe di and triblock copolymer. Time dependence of the GPC traces for the unreacted polymers reflect the kinetics for hydrolysis of three types of core cross linked micelles.

7.5.6 Drug loading content and releasing kinetics for micelles from PMCL$_{60}$-*b*-PEG$_{45}$-OMe, PCL$_{40}$-*b*-PMCL$_{20}$-*b*-PEG$_{45}$-OMe and PMCL$_{20}$-*b*-PCL$_{40}$-*b*-PEG$_{45}$-OMe

During the formation of these three core cross linkable block copolymer micelles, both drug and initiator will be loaded into the core of the micelles. So, the initiator will take some space of the core. Since the length of the hydrophobic segments is constant, the core size of the micelles from PMCL$_{60}$-*b*-PEG$_{45}$-OMe, PCL$_{40}$-*b*-PMCL$_{20}$-*b*-PEG$_{45}$-OMe and PMCL$_{20}$-*b*-PCL$_{40}$-*b*-PEG$_{45}$-OMe should be comparable. The actual drug loading content of the micelle cores might be different for these three types of micelles due to the double bonds on PMCL segment may have some affects on the drug loading and they all locate at different regions of the cores. The lipase catalyzed drug releasing kinetics for micelles from PMCL$_{60}$-*b*-PEG$_{45}$-OMe, PCL$_{40}$-*b*-PMCL$_{20}$-*b*-PEG$_{45}$-OMe and PMCL$_{20}$-*b*-PCL$_{40}$-*b*-PEG$_{45}$-OMe is very worth well to be studied since different regions of the micelle cores are cross linked and this may result in totally different releasing kinetic.

7.5.7 Cross linking of PCL-*b*-PEG-OMe micelle through hydrophobic cross linking agent

The above discussed three types of core cross linkable micelles are based upon the cross linking of double bond on PMCL segment. There is another very convenient method to achieve the PCL core cross linking. During the self assembly process of PCL_{60}-*b*-PEG_{45}-OMe diblock copolymers, the hydrophobic drug, initiator (lauroyl peroxide) and cross linking agent (ethylene glycol diacrylate) would be loaded into the PCL core at the same time. After heating the micelle, the ethylene glycol diacrylate will form the interpenetrating network in the core to restrict the movement of PCL chains and loaded drugs. The lipase catalyzed degradation of such polymer micelle and drug releasing experiments will be evaluated.

7.6 Preparation of an ultimate micelle with high drug loading content, no burst release and high stability at acidic and enzymatic medium

According to the obtained results from Chapters 2-6 and the predicted results in Chapter 7, the ultimate goal is to prepare the [PCL_{max}-*b*-$PMCL_{20}$-*b*-PBO_6-*b*-PEG_{32}-$RSO_3]^-Na^+$ micelle. From the structure of this micelle, inserting 6 units of PBO segment between PEG and PCL core could protect the interface ester groups and thus increases the micelle stability at acidic medium. Introducing the negative charge at the terminus of PEG corona could increase the stability of the micelle in aqueous medium and also stabilize the micelle with a longer hydrophobic PCL segments. The large PCL core also increases the drug loading content. The interfacially cross linkable PMCL segment could increase the micelle stability at the presence of lipase enzymes. So, the interfacially cross linked $[PCL_{max}\text{-}b\text{-}PMCL_{20}\text{-}b\text{-}PBO_{6}\text{-}b\text{-}PEG_{32}\text{-}RSO_{3}]^{-}Na^{+}$ micelle with negatively charged corona (Figure 7.2) probably is the ideal candidate for drug delivery system.

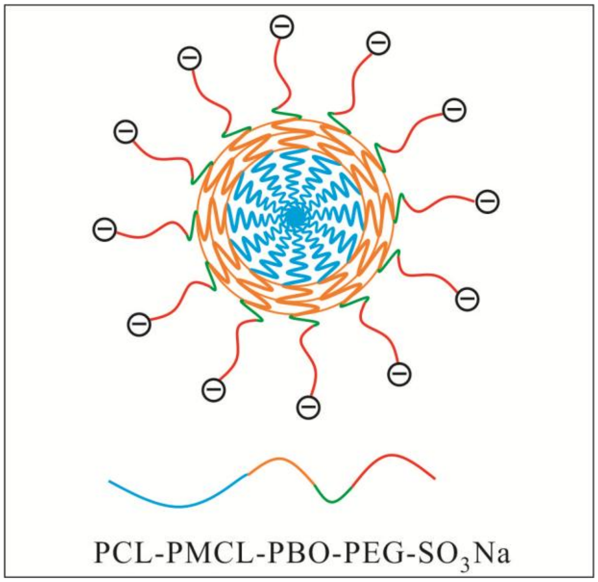

Scheme 7.2: Chemical structure of interfacially cross linked $[PCL_{max}\text{-}b\text{-}PMCL_{20}\text{-}b\text{-}PBO_{6}\text{-}b\text{-}PEG_{32}\text{-}RSO_{3}]^{-}Na^{+}$ micelle with negatively charged corona.

7.7 References

(1) Elhasi, S.; Astaneh, R.; Lavasanifar, A. *Eur. J. Pharm. Biopharm.* 2007, 65, 406-413.

(2) Shi, B.; Fang, C.; You, M.; Zhang, Y.; Fu, S.; Pei, Y. *Colloid. Polym. Sci.* 2005, 283, 954-967.

(3) Letchford, K.; Liggins, R.; Burt, H. *J. Pharm. Sci.* 2008, 97, 1179-1190.

(4) Kim, S.; Shi, Y.; Kim, J. Y.; Park, K.; Cheng, J.-X. *Expet Opin Drug Deliv.* 2010, 7, 49-62.

(5) Tyrrell, Z. L.; Shen, Y.; Radosz, M. *Prog. Polym. Sci.* 2010, 35, 1128-1143.

(6) Shuai, X.; Ai, H.; Nasongkla, N.; Kim, S.; Gao, J. *J. Controlled Release* 2004, 98, 415-426.

(7) Berg, O. G.; Gelb, M. H.; Tsai, M.-D.; Jain, M. K. *Chem. Rev.* 2001, 101, 2613-2654.

(8) van Tilbeurgh, H.; Egloff, M.-P.; Martinez, C.; Rugani, N.; Verger, R.; Cambillau, C. *Nature* 1993, 362, 814-820.

(9) Schmid, R. D.; Verger, R. *Angew. Chem. Int. Ed.* 1998, 37, 1608-1633.

(10) Sörensen, M. H.; Ng, J. B. S.; Bergström, L.; Alberius, P. C. A. *J. Colloid Interface Sci.* 2010, 343, 359-365.

(11) Sutton, D.; Wang, S.; Nasongkla, N.; Gao, J.; Dormidontova, E. E. *Exp. Biol. Med.* 2007, 232, 1090-1099.

(12) Takeda, K.; Imaoka, I.; Yoshii, E. *Tetrahedron* 1994, 50, 10839-10848.

(13) Sinnwell, S.; Ritter, H. *Macromolecules* 2006, 39, 2804-2807.

(14) Schubert, S.; Delaney, J. J. T.; Schubert, U. S. *Soft Matter* 2011, 7, 1581-1588.

(15) Chung, T. W.; Cho, K. Y.; Lee, H.-C.; Nah, J. W.; Yeo, J. H.; Akaike, T.; Cho, C. S. *Polymer* 2004, 45, 1591-1597.

(16) Giacomelli, C.; Borsali, R. *Macromol. Symp.* 2006, 245-246, 147-153.

(17) Lassalle, V.; Ferreira, M. L. *Macromol. Biosci.* 2007, 7, 767-783.

(18) Yang, R.; Meng, F.; Ma, S.; Huang, F.; Liu, H.; Zhong, Z. *Biomacromolecules* 2011, 12, 3047-3055.